Vol. 65 April, 1961 No. 4

THE JOURNAL OF PHYSICAL CHEMISTRY

(Registered in U. S. Patent Office)

CONTENTS

NOTES

COMMUNICATIONS TO THE EDITOR

THE JOURNAL OF PHYSICAL CHEMISTRY

(Registered in U. S. Patent Office)

Published monthly by the American Chemical Society at 20th and Northampton Sts., Easton, Pa.

Second-class mail privileges authorized at Easton, Pa. This publication is authorized to be mailed at the special rates of postage prescribed by Section 131.122.

The *Journal of Physical Chemistry* is devoted to the publication of selected symposia in the broad field of physical chemistry and to other contributed papers.

Manuscripts originating in the British Isles, Europe and Africa should be sent to F. C. Tompkins, The Faraday Society, 6 Gray's Inn Square, London W. C. 1, England.

Manuscripts originating elsewhere should be sent to W. Albert Noyes, Jr., Department of Chemistry, University of Rochester, Rochester 20, N. Y.

Correspondence regarding accepted copy, proofs and reprints should be directed to Assistant Editor, Allen D. Bliss, Department of Chemistry, Simmons College, 300 The Fenway, Boston 15, Mass.

Business Office: Alden H. Emery, Executive Secretary, American Chemical Society, 1155 Sixteenth St., N. W., Washington 6, D. C.

Advertising Office: Reinhold Publishing Corporation, 430 Park Avenue, New York 22, N. Y.

Articles must be submitted in duplicate, typed and double spaced. They should have at the beginning a brief Abstract, in no case exceeding 300 words. Original drawings should accompany the manuscript. Lettering at the sides of graphs (black on white or blue) may be pencilled in and will be typeset. Figures and tables should be held to a minimum consistent with adequate presentation of information. Photographs will not be printed on glossy paper except by special arrangement. All footnotes and references to the literature should be numbered consecutively and placed in the manuscript at the proper places. Initials of authors referred to in citations should be given. Nomenclature should conform to that used in *Chemical Abstracts*, mathematical characters be marked for italic, Greek letters carefully made or annotated, and subscripts and superscripts clearly shown. Articles should be written as briefly as possible consistent with clarity and should avoid historical background unnecessary for specialists.

Notes describe fragmentary or incomplete studies but do not otherwise differ fundamentally from articles and are subjected to the same editorial appraisal as are articles. In their preparation particular attention should be paid to brevity and conciseness. Material included in Notes must be definitive and may not be republished subsequently.

Communications to the Editor are designed to afford prompt preliminary publication of observations or discoveries whose value to science is so great that immediate publication is imperative. The appearance of related work from other laboratories is in itself not considered sufficient justification for the publication of a Communication, which must in addition meet special requirements of timeliness and significance. Their total length may in no case exceed 1000 words or their equivalent. They differ from Articles and Notes in that their subject matter may be republished.

Symposium papers should be sent in all cases to Secretaries of Divisions sponsoring the symposium, who will be responsible for their transmittal to the Editor. The Secretary of the Division by agreement with the Editor will specify a time after which symposium papers cannot be accepted. The Editor reserves the right to refuse to publish symposium articles, for valid scientific reasons. Each symposium paper may not exceed four printed pages (about sixteen double spaced typewritten pages) in length except by prior arrangement with the Editor.

Remittances and orders for subscriptions and for single copies, notices of changes of address and new professional connections, and claims for missing numbers should be sent to the American Chemical Society, 1155 Sixteenth St., N. W., Washington 6, D. C. Changes of address for the *Journal of Physical Chemistry* must be received on or before the 30th of the preceding month.

Claims for missing numbers will not be allowed (1) if received more than sixty days from date of issue (because of delivery hazards, no claims can be honored from subscribers in Central Europe, Asia, or Pacific Islands other than Hawaii), (2) if loss was due to failure of notice of change of address to be received before the date specified in the preceding paragraph, or (3) if the reason for the claim is "missing from files."

Subscription rates (1961): members of American Chemical Society, $12.00 for 1 year; to non-members, $24.00 for 1 year. Postage to countries in the Pan-American Union $0.80; Canada, $0.40; all other countries, $1.20. Single copies, current volume, $2.50; foreign postage, $0.15; Canadian postage $0.10; Pan-American Union, $0.10. Back volumes (Vol. 56–64) $30.00 per volume; foreign postage, per volume $1.20, Canadian, $0.40; Pan-American Union, $0.80. Single copies: back issues, $3.00; for current year, $2.50; postage, single copies: foreign, $0.15; Canadian, $0.10; Pan-American Union, $0.10.

The American Chemical Society also publishes *Journal of the American Chemical Society, Chemical Abstracts, Industrial and Engineering Chemistry*, International Edition of *Industrial and Engineering Chemistry, Chemical and Engineering News, Analytical Chemistry, Journal of Agricultural and Food Chemistry, Journal of Organic Chemistry, Journal of Chemical and Engineering Data, Chemical Reviews, Chemical Titles* and *Journal of Chemical Documentation*. Rates on request.

THE JOURNAL OF PHYSICAL CHEMISTRY

(Registered in U. S. Patent Office) (© Copyright, 1961, by the American Chemical Society)

VOLUME 65 MAY 1, 1961 NUMBER 4

A THERMODYNAMIC CALCULATION OF SELECTIVITY COEFFICIENTS FOR STRONG-BASE ANION EXCHANGERS[1]

BY G. E. BOYD, S. LINDENBAUM AND G. E. MYERS

Oak Ridge National Laboratory, Oak Ridge, Tennessee

Received May 26, 1960

A computation of the equilibrium selectivity coefficients for the exchange of bromide with chloride, iodide or fluoride ions present in dilute aqueous solutions was performed for a series of cross-linked strong-base anion exchangers (polystyrene quaternary ammonium type) using the Gibbs–Donnan equation. Swelling pressures, P, and activity coefficient ratios, log $(\gamma_{X^-}/\gamma_{Br^-})_r$, were evaluated from weight swelling measurements conducted in isopiestic vapor pressure experiments on virtually uncross-linked and on cross-linked exchangers. Partial molar volume differences, $(\bar{v}_{X^-} - \bar{v}_{Br^-})$, needed for the swelling free energy estimate were derived from density measurements on a weakly cross-linked exchanger. The calculated selectivity coefficients were in satisfactory agreement with independently measured experimental values except with the most highly cross-linked exchangers. When the values for the latter were corrected for their lower exchange capacities good agreement apparently was obtained. The thermodynamic treatment reported has led to the important generalization that, at constant temperature in the absence of specific interactions in the aqueous electrolyte phase, the selectivity coefficient, D_1^2, is a function solely of the weight swelling of the exchanger; whatever changes the swelling, be it the exchanger cross-linking, ionic composition or external electrolyte concentration, also will change D_1^2 in a manner that may be estimated from the Gibbs–Donnan equation.

This paper continues the program of thermodynamic calculations of the ionic selectivity coefficients shown by organic ion exchangers when they are in equilibrium with dilute aqueous electrolyte mixtures[2]; specifically, the extent of the selective uptake of halide ions by variously cross-linked strong base anion exchangers will be computed.

The basis for the calculation of ion-exchange reaction equilibrium constants is the exact Gibbs–Donnan equation for a membrane equilibrium in the presence of an hydrostatic pressure[3a,b]

$$RT \ln K_a = P(z_2\bar{v}_1 - z_1\bar{v}_2) \qquad (1)$$

In eq. 1 K_a is the mass law activity product ratio for an ion-exchange reaction involving the replacement of ion 1 by ion 2, P is the pressure, $\bar{v}_1$ and $\bar{v}_2$ are the partial molal volumes of the exchanger salts, and z_1 and z_2 are the charges carried by 1 and 2, respectively. The equation for the experimentally measured mass law concentration product ratio, or selectivity coefficient, D_1^2, for the exchange of singly charged anions follows from eq. 1

$$\log D_1^2 = P(\bar{v}_1 - \bar{v}_2)/2.3RT + \log(\gamma_1/\gamma_2)_r - 2\log(\gamma_1/\gamma_2)_w \qquad (2)$$

where the subscripts, r and w, denote the exchanger and external aqueous solution phases, respectively, and γ_1 and γ_2 are the mean molal activity coefficients for the halide salts 1 and 2.

In applying eq. 2 it will be assumed that the organic anion exchanger can be regarded as a polyelectrolyte solution or homogeneous gel phase in which water acts as solvent and resin halide salts 1 and 2 are solutes. A molal, or weight normal, concentration scale will be used for the ion exchanger and for the equilibrium aqueous electrolyte solution. The limited swelling of cross-linked ion exchangers is taken into account by the inclusion of a pressure–volume term in eq. 2. The swelling pressure, P, is defined by the variation of the free energy of the polymeric network with volume consequent to the osmotic penetration of water molecules into the exchanger.[4] The standard and refer-

(1) Presented before the Division of Colloid Chemistry, American Chemical Society 132nd National Meeting, New York, N. Y., September 8–13, 1957.

(2) G. E. Myers and G. E. Boyd, *J. Phys. Chem.*, **60**, 521 (1956).

(3) (a) F. G. Donnan and E. A. Guggenheim, *Z. physik. Chem.*, **162A**, 346 (1932); (b) F. G. Donnan, *ibid.*, **168A**, 369 (1934).

(4) No actual hydrostatic pressure exists inside the exchanger that can be detected and measured by conventional techniques (*i.e.*, probes, etc.). However, the elastic response of the cross-linked polymeric network to its osmotic penetration by water gives a strain energy whose change with volume at equilibrium is formally equivalent to the

ence state choices for the activity coefficients and the definition of the selectivity coefficient are the same as in our calculations on cation exchangers.[2,5]

That further confusion might be avoided regarding the methods employed in this and in our earlier paper, it is emphasized that the use made of eq. 1 is not a "... test of the thermodynamic theory of ion-exchange processes of Gregor ...."[6] In this latter, non-thermodynamic treatment[7] which starts with eq. 1, the solvent was chosen as the "free water" remaining in the exchanger after a fixed amount of the total water was assigned, arbitrarily, to the ions as water of hydration. The partial molar volumes in eq. 1 were then identified with the molar volumes of the hydrated ions derived from conductivity measurements, and the activity coefficient ratios in ln K_a were taken as approximately unity. In some cases an apparent qualitative concordance is given with experiment by this simplification; in general, however, a quantitative account cannot be obtained without assuming a variable ionic hydration. Further, it is not possible to account, even qualitatively, for observed selectivity coefficient increases with increasing amounts of the preferred ion[8] in the exchanger, or for selectivity coefficient reversals. When experimentally defined stoichiometric partial molal volumes, concentrations and activity coefficients are employed in eqs. 1 and 2 the second member of the right hand of eq. 2 has been found[9,10] to determine the magnitude of log D_1^2.

This paper will demonstrate that each of the three right-hand members of eq. 2 can be evaluated by using exact thermodynamic equations. The estimates of log D_1^2 thus derived will be shown to be in agreement with the selectivity coefficients measured directly by experiment. Evidence will be presented for the important generalization that, at constant temperature in the absence of specific interactions (*e.g.*, complex ions, etc.,) in the aqueous electrolyte phase, D_1^2 is a function only of the weight swelling of the exchanger[11]; whatever changes the swelling, be it (a) the exchanger cross-linking, (b) the ionic composition or (c) the external electrolyte concentration, also will change the selectivity coefficient in a manner that may be estimated using eq. 2.

Evaluation of Terms in Fundamental Equation 2.—The first term of the right-hand member of eq. 2 contains two quantities which require independent estimates.

The swelling pressure for cross-linked ion exchangers may be computed[10] by eq. 3 where $\bar{v}_w$

$$P = (RT/\bar{v}_w) \ln (a_w'/a_w) \qquad (N_m \text{ constant}) \quad (3)$$

is the partial molal volume of water in the exchanger. The use of eq. 3 requires that the water activity, a_w', in a cross-linked exchanger be compared with the activity, a_w, in a chemically identical unlinked exchanger containing the same amount of water per equivalent. In this investigation the cross-linked exchangers were in equilibrium with 0.1 molal pure or mixed 1–1 electrolytes; hence, log a_w' may be computed from known osmotic coefficients, ϕ, at this concentration. The pressure is therefore given by

$$P(\text{atm.}) = \frac{5.6339 \times 10^4}{\bar{v}_w} [-0.00156\phi - \log a_w] N_m \quad (3a)$$

Required values of log a_w for a non-cross-linked exchanger of the same weight normality, N_m, as the cross-linked preparation may be interpolated from values of log a_w determined on a very weakly cross-linked exchanger as a function of N_m in isopiestic vapor pressure experiments. A small, usually negligible, correction to the value of P estimated in eq. 3a can then be made for the pressure, P_0, in the weakly cross-linked exchanger when it is in equilibrium with pure water using

$$P_0 = (RTM_w/1000\bar{v}_w)\, \nu\phi^\circ N_m^\circ = 24.4\, \nu\phi^\circ N_m^\circ \quad (3b)$$

where M_w is the molar mass and $\bar{v}_w$ the partial molal volume of water, $\nu\phi^\circ$ and N_m° are the molal osmotic coefficient and weight normality of the fully swollen exchanger, respectively. The necessary value of $\nu\phi^\circ$ may be found by extrapolating the experimentally determined curve for the variation of $\nu\phi$ with N_m to N_m°. The magnitude of $\bar{v}_w$ varies with N_m and to a much lesser extent with P[12]; however, the value 18.069 ml. mole^{-1} may be used with less than 1% error in some cases (*cf.*, Tables IV and V).

The partial molal volume difference, $(\bar{v}_1 - \bar{v}_2)$, may be evaluated from experimental measurements of the equivalent volumes, V_e, of resins of varying water content and ionic composition[2]

$$(\bar{v}_1 - \bar{v}_2) = (V_1 - V_2) - \int_0^{x_w} (\partial\bar{v}_w/\partial x_2)_{x_w}\, dx_w \quad (4)$$

where V_1 and V_2 are the molar volumes of the dry resinates 1 and 2, respectively, x_2 is the equivalent fraction of 2 (*i.e.*, "loading"), and x_w the equivalent water content. Equation 4 is exact and does not assume that $\bar{v}_w$ remains constant, independent of the weight normality (*i.e.*, x_w), or composition (x_2) of the exchanger. In special cases it may be acceptable to assume $\bar{v}_w$ is independent of x_w and x_2; then the labor in estimating $(\bar{v}_1 - \bar{v}_2)$ may be

hydrostatic pressure that would be needed if no cross-linking were present. Thus, the thermodynamic properties and, hence, the ionic selectivity of a cross-linked exchanger can be modified by the action of an external hydrostatic pressure which would expel water and increase the concentration of the polyelectrolyte phase.

(5) The absence of a coefficient to the second term in the right-hand side of eq. 2 is a consequence of the hypothesis that the polycation of the anion exchanger carries a large number of positive charges. The exchanger may be regarded as an n, 1 electrolyte where n is very large. The mean molal activity coefficient of the resinate salt is $\gamma_\pm = \gamma^{\nu_+}/^{\nu}.\gamma^{\nu_-}/^{\nu}$ where the total number of ions, ν, is given by $\nu = \nu_+ + \nu_- = 1 + \nu_-$. The quantity ν is very large so that to a good approximation ν_+/ν is zero, $\nu_- = \nu$ and $\gamma_+ = \gamma_-$. Physically, the foregoing statement means that the thermodynamic properties of a high molecular weight ion exchanger are determined by its mobile counterions, and that the contributions from the structurally-bound ionic exchange groups may be taken as negligibly small. The coefficient to the second term on the right-hand side of eq. 2 differs from unity accordingly by a negligibly small amount.

(6) H. P. Gregor, *Ann. Rev. Phys. Chem.*, **8**, 470 (1957).

(7) H. P. Gregor, *J. Am. Chem. Soc.*, **70**, 1293 (1948); **73**, 642 (1951).

(8) The preferred ion is defined as that ion taken up selectively when present in the system in micro-amounts.

(9) E. Glueckauf, *Proc. Roy. Soc. (London)*, **214**, 207 (1952).

(10) G. E. Boyd and B. A. Soldano, *Z. Elektrochem.*, **57**, 162 (1953).

(11) The quantitative measure of weight swelling is the equivalent water content, x_w, given in g. equiv.$^{-1}$, or, its inverse, the weight normality, $N_m = 1000/x_w$.

(12) The compressibility of water is sufficiently small that the pressure dependence of $\bar{v}_w$ will be ignored. For example, there is less than 3% decrease in $\bar{v}_w^\circ$ even when P = 500 bars.

reduced.[13] Generally, however, and especially where the exchange of multi-charged anions (or cations with cation exchangers) occurs, it will be necessary to employ eq. 4.[14]

The second term of the right-hand member of eq. 2 reflects the contribution of the ionic interactions in the exchanger to $\log D_1^2$. It may be evaluated by means of eq. 5 from measurements of the variation of x_w for a weakly cross-linked exchanger with ionic composition for a range of water activities, a_w, in an isopiestic vapor pressure experiment

$$\log (\gamma_1/\gamma_2)_r - \log (\gamma_1^*/\gamma_2^*)_r = 0.05551 \int_0^{\log a_w} (\partial x_w/\partial x_2)a_w \, d \log a_w = 0.05551 I_R \quad (5)$$

In addition to the measurements from which I_R is estimated, it is necessary to evaluate the term $\log (\gamma^*_1/\gamma^*_2)_r$. This was accomplished by experimental selectivity coefficient measurements on the same exchanger in 0.01 N electrolyte, because, when $P = 0$, eq. 2 then gives $\log D^* = \log (\gamma^*_1/\gamma^*_2)_r$.[15]

The third term in the right hand of eq. 2 for the mean molal ionic activity coefficient ratio for the dilute aqueous mixed electrolyte may be evaluated following Robinson and Stokes[16]

$$\log (\gamma_1/\gamma_2)_w = \log (\gamma_{1(0)}/\gamma_{2(0)}) - (b_1' - b_2')m \quad (6)$$

In eq. 6 $\gamma_{1(0)}$ and $\gamma_{2(0)}$ are the activity coefficients for electrolytes 1 and 2 when present alone in aqueous solution at molality m, and the parameters b_1' and b_2' are related to the β's tabulated by Guggenheim[17] by $b' = 0.4342\beta$

It may be useful to note several features, as well as limitations, of the program of calculations outlined above.

(a) The applicability of eq. 5 is based on the assumption that an ion exchanger when it is in equilibrium with a dilute aqueous electrolyte may be regarded as a ternary mixture of polyelectrolyte salts 1 and 2 and water. When the concentration of external aqueous solution is small (*i.e.*, 0.1 M or less) Donnan invasion of cross-linked exchangers by electrolyte can be neglected, and the foregoing assumption holds to a good approximation. However, when high concentrations of electrolyte or very weakly cross-linked exchangers are employed, electrolyte penetration may become appreciable, and eq. 5 will be inapplicable.[18]

(b) It will be seen from eq. 5 that the calculation of $\log (\gamma_1/\gamma_2)_r$ on an absolute basis will not be accomplished. Hence, the selectivity coefficients estimated with eq. 2 will be relative to those for the weakly cross-linked exchanger upon which the isopiestic weight swelling measurements were made. An absolute estimation may be realized when $\log (\gamma^*_1/\gamma^*_2)_r = \log D^* = 0$, as was the case to a good approximation for the exchange of Na^+ with H^+ ion and with several alkali metal cations[2]; with strong-base anion exchangers, however, large selectivity coefficients were observed even with the most lightly cross-linked preparations.

(c) The calculation using eq. 2 assumes that the properties of highly cross-linked exchangers may be estimated from measurements on a very weakly cross-linked exchanger. It is postulated that cross-linking does not change the thermodynamic properties of the polyelectrolyte, so that all exchangers of the same chemical type and exchange capacity (dry basis) will show the same values of $\log (\gamma_1/\gamma_2)_r$ and $(\bar{v}_1 - \bar{v}_2)$ if they are of identical weight swelling. Comparisons between cross-linked and uncross-linked exchangers are presumed to be valid after correcting for the differences in their free energies of swelling. Stated alternatively, the selectivity coefficient of a weakly cross-linked exchanger could be increased by the application of an external pressure sufficient to expel water from it, and its coefficient could be made identical with that for a more highly cross-linked exchanger if N_m were increased to the same value as that for the latter exchanger. In principle, an "ionic pump" could be based on these ideas.

Experimental

The strong-base anion exchangers employed were derived from polystyrene–divinylbenzene copolymer spheres into which positively charged quaternary ammonium groups (benzyldimethylethanol) were structurally bound. These preparations (Dowex-2) were received from the Physical Research Laboratory of the Dow Chemical Company, Midland, Michigan, in two different series. Their cross-linkings, measured approximately by the nominal per cent. of divinylbenzene (DVB) used in preparing the copolymer, varied from 0.5 to 24% DVB. Acidimetric titration showed the preparations to be nearly monofunctional (*i.e.*, less than *ca.* 3% weak-base capacity). The desired homo-ionic and mixed salt-forms were prepared with 1 M solutions of reagent-grade sodium halide after a pre-treatment of the exchangers to remove tertiary amine impurities, linear polyelectrolyte and defective particles. Excess salt solution was rinsed from the chloride, bromide and iodide salt-forms with demineralized water. Initially tenth normal hydrofluoric acid solution was used to rinse the fluoride salts; however, it was observed that this treatment gave fluoride ion contents approximately 10% above the exchange capacity, presumably because of the strong absorption of HF_2^- ion. Neutral 0.1 N sodium fluoride solution was employed thereafter.

Chemical analyses were conducted on the initial pure and mixed resin halides of the 0.5% DVB preparations used for the water absorption measurements (Table III) and on the equilibrium resins from the selectivity coefficient measurements, so that the equivalent fraction of a given halide in the exchanger might be estimated. Analyses of the fluoride salt forms were performed on $NaNO_3$ solutions used to displace fluoride ion quantitatively from the exchanger. Lead chlorofluoride was precipitated,[19] dried, weighed and redissolved in acid, and chloride ion was determined volumetrically using the Volhard procedure. The other halides were estimated by argentometric titration using a silver wire and a calomel reference electrode. The exchange capacities of the dry chloride salt-forms of the variously

(13) E. Högfeldt, *Acta Chem. Scand.*, **12**, 182 (1958).

(14) The difference, $(\bar{v}_1 - v_2)$, is a function of P as well as of N_m. However, the dependence of $\Delta\bar{v}$ on P is so slight that it can be neglected within the limits of error of the calculations in this paper.

(15) The accurate evaluation of $\log D^*$ requires that (a) the measured $\log D_1^2$ values be extrapolated to infinite dilution and (b) corrected for the fact that the pressure is not zero. Neglect of these refinements introduces an error well below that of the measurements themselves, however.

(16) R. A. Robinson and R. H. Stokes, "Electrolyte Solutions," Butterworth's, London, 1955, p. 440.

(17) E. A. Guggenheim and J. C. Turgeon, *Trans. Faraday Soc.*, **51**, 747 (1955).

(18) The molal Donnan distribution coefficient, λ_D, for the equilibrium between a nominal 2% DVB cross-linked Dowex-2 (Preparation J, Table I) exchanger and 0.1 N sodium chloride solution is 0.2. The concentration of NaCl in the exchanger is therefore 0.02 N which is negligibly small compared with $N_m = 1.92$, the weight normality of resin chloride.

(19) W. F. Hillebrand and G. E. F. Lundell, "Applied Inorganic Analysis," John Wiley and Sons, New York, N. Y., 1929, p. 604.

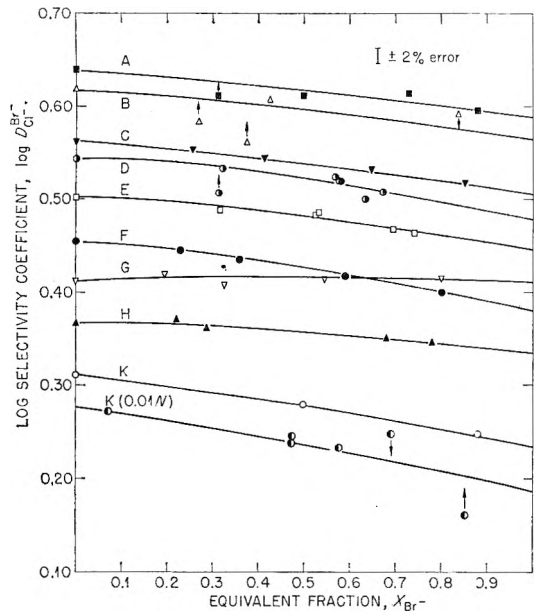

Fig. 1.—Selectivity coefficients at 25° for the bromide–chloride ion exchange equilibrium between variously cross-linked Dowex-2 and 0.1 *N* Na(Cl + Br) solutions. (Measurements on preparations A, C, F, G and H taken from ref. 25.)

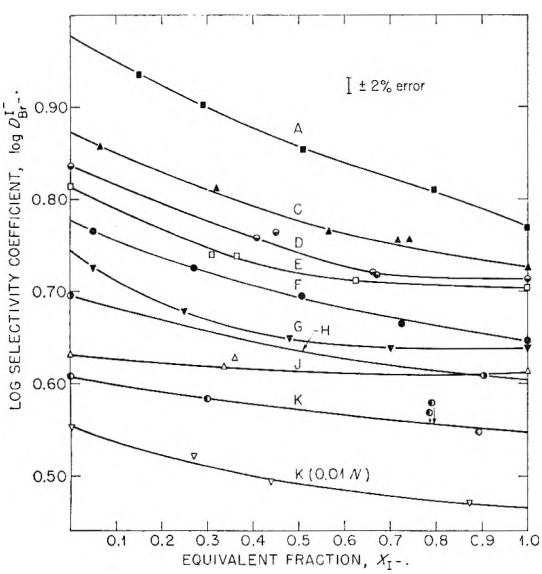

Fig. 2.—Selectivity coefficients at 25° for the iodide–bromide ion-exchange equilibrium between variously cross-linked Dowex-2 and 0.1 *N* Na(Br + I) solutions. (Measurements on preparations A, C, F, G and H taken from ref. 25.)

cross-linked exchangers are given in Table I. If an ion-exchange group were present on every benzene ring in the exchanger, a capacity of 4.14 meq./g. dry Cl-form would have been found. The observed capacities varied from 95 to 46% of this theoretical value.

Several methods to determine the water contents of the salt-forms of the cross-linked preparations in equilibrium with 0.1 *N* electrolyte solutions were employed. Centrifugation techniques[20] could be used on the more highly cross-linked exchangers to yield equivalent water content values of fair accuracy when care was exercised to standardize the procedure. Determination of water in the weakly cross-linked exchangers (*i.e.*, < 6% DVB) presented a more difficult problem. Accurate x_w values were obtained by using isopiestic equilibration techniques[10] which, unfortunately, were inconvenient. An attempt was made to devise a rapid, accurate and convenient method using radioactive lanthanum ion as a tracer. It was assumed that water, but not La^{+++} ion, would be taken up on immersing dry anion exchanger in a 0.1 *N* sodium halide solution containing radio-lanthanum. Unfortunately, La^{+++} was absorbed; measurements of this absorption at varying lanthanum concentrations would be required to effect a correction, and this detracted from the apparent convenience of the method.

(20) (a) H. P. Gregor, K. M. Held and J. Bellin, *Anal. Chem.*, **23**, 620 (1951). (b) K. W. Pepper, D. Reichenberg and D. K. Hale, *J. Chem. Soc.*, 3129 (1952).

TABLE I

EXCHANGE CAPACITIES AND EQUIVALENT WATER CONTENTS OF HALIDE SALT-FORMS OF CROSS-LINKED DOWEX-2 PREPARATIONS

Identity[a]	Nominal % DVB content	Capacity (meq./g. dry Cl-form)	Water content[b] (g. H_2O/eq.) RF	RCl	RBr	RI
A	16	1.91	128	114	87.1	65.4
B	24	2.17	..	139	103	...
C	8	3.10	185	139	100	66.7
D	10	3.03	247	141	108	(101)
E	6	3.21	..	177	119	(102)
F	4	3.47	294	233	159	83.3
G	2	3.79	345	264	181	84.9
H	1	3.71	424	333	215	86.3
I	4	3.73	497	318	234	105
J	2	3.51	763	521	326	112
K	0.5	3.95	..	..	..	...
L	0.5	3.66	2100	1428	842	...

[a] Preparations A, C, F, G and H from Series 1; the remainder from Series 2. [b] Equivalent water contents for exchangers in equilibrium with decinormal aqueous sodium halide solution containing same anion.

Equivalent water values for the homo-ionic salt-forms are summarized in Table I; only an approximate correspondence holds between x_w and the nominal DVB content. The sequence of decreasing x_w for constant cross-linking was $F^- > Cl^- > Br^- > I^-$. Measurements (data not given) on mixed halide exchangers showed a linear decrease of x_w with the equivalent fraction of the preferred halide ion in the exchanger excepting for the weakly cross-linked preparations, H, I, J, K and L, where small positive deviations were observed.

Selectivity coefficient measurements were performed by batch equilibrium techniques with weighed amounts of the pure exchanger salt forms and 0.1 *N* sodium halide solutions. Radioactive tracers (1.87 h F^{17}, 35.5 m Cl^{38}, 35.9 h Br^{82} and 8.05 d I^{131}) were employed; both exchanger and aqueous phases were analyzed and material balances were established for all of the experiments reported. The rate of anion exchange was rapid and equilibrium appeared to be attained in much less than one hour. In many cases the equilibrium point was approached from both sides. The experimental errors were such that D_1^2 values appeared to be certain to ±2%. The measurements on the preparations listed in Table I are presented in Figs. 1, 2 and 3 where D_1^2 is plotted (log scale) as a function of the equivalent fraction of the preferred ion in the exchanger.

Several features seem noteworthy: (a) There was relatively little dependence of the selectivity coefficient on the equivalent fraction of the preferred ion in the exchanger (*i.e.*, on the "loading") in the exchanges of bromide with chloride or with iodide ion; with fluoride ion large values of $D_{F^-}^{Br^-}$ were observed, and a strong dependence of the selectivity coefficient on x_{Br^-} was found. (b) Selectivity coefficients greatly different from unity were observed even with the most weakly cross-linked anion exchangers; this behavior contrasts strongly with that for 0.5% DVB Dowex-50, where, in the alkali metal cation exchanges, selectivity coefficients close to unity were found. (c) In all cases the selectivity coefficient decreased with the equivalent fraction of the preferred ion; in the bromide–fluoride exchange log $D_{F^-}^{Br^-}$ decreased linearly with x_{Br^-}, whereas the decrease of log $D_{Cl^-}^{Br^-}$ was concave to the x_{Br^-}

axis and log $D_{Br^-}^{I^-}$ was convex to the x_{I^-} axis. (d) As a possible general rule, the higher the selectivity coefficient the greater its dependence on the equivalent fraction of the preferred ion.

Equivalent volume, V_e measurements on various salt-forms of preparation I (Table I) in the dry state and with varying equivalent water content were conducted pycnometrically using dry *n*-octane as a displacement liquid.[21] Uncracked beads were selected, and care was exercised to ensure the removal of occluded air during the pycnometric operations. The desired degrees of exchanger hydration were established by isopiestic vapor pressure equilibrations. Equivalent water contents, X_w, in *moles* per equivalent were determined from the weight losses observed on heating the exchanger at 65° for 48 hours in a vacuum oven connected to a trap immersed in liquid nitrogen. The precision of the V_e values was ±0.2%; the X_w values probably were no better than ±1%. The data were fitted to equations of the form, for x_2 constant

$$V_e = V_a + \phi_w X_w \qquad (7a)$$

$$\phi_w = \phi_w^\circ X_w/(b + X_w) \qquad (7b)$$

where V_a is the equivalent volume of the anhydrous exchanger salt, and ϕ_w is the apparent molal volume of water in the exchanger. In earlier publications[10,20b] ϕ_w has been taken as equal to ϕ_w°, the molar volume of pure water (18.069 ml). In general, however, ϕ_w must be a function of N_m (or x_w) as is true with ordinary aqueous electrolyte solutions, and ϕ_w should approach ϕ_w° at infinite dilution (*i.e.*, indefinitely large x_w). Values of V_a and b derived from the volume measurements are listed in Table II together with corresponding values for the partial molal volume of the exchanger salt at infinite dilution, $\bar{v}_a^\circ$. The magnitude of difference ($V_a - \bar{v}_a^\circ$) may be a measure of the electrostriction experienced by water on entering the dry exchanger; this difference is greatest for the fluoride and least for the iodide salt form. The fractional molar electrostriction, $(V_a - \bar{v}_a^\circ)/\phi_w^\circ$, appears to be the same numerically as the empirical constant, b, as is necessary by thermodynamics.

TABLE II

VARIATION OF EQUIVALENT VOLUMES, V_e, OF ANION EXCHANGER SALT-FORMS (ML.) WITH EQUIVALENT WATER CONTENT, X_w (MOLES EQUIV.$^{-1}$)

$$V_e = V_a + \phi_w X_w = V_a + \phi_w^\circ X_w^2/(b + X_w)$$

Salt-form	V_a	$\bar{V}_a^\circ$	b	$V_a - \bar{v}_a^\circ$	$(V_a - \bar{v}_a^\circ)/\phi_w^\circ$
Fluoride	210.9	199.3	0.648	11.6	0.642
Chloride	225.3	218.5	.378	6.8	.376
Bromide	231.8	226.5	.292	5.3	.293
Iodide	242.2	238.9	.181	3.3	.183
Fluoride–bromide[a]	220.2	213.7	.361	6.5	.360
Chloride–bromide[a]	228.5	222.0	.359	6.5	.360
Iodide–bromide[a]	238.3	233.3	.276	5.0	.277

[a] Equimolar mixture, $x_{Br^-} = 0.5$.

The equivalent water contents of the salt-forms of the weakly cross-linked (nominal 0.5% DVB) preparations used as the reference exchangers in this work were measured as a function of ionic composition for various water activities, a_w, using a gravimetric isopiestic method.[2] The values given in Table III are precise to ± 0.15%; their accuracy is almost certainly lower principally because of uncertainties in the attainment of isopiestic equilibrium. In contrast to the alkali metal cation salts of a nominal 0.5% DVB linked polystyrene sulfonate, the rate of approach to isopiestic equilibrium by the anion exchanger salts was low, and as many as 14 days frequently were required to attain constant water absorptions. In addition, difficulty was experienced with the fluoride salt form because of its apparent instability. It was not possible using the isopiestic method to measure x_w values for $a_w = 1.00$ reliably; the values in Table III were determined by centrifugation with an accuracy which was surely no better than ±2%.

(21) The very slight pressure dependence of the partial molal volume of water will be ignored. Accordingly, $\bar{v}_w$ will be assumed to depend on N_m only and to be independent of the exchanger cross-linking. Preparation I was chosen for reasons of convenience.

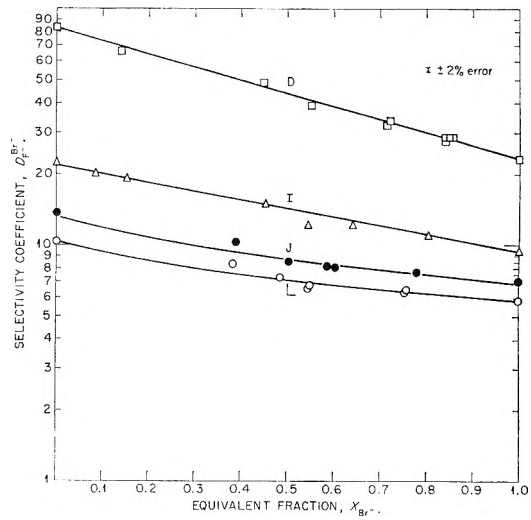

Fig. 3.—Selectivity coefficients at 25° for the bromide–fluoride ion-exchange equilibrium between variously cross-linked Dowex-2 and 0.1 *N* Na(F + Br) solutions (log scale for $D_{F^-}^{Br^-}$).

Treatment of Experimental Data.—The experimental weight swelling and equivalent volume measurements on the weakly cross-linked reference exchanger will be treated so as to compute log D_1^2 as a function of the weight normality, N_m. It is convenient to proceed in this manner because with cross-linked exchangers N_m varies with the degree of cross-linking for constant composition, x_2, and external ionic strength, μ; with x_2 for constant cross-linking and μ; or, with μ, for constant x_2 and crosslinking. Accordingly, to evaluate the terms in eq. 2 the data of Table III were fitted by least-squares methods to empirical equations of the form

$$x_w = a + bx_2 + cx_2^2 \qquad (8)$$

where x_2 is the equivalent fraction of bromide or iodide ion in the exchanger for the various $-\log a_w$ employed. Next, x_w values computed from eq. 8 for $x_2 = 0.0$, 0.5 and 1.0 were fitted to

$$-1000 \log a_w = \alpha + \beta N_m + \gamma N_m^2 \qquad (9)$$

where $N_m \equiv 1000/x_w$.[22]

The first step in the numerical calculations consisted in evaluating the swelling pressure–volume term in eq. 2. Values of $-\log a_w$ from eq. 9 and of $\bar{v}_w = (\partial V_e/\partial x_w)_{x_2}$ found by differentiating eq. 7 were substituted into eq. 3a; P was found to vary between zero and 600 atmospheres, to increase with N_m and to depend on the salt-form of the exchanger (Tables IV, V and VI). The partial molal volume of water in the exchanger decreased with increasing resinate concentration, and, for a given N_m, was smallest for the fluoride and largest for the iodide salt-form. The variation of $\bar{v}_w$ with ionic composition, x_2, was linear within experimental error so that the partial molal volume differences, $(\bar{v}_1 - \bar{v}_2)$, evaluated using eq. 4 were independent of x_2. The integration in eq. 4 was performed analytically using eq. 7 to give $(\bar{v}_1 - \bar{v}_2)$ as a function of N_m. A comparison of these values is made in Fig. 4 with the corresponding

(22) The "least squares" constants for eqs. 8 and 9 will be supplied on request to the senior author.

Table III

Equivalent Water Absorption (g. H_2O/Eq.) by Various Halide Salts of Nominal 0.5% DVB Cross-linked Dowex-2 as a Function of Water Vapor Activity

Equivalent fraction	−log a_w 0.00000	0.00346	0.00877	0.03395	0.04484	0.07438	0.09307	0.12332	0.14978	0.20901	0.27687
					Bromide–Chloride[a]						
x_{Br^-}											
0.000	2375	654	353	169	143	106	93.6	79.1	71.6	58.4	50.2
.235	2300	618	331	147.4	129.6	99.3	85.9	71.4	64.9	53.1	45.1
.471	2176	547	295	136.1	120.1	(93.2)	80.6	67.3	61.2	50.6	42.7
.735	2049[c]	493	257	120	106.6	82.7	71.3	59.7	55.2	45.6	38.7
1.000	1930	406	215	114	100.8	75.5	67.7	55.6	50.5	42.1	36.6
					Iodide–Bromide[a]						
x_{I^-}											
0.000	1930	406	215	114	100.8	75.5	67.7	55.6	50.5	42.1	36.6
.194	1880	339	177.6	89.0	83.6	66.0	56.2	46.5	44.7	37.4	32.0
.416	1770	263	154.3	81.1	72.9	58.1	49.5	42.4	40.9	34.7	29.6
.689	1330	190.4	122.6	71.1	65.7	(52.9)	46.6	40.9	38.6	33.1	28.2
1.000	196	135.1	96.6	(62.3)	50.9	40.7	40.3	36.0	33.2	29.0	25.7
					Bromide–Fluoride[b]						
	0.00000	0.00157	0.00184	0.00306	0.00877	0.03395	0.04484	0.07438	0.09307	0.12332	0.14978
x_{Br^-}											
0.000	2823	1362	1221	931	598	265	225	165.1	145.0	122.5	..
.250	2745	1192	1060	783	488	217	180.9	138.4	118.6	99.8	..
.500	2561	1010	885	639	393	176.7	147.4	114.9	98.0	84.7	..
.750	2301	791	693	485	289	137.1	115.7	89.5	78.9	68.7	..
1.000	1697	514	443	309	186	100.3	87.5	68.0	61.7	51.4	..

[a] Preparation K, Table I. [b] Preparation L, Table I. [c] Value for $x_{Br^-} = 0.848$.

Table IV

Computation of Log $D_{Cl^-}^{Br^-}$ as a Function of Resinate Weight Normality in the Bromide–Chloride Ion Exchange ($\mu = 0.10$)

$$\log D_{Cl^-}^{Br^-} = P(\bar{v}_{Cl^-} - \bar{v}_{Br^-})/2.3RT - 55.51\, I_R + \log (\gamma^*_{Cl^-}/\gamma^*_{Br^-})_r - 2 \log (\gamma_{NaCl}/\gamma_{NaBr})_w$$

Weight normality, N_m	x_{Br^-}	−log a_w	$-55.51 I_R$	log $(\gamma^*_{Cl^-}/\gamma^*_{Br^-})_r$	$\bar{v}_w$ (ml.)	P (atm.)	$(\bar{v}_{Cl^-} - \bar{v}_{Br^-})$	$P\Delta\bar{v}/2.3RT$	log $D_{Cl^-}^{Br^-}$
	0.0	0.00156	0.0172	0.2780	18.068	2.0	−8.1	−0.0003	0.2975
1	0.5	.00101	.0220	.2420	18.068	−0.2	−8.1	.0000	.2664
	1.0	.00090	.0224	.1965	18.068	−0.9	−8.1	+ .0001	.2216
	0.0	.00560	.0561	.2780	18.066	14.6	−8.1	− .0021	.3346
2	0.5	.00374	.0652	.2420	18.066	8.4	−8.1	− .0012	.3086
	1.0	.00250	.0693	.1965	18.067	4.1	−8.1	− .0006	.2678
	0.0	.01109	.0972	.2780	18.062	31.7	−8.1	− .0046	.3732
3	0.5	.00785	.1093	.2420	18.063	21.2	−8.1	− .0031	.3508
	1.0	.00513	.1138	.1965	18.064	12.3	−8.1	− .0018	.3111
	0.0	.01775	.1362	.2780	18.056	52.5	−8.0	− .0075	.4093
4	0.5	.01279	.1452	.2420	18.059	36.6	−8.0	− .0052	.3846
	1.0	.00900	.1572	.1965	18.062	24.3	−8.0	− .0035	.3528
	0.0	.03457	.2093	.2780	18.040	105.1	−8.0	− .0149	.4750
6	0.5	.02516	.2050	.2420	18.045	75.3	−8.0	− .0107	.4389
	1.0	.01854	.2200	.1965	18.051	54.1	−8.0	− .0077	.4114
	0.0	.05606	.2772	.2780	18.018	172.5	−7.9	− .0242	.5336
8	0.5	.04084	.2527	.2420	18.027	124.3	−7.9	− .0174	.4799
	1.0	.03050	.2669	.1965	18.036	91.5	−7.9	− .0128	.4532
	0.0	.08223	.3384	.2780	17.992	254.6	−7.9	− .0357	.5833
10	0.5	.05984	.2961	.2420	18.006	183.9	−7.9	− .0258	.5149
	1.0	.04487	.3037	.1965	18.020	136.6	−7.9	− .0191	.4837
	0.0	.11307	.3971	.2780	17.962	351.9	−7.8	− .0487	.6290
12	0.5	.08216	.3351	.2420	17.983	254.1	−7.8	− .0352	.5445
	1.0	.06165	.3340	.1965	18.003	189.2	−7.8	− .0262	.5069

volume differences evaluated from density data on concentrated aqueous potassium and cesium halide solutions.[23] The agreement, especially for $N_m = 0$, was gratifying. In passing, it is noted that the volume differences were negative.

Calculations of the resin halide mean molal

TABLE V

COMPUTATION OF LOG $D_{Br^-I^-}$ AS A FUNCTION OF RESINATE WEIGHT NORMALITY IN THE IODIDE–BROMIDE ION EXCHANGE ($\mu = 0.10$)

$$\log D_{Br^-I^-} = P(\bar{v}_{Br^-} - \bar{v}_{I^-})/2.3RT - 55.51I_R + \log (\gamma^*_{Br^-}/\gamma^*_{I^-})_r - 2 \log (\gamma_{NaBr}/\gamma_{NaI})_w$$

Weight normality, N_m	x_{I^-}	$-\log a_w$	$-55.51I_R$	$\log (\gamma^*_{Br^-}/\gamma^*_{I^-})_r$	$\bar{v}_w$(ml.)	P(atm.)	$(\bar{v}_{Br^-} - \bar{v}_{I^-})$	$P\Delta\bar{v}/2.3RT$	$\log D_{Br^-I^-}$
	0.0	0.00090	0.0215	0.5441	18.067	−0.9	−12.4	+0.0002	0.5688
1	0.5	.00045	.0110	.5250	18.067	−1.6	−12.4	+ .0003	.5393
	1.0	.00000	....	.4983	18.068	−2.3	−12.4	+ .0005	.5018
	0.0	.00513	.0952	.5441	18.066	12.3	−12.3	− .0027	.6396
3	0.5	.00229	.0444	.5250	18.066	4.1	−12.3	− .0009	.5715
	1.0	.00000	....	.4983	18.067	−2.3	−12.3	+ .0005	.5018
	0.0	.01347	.1843	.5441	18.058	38.3	−12.3	− .0084	.7230
5	0.5	.00502	.0832	.5250	18.061	12.6	−12.3	− .0028	.6084
	1.0	.00000	....	.4983	18.064	−2.3	−12.3	+ .0005	.5018
	0.0	.02422	.2520	.5441	18.044	71.9	−12.3	− .0157	.7834
7	0.5	.01047	.1352	.5250	18.052	29.7	−12.3	− .0065	.6567
	1.0	.00262	.0312	.4983	18.059	5.9	−12.3	− .0013	.5312
	0.0	.03738	.3142	.5441	18.028	113.1	−12.2	− .0245	.8368
9	0.5	.01759	.1807	.5250	18.041	51.9	−12.2	− .0112	.6975
	1.0	.00487	.0518	.4983	18.054	12.9	−12.2	− .0028	.5503
	0.0	.05295	.3697	.5441	18.012	161.9	−12.2	− .0351	.8817
11	0.5	.02637	.2200	.5250	18.026	79.4	−12.2	− .0172	.7308
	1.0	.00899	.0778	.4983	18.040	25.8	−12.2	− .0056	.5735
	0.0	.07094	.4243	.5441	17.994	218.4	−12.2	− .0473	.9241
13	0.5	.03682	.2563	.5250	18.016	112.1	−12.2	− .0243	.7600
	1.0	.01500	.0969	.4983	18.038	44.6	−12.2	− .0097	.5885
	0.0	.09134	.4797	.5441	17.975	282.5	−12.1	− .0606	.9662
15	0.5	.04894	.2883	.5250	18.003	150.1	−12.1	− .0322	.7841
	1.0	.02288	.1140	.4983	18.030	69.2	−12.1	− .0149	.6004

TABLE VI

COMPUTATION OF LOG $D_{F^-Br^-}$ AS A FUNCTION OF RESINATE WEIGHT NORMALITY IN THE BROMIDE–FLUORIDE ION EXCHANGE ($\mu = 0.10$)

$$\log D_{F^-Br^-} = P(\bar{v}_{F^-} - \bar{v}_{Br^-})/2.3RT - 55.51I_R + \log (\gamma^*_{F^-}/\gamma^*_{Br^-})_r - 2 \log (\gamma_{NaF}/\gamma_{NaBr})_w$$

Weight normality, N_m	x_{Br^-}	$-\log a_w$	$-55.51I_R$	$\log (\gamma^*_{F^-}/\gamma^*_{Br^-})_r$	$\bar{v}_w$ (ml.)	P (atm.)	$(\bar{v}_{F^-} - \bar{v}_{Br^-})$	$P\Delta\bar{v}/2.3RT$	$\log D_{F^-Br^-}$
	0.0	0.00279	0.0821	0.9270	18.067	6.0	−27.2	−0.0029	1.0158
1	0.5	.00123	.0640	.8330	18.067	0.6	−27.2	− .0003	0.9063
	1.0	.00090	.0470	.6410	18.068	−0.9	−27.2	+ .0004	.6980
	0.0	.01066	.2510	.9270	18.060	30.5	−27.1	− .0146	1.1730
2	0.5	.00535	.1990	.8330	18.064	13.5	−27.1	− .0065	1.0351
	1.0	.00250	.1150	.6410	18.067	4.1	−27.1	− .0020	0.7636
	0.0	.02070	.4000	.9270	18.048	61.9	−27.0	− .0297	1.3069
3	0.5	.01069	.3090	.8330	18.055	30.1	−27.0	− .0144	1.1372
	1.0	.00513	.2045	.6410	18.064	12.3	−27.0	− .0059	0.8492
	0.0	.03292	.5310	.9270	18.032	100.1	−26.9	− .0478	1.4198
4	0.5	.01725	.4050	.8330	18.047	50.6	−26.9	− .0242	1.2234
	1.0	.00900	.2990	.6410	18.062	24.3	−29.9	− .0116	0.9380
	0.0	.04732	.6500	.9270	18.013	145.3	−26.8	− .0691	1.5175
5	0.5	.02503	.4930	.8330	18.036	75.0	−26.8	− .0357	1.2999
	1.0	.01347	.3835	.6410	18.058	38.3	−26.8	− .0182	1.0159
	0.0	.08266	.8640	.9270	17.964	256.5	−26.6	− .1211	1.6795
7	0.5	.04424	.6502	.8330	18.004	135.2	−26.6	− .0638	1.4290
	1.0	.02422	.5225	.6410	18.044	71.9	−26.6	− .0339	1.1392
	0.0	.12670	1.0630	.9270	17.901	396.0	−26.4	− .1856	1.8140
9	1.5	.06832	0.7920	.8330	17.965	211.0	−26.4	− .0989	1.5357
	1.0	.03738	.6345	.6410	18.028	113.1	−26.4	− .0530	1.2321
	0.0	.19143	....	.9270	17.830	602.2	−26.2	− .2801	....
11	0.5	.10397	.9420	.8330	17.921	323.7	−26.2	− .1505	1.6341
	1.0	.05295	.7325	.6410	18.012	161.9	−26.2	− .0753	1.3078

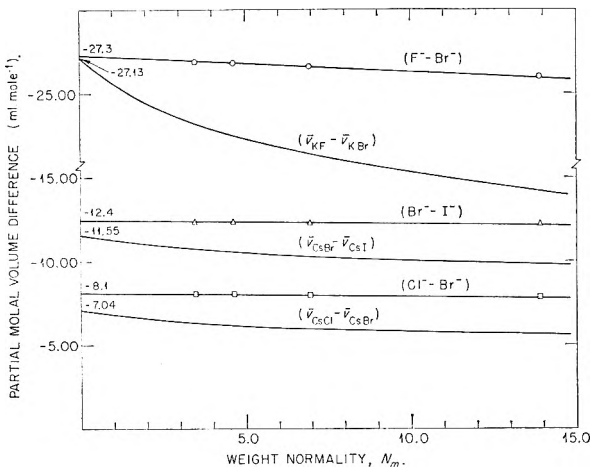

Fig. 4.—Variations of partial molal volume differences of resin halides with weight normality.

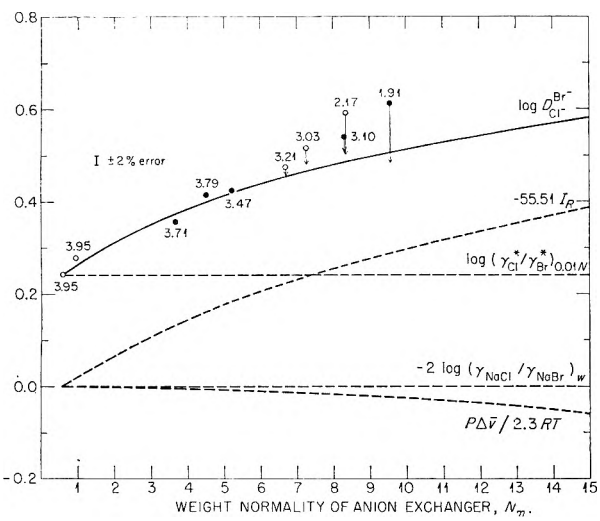

Fig. 5.—Summary of calculations and comparison with experiment for the bromide-chloride ion exchange at $x_{Br^-} = 0.5$. (Exchange capacity indicated adjacent to point for each preparation. Arrows show correction of selectivity coefficient value to that expected if capacity were 3.95 meq./g. Cl-form. Data plotted as filled circles are taken from ref. 25).

activity coefficient ratio, log $(\gamma_1/\gamma_2)_r$, according to eq. 5 require that eq. 8 be differentiated to find $(\partial x_w/\partial x_2)_{aw}$; then the variation of this coefficient must be integrated over a range of log a_w. This integration was performed analytically when a suitable empirical equation relating $(\partial x_w/\partial x_2)_{aw}$ and log a_w could be found by least squares methods; alternatively, the integral I_R was evaluated numerically or graphically when the empirical equations found by least squares could not be integrated analytically in terms of closed functions. Values of the integral were computed as a function of log a_w, the upper limit, and these were plotted to give a smooth $(0.05551I_R, -\log a_w)$ curve for $x_2 = 0.0$, 0.5 and 1.0, respectively. The values of $0.05551\ I_R$ listed in column four of Tables IV, V and VI were found by graphical interpolation from the $-\log a_w$ values estimated by eq. 9 for each N_m. The errors in the calculated I_R by the procedure outlined arise from the errors in b and c of eq. 8 and in α, β and γ of eq. 9.

(23) H. S. Harned and B. B. Owen, "The Physical Chemistry of Electrolyte Solutions," Reinhold Publ. Corp., New York. N. Y., 1959, 3rd Ed., p. 361.

Discussion

The Bromide–Chloride Ion-Exchange Equilibrium.—The computation of log $D_{Cl^-}^{Br^-}$ as a function (a) of equivalent fraction of bromide ion in the exchanger for constant N_m and (b) of N_m for constant x_{Br^-} is summarized in Table IV. Values of $0.05551I_R$ were computed for $x_{Br^-} = 0$ by integrating the equation

$$(\partial x_w/\partial x_2)_{aw} = 1/(4.801 + 324.9y - 742.0y^2) \quad (10a)$$

for $x_{Br^-} = 0.5$ by integrating the equation

$$(\partial x_w/\partial x_2)_{aw} = 1/(2.292 + 533.9y - 1680.1y^2) \quad (10b)$$

and for $x_{Br^-} = 1.0$ by numerical integration of the least squares equation

$$(\partial x_w/\partial x_2)_{aw} = 1/(1.461 + 629.5y^{1.044}) \quad (10c)$$

where $y \equiv -\log a_w$. The value of -2 log $(\gamma_{NaCl}/\gamma_{NaBr})_w$ for $\mu = 0.10$ was 0.0026 and independent of the composition of the mixed electrolyte (eq. 6).

The relatively large contribution of (log $\gamma^*_{Cl^-}/\gamma^*_{Br^-})_r$ and the relatively small contributions from $P(\bar{v}_{Cl^-} - \bar{v}_{Br^-})$ and log $(\gamma_{NaCl}/\gamma_{NaBr})_w^2$ terms to log $D_{Cl^-}^{Br^-}$ may be noted. The calculated selectivity coefficients are seen (Table IV) to increase with N_m and, hence, the exchanger cross-linking for constant x_{Br^-} and to remain constant within the errors involved or to decrease with increasing x_{Br^-} when N_m is held constant.

A comparison of the experimentally measured (Fig. 1) and the calculated values for log $D_{Cl^-}^{Br^-}$ at $x_{Br^-} = 0.5$ is afforded by Fig. 5. Agreement to within ± 2% is indicated to $N_m = 7$. The disagreement for the more highly crosslinked exchangers is considerably larger than the errors in either the selectivity coefficient measurements or in the calculations. It seems unlikely, since the experiments were performed with neutral aqueous electrolyte solutions, that the presence of a small number of weakly basic anion-exchange groups in the cross-linked preparations was the cause of the discrepancy. The fact that the more highly crosslinked exchangers possessed appreciably lower exchange capacities than the more weakly crosslinked preparations, especially than the nominal 0.5% DVB reference exchanger, is believed significant. The thermodynamic treatment assumes implicitly that the equivalent weight of the exchanger remains constant; yet between preparations K and A a twofold increase occurred (Table I).

Recent measurements of bromide–chloride ion-exchange selectivity coefficients for variable capacity Dowex-1 preparations have shown that $D_{Cl^-}^{Br^-}$ *increased* as the capacity diminished.[24] If the reported capacity dependence of $D_{Cl^-}^{Br^-}$ is employed to correct the values plotted in Fig. 5 to a constant equivalent weight of 253, a satisfactory agreement between the calculated and observed log $D_{Cl^-}^{Br^-}$ is obtained for the entire range of N_m.

It is important to note in Fig. 5 that the agreement between the log $D_{Cl^-}^{Br^-}$ for two independent

(24) S. Lindenbaum, C. F. Jumper and G. E. Boyd, *J. Phys. Chem.*, **63**, 1924 (1959).

series of cross-linked exchangers[25] is quite satisfactory when the values are plotted against N_m, but that a correlation cannot be made with the cross-linking as indicated by the nominal per cent. DVB in the preparations. Values of $D_{Cl^-}^{Br^-}$ have been published for only a few commercial type strong-base anion exchangers[26-28]; unfortunately, these cannot be plotted in Fig. 5 because the x_w values for the preparations have not been given.

The dependence of log $D_{Cl^-}^{Br^-}$ on x_{Br^-} for a given exchanger may be obtained from log $D_{Cl^-}^{Br^-}$, N_m curves for $x_{Br^-} = 0.0$, 0.5 and 1.0 using the measured weight swellings of the exchanger, and satisfactory agreement with the data in Fig. 1 may be demonstrated.

The Iodide–Bromide Ion-exchange Equilibrium.—The computations of the dependence of log $D_{Br^-}^{I^-}$ on ionic composition and exchanger cross-linking are summarized in Table V. Values for $0.05551I_R$ were computed for $x_{I^-} = 0.0$ by integrating the equation

$$(\partial x_w/\partial x_2)_{aw} = 1/(2.120 + 378.3y - 1846y^2) \quad (11a)$$

for $x_{I^-} = 0.5$ by integrating the equation

$$(\partial x_w/\partial x_2)_{aw} = 1/(2.317 + 475.2y - 1004y^2) \quad (11b)$$

and for $x_{I^-} = 1.0$ by graphical integration of the equation

$$(\partial x_w/\partial x_2)_{aw} = 1/(0.173 + 3600y^{1.097}) \quad (11c)$$

The value of -2 log $(\gamma_{NaBr}/\gamma_{NaI})_w$ for $\mu = 0.1$ was 0.0030 and independent of the composition of the mixed electrolyte (eq. 6).

It may be observed in Table V that the dominant contribution to the selectivity coefficient again comes from the activity coefficient ratio term for the exchanger, log $(\gamma_{Br^-}/\gamma_{I^-})_r$. A comparison of the experimental selectivity coefficient values taken from Fig. 2 for $x_{I^-} = 0.5$ with those calculated is given in Fig. 6, where a fair agreement appears to hold for exchanger weight normalities up to 10. Initially, log $D_{Br^-}^{I^-}$ increases rapidly with N_m and then more slowly and nearly linearly. The disagreement between the observed and calculated values for $N_m > 10$ is assumed to arise from the same cause as in the bromide–chloride anion-exchange equilibrium (*viz.*, to a "capacity" effect).

The Bromide–Fluoride Ion-exchange Equilibrium.—The calculations of log $D_{F^-}^{Br^-}$ for this system are summarized in Table VI. Values of $0.05551I_R$ were computed for $x_{Br^-} = 0.0$ by integrating the equation

$$(\partial x_w/\partial x_2)_{aw} = 1/(1.696 + 140.7y - 365.1y^2) \quad (12a)$$

for $x_{Br^-} = 0.5$ by numerically integrating

$$(\partial x_w/\partial x_2)_{aw} = 1/(0.769 + 77.72y^{0.759}) \quad (12b)$$

and for $x_{Br^-} = 1.0$ by integrating

$$(\partial x_w/\partial x_2)_{aw} = 1/(0.985 + 180.4y - 40.50y^2) \quad (12c)$$

The value of -2 log $(\gamma_{NaF}/\gamma_{NaBr})_w$ for $\mu = 0.10$ was 0.0096 and independent of the composition of the mixed electrolyte (eq. 6).

Large selectivity coefficients and a strong dependence of $D_{F^-}^{Br^-}$ on ionic composition were characteristic of this system (Fig. 3). The magnitude of the pressure–volume term, particularly for $x_{Br^-} = 0.0$, was large in comparison with the bromide–chloride and iodide–bromide ion exchanges; relative to the log $(\gamma_{F^-}/\gamma_{Br^-})_r$ term, however, it was unimportant. A comparison of the experimental with calculated selectivity coefficients for three values of the bromide ion equivalent fraction is afforded by Fig. 7. Excepting for preparation D (Table I), the agreement appears reasonably satisfactory in view of the experimental difficulties encountered.

A strong dependence of log $D_{F^-}^{Br^-}$ on N_m is indicated for $x_{Br^-} = 0.0$ while, for $x_{Br^-} = 1.0$ a much smaller variation is calculated. This behavior

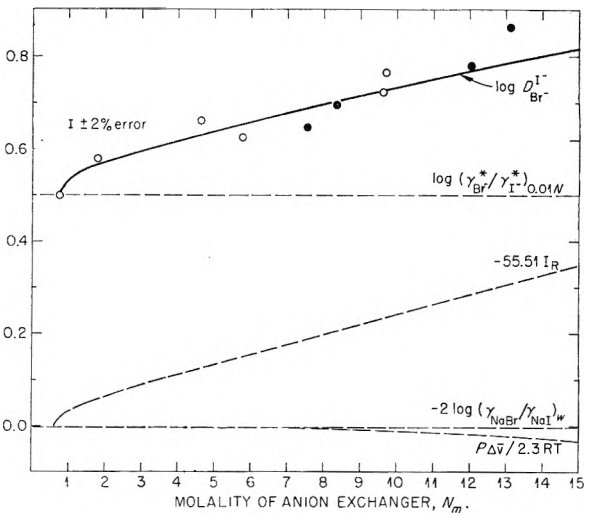

Fig. 6.—Summary of calculations and comparison with experiment for the iodide–bromide ion exchange at $x_{I^-} = 0.5$. (Values plotted with filled circles taken from ref. 25.)

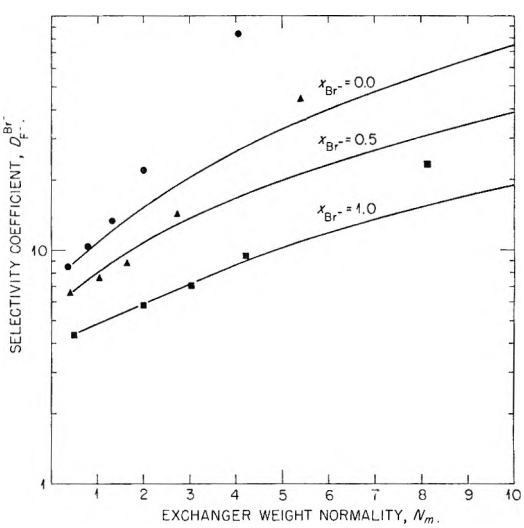

Fig. 7.—Summary of calculations and comparison with experiment for the bromide–fluoride ion exchange at $x_{Br^-} = 0.0$, 0.5 and 1.0. The log $D_{F^-}^{Br^-}$ values for the lowest N_m were obtained with preparation L in equilibrium with 0.01 *N* mixed aqueous NaCl + NaBr solution. These data do not appear in Fig. 3.

(25) Data for Series 1 from B. Soldano and D. Chesnut, *J. Am. Chem. Soc.*, **77**, 1334 (1955), *cf.* Table 1.

(26) R. Kunin and F. X. McCarthy, *Ind. Eng. Chem.*, **41**, 12 (1949).

(27) R. M. Wheaton and W. C. Bauman, *ibid.*, **43**, 1088 (1951).

(28) H. P. Gregor, J. Belle and R. A. Marcus, *J. Am. Chem. Soc.*, **77**, 2713 (1955).

gives rise to the observed (Fig. 3) strong dependence of the selectivity coefficient on the equivalent fraction of the bromide ion, particularly with the most highly cross-linked exchangers.

General Conclusions.—In the first place it is believed that the applicability of the Gibbs–Donnan equation (eq. 2) has been demonstrated by the concordance of the calculated and observed selectivity coefficient values reported in this paper. Thus, in Fig. 5 agreement of observation with theory was obtained when corrections were made to a uniform equivalent weight, and it seems reasonable to suppose the same would be true for Fig. 6 if the capacity dependence of $D_{Br^-}^{1^-}$ were known. Further, as may be shown from Tables IV, V and VI, the observed variation of the selectivity coefficients with the ionic composition of the exchanger (Figs. 1, 2 and 3) was obtained from the calculations. It becomes possible, therefore, to conclude that the nature of the cross-linking in an exchanger is not important so long as the equivalent weight remains practically constant.

The treatment given above has suggested also that the logarithm of the selectivity coefficient should be a smoothly increasing function of the resinate weight normality for constant exchanger "loading," and this has been verified. Accordingly, log D_1^2, N_m curves, which of course are empirical, may be used to predict selectivity coefficients for any changes which alter the weight swelling (*viz.*, cross-linking, ionic composition or external ionic strength within limits). In addition, these curves afford a basis hitherto lacking for comparing selectivity coefficient measurements by different investigators and, hence, are useful in reducing errors. The utility of the concept of exchanger weight normality as a means for the correlation of equilibrium selectivity coefficient data serves to direct attention to the general importance of weight swelling measurements on cross-linked ion exchangers. Convenient and reliable experimental methods for the estimation of equivalent water contents of exchangers in equilibrium with aqueous electrolyte mixtures are needed, and x_w values should be reported in experimental papers.

For the ion-exchange systems measured in this investigation the largest contribution to the selectivity coefficient value came from the term in eq. 2 which reflects the ionic interactions within the ion exchanger (*i.e.*, log $(\gamma_1/\gamma_2)_r$). The pressure–volume term was relatively much smaller. In fact, since $\Delta\bar{v}$ was negative in sign, swelling of the ion exchange polymer acted so as to reduce slightly the selectivity coefficient. A significant limitation of the calculation presented in this paper was the large value of the term log $(\gamma_1^*/\gamma_2^*)_r$ and, hence, its contribution to log $(\gamma_1/\gamma_2)_r$. This unexpected result was a consequence of the exceptionally high selectivity coefficients shown by very weakly cross-linked (*e.g.*, nominal 0.5% DVB) anion exchangers which served as reference points. Evidently, isopiestic vapor pressure experiments might better have been done on dilute solutions of linear polyelectrolyte of identical equivalent weight so that the integral, $0.05551I_R$, would have been a larger fraction of log $(\gamma_1/\gamma_2)_r$, eq. (5).

The large selectivity coefficients found with the most weakly cross-linked exchanger available suggests, however, that with anion exchangers based on structurally-bound benzyldimethylethanolammonium groups that ion binding must, in contrast with analogously linked cation exchangers, be quite strong. Support for this view appears in several types of data published on the behavior of several strong electrolyte halide salt solutions. Thus, measurements on the activity coefficient ratio for bromide and chloride ions in mixed aqueous KCl + KBr solutions[29] give for $N_m = 4.5$, $x_{Br^-} = 0.5$, log $(\gamma_{KCl}/\gamma_{KBr}) = -0.0162$. This value is much smaller than the value log $(\gamma_{R_4NCl}/\gamma_{R_4NBr}) = 0.161$, interpolated from Fig. 5, and this difference suggests that a considerably more specific interaction occurs with bromide and chloride ion and the quaternary ammonium ions of Dowex-2 than with potassium ion. Further, although activity coefficient measurements on aqueous tetramethylammonium iodide and tetraethylammonium iodide solutions have been performed only over a relatively narrow concentration range,[30] these are much smaller than the activity coefficients of the alkali metal iodides at comparable concentrations, again suggesting an increased ion association. Finally, measurements of the freezing point lowering conducted on dilute solutions of a series of tetra-*n*-alkyl-ammonium chlorides and iodides[31] may be cited where strong, specific interactions were evident.

The Gibbs–Donnan equation for the selectivity coefficients observed in ion-exchange equilibria promises to be of general usefulness in the future. From eq. 2 it is observed that if three terms are measured the fourth may be computed; thus, this equation affords a means for estimating log $(\gamma_1/\gamma_2)_r$ from selectivity coefficient measurements to which minor corrections for the pressure–volume and external aqueous electrolyte activity coefficient ratio have been made. Conversely, when log $(\gamma_1/\gamma_2)_r$ is known, either the pressure–volume or the aqueous activity coefficient ratio may be estimated. In the next paper, we shall demonstrate that eq. 2 also may be employed to estimate the effect of the ionic strength, μ, of the external electrolyte mixture on log D_1^2 through the influence of μ on the weight swelling of the exchanger.

(29) W. H. McCoy and W. E. Wallace, *J. Am. Chem. Soc.*, **78**, 1830 (1956).

(30) B. E. Conway, "Electrochemical Data," Elsevier Publishing Co., Amsterdam, 1952, pp. 89–90.

(31) J. Lange, *Z. physik Chem.*, **168A**, 147 (1934).

METHANE–OXYGEN FLAME STRUCTURE. III. CHARACTERISTIC PROFILES AND MATTER AND ENERGY CONSERVATION IN A ONE-TWENTIETH ATMOSPHERE FLAME[1]

BY R. M. FRISTROM, C. GRUNFELDER AND S. FAVIN

Applied Physics Laboratory, The Johns Hopkins University, Silver Spring, Maryland

Received July 21, 1960

A set of characteristic profiles is presented for an oxygen-diluted methane flame (premixed, flat and laminar) giving local temperature, aerodynamics and composition as functions of distance through the flame front. The description provided by these profiles is complete with the exception of the concentrations of the radical and atomic species which could not be determined by the techniques used. Their concentrations were assumed to be quantitatively negligible. The validity of a one-dimensional description for this flame was tested experimentally by checking the invariance of the measured profiles with radial distance in the burner, and by analyzing the deduced fluxes for material and energy conservation at a number of stations through the flame front. Agreement was considered satisfactory for quantitative study. To a reasonable approximation, the flame can be separated into three spatially distinct regions: a transport region, a methane reaction region and a carbon monoxide reaction region. The standard Lewis number assumption ($\rho C_p D/\lambda = 1$) used in many flame theories was tested with respect to the reactions of CH_4 and CO in this flame and found to provide a satisfactory first approximation.

Introduction

This paper is the third in a series of studies of physical processes and chemical kinetics in premixed, laminar methane–oxygen flame fronts. In the first two papers[2] (referred to hereafter as I and II) data were presented for a tenth atmosphere methane flame with excess oxygen (CH_4, 0.078; O_2, 0.919) together with a detailed analysis of the flux of matter and energy. The present paper, III, contains data and a similar analysis for a flame of the same composition but at one-twentieth atmosphere pressure. Comparisons between these two sets of data should allow conclusions to be drawn as to the reliability of the techniques and give an indication of the order of the dominant reactions in the flame. In the following paper,[3] IV, a discussion is given of chemical kinetics in these flames.

Experimental

The system under study was a flat flame supported on a circular screen burner.[4] The principal change from the one-tenth atmosphere system[2a] was the use of a larger burner and housing scaled to accommodate equal mass flows for the two flames. (The burner diameter was scaled up a factor of $\sqrt{2}$ from 3.15 to 4.44 cm.) Local aerodynamics were measured using the particle-track technique.[2a,5] Local temperature was determined using silica-coated Pt–Pt, 10% Rh thermocouples.[2a,6] The total diameter of thermocouple bead and coating was 0.004 cm. Local composition was measured using microprobe sampling techniques.[2a,7–9] A quartz probe with an orifice diameter of 0.003 cm. and a low pressure flow system were used for sampling. Flame gases were analyzed with a mass spectrometer (Consolidated Electrodynamics Corporation #21–620). The gases used were of high purity and analyzed by us prior to use (see Table I).

TABLE I

INITIAL AND FINAL STATES OF THE FLAME GASES

	Initial	Final (calcd.)	Final (expt.)
T(°K.)	400	1990	1980
V_s[a] (cm./sec.)	93.0	323.0	312.0
X_{CH_4}	0.0785	0	0
X_{O_2}	0.919	0.756	0.763
X_{Ar}	.00018	.00018	.00018
X_{N_2}	.00060	.00060	.00060
X_{H_2}	0	.00023	.0008
X_{OCH_2}	0	0	0
X_{CO}	0	0.00056	0.00305
X_{CO_2}	0.00147	.0792	.0788
X_{H_2O}	0.00038	.153	.154
X_H	0	.00011	....
X_{OH}	0	.00626	....
X_O	0	.00285	....
X_{NO}	0	.00042	....

[a] Evaluated at the screen surface where the temperature is 400°K.

Results

The results are presented in the form of profiles giving the intensive properties as a function of distance through the flame front (Figs. 1, 2). The

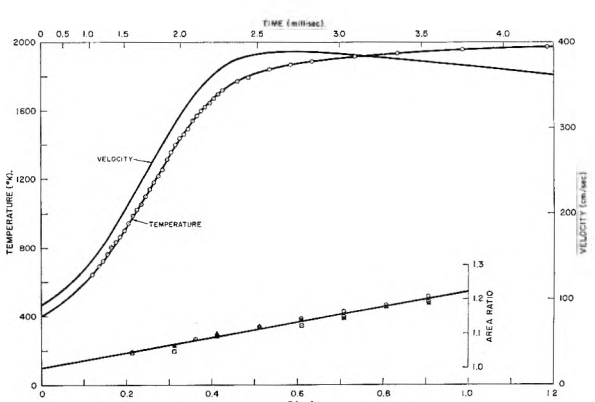

Fig. 1.—Temperature, velocity and area ratio profiles.

description given by these profiles which specify temperature, velocity and composition is complete except for the neglect of atom and free radical species concentrations which are presumed to be small. The validity of using a one-dimensional

(1) Work supported by the Bureau of Naval Weapons.

(2) (a) R. M. Fristrom, C. Grunfelder and S. Favin, *J. Phys. Chem.*, **64**, 1386 (1960); (b) A. A. Westenberg and R. M. Fristrom, *ibid.*, **64**, 1393 (1960).

(3) A. A. Westenberg and R. M. Fristrom, *ibid.*, **65**, 591 (1961).

(4) R. M. Fristrom and S. D. Raezer, Applied Physics Laboratory, The Johns Hopkins University Report CM-912 (1956).

(5) R. M. Fristrom, R. Prescott, W. H. Avery and J. Mattuck, *J. Chem. Phys.*, **22**, 106 (1954).

(6) R. Friedman, "Fourth Symposium on Combustion," The Williams & Wilkins Co., Baltimore, Md., 1953, p. 259.

(7) R. Prescott, S. Foner, R. Hudson and W. H. Avery, *J. Chem. Phys.*, **22**, 145 (1954).

(8) R. M. Fristrom, R. Prescott, W. H. Avery and C. Grunfelder, *Combustion and Flame*, **1**, 102 (1957).

(9) R. M. Fristrom, W. H. Avery and C. Grunfelder, "Seventh Symposium on Combustion," Butterworths, London, 1959, p. 304.

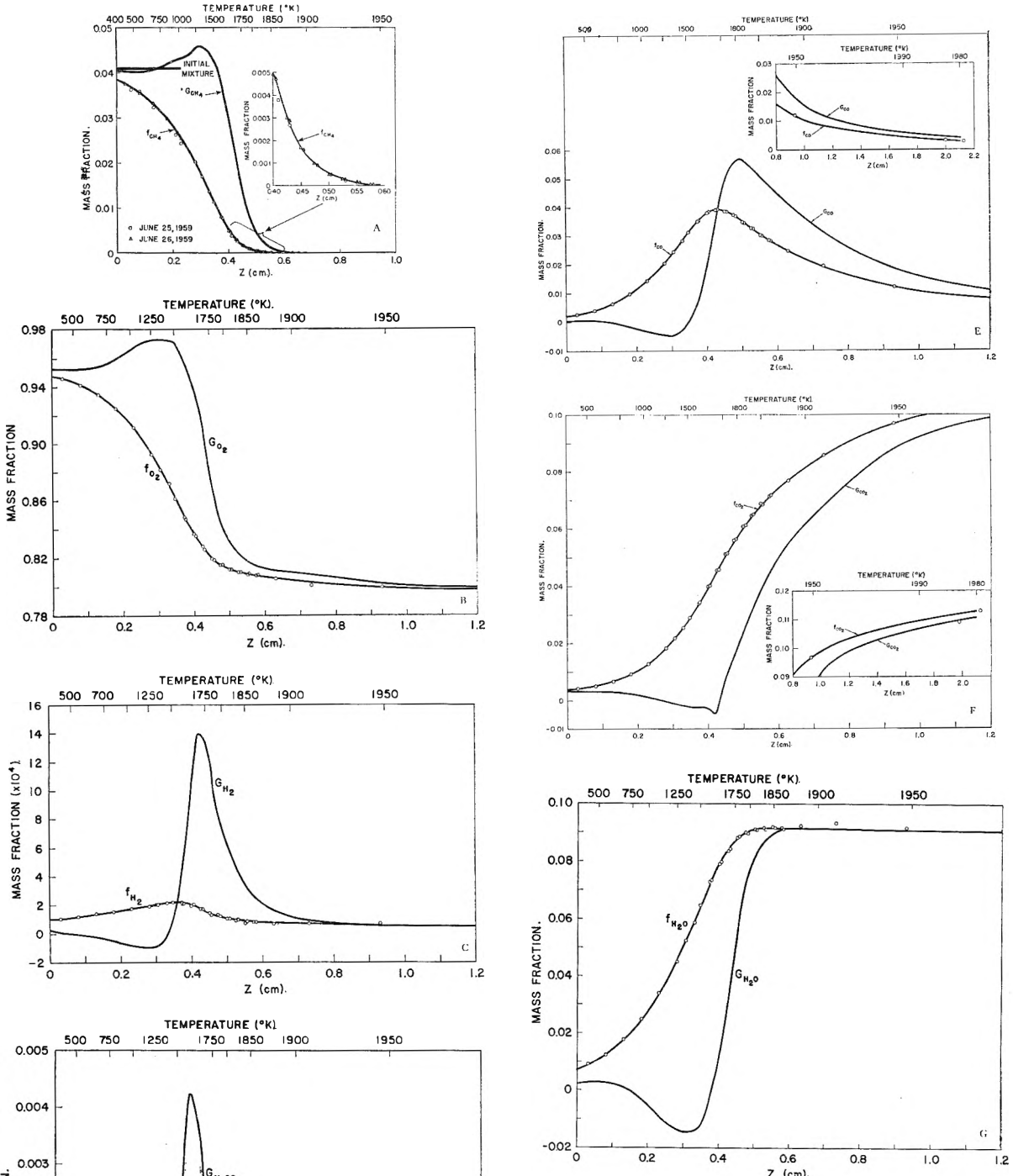

Fig. 2.—Composition and flux profiles. Mass fraction f_i and fractional mass flux G_i *vs.* distance z (cm.), and temperature (°K.): A, methane, CH_4; points are given for two successive runs to show reproducibility; B, oxygen, O_2; C, hydrogen, H_2; D, formaldehyde, H_2CO; E, carbon monoxide, CO; F, carbon dioxide, CO_2; G, water, H_2O.

description for this flame was checked experimentally by measuring profiles both on and off the axis. As in previous studies of flames of this type,[2a,5,8,9] there was no significant variation in profiles in the central region (±2 cm. from the axis) and a one-dimensional model was considered satisfactory for quantitative work.

Duplicate runs were found to be in substantial agreement (for example see Fig. 2A). The results of the most complete set of runs are presented, together with the analysis of the individual species

fluxes.[2b,10] Using eq. 1, these fluxes were calculated from the composition curves and measured temperatures using the diffusion coefficient data of Walker and Westenberg.[11]

$$G_i = f_i(v + V_i)/v;\ V_i = -(D_i/X_i)(dX_i/dz) \quad (1)[12]$$

To provide an estimate of the reliability of the data and the applicability of the one-dimensional model, the fluxes were also analyzed for conservation of the atomic fluxes. The flux of each atomic species as determined using eq. 2 should have been individually conserved at every point in the flame, provided the data were satisfactory and the interpretation valid.

$$\sum_i n_i G_i/M_i = \text{constant} \quad (2)$$

TABLE II

DEFINITION OF SYMBOLS

A	Stream tube area ratio
C_p	Heat capacity at constant pressure (cal./°K./g.)
D_i	Binary diffusion coefficient of species i with oxygen (cm.²/sec.)
f	Subscript indicating final conditions
F	Fractional molar flux
f_i	Mass fraction of species i
G_i	Fraction of total mass flow rate due to species i
H_i	Molar enthalpy of species i (cal./mole)
$\hat{H}$	Specific enthalpy of mixture (cal./g.)
M_i	Molecular weight of species i
n_i	No. of atoms of an element in a molecule of species i
N_i	Concn. of species i (moles/cm.³)
o	Subscript indicating initial conditions
T	Temperature (°K.)
v	Mass average velocity (cm./sec.)
V_i	Diffusion velocity of species i (cm./sec.)
X_i	Mole fraction of species i
z	Distance (cm.)
θ	Fractional temp. rise, $(T - T_0)/(T_f - T_0)$
λ	Thermal conductivity (cal./cm./sec./°K.)
ρ	Density (g./cm.³)

The energy fluxes through the flame were calculated from the data using eq. 3

$$\rho_0 v_0 \hat{H} - A\lambda(dT/dz) + A\sum_i N_i H_i V_i = \rho_0 v_0 \hat{H}_0 = \text{constant} \quad (3)$$

They were separated into contributions from convection, conduction and diffusion. Conservation of energy dictates that the sum of these three contributions should be constant and equal to the initial enthalpy flux of the flame gases.

Discussion of Results

The precision of these data was somewhat better than that obtained in the one-tenth atmosphere study.[2a] This was expected to be the case since the one-twentieth atmosphere flame was twice as thick as the one-tenth atmosphere flame and better spatial resolution and derivatives should have been obtained. An exception to this was the particle-track measurements. Here, difficulty was experienced in the region of acceleration and errors from lag were appreciably higher than in the one-tenth atmosphere study. Satisfactory area profiles and final velocity measurements were obtained however, and since these were the only aerodynamic parameters used in the analysis,[13] the problem was not pursued. The difficulty may have been associated with using particles small compared with the mean free path with the resulting reduction in drag coefficient.

Analysis of the flux of the individual atomic species (C, H, O) indicated satisfactory conservation of matter for each of these fluxes individually. This must be the case in flames since no nuclear reactions are involved. For the flux of hydrogen, the average deviation was 2.5% and the maximum deviation −7% while for carbon the average deviation was 2.2% and the maximum deviation was +10%. The results for oxygen were an order of magnitude better but this was not considered significant because of the large excess of oxygen and the small change in its concentration. These conservation considerations provide a reasonable test of the data since they involve not only all of the thermal, aerodynamic and composition data, but also the first spatial derivative of the composition data and the various diffusion coefficients.

Analysis of the flux of energy in this flame was less satisfactory but still within the limits of experimental error dictated by our lack of knowledge of the concentrations of the very energetic free radical species and the thermal conductivities of the high temperature gas mixtures. The energy flux curves were essentially the same as found with the one-tenth atmosphere flame[2b] provided the distance is scaled according to inverse pressure. The dominant fluxes are due to thermal conduction and molecular diffusion; over much of the flame they are large compared with the initial enthalpy flux.

The energy fluxes due to thermal conduction and molecular diffusion are of opposite signs and magnitude throughout most of this flame. This approximate balance suggests that this flame might be represented by a model in which the effective Lewis number $\rho C_p D/\lambda$ is unity. In such a flame the thermal and concentration fields are similar and the number of differential equations considered for the flames can be reduced.[14] As Hirschfelder pointed out,[15] this can only be the case if the Lewis numbers of all of the species are separately equal to unity but, as mentioned by Klein,[16] a good first approximation should be provided if a fuel can be defined whose disappearance is directly connected with the heat release and whose effective Lewis number is unity. Under these conditions, there should be a linear relationship between fuel disappearance and temperature rise. In this flame, methane and carbon monoxide can be considered as fuels in their respective spatial regions. Despite the fact that

(10) R. M. Fristrom and A. A. Westenberg, *Combustion and Flame*, **1**, 217 (1957).

(11) R. E. Walker and A. A. Westenberg, *J. Chem. Phys.*, **32**, 436 (1960).

(12) See Table II for definition of symbols.

(13) For the analysis, the velocities of Fig. 1 were deduced from the temperature and composition data using the equation: $v = (\rho_0 v_0 RT)/(AP\bar{M})$ which is derived from the continuity equation and ideal gas law.

(14) J. O. Hirschfelder, C. F. Curtiss and R. B. Bird, "Molecular Theory of Gases and Liquids," John Wiley and Sons, Inc., New York, N. Y., 1954.

(15) J. O. Hirschfelder, *Phys. Fluids*, **3**, 109 (1960).

(16) G. Klein, *Phil. Trans. Roy. Soc.*, **A249**, 389 (1957).

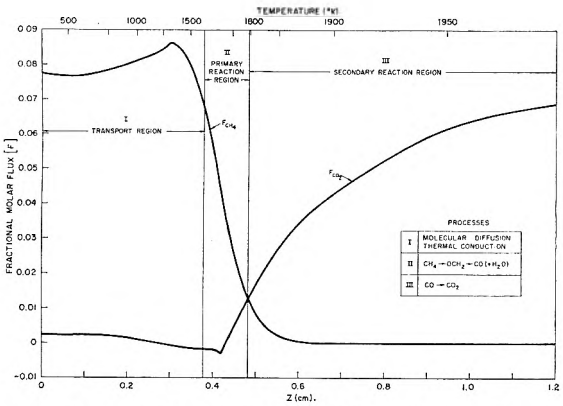

Fig. 3.—Spatial separation in the methane flame: F_{CH_4} and F_{CO_2} *vs.* distance.

their Lewis numbers are not always close to unity, ($N_{Le}(CH_4)$ = 1–1.25; $N_{Le}(CO)$ = 1–1.1), the unity Lewis number approximation appears to be a reasonable one, as was the case for the one-tenth atmosphere flame.[2b]

It is interesting to note that this flame can be conveniently divided into three spatially distinct regions (Fig. 3). In the first region, no reactions occur despite major changes in concentration and temperature due to the transport processes of thermal conduction and molecular diffusion. In the second region, the methane is attacked and converted to water and carbon monoxide. In the third region, the carbon monoxide reacts. This division is not, of course, absolute, but it is sufficiently sharp to provide a convenient description of the flame. This behavior is similar to that of the one-tenth atmosphere flame.[2b] If the division is determined by taking the point at which the methane flux was equal to the carbon dioxide flux, the assigned temperature in this flame was within 25°K. of that found for the one-tenth atmosphere flame. Spatial separation occurs because of the difference between the relative rates of reaction of methane and carbon monoxide and is characteristic of many hydrocarbon flames. These questions are discussed in detail in the following paper.[3]

The principal limitation of these data is our present inability to measure the concentrations of atomic and radical species. These concentrations are of the order of a few tenths of a per cent. or less in the equilibrium burned gases (see Table I) and probably of the order of 1% in the reaction zone. Thus the contribution of recombined radicals to the major stable species which are measured will be minor although probably not negligible. It might be possible to assign certain peculiarities in the flux curves such as the initial negative flux of water to this source of error. In the case of the trace species the problem is more serious since their concentrations are of the same order as that expected for radical species. For example, it would be possible to interpret the observed hydrogen as due in part to recombined hydrogen atoms and the formaldehyde to methyl radical. In the absence of other information, we prefer to take the observed species curves at face value, but the alternative interpretation cannot be excluded at present. Beyond the effects of the data, the lack of radical concentration information is unfortunate because most of the reactions which we believe to be important in this flame[3] involve radical or atomic species. The effect of uncertainty in radical concentrations on the energy fluxes is also serious since they are high energy species, and the observed deviations from energy conservation probably are due to this source.

Since it is not safe to apply the steady-state approximation in flame systems,[17] the problem is an experimental one. Techniques for making such measurements directly are under development[18–20] and it is hoped that this information eventually will be available for this system thus allowing a complete analysis to be made.

Acknowledgment.—The authors wish to thank Dr. W. H. Avery for his interest and encouragement in this work, and Dr. A. A. Westenberg for many helpful discussions.

(17) E. S. Campbell, J. O. Hirschfelder and L. M. Schalit, "Seventh Symposium (International) on Combustion," Butterworths, London, 1959, p. 332–38.

(18) C. J. James and T. M. Sugden, *Proc. Roy. Soc. (London)*, **A227**, 312 (1955).

(19) W. E. Kaskan, *Combustion and Flame*, **2**, 229 (1958).

(20) T. Grewer and H. Gg. Wagner, *Z. physik Chem. (Frankfort)*, **20**, 371 (1959).

METHANE-OXYGEN FLAME STRUCTURE. IV. CHEMICAL KINETIC CONSIDERATIONS

BY A. A. WESTENBERG AND R. M. FRISTROM

Applied Physics Laboratory, The Johns Hopkins University, Silver Spring, Maryland

Received July 21, 1960

Experimental data on temperature, composition and aerodynamic profiles in the reaction zone of oxygen–diluted methane flames (premixed, flat and laminar) at pressures of 1/10 and 1/20 atm. which have been given in previous papers of this series are discussed in terms of the chemical kinetics of the flame reactions. It is shown that the profiles of net reaction rates for the stable species as determined from the data are internally consistent, and that the data at the two pressures indicate the predominance of bimolecular processes. The results of an exhaustive study of the possible elementary reactions which might occur are given, and a reaction mechanism proposed which accounts most simply for the observations. It is shown conclusively that the primary mechanism of CH_4 disappearance cannot be by direct O_2 attack (as in low temperature studies), but must be mainly by reaction with OH (and possibly O). The appearance of CO_2 is attributed solely to the CO + OH → CO_2 + H reaction, and by combining the present data with those of other workers a reasonable value for the rate constant is obtained. It is then possible to compute a profile of OH radical concentration, which exhibits a moderate non-equilibrium maximum in the fast reaction zone. The OH profile also enables a reasonable estimate of the rate constant for the reaction $CH_4 + OH \rightarrow CH_3 + H_2O$ to be made. Finally, the question of over-all kinetics for the CO reaction is discussed. It is shown that, if the assumption is made that the OH concentration near the hot boundary is determined by its equilibrium with O_2, H_2O and O, an over-all expression for the appearance rate of CO_2 can be written which leads to significant agreement between the present work and that of several other authors.

Introduction

Previous papers[1-3] (referred to as I, II and III) in this series have reported various aspects of the study of laminar flame structure in a premixed methane–oxygen system. Paper I described the experimental techniques used, and presented a set of data on profiles of temperature, composition and aerodynamics measured in a flat flame at one-tenth atm. pressure and of initial composition (mole fractions) $X_{CH_4} = 0.078$, $X_{O_2} = 0.914$. Paper II covered the application of molecular transport properties to these data and examined them in terms of conservation of matter and energy. Paper III contained the data and similar analysis for a flame of the same mixture burning at a pressure of one-twentieth atm. In the present paper, the structure data for both flames are considered from the point of view of chemical kinetics.

Determination of Net Reaction Rates.—The original experimental data consisted of a set of profiles of temperature T, mass average gas velocity v, and mole fraction X_i of all the chemical species (excluding free radicals and atoms) as functions of the distance z through the flame zone. After appropriate correction for molecular diffusion (*i.e.*, determining profiles of diffusion velocity V_i for each species) the flux variables G_i defined by

$$G_i = f_i(v + V_i)/v \qquad (1)$$

were computed[2] (f_i is mass fraction of species i). G_i represents the fraction of the total mass flux at any point in the flame due to species i. It may then be shown[4] that the equation of continuity for species i can be written in terms of G_i as

$$K_i = (\rho v/M_i)(dG_i/dz) \qquad (2)$$

where ρ is density, M_i is molecular weight, and K_i is the net rate of appearance (positive) or disappearance (negative) of i per unit volume per unit time due to chemical reaction. In the usual c.g.s. units, K_i has dimensions of moles cm.$^{-3}$ sec.$^{-1}$. A profile of this rate variable was computed for each species by numerically differentiating the G_i curve and using the appropriate profiles of ρ and v. (The product ρv is not constant in a real flat flame because of lateral expansion of stream-tubes.[2]) These rate profiles for both the 1/10 and 1/20 atm. flames are given in Figs. 1 and 2.

These K_i profiles are interesting in a qualitative sense. It will be noted that the flames can be divided conveniently into three zones. The first, extending from the screen ($z = 0$) to about $z = 0.2$ cm. and $z = 0.3$ cm. in the two flames, respectively, is a region where all changes in composition and temperature are due simply to molecular transport processes. In neither flame is there any appreciable chemical reaction until a temperature of about 1300°K. is reached. Then the second zone, in the approximate ranges $z = 0.2$–0.3 cm. and $z = 0.3$–0.6 cm. of Figs. 1 and 2, is the region where the fast reactions occur. The CH_4 disappears with the formation of most of the H_2O and H_2. Finally, the third zone, where CO is converted slowly to CO_2, extends out to the hot boundary.

It should be kept in mind that the determination of the V_i requires a differentiation of the experimental composition profile, so that obtaining the rate variables K_i really involves a double differentiation of the experimental data. This is an obvious source of error in a study of this kind. Since the gas velocity v and the diffusion velocity V_i generally are of about equal importance in determining G_i over most of the flame zone, the quantity dG_i/dz does not bring in a direct double differentiation of the composition profiles. (At some points the V_i are greater than v, however.) Still, the process might be expected to reduce the precision of the composition profiles (estimated to be several per cent.) by a factor of four or so. This, of course, is a source of error resulting purely from data manipulation and has nothing to do with other experimental errors. The latter have been discussed.[1]

There are certain procedures which may be used

(1) R. M. Fristrom, C. Grunfelder and S. Favin, *J. Phys. Chem.*, **64**, 1386 (1960).

(2) A. A. Westenberg and R. M. Fristrom, *ibid.*, **64**, 1393 (1960).

(3) R. M. Fristrom, C. Grunfelder and S. Favin, *ibid.*, **65**, 587 (1961).

(4) J. O. Hirschfelder, C. F. Curtiss and R. B. Bird, "The Molecular Theory of Gases and Liquids," John Wiley and Sons, New York, N. Y., 1954, p. 748.

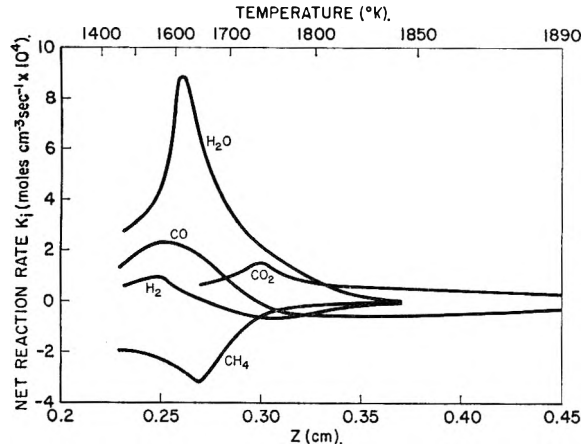

Fig. 1.—Net reaction rates of major species in CH_4–O_2 flame at 1/10 atm. pressure. K_{CO} and K_{CO_2} actually extend to $z = 0.85$ cm. (K_{H_2CO} too small to be shown.)

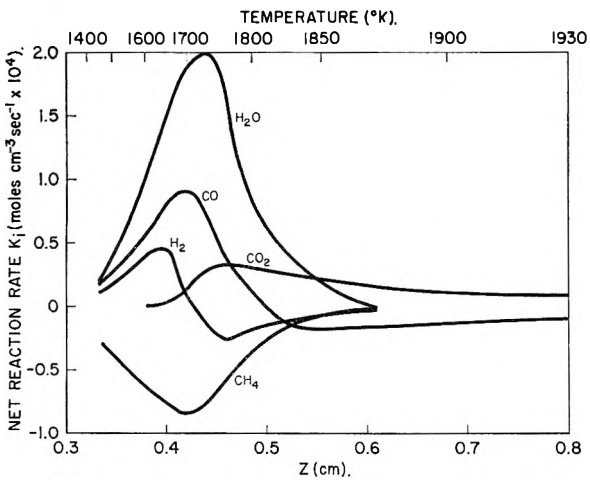

Fig. 2.—Net reaction rates of major species in CH_4–O_2 flame at 1/20 atm. pressure. K_{CO} and K_{CO_2} actually extend to $z = 1.7$ cm. (K_{H_2CO} too small to be shown.)

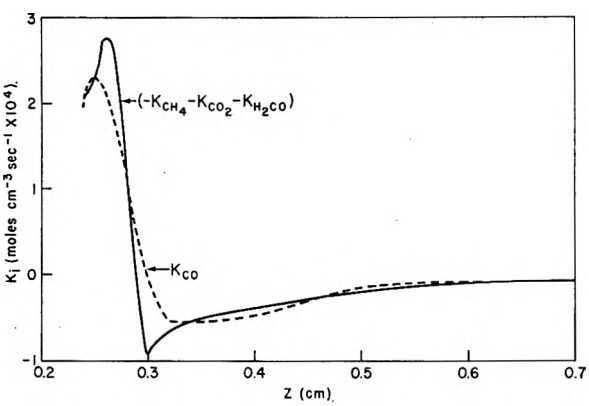

Fig. 3.—Comparison of K_{CO} with combined rate ($-K_{CH_4} - K_{CO_2} - K_{H_2CO}$) in 1/10 atm. flame.

to check the rates derived in this way. These make use of the requirement that matter be conserved in the flame reactions. This fact was invoked in paper II to check the composition profiles and the data analysis, and it is also useful in checking the manipulations necessary to obtain K_i. If n_i is the number of atoms of a particular element in a molecule of species i, conservation of matter requires that

$$\sum_i n_i K_i = 0 \qquad (3)$$

Applying this condition to carbon gives

$$K_{CO} = -K_{CH_4} - K_{CO_2} - K_{H_2CO} \qquad (4)$$

if the contributions of carbon-containing free radicals are assumed to be negligible. Similarly, for hydrogen we have

$$K_{H_2O} = -2K_{CH_4} - K_{H_2} - K_{H_2CO} \qquad (5)$$

Since the diffusion velocity for O_2—and hence the G_{O_2} and K_{O_2}—was not determined independently, a rate balance for oxygen was not carried out. Figures 3 and 4 show the comparison of the quantities on either side of eq. 4 for both flames, while Figs. 5 and 6 show similar comparisons according to eq. 5. In general, the two curves in each case are qualitatively similar, and in fairly good quantitative agreement—especially in the region beyond the fast reaction zone for the carbon case where the slow conversion of CO to CO_2 is the only reaction of importance. These checks for the one-twentieth atm. flame are somewhat better than for the one-tenth atm. flame, as might be expected since the work is easier at lower pressure. Discrepancies undoubtedly are the result of neglect of radical contributions as well as experimental errors.

Reaction Mechanism.—Before discussing details of the mechanism, some significant clues as to the nature of the flame kinetics may be obtained by comparing the structural data at the two pressures. It can be shown theoretically[5] that, if all the reactions involved in a flame are of order α, all distances should scale proportional to $P^{-\alpha/2}$, where P is pressure. Thus if most of the important reactions are second order, as seems likely, the distance coördinate should be proportional to P^{-1}. In the present case, the two flames were studied at pressures differing by a factor of two, so that a given profile in the 1/10 atm. flame should be compared with its counterpart in the 1/20 atm. flame plotted with its distance coördinate halved. Such a comparison is shown in Fig. 7 for the two temperature profiles, and in Fig. 8 for the concentration profiles of one of the species, X_{H_2O}. The circled points are the direct experimental data for the 1/10 atm. flame and the triangles are the 1/20 atm. data plotted against $z/2$. (The latter were translated downstream $\approx$ 0.04 cm. after halving to show the congruence better.) The similarity of the curves in each case is striking, and this provides support for the postulate of the flame reactions being predominantly second order (*i.e.*, bimolecular).

Additional proof of this point is provided by comparing the rate profiles at the two pressures. Consider the case of K_{H_2O}. If we assume that the net rate of water formation at any point is by way of bimolecular steps, we can write

$$K_{H_2O} = (P/RT)^2 \sum_J k_J (X_i X_k)_J \qquad (6)$$

where k_J is the rate constant of the Jth reaction involved in H_2O formation (or destruction—negative k_J), and $(X_iX_k)_J$ denotes the mole fraction product of whatever species enter into the Jth

(5) See work cited in ref. 4, p. 765.

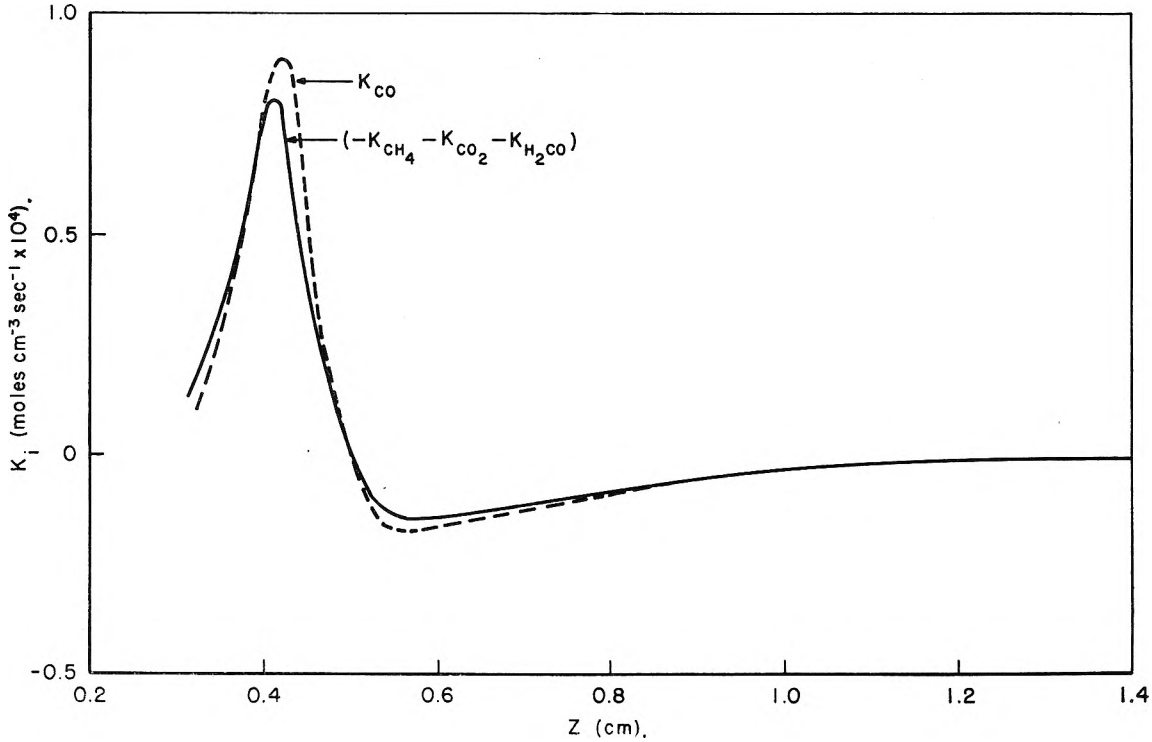

Fig. 4.—Comparison of K_{CO} with combined rate $(-K_{CH_4} - K_{CO_2} - K_{H_2CO})$ in 1/20 atm. flame.

reaction. It is apparent from this equation that, in comparing flames at different pressures, if the temperature and mole fraction profiles are congruent when plotted on the proper distance scales, then the rate profiles should be congruent keeping in mind that $K_i \propto P^2$. Figure 9 shows K_{H_2O} treated in this way. Solid curves A and B are the rate profiles for the 1/10 and 1/20 atm. flames plotted against z and $z/2$, respectively. The dashed curve C is curve B with its ordinate multiplied by four to account for the pressure effect on K_{H_2O}. The comparisons for other K_i profiles show similar congruence when plotted on a P^2 basis.

The mechanism of reaction in the methane–oxygen system has been investigated many times by different techniques and under varying conditions. Many of these results and speculations have been summarized by Lewis and von Elbe,[6] Semenov,[7] and others. Most of this work was done at considerably lower temperatures than in the flames considered here, and under conditions where wall effects were likely to be of importance. Recently, Fenimore and Jones[8] have reported some results of structure studies of flames containing CH_4 and O_2 (among others) which have points of similarity to the present work. We have proceeded, first, by examining anew all the likely elementary bimolecular reactions involving simple species which might occur in the flames under consideration. These have then been boiled down to the simplest set which seems to "explain" most of the observations.

(6) B. Lewis and G. von Elbe, "Combustion, Flames and Explosions of Gases," Academic Press, New York, N. Y., 1951, Chap. IV.

(7) N. N. Semenov, "Some Problems in Chemical Kinetics and Reactivity," Princeton University Press, Princeton, N. J., 1958, Vol. II, Chap. XII.

(8) C. P. Fenimore and G. W. Jones, *J. Phys. Chem.*, **63**, 1834 (1959).

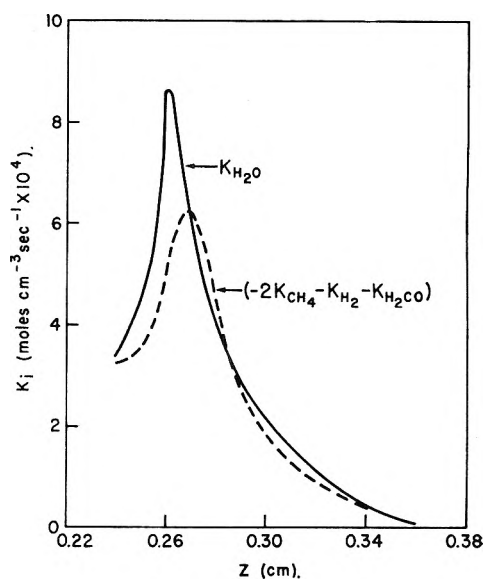

Fig. 5.—Comparison of K_{H_2O} with combined rate $(-2K_{CH_4} - K_{H_2} - K_{H_2CO})$ in 1/10 atm. flame.

Methane Disappearance.—

$$CH_4 + O_2 \longrightarrow CH_3 + HO_2$$

This is a reaction commonly postulated in the low temperature oxidation of methane.[7] However, in the present case it may be shown easily that such a direct oxygen attack cannot be of importance in the disappearance of methane. The above reaction is endothermic by about 55 kcal./mole. Using this as the minimum possible activation energy (a value which has been confirmed by shock tube experiments[9]), and a maximum collision theory frequency

(9) G. B. Skinner and R. Ruehrwein, *ibid.*, **63**, 1736 (1959).

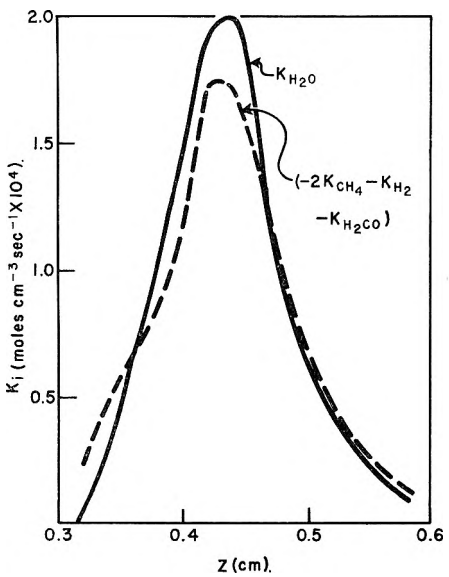

Fig. 6.—Comparison of K_{H_2O} with combined rate ($-2K_{CH_4} - K_{H_2} - K_{H_2CO}$) in 1/20 atm. flame.

factor of 10^{14} cm.^{3} mole^{-1} sec.$^{-1}$, the disappearance rate of CH_4 would be

$$K_{CH_4} = -10^{14} e^{-56000/RT} [CH_4][O_2]$$

where $[CH_4]$ denotes the methane concentration in mole cm.$^{-3}$, etc. The actual data from the 1/10 atm. flame at the point where $T = 1600°K.$, for example, give a value of $K_{CH_4} \approx 10^{-8}$ when this equation is used, while the experimental value of K_{CH_4} at this point is 2.7×10^{-4}. Thus the maximum possible rate predicted on the basis of this reaction is too low by a factor of the order of 10^{-4} compared to the experimental rate, so the direct reaction of CH_4 and O_2 cannot be important in this flame. Since the direct reaction would presumably be one of the major sources of any HO_2 in the flame, its elimination also provides a strong reason for not considering this radical in the flame mechanism.

$$CH_4 + OH \longrightarrow CH_3 + H_2O$$

This reaction is exothermic by 17.5 kcal./mole and has an estimated[10] activation energy $E \approx 8.5$. It is the likely main reaction in CH_4 disappearance under these flame conditions, as will be discussed more fully later.

$$CH_4 + H \longrightarrow CH_3 + H_2$$

Energetically this step is feasible, since it is slightly exothermic and has $E \approx 6$–13 depending on the steric factor assumption.[11] It seems likely, however, that in view of the large excess of O_2 present the H concentration would be very low compared to that of OH (the calculated mole fraction ratios X_{OH}/X_H in the final burned gas are about 70 and 60 for the 1/10 atm. and 1/20 atm. flames, respectively), so that this reaction can be neglected as far as CH_4 disappearance is concerned. Further support for this neglect is the fact that very low H_2 concentrations were observed in these flames. This was not the case in the propane–air flame previous studied.[12]

$$CH_4 + O \longrightarrow CH_3 + OH$$

There is less known about this reaction than the others. It is probable that the activation energy is low and similar to that of the foregoing reactions (Steacie[11] quotes one estimate of $E \approx 8$). The O concentration at the hot boundary is approximately half that of OH for both flames, so it would appear that this reaction should be included.

Intermediate Formation.—The stable intermediates included here are CO, H_2 and H_2CO. The latter two are present at such low concentrations—nowhere greater than about 0.3 mole %—that it is hardly necessary to account for them quantitatively, and it is possible that they may partially represent radical recombination products. But it is of interest to see how they might enter into the general scheme of things.

A likely possibility is the step frequently invoked[6,7] wherein a peroxide is formed

$$CH_3 + O_2 \longrightarrow H_3COO$$

with essentially zero activation energy and a frequency factor of about 10^{11} cm.^{3} mole^{-1} sec.$^{-1}$. This could then be followed by

$$H_3COO \longrightarrow H_2CO + OH$$

Semenov[7] suggests that the second step actually involves isomerization (to H_2COOH) and then decomposition. Such an isomerization probably involves a fairly large activation energy, but since it is a unimolecular process its over-all *rate* will always be much faster than a bimolecular process such as is involved in the peroxide formation. However, if the C–O–O bond angle is about 90°, as is normal for such compounds, the terminal O atom would lie close to an H atom and isomerization might be unnecessary. In any case, the above two steps can be combined into one effective reaction

$$CH_3 + O_2 \longrightarrow H_2CO + OH$$

with $E \approx 0$ and $k \approx 10$.[11] The low value of k implies a steric factor of about 10^{-3}, which is not unreasonable in this case. No other plausible mechanism of H_2CO formation is apparent to us.

$$H_2CO + M \longrightarrow H_2 + CO + M$$

where M is any particle. This reaction is thermally neutral but seems improbable on steric grounds.

$$H_2CO + M \longrightarrow HCO + H + M$$

This reaction is so endothermic ($\approx$ 78 kcal./mole) as to be dismissed easily from consideration.

$$H_2CO + OH \longrightarrow HCO + H_2O$$

This is frequently postulated in hydrocarbon and formaldehyde oxidation mechanisms and seems plausible. It is exothermic by 40 kcal./mole and undoubtedly has very low activation energy. Since so little H_2CO accumulates in the flame, this reaction must proceed fast enough to remove H_2CO as soon as it is formed.

The HCO formed above may then react by way of

(10) L. I. Avramenko and R. V. Lorentso, *Doklady Akad. Nauk USSR*, **67**, 867 (1949).

(11) E. W. R. Steacie, "Atomic and Free Radical Reactions," Vol. II, Reinhold Publ. Corp., New York, N. Y., 1954.

(12) R. M. Fristrom and A. A. Westenberg, *Combustion and Flame*, **1**, 217 (1957).

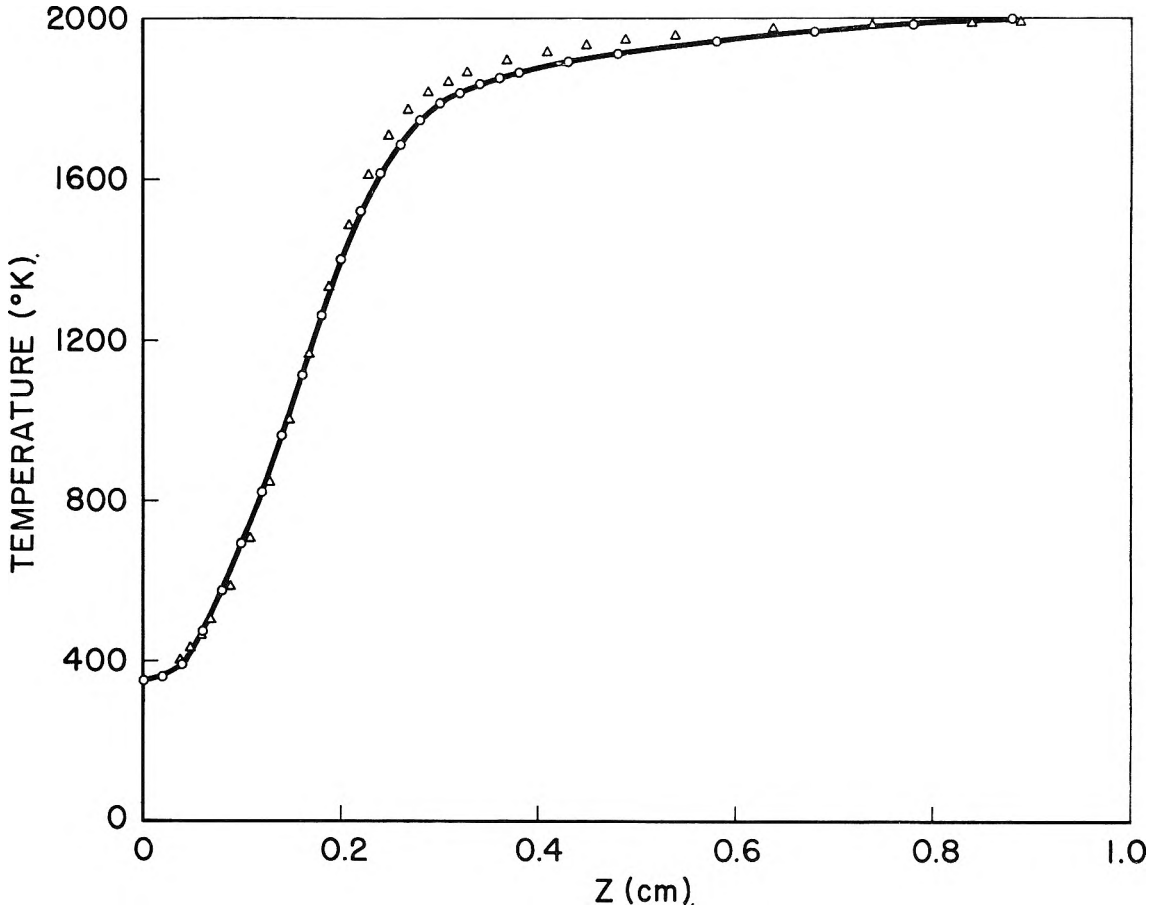

Fig. 7.—Plot showing congruence of the flame temperature profiles at two different pressures: O, data for 1/10 atm. flame; △, data for 1/20 atm. flame plotted against $z/2$.

$$HCO + OH \longrightarrow CO + H_2O, \text{ or}$$
$$HCO + M \longrightarrow H + CO + M, \text{ or}$$
$$HCO + O_2 \longrightarrow CO_2 + OH$$

The second of these reactions is fairly endothermic (26 kcal./mole) and must make only a minor contribution. The third is sterically improbable and does not allow for the production of CO in the flame. Presumably the first reaction accounts for the main rate of CO formation.

In the presence of O atoms, it seems plausible to consider

$$O + H_2CO \longrightarrow CO + H_2O$$

as a likely step in the removal of formaldehyde. However, since the O atoms presumably would be in their normal triplet state (^3P) while the other three participants in the reaction would be in singlet states, this violation of the spin conservation rules[13] should rule the reaction out as being much too slow. It also seems rather unlikely on steric grounds.

Carbon Monoxide Disappearance.—Certainly the most likely (and most commonly postulated) step is

$$CO + OH \longrightarrow CO_2 + H$$

The two estimates of the rate constant which have been made are in fair agreement (Avramenko and Lorentso[14]: $k \approx 3 \times 10^{12}\, e^{-7000/RT}$, Fenimore and Jones[15]: $k \approx 2 \times 10^{13}\, e^{-10000/RT}$). The rate constant for the reverse reaction consistent with these and the equilibrium constant is nearly comparable in the temperature range (1500–2000°) of interest, but in view of the probable low concentration of H atoms it is felt that the reverse reaction is of minor importance. This point is amplified later.

$$M + CO + O \longrightarrow CO_2 + M$$

For all species in ground electronic states, this reaction can be eliminated because it violates spin conservation. Also, it has been shown that the main reaction steps must be bimolecular.

$$CO + O_2 \longrightarrow CO_2 + O$$

This reaction is all right from the electron spin viewpoint, and also probably from the energetic viewpoint, since it is exothermic by 8 kcal./mole—although we are unaware of any estimates of actual activation energy. The main point is that if this reaction contributes appreciably it is hard to explain the pronounced catalytic effects of H_2O or H_2 (*i.e.*, OH) on the reaction or why dry CO–O_2 mixtures are stable up to moderately high temperatures, although at flame temperatures there may be some direct O_2 attack. CO–O_2 mixtures which are really dry have exceedingly low burning velocities or cannot be ignited at all.[16] It seems quite unlikely,

(13) K. J. Laidler, "Chemical Kinetics," McGraw-Hill Book Co., New York, N. Y., 1950, p. 386.

(14) L. I. Avramenko and R. V. Lorentso, *Zhur. Fiz. Khim.*, **24**, 207 (1950).

(15) C. P. Fenimore and G. W. Jones, *J. Phys. Chem.*, **62**, 1578 (1958).

(16) R. A. Wires, L. A. Watermeier and R. A. Strehlow, *ibid.*, **63**, 989 (1959).

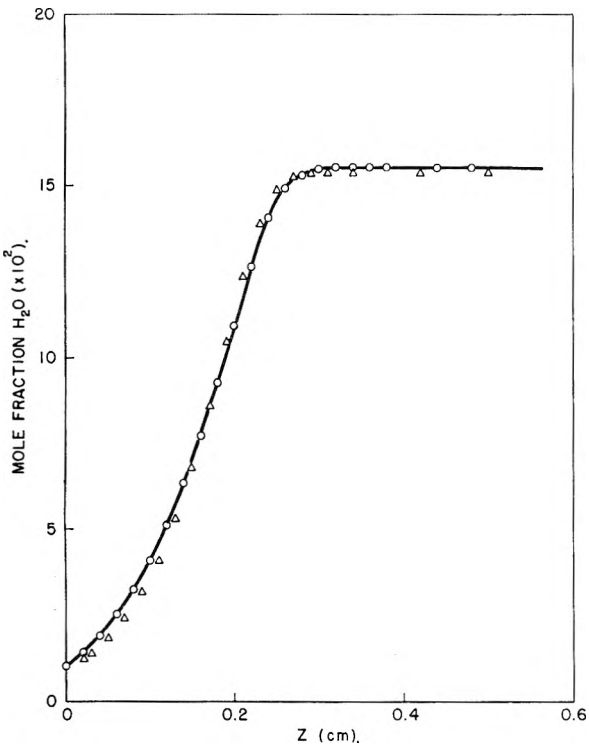

Fig. 8.—Plot showing congruence of the H_2O concentration profiles at two different pressures: O, data for 1/10 atm. flame; △, data for 1/20 atm. flame plotted against $z/2$.

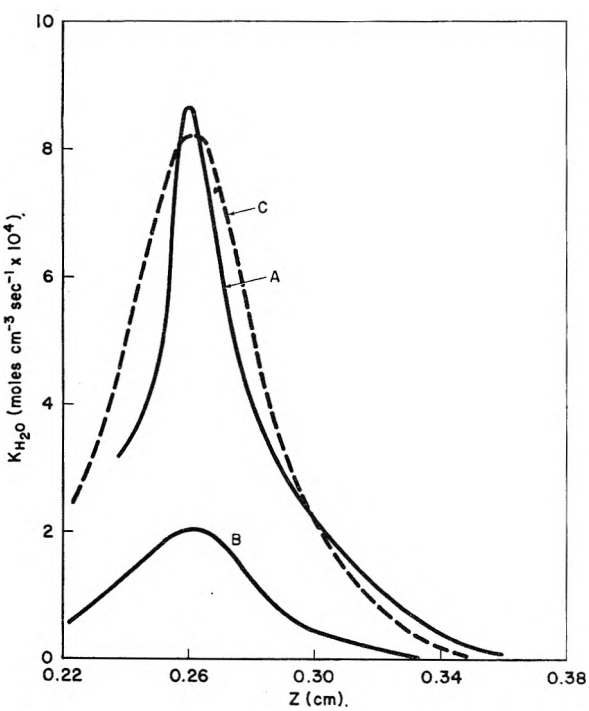

Fig. 9.—Plot showing congruence of the K_{H_2O} profiles at two different pressures: A, data for 1/10 atm. flame; B, data for 1/20 atm. flame plotted against $z/2$; C, data for 1/20 atm. flame plotted against $z/2$ and multiplied by 4.

therefore, that this reaction needs to be included.

Miscellaneous Reactions.—The reactions discussed in the foregoing sections include those which might account for the disappearance or appearance of the main stable species found in the flames without bringing in three-body reactions or the many complex or unlikely intermediate species so often suggested in kinetic studies at lower temperatures. The radical HO_2 has not been postulated because, as stated previously, its formation by direct reaction of O_2 with CH_4 is definitely not quantitatively significant in this case, and because the only other feasible source of HO_2, *i.e.*, by three-body combination with H atom *via* $H + O_2 + M \rightarrow HO_2 + M$, would be much too slow at these pressures compared with the two-body process

$$H + O_2 \longrightarrow OH + O$$

The latter reaction has been estimated by Fenimore and Jones[17] to have a rate constant of $5 \times 10^{14}\ e^{-18000/RT}$. It is a chain branching step which presumably is a major contributor to removing H from the system. With regard to HO_2, it may be noted also that a search for it by mass spectrometric analysis in a CH_4–O_2 diffusion flame was unsuccessful.[18]

Several other reactions ought to be mentioned.

$$H + H_2O \longrightarrow OH + H_2$$

This reaction has been estimated[8] to have a rate constant of $10^{15}\ e^{-25000/RT}$. It may partly account for the appearance of H_2 in the system while the reverse reaction contributes to H_2 removal.

$$O + H_2 \longrightarrow OH + H$$

This presumably contributes to H_2 removal. The reaction to form H_2O directly would be a spin violation.

$$H_2 + O_2 \longrightarrow OH + OH$$

This is quite improbable, energetically and sterically.

$$O + H_2O \longrightarrow OH + OH$$

This is endothermic by about 18 kcal./mole and would seem to be rather unimportant. The reverse reaction is the most likely mechanism for OH removal.

$$O + H_2O \longrightarrow H_2 + O_2$$

This reaction is about thermally neutral, and we are unaware of any data on it otherwise. It does not seem very probable sterically.

$$O + O + M \longrightarrow O_2 + M$$

The most important recombination reaction is probably that of O atoms. Three-body recombinations of H and OH also could provide chain termination, but these both involve H atoms which are low in concentration in this flame.

Summarizing the discussion of the possibilities, and after eliminating the impossible or improbable steps, the simplest set of reactions which accounts for the main features of the flame chemistry is

$$\left.\begin{array}{ll} \text{(I)} & CH_4 + OH \xrightarrow{k_1} CH_3 + H_2O \\ \text{(II)} & CH_4 + O \xrightarrow{k_2} CH_3 + OH \end{array}\right\} \begin{array}{l} \text{Methane disappearance.} \\ \text{Water formation.} \end{array}$$

(17) C. P. Fenimore and G. W. Jones, *ibid.*, **63**, 1154 (1959).

(18) S. N. Foner and R. L. Hudson, *J. Chem. Phys.*, **21**, 1374 (1953).

(III) $CH_3 + O_2 \xrightarrow{k_3} H_2CO + OH$ } Formaldehyde formation and disappearance.

(IV) $H_2CO + OH \xrightarrow{k_4} HCO + H_2O$ } Water formation.

(V) $HCO + OH \xrightarrow{k_5} CO + H_2O$ } Carbon monoxide formation and disappearance.

(VI) $CO + OH \xrightarrow{k_6} CO_2 + H$ } Carbon dioxide formation.

(VII) $H + H_2O \xrightarrow{k_7} OH + H_2$ } Hydrogen formation and disappearance.

(VIII) $O + H_2 \xrightarrow{k_8} OH + H$ }

(IX) $OH + OH \xrightarrow{k_9} H_2O + O$

(X) $H + O_2 \xrightarrow{k_{10}} OH + O$

(XI) $O + O + M \xrightarrow{k_{11}} O_2 + M$

The chemistry of the oxygen-diluted flame is different and somewhat simpler than its fuel-rich or stoichiometric counterparts. It would seem that the principal reason for this difference is that the concentration of oxygen *in the reaction zone* (as opposed to the inlet concentration) determines whether the radicals OH and O or H predominate in the initial reaction with fuel. In fuel-rich or even stoichiometric flames it is the H atom which predominates, because the effect of diffusion is to reduce drastically the oxygen concentration in the reaction zone—and hence that of OH and O also. Thus these flames are characterized by relatively high intermediate concentrations[12] of H_2 formed by reactions like VII or by direct reaction of H atom with the hydrocarbon. In any CH_4–O_2 flame, however, the initial attack of OH, O or H on the CH_4 molecule leaves a CH_3 radical which must then react (more or less, depending on the O_2 concentration) with O_2 *via* reaction III. The O_2 disappearance in flames containing considerable H atom concentration, *i.e.*, those not oxygen-diluted, must undoubtedly be attributed also to reaction X, and in some cases this may be the major mechanism as advocated by Fenimore and Jones.[8] It is difficult to see how reaction III could be excluded entirely, however, and still account plausibly for the appearance of H_2CO and CO.

Since all of the steps in the proposed reaction scheme involve free radicals, this brings up the question of chain initiation, branching and breaking reactions, and what we believe is an important distinction between flames and reacting systems which are homogeneous over relatively much longer distances. It is clear that the source of radicals in the fast reaction zone of a flame cannot be simply by diffusion from the burned equilibrium gas at the hot boundary since, as is brought out later, the evidence from this work and that of many other investigators is that the radical concentration in this zone goes through a maximum. The cause of this non-equilibrium maximum must be the reaction itself. In a flame there are no surfaces for radical recombination, so that the only mechanism (other than slow three-body radical recombinations) for opposing the chain reactions and thus limiting the chemical rate processes is the loss of radicals from the fast reaction zone by diffusion upstream and downstream from the radical maximum. The net result is that a relatively high non-equilibrium concentration of radicals may be maintained in this zone. Since the fast bimolecular reactions have the effect of merely exchanging unpaired electrons between radicals, it has been pointed out by Sugden and co-workers[19] that the attainment of final equilibrium values must be by way of three-body radical recombinations such as XI. On the other hand, chain initiating steps need not be important in flame kinetics because high radical concentrations already exist and are communicated to the incoming gas by diffusion.

Interpretation of the Data in Terms of the Mechanism.—Since most of the chemical activity in these flames has been attributed to the OH radical, it is natural to examine first the consequences of this assumption. The concentration of H atoms is kept very low (final burned gas mole fraction $X_H \approx 10^{-4}$) by the excess of O_2 and H_2O *via* reactions X and VII. Oxygen atom activity is largely confined to probable participation in CH_4 disappearance *via* II and provides a mechanism for equilibration of the system *via* XI. It will be noted that in the postulated mechanism the only step involving CO_2 is VI. If we accept this postulate and consider both forward and reverse directions of VI, we can write

$$K_{CO_2} = k_6[CO][OH] - k_{-6}[CO_2][H]$$

or using the equilibrium constant[20] relation $K_6 = k_6/k_{-6}$

$$K_{CO_2} = k_6N^2[X_{CO}X_{OH} - X_{CO_2}X_H/K_6] \qquad (7)$$

where N is the total molar density at any point in the flame. It is clear that eventually the reverse reaction term must become equal in magnitude to the forward term since equilibrium is approached at the hot boundary. In the earlier stages of the CO afterburning region, of course, the reverse reaction will be of less importance. At any rate, it is possible to estimate k_6 by assuming that *near the hot boundary* the mole fractions X_{OH} and X_H are close to the computed equilibrium values as given in Table I. This would seem to be a reasonable assumption. The experimental K_{CO_2} data may then be used in eq. 7, together with the experimental data on X_{CO} and X_{CO_2} and the known equilibrium constant K_6, to compute k_6 near the hot boundary. In this way the data from the flames at both pressures give a value of $k_6 \approx 9 \times 10^{11}$ cm.^{3} mole^{-1} sec.$^{-1}$ at $T \approx 1950$°K. As mentioned previously, there have been two published experimental estimates of k_6 expressed in the simple Arrhenius form $A \exp(-E/RT)$. Avramenko and Lorentso's expression[14] $k_6 \approx 3 \times 10^{12} \exp(-7000/RT)$ (obtained by a flow technique at considerably lower temperatures) gives $k_6 = 5 \times 10^{11}$ at 1950°K. while that of Fenimore and Jones,[15] $k_6 \approx 2 \times 10^{13} \exp(-10000/RT)$, (obtained by a flame study at temperatures comparable to ours) gives $k_6 \approx 1.5 \times 10^{12}$ at 1950°K. Considering the variety of techniques employed this degree of agreement may be

(19) E. M. Bulewicz, C. G. James and T. M. Sugden, *Proc. Roy. Soc. (London)*, **A235**, 89 (1956).

(20) The equilibrium constant symbol such as K_6 should not be confused with the K_i used for net reaction rates.

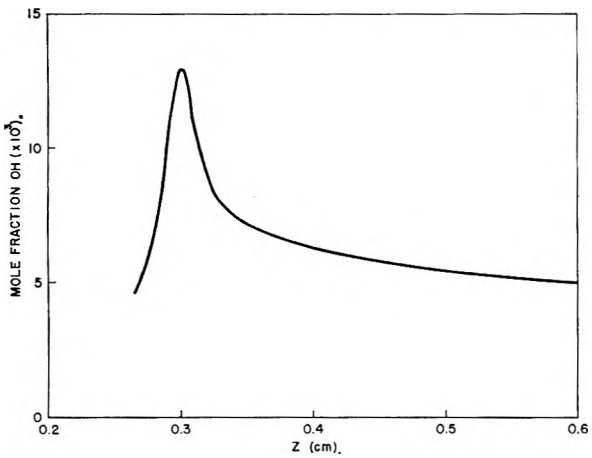

Fig. 10.—Profile of OH radical concentration in 1/10 atm. flame obtained from the CO_2 formation rate profile by fitting to the equilibrium concentration of OH at the hot boundary.

considered reasonably satisfactory. It was not possible to obtain an independent value of E_6 from this work. Using Avramenko and Lorentso's value $E_6 = 7$ kcal./mole and our value of k_6 at 1950°K., the expression for k_6 obtained was

$$k_6 \approx 5 \times 10^{12} e^{-7000/RT} \qquad (8)$$

TABLE I

CALCULATED FINAL (HOT BOUNDARY) EQUILIBRIUM GAS COMPOSITION; T, 2000°K.

Species	Mole fractions 1/10 atm.	1/20 atm.
H_2O	0.15473	0.15349
CO_2	.08022	.07918
O_2	.75273	.75612
CO	.00040	.00056
H_2	.00016	.00023
N_2	.00060	.00060
NO	.00042	.00042
Ar	.00340	.00018
OH	.00528	.00626
O	.00201	.00285
H	.00007	.00011

Once k_6 was determined in this way, it was possible to estimate a profile of X_{OH}. In order to do this using eq. 7, the reverse reaction term must be neglected. This is justifiable, as pointed out before, in a region far enough upstream of the hot boundary. Indeed, in the region used for the fitting procedure to get k_6 at 1950°K. which was described, the reverse term, *i.e.*, the second term in brackets in eq. 7, was only about 1/10 as large as the forward term, so that its neglect upstream of this would certainly be warranted. A profile of X_{OH} for the 1/10 atm. flame computed in this way is shown in Fig. 10. It will be noted that X_{OH} is nearly constant in the latter (hotter) part of the flame where the main reaction is the conversion of CO to CO_2, but rises to a maximum in the region where the fast reactions occur. This general behavior of unstable intermediates in flames has been noted by several authors. Experimentally, radical concentrations in the nearly burned gas regions of flames have been measured with an isotope labeling technique,[21] spectroscopically,[22,23] and photometrically.[19] The general conclusions of these studies have been that although radical concentrations (H and OH) may show a maximum two or three orders of magnitude above equilibrium values in the nearly burned gas of rich hydrogen flames and several times greater than equilibrium in lean hydrogen flames, in hydrocarbon flames values only slightly above equilibrium are reported. (The latter conclusion supports our use of the equilibrium X_{OH} in computing k_6.) In the present case, $(X_{OH})_{max}$ occurs at $z = 0.3$ cm. where the temperature is 1750°K. The ratio of $(X_{OH})_{max}$ to the equilibrium value at this temperature is about 10. This maximum lies near the fast reaction region and would not be in the region studied by the optical techniques quoted above. In the slow reaction region the X_{OH} values are closer to equilibrium, in agreement with these studies.

The disappearance of CH_4 in the flame has been attributed to OH radicals and/or O atoms *via* reactions I and II. Which of these—if either one—is more important is not possible to state for sure at this time. In view of the fact that the final equilibrium X_{OH} is more than twice X_O (see Table I), and that there are more sources of OH than O in the proposed mechanism, it seems likely that I would be more important. (Presumably II could not occur without I, since II generates OH, but the converse is not true.) If we neglect reaction II for the moment, the X_{OH} profile obtained from the CO_2 production rate may be used to obtain a rate constant for I. Thus

$$K_{CH_4} = -k_1 N^2 X_{CH_4} X_{OH} \qquad (9)$$

and solving for k_1, using X_{OH} profiles individually fitted at the hot boundary of each flame, we obtain from the 1/10 atm. flame (cm.^{3} mole^{-1} sec.$^{-1}$)

$$k_1(1650\text{–}1790°\text{K.}) = 3 \times 10^{13}$$

and from the 1/20 atm. flame

$$k_1(1660\text{–}1840°\text{K.}) = 1 \times 10^{13}$$

Over the temperature range in the flame where both K_{CH_4} and X_{OH} data were available, k_1 was independent of temperature. The only available estimate of E_1 is about 8.5 kcal./mole (quoted in ref. 7). From 1650 to 1840°K. the factor $\exp(-8500/RT)$ varies only from 0.08 to 0.10, which is well within the scatter of the k_1 values determined, so that such a small temperature dependence would be undetectable. The point really is that an average k_1 value of about 2×10^{13} is entirely reasonable. Taken at face value, this would imply a steric factor about 10 times larger than that for reaction VI (the activation energies are probably roughly equal). This may be sensible in view of the spherical symmetry of the CH_4 molecule. If part of the measured CH_4 disappearance rate is due to O atoms, however, the estimate of k_1 obtained by assuming it is all due to OH reaction would be too high, which would tend to overestimate the steric factor of reaction I.

(21) C. P. Fenimore and G. W. Jones, *J. Phys. Chem.*, **62**, 693 (1958).

(22) (a) W. E. Kaskan, *Combustion and Flame*, **2**, 229, 286 (1958); (b) A. G. Gaydon and H. G. Wolfhard, *Proc. Roy. Soc. (London)*, **A194**, 169 (1948).

(23) T. Grewer and H. G. Wagner, *Z. physik. Chem.*, **20**, 371 (1959).

It should be noted that Fenimore and Jones[8] rule out reaction I as an important reaction in methane flames on the basis of indirect arguments involving the relative rates of H_2O and CO_2 formation in near-stoichiometric CH_4–H_2–O_2–Ar flames. Since (as far as we can tell) they made no actual measurements of H_2O concentration, we do not regard their argument as very convincing.

Over-all Kinetics.—It is interesting to examine data from flame studies of this kind in terms of so-called over-all kinetics, and a comparison with the results of other workers may be of some significance. A general picture[24] of what must be happening as a complex reacting mixture such as exists in the afterburning regions of a flame approaches its final equilibrium state has emerged principally from the work of Bulewicz, James and Sugden[19] and Kaskan.[21,25] They have shown that a mechanism which includes only reactions such as (in this case) VI through IX cannot lead to final equilibration of an arbitrary mixture of the radicals and molecules present in the flame gases. These bimolecular steps, which simply exchange unpaired electrons amongst the various species, would be expected to lead eventually to a state where certain relations between the species concentrations would be the same as at equilibrium, but where actual concentrations might be higher or lower than for complete equilibrium. Kaskan[25] has pointed out that, for the mixture under consideration here, the quantity

$$[OH] + 2[O] + 3[H] + 2[CO] + 2[H_2]$$

cannot change with time if only reactions VI–IX are considered. In order to reach final equilibrium some other reactions—presumably three-body recombinations—must be included. This appears to be a perfectly valid argument. It says nothing, however, about the chemical kinetic rates of the individual species in the afterburning region.

Kaskan[25] has presented evidence from spectroscopic measurements in various lean flames that reactions VI, VII, VIII and X reach a state of equilibration very quickly beyond the fast reaction (luminous) zone. If we assume equilibration of VI and VII, this implies that the water gas equilibrium must be satisfied. This is something that

$$CO + H_2O \rightleftharpoons CO_2 + H_2$$

is subject to experimental test in our flames since all of the above four species were directly measured. If we define the water gas equilibrium constant as

$$K_{wg} = \left(\frac{[CO_2][H_2]}{[CO][H_2O]}\right)_{equil} \qquad (10)$$

we can compare the measured ratio $Q_{wg} = ([CO_2]\cdot[H_2]/[CO][H_2O])_{meas}$ with K_{wg} to determine the extent of deviation from equilibrium. This comparison is shown in Table II. It is clear that the water gas equilibrium definitely is not attained until the hot boundary is reached, so that the equilibration of *both* reactions VI and VII is not borne out by these data. Since the region of the flame covered in Table II is one where both $[H_2O]$ and $[H_2]$ have attained essentially constant values, it is quite possible that VII may be equilibrated, but if so, VI cannot be. Previous evidence[19,21] indicates that VII may be equilibrated in such flames as these. The lack of equilibration of VI was commented on earlier in the present paper, of course, when only the forward reaction was used to estimate a profile of X_{OH}.

TABLE II

TEST OF ATTAINMENT OF THE WATER GAS EQUILIBRIUM IN THE AFTERBURNING REGION

$K_{wg} = ([CO_2][H_2]/[CO][H_2O])_{equil}$, $Q = ([CO_2][H_2]/[CO][H_2O])_{meas}$

z, cm.	T, °K.	Q_{wg}	K_{wg}	Q_{wg}/K_{wg}
		1/10 atm. flame		
0.30	1748	0.011	0.266	0.041
.38	1852	.013	.240	.054
.45	1890	.021	.233	.090
.60	1940	.041	.224	.18
.80	1988	.11	.215	.52
.90	2000	.24	.215	≈1
		1/20 atm. flame		
0.56	1853	0.013	0.240	0.054
.66	1893	.016	.233	.069
.82	1931	.027	.225	.12
1.0	1957	.043	.220	.20
1.5	1988	.089	.215	.41
2.1	1990	.19	.215	.89

If we assume, then, that reaction VI is *not* equilibrated in the afterburning zone of these flames, the question arises as to whether or not the disappearance rate of CO can be related to the concentrations of other major species in any reasonable way. It seems evident that, as pointed out before, the eventual equilibration of the excess radicals present in the flame must be by way of recombination reactions, such as the reaction XI which we have postulated as being most important in our case. Simultaneously, it appears reasonable that the CO is being converted to CO_2 *via* VI, with the reverse reaction becoming important in the later stages as the concentration of CO decreases and CO_2 increases. In rigorous detail, these processes of radical decay and CO conversion are coupled, of course. However, in a case such as this where O_2 and H_2O are present in *large excess* compared to CO, the radical concentrations are probably not much out of equilibrium, so that it is perhaps useful and instructive to *approximate* the situation by regarding the CO as immersed in a bath composed of O_2, H_2O, OH and O at equilibrium. This amounts to a steady-state treatment of OH and O. From the equilibrated reactions IX and XI one can derive an expression for X_{OH} of the form

$$X_{OH} = \frac{(X_{H_2O})^{1/2}(X_{O_2})^{1/4}}{K_9^{1/2}K_{11}^{1/4}P^{1/4}} \qquad (11)$$

where the equilibrium constants K_9 and K_{11} are in partial pressure units, *i.e.*

$$K_9 = \frac{p_{H_2O}p_O}{(p_{OH})^2}; \quad K_{11} = \frac{p_{O_2}}{(p_O)^2}$$

The presence of small amounts of CO will not appreciably alter the values of X_{OH} computed from (11).

(24) The authors are indebted to the referees of this paper for helpful discussion and several constructive suggestions about this matter.

(25) W. E. Kaskan, *Combustion and Flame*, **3**, 49 (1959).

TABLE III

COMPARISON OF CO DISAPPEARANCE RATES COMPUTED FROM EQ. 14 AND THOSE MEASURED EXPERIMENTALLY BY VARIOUS AUTHORS

Author	Flame system	$K_{CO_2}/[CO]$ eq. 14 (sec.$^{-1}$)	$K_{CO_2}/[CO]$ Exptl. (sec.$^{-1}$)
This work	CH_4–O_2 at 0.1 atm. ($X_{O_2} = 0.75$, $X_{H_2O} = 0.15$, $T = 1950$°K.)	2900	3000
This work	CH_4–O_2 at 0.05 atm. ($X_{O_2} = 0.76$, $X_{H_2O} = 0.15$, $T = 1950$°K.)	1400	1500
Friedman and Cyphers[27]	C_3H_8–air at 0.06 atm. ($X_{O_2} = 0.095$, $X_{H_2O} = 0.084$, $T = 1600$°K.)	73	231
Friedman and Nugent[28]	CO–O_2 at 0.04 atm. ($X_{O_2} = 0.77$, $X_{H_2O} = 0.033$, $T = 1780$°K.)	210	185
Fenimore and Jones[29]	C_2H_2–air at 1 atm. ($X_{O_2} = 0.052$, $X_{H_2O} = 0.061$, $T = 1885$°K.)	2900	700

We may now use eq. 7 with the reverse reaction (second) term neglected—an approximation which should certainly be good in the initial stages of the CO disappearance as previously noted. Substituting eq. 11 for X_{OH} in (7) gives

$$K_{CO_2} = \frac{k_6 N^2 X_{CO}(X_{H_2O})^{1/2}(X_{O_2})^{1/4}}{K_9^{1/2}K_{11}^{1/4}P^{1/4}} = \frac{k_6[CO][H_2O]^{1/2}[O_2]^{1/4}}{K_9^{1/2}K_{11}^{1/4}(RT)^{1/4}} \quad (12)$$

which is an over-all kinetic relation for the initial rate of CO_2 formation from CO reacting in a shifting equilibrium mixture of O_2, H_2O, O and OH. The "over-all rate constant" for this case would be given by

$$k = k_6/K_9^{1/2}K_{11}^{1/4}(RT)^{1/4} \quad (13)$$

in units of (cm.^{3} mole^{-1})$^{0.75}$ sec.$^{-1}$. The equilibrium constants K_9 and K_{11} are known functions of temperature, of course—approximately of the form $\ln K \propto (1/T)$. Since k_6 is of the same form, an Arrhenius plot of $\ln k$ *vs.* $1/T$ with k evaluated according to eq. 13 should be linear (the $T^{1/4}$ factor is unimportant) with a slope giving an "over-all activation energy." This procedure, using eq. 8 for k_6, gave the result

$$K_{CO_2} = 3 \times 10^{13} e^{-45000/RT}[CO][H_2O]^{1/2}[O_2]^{1/4} \quad (14)$$

It should be emphasized that this expression would not be expected to be a reasonable approximation under conditions (such as in flames rich in H_2) where high excess OH concentrations are found or where the reaction has proceeded long enough so that the reverse reaction of VI should be included. Both of these conditions have been noted by Kaskan.[25] But where small amounts of CO are present with excesses of O_2 and H_2O it should be valid. In this connection it is noteworthy that the concentration dependences of the CO conversion rate given by eq. 14 are exactly the same as those found empirically by Kozlov[26] in a conventional flow reactor experiment, and stated by him as having been verified by several other Russian workers in various burning velocity studies for O_2 concentrations greater than 5%. It seems likely that this is significant. His over-all activation energy is lower (32 kcal./mole), however.

(26) G. I. Kozlov, "Seventh Symposium on Combustion," Butterworths, London, 1959, p. 142.

(27) R. Friedman and J. A. Cyphers, *J. Chem. Phys.*, **23**, 1875 (1955).

(28) R. Friedman and R. G. Nugent, "Seventh Symposium on Combustion," Butterworths, London, 1959, p. 311.

(29) C. P. Fenimore and G. W. Jones, *J. Phys. Chem.*, **61**, 651 (1957).

Using eq. 14, it is of interest to compare the present results with those of other flame studies. For each case, the quantity $K_{CO_2}/[CO]$ was computed from (14) and compared with the experimentally measured value. The results are given in Table III. For the data of this work, the two agree closely, of course, because the numerical value of k_6 which enters into the over-all rate constant *via* eq. 13 was fitted to the experimental data by the same equilibrium OH assumption used in deriving (14). For the three other works cited, the predictions of eq. 14 are at least fairly satisfactory, considering the variety of experimental conditions and techniques employed. The validity of (14) is by no means proven, however, and is simply suggested as being interesting at this time.

Fenimore and Jones[28] report several other sets of data for flames having considerably less O_2 in the burned gas, and the experimental values of $K_{CO_2}/[CO]$ for these are much lower than the computed values—the discrepancy being considerably worse than the case cited in Table III. Indeed, in this connection it is again interesting to note that Kozlov[26] also mentions that the $^1/_4$ power concentration dependence for O_2 holds only for $X_{O_2} > 5\%$. It would seem that this is to be expected under the interpretation suggested here, since with very little O_2 present the H atom concentration would be much higher, and the reverse of reaction VI should be included. Thus, calculated values of $K_{CO_2}/[CO]$ would tend to be lower than those computed neglecting the reverse reaction and this would improve the agreement shown in Table III for the data of Fenimore and Jones. The probable inadequacy of neglecting the reverse reaction in their work also has been remarked by Fenimore and Jones.[15] The effect of the reverse reaction can be included by assuming an equilibrium concentration of H also, so that using the complete eq. 7 one gets

$$K_{CO_2} = k_6 N^2 (X_{H_2O})^{1/2}\left[\frac{X_{CO}(X_{O_2})^{1/4}}{K_9^{1/2}K_{11}^{1/4}P^{1/4}} - \frac{X_{CO_2}}{K_6 K_9^{1/2}K_{11}^{3/4}K_{10}P^{3/4}(X_{O_2})^{1/4}}\right] \quad (15)$$

This shows that the larger X_{O_2}, the less important the second term (reverse reaction), although it is only a $^1/_4$ power dependence. The over-all $^1/_2$ power dependence on X_{H_2O}, remains, however,

which also accords with Kozlov's results. The usefulness of such a complex expression as (15) is questionable, of course.

Acknowledgment.—The authors are pleased to note that they have benefited from discussions of this work with Dr. W. H. Avery, and from the able assistance of Mr. S. Favin in the numerical calculations.

THE ABSOLUTE ADSORPTION ISOTHERMS OF VAPORS OF NITROGEN, BENZENE AND *n*-HEXANE, AND THE HEATS OF ADSORPTION OF BENZENE AND *n*-HEXANE ON GRAPHITIZED CARBON BLACKS. I. GRAPHITIZED THERMAL BLACKS

BY A. A. ISIRIKYAN AND A. V. KISELEV

Adsorption Laboratory, Department of Chemistry, M. V. Lomonosov Moscow State University, Surface Chemistry Group, Institute of Physical Chemistry, U.S.S.R. Academy of Sciences, Moscow, Russia

Received August 1, 1960

Unified absolute adsorption isotherms for nitrogen at −195°, and *n*-hexane and benzene at 20° have been measured using a series of "graphitized" medium thermal carbon blacks as adsorbents. Differential heats of adsorption as a function of surface coverage were also measured. The initial portion of the nitrogen isotherms is slightly convex and well described in terms of localized adsorption, taking into account interaction of adsorbate molecules. The adsorption isotherm for benzene, on the other hand, is initially concave, and the heat of adsorption is found to be practically constant over the entire monolayer coverage. In the case of *n*-hexane, the heat of adsorption rises by about 15% during monolayer coverage, and the initial portion of the isotherm, like nitrogen, is slightly convex. The newly-measured heats of adsorption are in good agreement with earlier calculated values of the potential energy of adsorption.

Introduction

In studies of adsorption on solid bodies, the measured quantities are usually relative. This is due to the indeterminate geometrical and chemical structure of most adsorbents. For this reason, there is an unfortunate gulf between experiment and theories of adsorption forces and adsorption equilibria, which, in quantitative form, refer specifically to homogeneous surfaces.[1,2] Even such a basic quantity as specific surface of the adsorbent frequently remains indeterminate, because at the basis of the BET method[3] lies (among other limitations) the assumption of a more homogeneous surface.

It is important, therefore, to employ adsorbents of homogeneous surface which will provide reproducible results in all laboratories. In this connection, adsorbents having their surface composed principally of planes of a single index, and of sufficient area for precise measurements, are most desired. One of the simplest adsorbents of this type is "graphitized" carbon black.[1,4−15] Thermal carbon blacks heated in absence of air to 3000° have an especially homogeneous surface.[5−9,11,14−16] As a result of heat treatment, the initially spherical particles become polyhedra,[5] with faces consisting mainly of homogeneous basal planes of single crystals of graphite. These single crystals are connected along the edges of the polyhedron. While these boundaries give rise to some residual heterogeneity, it is so small it does not influence adsorbate–adsorbent interaction. A comparison of adsorption isotherms and heats of adsorption measurements carried out on such carbon blacks in many laboratories demonstrates the excellent reproducibility of both the measurements and the surface uniformity.

Using a number of graphitized thermal blacks, we have investigated the adsorption of nitrogen at −195°: first, because reliable data are already available in the region of small[6] and large[9] coverages and, second, because nitrogen usually is used in determining specific surface by the BET method. Isotherms and differential heats of adsorption of benzene and *n*-hexane were also obtained. Al-

(1) A. V. Kiselev, *Vestnik Akademii Nauk SSSR*, No. 10, 43 (1957); N. N. Avgul, A. A. Isirikyan, A. V. Kiselev, I. A. Lygina and D. P. Poshkus, *Izvestia Akademii Nauk SSSR, Dept. Chem. Sci.*, 1314 (1957); N. N. Avgul, A. V. Kiselev, I. A. Lygina and D. P. Poshkus, *ibid.*, 1196 (1959).

(2) A. V. Kiselev, D. P. Poshkus, *Dokl. Akad. Nauk SSSR*, **132**, 148 (1960).

(3) S. Brunauer, P. H. Emmett and E. Teller, *J. Am. Chem. Soc.*, **60**, 309 (1938).

(4) R. A. Beebe, J. Biscoe, W. R. Smith and C. B. Wendell, *J. Am. Chem. Soc.*, **69**, 95 (1947); C. Pierce and R. N. Smith, *ibid.*, **75**, 846 (1953); R. A. Beebe and D. M. Young, *J. Phys. Chem.*, **58**, 93 (1954).

(5) W. D. Schaeffer, W. R. Smith and M. H. Polley, *Ind. Eng. Chem.*, **45**, 1721 (1953).

(6) S. Ross and W. Winkler, *J. Coll. Sci.*, **10**, 319, 330 (1955); S. Ross and W. W. Pultz, *ibid.*, **13**, 397 (1958).

(7) A. V. Kiselev and E. V. Khrapova, *Kolloidn. zhurn.*, **23**, 2 (1961).

(8) A. A. Isirikyan and A. V. Kiselev, *ibid.*, in press.

(9) R. A. Beebe and J. M. Holmes, *J. Phys. Chem.*, **61**, 1684 (1957).

(10) A. V. Kiselev, *Kolloidn. zhurn.*, **20**, 338 (1958); A. V. Kiselev, N. V. Kovaleva, V. A. Sinitsyn and E. V. Khrapova, *ibid.*, **20**, 444 (1958).

(11) R. A. Beebe, J. M. Holmes, A. V. Kiselev and N. V. Kovaleva, *J. Phys. Chem.*, in press.

(12) N. N. Avgul, A. V. Kiselev, A. Ya. Korolev and I. A. Lygina, *Kolloidn. zhurn.*, **20**, 298 (1958).

(13) N. N. Avgul, G. I. Berezin, A. V. Kiselev and I. A. Lygina, *Zhurn. fiz. Khimii*, **30**, 2106 (1956); *Izv. Akad. Nauk SSSR, Dpt. Chem. Sci.*, 1304 (1956); 1021 (1957); 787 (1959); A. V. Kiselev, "Proc. Second Internat. Congress on Surface Activity," Vol. 2, London, 1957, p. 168.

(14) W. B. Spencer, C. H. Amberg and R. A. Beebe, *J. Phys. Chem.*, **62**, 719 (1958).

(15) N. N. Avgul, G. I. Berezin, A. V. Kiselev and I. A. Lygina, *Izv. Akad. Nauk SSSR, Dept. Chem. Sci.*, in press.

(16) M. H. Polley, W. D. Schaeffer and W. R. Smith, *J. Phys. Chem.* **57**, 469 (1953).

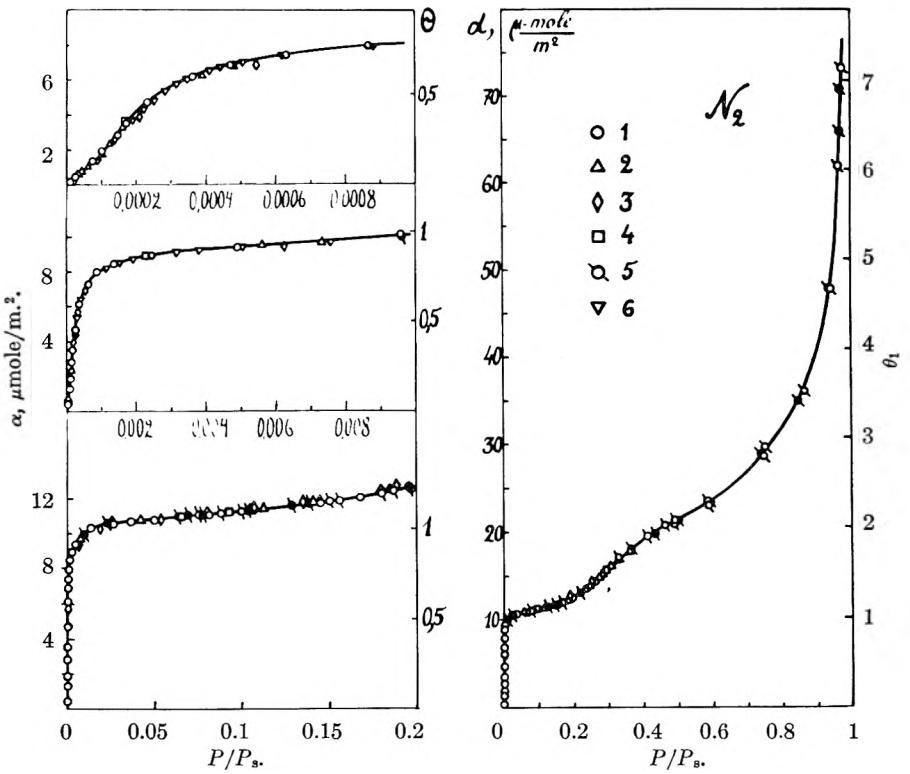

Fig. 1.—Absolute adsorption isotherm of nitrogen vapor at −195° on graphitized thermal blacks: (1) MT-1 (3100°); (2) FT (2800°); (3) T-1 (3000°); (4) T-3 (3200°); (5) MT (3100°) data from (9); (6) FT (2800°) data from (6).

though these molecules contain the same number of carbon atoms, they are radically different in structure. Benzene, though non-polar, has an uneven density distribution of π-electrons. For this reason, adsorption of benzene is sensitive to presence of surface hydroxyl groups as are all molecules with large quadrupole moments.[17-21] *n*-Hexane is practically insensitive to this factor. Benzene molecules are planar and, in the case of adsorption on a non-polar adsorbent, the weak electrokinetic (dispersion) attraction between them is, apparently, balanced by the weak electrostatic repulsion of the CH dipoles and quadrupoles formed by π-electron clouds, so that the heat of adsorption remains nearly constant during filling of the monolayer.[12] On the other hand, molecules of *n*-hexane are strongly attracted to each other and the heat of adsorption passes through a maximum.[8,13]

Experimental

Adsorbents.—The adsorbents used in the present study were thermal carbon blacks graphitized at 3000 ± 300° in the absence of air. The thermal blacks T-1 and T-3 were prepared in this Laboratory and subsequently graphitized by us. The graphitized samples Sterling FT (2800°) and Sterling MT (3100°) were obtained from Dr. W. R. Smith of Cabot Corporation, and were from the same lot as the samples previously supplied Dr. Ross and Dr. Beebe.[6,9] The Sterling MT-1 (3100°) was a freshly prepared sample obtained from Dr. Smith at a somewhat later date. The samples T-1 and T-3 were graphitized in our laboratory at 3000° for 45 and 10 minutes, respectively. The Sterling MT and FT samples supplied by Dr. Smith had been heat treated for two hours. Earlier studies have shown that graphitization at 3000° is very rapid and it can be assumed that all the above samples are at about the same degree of graphitization.

Prior to the experiments, the samples were evacuated in the system at 450° for 6–10 hours.[22]

Absorbates.—Nitrogen was obtained first from sodium azide and then by purification of tank nitrogen. The benzene and *n*-hexane were the same as used in earlier work.[8,22] Adsorption of nitrogen was measured on two devices with accurately calibrated gas burets, first directly in the calorimetric cartridge,[8,17,22] and then separately.[23] In the low pressure region, corrections were introduced in accordance with Chu Liang.[24] The saturation pressure, P_s, was measured with a nitrogen thermometer, and ranged from 780 to 810 mm.

Measurements of the adsorption and heats of adsorption of benzene and *n*-hexane were carried out with the vacuum capillary microburet for liquids, and a calorimeter with constant heat exchange as described earlier.[22]

Results and Discussion

Determination of Specific Surfaces.—Data from Ross[6] and Beebe[9] for the adsorption of nitrogen on similar samples of graphitized thermal blacks were included with our data in preparing BET plots. All the data provided linear plots over relative pressures ranging from 0.0003 to 0.09. Values for the monolayer capacity a_m, in micromoles per

(17) A. V. Kiselev, *Dokl. Akad. Nauk SSSR*, **106**, 1046 (1956); A. A. Isirikyan and A. V. Kiselev, *ibid.*, **115**, 343 (1957); A. V. Kiselev and L. D. Belyakova, *ibid.*, **119**, 298 (1958); "The Structure and Properties of Porous Materials," Ed. D. H. Everett and F. Stone, London, 1958, p. 195.

(18) A. V. Kiselev and D. P. Poshkus, *Dokl. Akad. Nauk SSSR*, **120**, 834 (1958).

(19) L. E. Drain, *Trans. Faraday Soc.*, **49**, 650 (1953); L. E. Drain and J. A. Morrison, *ibid.*, **49**, 654 (1953).

(20) T. Hayakawa, *Bull. Chem. Soc. Japan*, **30**, 236 (1957).

(21) G. J. C. Frohrsdorff and G. L. Kington, *Trans. Faraday Soc.*, **55**, 1173 (1959).

(22) A. A. Isirikyan and A. V. Kiselev, *Zhurn. fiz. khim.*, **31**, 2127 (1957); **32**, 679 (1958); A. A. Isirikyan, A. V. Kiselev and G. G. Muttik, "Proc. Second Intern. Congress on Surface Activity," Vol. 2, London, 1957, p. 214.

(23) B. G. Aristov, A. P. Karnaukhov and A. V. Kiselev, *Kolloidn. zhurn* (in press).

(24) S. Chu Liang, *J. Appl. Phys.*, **22**, 148 (1951).

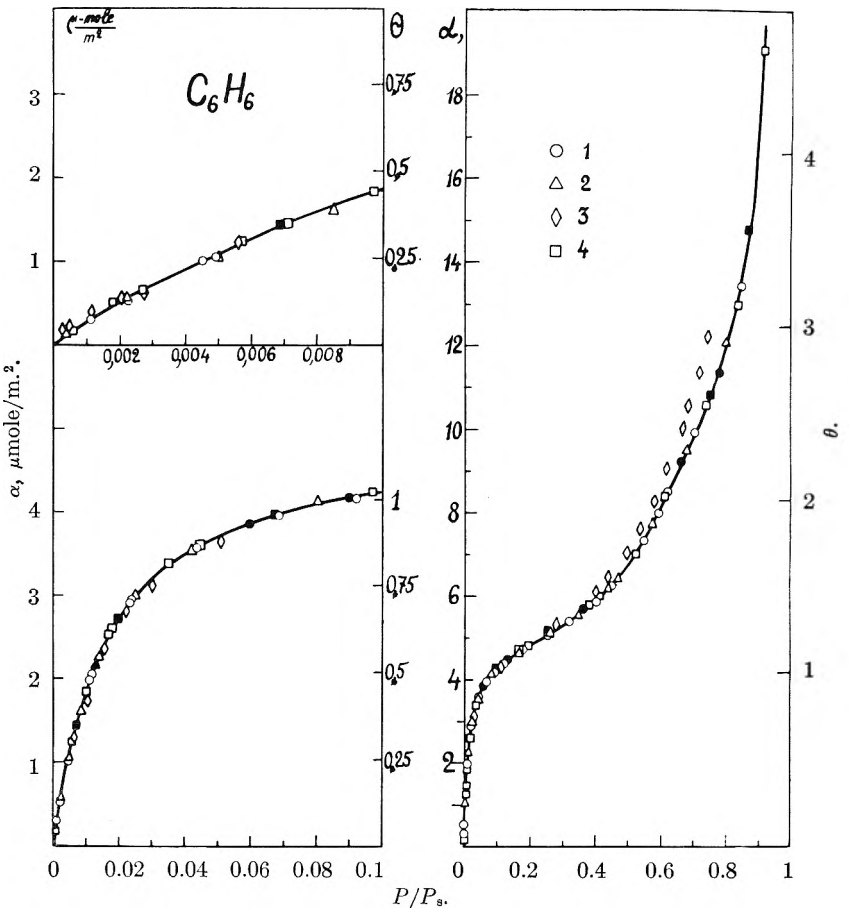

Fig. 2.—Absolute adsorption isctherm of benzene vapor at 20° on graphitized thermal blacks: (1) MT-1 (3100°); (2) FT (2800°); (3) T-1 (3000°); (4) T-3 (3200°).

gram, and specific areas, s, using 16.2 Å.² for nitrogen cross-sectional area, were computed from these plots and are reported in columns 2 and 3 of Table I.

TABLE I

CHARACTERISTICS OF SAMPLES OF GRAPHITIZED CARBON BLACKS USED

	Results of applying BET method					
	Nitrogen ω_m = 16.2 Å.²		Benzene ω_m = 40 Å.²		*n*-Hexane	
Adsorbent	a_m, μmole/g.	s, m.²/g.	a_m, μmole/g.	s, m.²/g.	a_m, μmole/g.	ω_m, Å.²
T-1 (3000°)	298.5	29.1	122.5	29.5	94.8	51.0
T-3 (3200°)	68.0	6.63	27.6	6.65	...	..
Sterling FT (2800°)	125.3	12.22	50.8	12.23	39.9	50.9
Sterling MT (3100°)	66.8	6.51	...	...	...	..
Sterling MT-1 (3100°)	78.4	7.65	31.9	7.68	25.06	50.8

The BET plots for benzene and *n*-hexane are linear over relative pressures from 0.04 to 0.12 for benzene, and 0.002 to 0.12 for *n*-hexane. The corresponding values of a_m are given in columns 4 and 6 of Table I. Assuming, for a plane benzene molecule, $\omega_m = v_m/N\tau$ where v_m is the molar volume of liquid benzene, N Avogadro's number, and τ, the van der Waals thickness of the molecule, as 3.70 Å., we obtain ω_m = 40.0 Å.² The corresponding values of specific area, s, given in column 5, are very close to those obtained with nitrogen on the same adsorbents.

Since it is difficult to make an independent determination of ω_m for *n*-hexane with a high degree of accuracy, this value was determined from the values of specific surface found with nitrogen, and the value ω_m as determined from the BET plot for the adsorption of *n*-hexane. The values of ω_m for *n*-hexane thus evaluated are given in column 7 of Table I. They are in good agreement, and provide an average value of 51.0 Å.² This value is close to the 54 A.² value estimated in earlier work,[13,25] from the density of the liquid assuming τ = 4 Å. and the van der Waals dimensions of *n*-hexane extended along the surface. Thus, using the BET method, it is feasible to determine the specific surface from the adsorption of *n*-hexane at 20°, employing ω_m = 51.0 Å. as the cross-sectional area of the adsorbate.

The Absolute Adsorption Isotherm of Nitrogen.—Figure 1 gives the isotherm, at −195°, of the absolute values of the adsorption of nitrogen (per unit area), $\alpha = a/s$,[26] and the extent of surface coverage, $\theta = \alpha/\alpha_m$. In the case of Sterling FT (2800°), the value of 12.22 m.²/g. that we determined coincides with that reported by Beebe, *et al.*,[14] which indicates that the samples were identical. This value was taken for recalcu-

(25) A. A. Isirikyan and A. V. Kiselev, *Zhurn. fiz. khim.* (in press).

(26) a is the measured value of adsorption per gram of adsorbent.

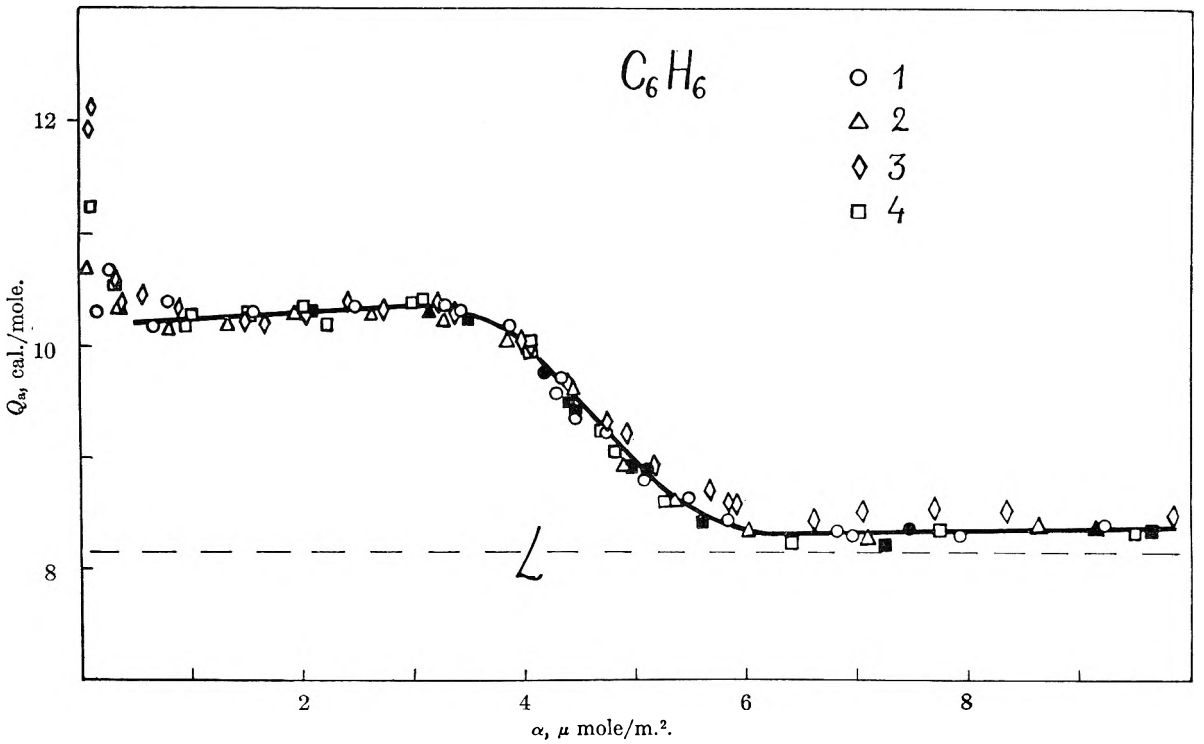

Fig. 3.—The differential heat of adsorption of benzene vapor at 20° as a function of the surface coverage of graphitized thermal blacks: (1) MT-1 (3100°); (2) FT (2800°); (3) T-1 (3000°); (4) T-3 (3200°).

lation of the data of Ross and co-workers[6] in terms of absolute values.[27] For our sample of Sterling MT (3100°), we obtained an area of 7.65 m.²/g., while Beebe, *et al.*,[14] report the value 6.3 m.²/g. for their sample. Thus, apparently these were different though very similar samples of graphitized thermal black. Therefore, in the determinations of absolute values from our data, we used s = 7.65 m.²/g. We find that the data of Beebe, *et al.*,[14] can be brought into agreement with our data on the basis of an area of 6.51 m.²/g., obtained from a BET plot in the same p/p_s interval, rather than their 6.3 value.

From Fig. 1 it is seen that for all thermal blacks, heated to about 3000°, the absolute values of adsorption, determined from both the measurements of Ross and Beebe,[6,9] as well as from our own, lie on one and the same isotherm.[28] The absolute isotherm thus obtained may be attributed to the adsorption of nitrogen on the basal plane of graphite. To facilitate reproduction of this isotherm as a standard, the interpolated values of α and p/p_s are provided in Table II.

A complete theoretical description of the isotherm for mono-molecular and, particularly, multi-molecular adsorption, requires a statistical-thermodynamic treatment, with account taken of the effect on the distribution function of the energies of adsorbate–adsorbent and adsorbate–adsorbate interactions and their variation with surface coverage. Since this has not been done as yet, use should be made of approximate equations, in which only the shape of the isotherm has been derived theoretically,

(27) In Paper 6 the reported value of s = 11.7 m.²/g., for this sample, was estimated from "point B."

(28) The same conclusion, though somewhat less precise, was made earlier, 7 ref., with the help of data from references 6 and 16.

TABLE II

ABSOLUTE VALUES OF ADSORPTION OF NITROGEN ON THE BASAL FACE OF GRAPHITE AT −195°

The surface is defined according to BET at ω_m = 16.2 A.² (see column 3 of Table I)

p/p_s	α, μmole/m.²	p/p_s	α, μmole/m.²	p/p_s	α, μmole/m.²
0.00003	0.50	0.0024	8.93	0.35	17.6
.00005	0.90	.0037	9.18	.40	19.0
.00008	1.45	.0055	9.45	.45	20.2
.00010	1.90	.0075	9.70	.50	21.2
.00013	2.55	.0095	10.00	.55	22.2
.00017	3.50	.014	10.35	.60	23.3
.00020	4.13	.025	10.59	.65	24.7
.00023	4.72	.040	10.72	.70	26.7
.00027	5.35	.06	10.91	.75	29.2
.00031	5.80	.08	11.05	.80	31.6
.00037	6.33	.10	11.27	.85	34.5
.00043	6.70	.13	11.60	.90	40.0
.00051	7.08	.16	11.95	.94	47.5
.00060	7.37	.19	12.46	.96	58.0
.00075	7.75	.22	13.15	.97	66.0
.00095	8.07	.26	14.36	.98	78.0
.0013	8.42	.30	16.00		

while the numerical values of the constants are found from experiment. The convex initial portion of the nitrogen isotherm on graphitized carbon black shows that in a more detailed description of the isotherm one cannot neglect adsorbate–adsorbate interactions as compared with adsorbate–adsorbent interactions. In the work of Ross,[6] the adsorption isotherm of nitrogen in the region of monolayer coverage was described by *three* equations: the Henry equation, the Hill equation for non-localized monomolecular adsorption, which

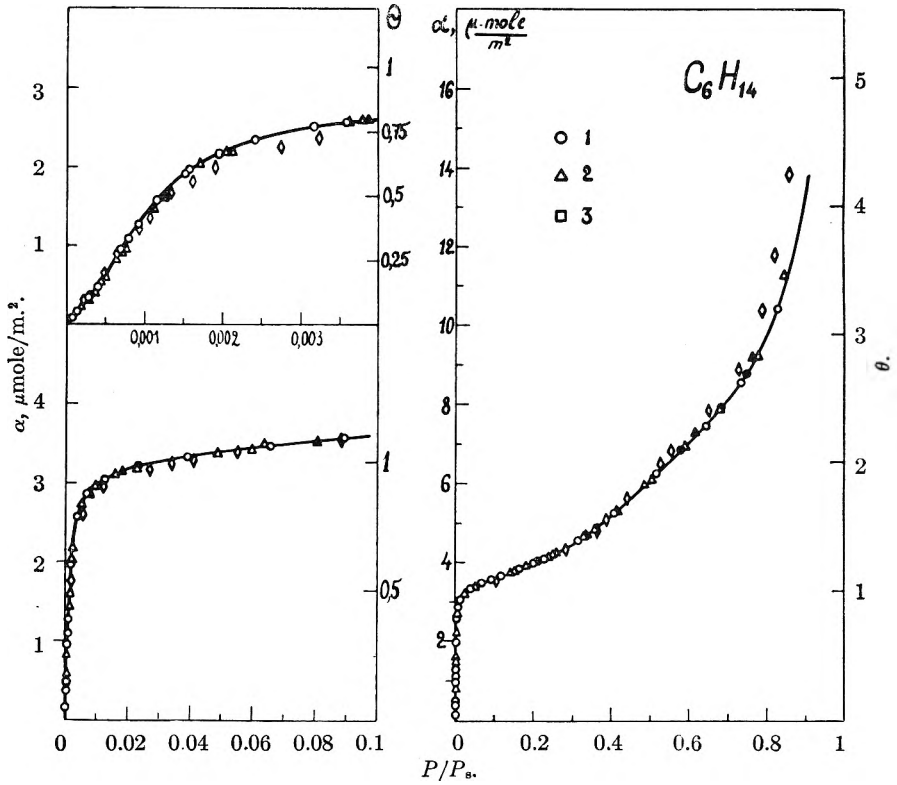

Fig. 4.—Absolute adsorption isotherm of *n*-hexane vapor at 20° on graphitized thermal blacks: (1) MT-1 (3100°); (2) FT (2800°); (3) T-1 (3000°).

accounts for adsorbate-adsorbate interaction,[29,30] and the Langmuir equation for localized adsorption without interaction. In papers[7,10] the entire region of monomolecular coverage was described by the following single equation, 1, which took into consideration the adsorbate-adsorbate interactions in the case of monomolecular localized adsorption[10]

$$p/p_s = \frac{\theta}{K_1(1 - \theta)(1 + K_n\theta)} \qquad (1)$$

where $\theta = \alpha/\alpha_m$, and K_1 and K_n are equilibrium constants of adsorbate-adsorbent and adsorbate-adsorbate interactions.

Up to $\alpha = 9$ μmole/m.² the isotherm in Fig. 1 is best described by equation 1 for $\theta = \alpha/9.23$ (*i.e.*, for $\omega_m = 18$ Å.²), $K_1 = 900$ and $K_n = 8$) hence

$$p/p_s = \frac{\alpha/9.23}{900(1 - \alpha/9.23)(1 + 8\alpha/9.23)} \qquad (2)$$

Equation 2 may be used as a good interpolation formula, because the isotherm calculated from it coincides with the experimental isotherm (up to $\alpha = 9$ μmole/m.² and relative pressure of 0.0025). In the region of lowest coverage, the experimental points lie somewhat higher. This may be attributed to enhanced adsorption at sites of residual inhomogeneity of the surface of the adsorbent.[31] Hill's equation of non-localized adsorption yields poorer results in this instance. Thus, nitrogen adsorption at −195° on the basal face of graphite is predominantly localized.

Adsorption and the Heat of Adsorption of Benzene.—Figure 2 presents an isotherm of the absolute values of adsorption of benzene vapor on the graphitized thermal blacks MT-1 (3100°), FT (2800°), T-2 (3200°) and T-1 (3100°). The data for these adsorbents lie close to a single general curve. Table III contains the appropriate interpolated values of α and p/p_s for the construction of this isotherm. In the region of monolayer adsorption, the isotherm is concave.

TABLE III

ABSOLUTE VALUES OF ADSORPTION OF BENZENE ON THE BASAL FACE OF GRAPHITE AT 20°

The surface is determined from nitrogen at −195° by the BET method, using $\omega_m = 16.2$ Å.²; $p_s = 75.4$ mm.

p/p_s	α, μmole/m.²	p/p_s	α, μmole/m.²	p/p_s	α, μmole/m.²
0.0005	0.15	0.030	3.24	0.40	5.86
.001	.27	.035	3.40	.45	6.25
.002	.50	.040	3.51	.50	6.77
.003	.71	.050	3.71	.55	7.35
.004	.90	.06	3.87	.60	8.08
.005	1.09	.07	4.00	.65	8.88
.006	1.28	.08	4.11	.70	9.80
.007	1.45	.09	4.19	.75	10.80
.008	1.60	.10	4.27	.80	11.90
.009	1.74	.15	4.61	.825	12.50
.010	1.87	.20	4.83	.850	13.40
.015	2.40	.25	5.06	.875	14.40
.020	2.74	.30	5.30	.900	16.20
.025	3.02	.35	5.56	.925	20.0

(29) T. L. Hill, *J. Chem. Phys.*, **14**, 441 (1946).

(30) J. H. de Boer, "The Dynamical Character of Adsorption," Oxford, 1953.

(31) When applying equation 2, one must bear in mind that the values of s used for constructing the absolute isotherm of Fig. 1 were determined from experimental isotherms by the BET method using $\omega_m = 16.2$ Å.² The BET equation does not describe a wave-like isotherm; for one thing, it does not describe the convex portion of its first wave.

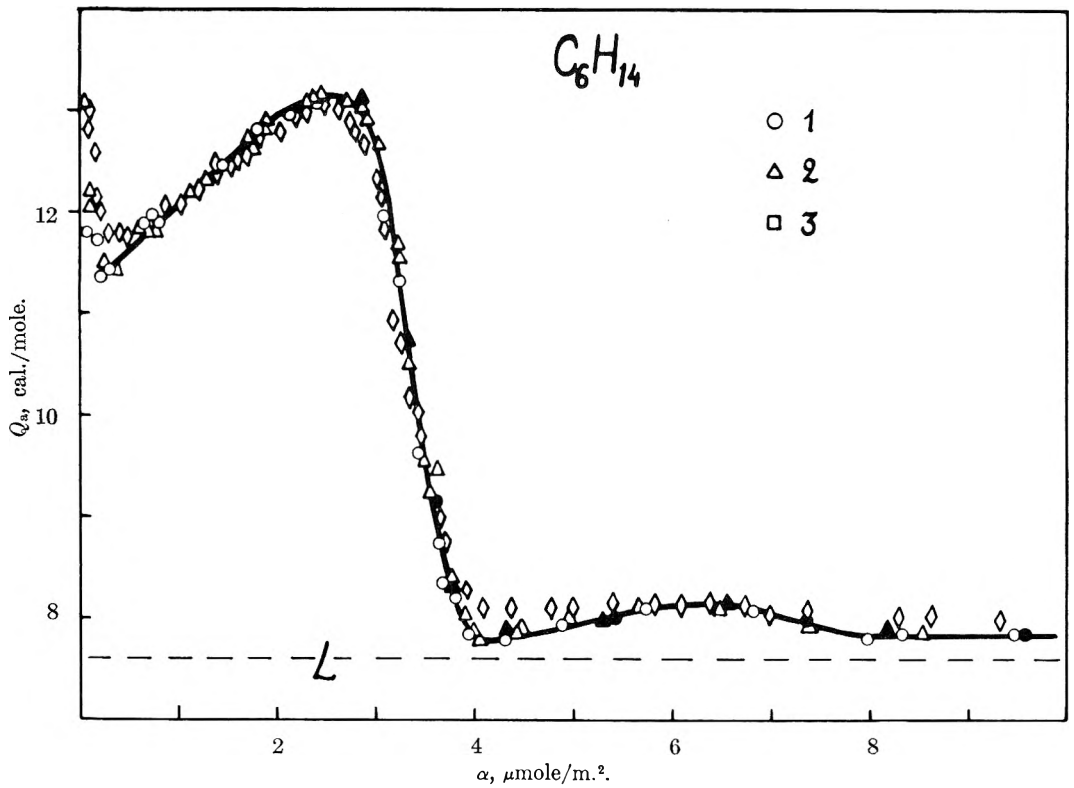

Fig. 5.—The differential heat of adsorption of *n*-hexane vapor at 20° as a function of surface coverage of graphitized thermal blacks: (1) MT-1 (3100°); (2) FT (2800°); (3) T-1 (3000°).

Figure 3 gives the differential heat of adsorption of benzene as a function of the surface coverage on the graphitized thermal blacks. All samples exhibit an initial region of enhanced heats, connected perhaps with penetration of the benzene molecules into grain boundaries of the single crystals of graphite. However, this region is small. Beginning with $\theta = 0.1$, the heat of adsorption is nearly constant to $\theta = 0.9$, after which it falls sharply in accordance with the transition to predominantly multilayer adsorption. The interpolated numerical data for the construction of this curve are given in Table IV. Extrapolating to zero coverage, we find 10.15 kcal./mole for Q_a. In a previous publication,[12] we have reported 10.2 and 10.3 kcal. for $\theta = 0$ and $\theta = 0.5$. These experimental values for the differential heats are in agreement with the value 10.3 kcal./mole calculated from theory.[1] It is observed from Fig. 3 that the net heat of adsorption is nearly constant over the monolayer, being 2.15 kcal./mole. It is further of interest that the net heat in the second layer is virtually constant at a value of 0.15 kcal./mole. Thus the adsorption of benzene at 20° on the basal face of "graphite" in the region of first and second layer coverage provides an example of a constant net heat, consistent with a basic assumption of the BET theory.

Adsorption and Heat of Adsorption of *n*-Hexane Vapor.—Figure 4 gives the absolute adsorption isotherms of hexane. The points for the three adsorbents MT-1 (3100°), FT (2800°) and T-1 (3000°) lie on nearly a single curve, although it may be noted that for the sample with the most homogeneous surface, Sterling MT (3100°), the points in the initial region lie somewhat lower,

TABLE IV

THE VALUES OF DIFFERENTIAL HEAT OF ADSORPTION OF BENZENE AT 20° FOR VARIOUS COVERAGES OF THE BASAL FACE OF GRAPHITE

α, μmole/m.²	Q_a, kcal./mole	α, μmole/m.²	Q_a, kcal./mole	α, μmole/m.²	Q_a, kcal./mole
0.2	(10.3)	3.2	10.38	5.5	8.50
0.6	10.20	3.6	10.30	6.0	8.35
1.0	10.22	4.0	10.00	7.0	8.30
1.4	10.25	4.4	9.55	8.0	8.30
2.0	10.28	4.8	9.05	9.0	8.30
2.6	10.33	5.2	8.70	10.0	8.30

while in the region of sharp inflection of the isotherm, about $\theta = 0.7$–0.9, they lie somewhat above the points for Sterling FT (2800°) and the somewhat less homogeneous sample T-1 (3000°). The data for Sterling MT (3100°) are closest to the absolute isotherm. Similar conclusions have been arrived at for adsorption of ammonia on this adsorbent.[9] For this reason, these data were given preference in construction of the absolute isotherm. The interpolated data for construction of this absolute isotherm are given in Table V.

The region of initial decline of the heats of adsorption, as shown in Fig. 5, extends to $\theta = 0.1$. Following this decline, they rise perceptibly in an approximately linear fashion and attain a maximum at $\theta = 0.9$. They then fall off sharply in accord with a transition to predominantly multilayer adsorption. The numerical data for constructing this curve are given in Table VI.

TABLE V

ABSOLUTE VALUES OF ADSORPTION OF *n*-HEXANE ON THE BASAL FACE OF GRAPHITE AT 20°

The surface is determined from nitrogen at −195° by the BET method, using ω_m = 16.2 Å.²

p/p_s	α, μmole/m.²	p/p_s	α, μmole/m.²	p/p_s	α, μmole/m.²
0.0001	0.12	0.004	2.63	0.35	4.79
.0002	0.23	.005	2.73	.40	5.18
.0004	0.48	.01	2.98	.45	5.61
.0006	0.79	.02	3.17	.50	6.06
.0008	1.10	.03	3.26	.55	6.58
.0010	1.38	.04	3.33	.60	7.00
.0012	1.62	.06	3.44	.65	7.51
.0014	1.82	.08	3.52	.70	8.09
.0016	1.97	.10	3.60	.75	8.77
.0018	2.10	.15	3.77	.80	9.63
.0023	2.31	.20	3.97	.85	11.0
.0028	2.43	.25	4.21	.90	13.5
.0034	2.54	.30	4.46		

TABLE VI

VALUES OF DIFFERENTIAL HEAT OF ADSORPTION OF *n*-HEXANE AT 20° AT VARIOUS COVERAGES OF THE BASAL FACE OF GRAPHITE

The value in parentheses has been extrapolated

α, μmole/m.²	Q_a, kcal./mole	α, μmole/m.²	Q_a, kcal./mole	α, μmole/m.²	Q_a, kcal./mole
0.1	(11.40)	2.6	13.8	4.8	7.90
.2	11.35	2.8	13.10	5.4	8.00
.4	11.50	3.0	12.70	6.0	8.12
.6	11.70	3.2	11.50	6.6	8.14
1.0	12.08	3.4	10.10	7.2	8.00
1.4	12.40	3.6	9.00	7.8	7.80
1.8	12.75	3.8	8.15	8.4	7.80
2.2	13.03	4.0	7.80	9.2	7.80
2.4	13.13	4.4	7.80	10.0	7.80

The pertinent data from Fig. 5 may be shown as

Coverage θ	Heat of adsorption Q_a	Net heat $Q_a - L$
0.1	11.3 kcal.	3.7
.5	12.6	5.0
.9	13.2	5.6
1.5	7.9	0.3

At a coverage of 0.5, the heat of adsorption for *n*-hexane is 12.6 kcal., in good agreement with the value 12.4 kcal. calculated from theory.[1] At this coverage, the heat of adsorption exceeds the heat of liquefaction by 65%, while at 1.5 coverage it is only 4% higher. However, during filling of the monolayer, *i.e.*, from a coverage of 0.1 to 0.9, the heat of adsorption increases by only 15%. The large value of the net heat and relatively small increase in the heat of adsorption during filling of the monolayer, coupled with a comparatively small net heat *after* completion of the monolayer, is responsible for the satisfactory manner in which the isotherms are described by the BET equation. However, the heat of adsorption does increase to a significant degree during monolayer coverage due to adsorbate–adsorbate interaction, and this is responsible for the fact that the adsorption isotherm is initially convex[32] (see data for MT (3100°) in Fig. 4). Since the heat of adsorption of *n*-hexane is large and the CH_3 and CH_2 groups in the molecule can locate over the sites of highest energy in the graphite planes (*i.e.*, mid-points of the carbon hexagons), the adsorption of *n*-hexane may be predominantly localized.

Specific Surface from Absolute Isotherms.—From the absolute isotherms provided by the data of Tables II, III and V, it is possible to obtain the specific surface of a carbon black adsorbent by measuring only a single adsorption point, a, at some convenient relative pressure. The corresponding value of α may be read from the absolute isotherm and the specific area, s, obtained from the relation $s = a/\alpha$.[33,34] Since the adsorption of *n*-hexane is insensitive to the degree of oxidation of the surface, the procedure should apply to all blacks as well as to the graphitized samples we have studied. This method would not, of course, be expected to apply to carbon blacks possessing any considerable degree of porosity. The use of *n*-hexane as an adsorbate provides a method not requiring a supply of liquid nitrogen.

Acknowledgment.—The authors express their gratitude to Dr. W. R. Smith of the Cabot Corporation for the samples of graphitized carbon black, FT (2800°) and MT-1 (3100°), and for his assistance in preparing our manuscript for publication. We also wish to thank Professor R. A. Beebe, Dr. J. M. Holmes and Dr. S. Ross for data on the adsorption of nitrogen on these carbon blacks. We also thank Dr. K. V. Chmutov for support of this work.

(32) The concave nature of the initial portion of the isotherm, as published earlier,[5,13] is now attributed to the lower degree of homogeneity of the adsorbents then in use.

(33) A. V. Kiselev, Collection of papers "Methods of Investigating the Structure of Highly Dispersive and Porous Bodies," U.S.S.R. Acad. of Sciences Press, Moscow, 1953, P. 86.

ON PHYSICAL ADSORPTION. XII. THE ADSORPTION ISOTHERM AND THE ADSORPTIVE ENERGY DISTRIBUTION OF SOLIDS[1]

BY SYDNEY ROSS AND JAMES P. OLIVIER

Department of Chemistry, Rensselaer Polytechnic Institute, Troy, N. Y.

Received August 17, 1960

A number of model adsorption isotherms have been computed, based on the concept of a two-dimensional non-ideal gas type of mobile film adsorbed on a solid substrate that displays a Gaussian distribution of adsorptive energies. These models were computed for a number of different adsorptive energy distributions of the substrate, designed to cover most physical situations. Experimental adsorption isotherms, chiefly of argon and nitrogen as adsorbates at temperatures of 77.5 and 90.1°K., were then compared with the computed models until the closest interpolated match was obtained. The model of a mobile adsorbed film was found to correspond with the observations and to predict correctly the variation of adsorption with temperature. A number of different adsorbents are thereby shown to be described adequately by a Gaussian distribution of adsorptive energies. The present method of obtaining a measure of the heterogeneity of a solid surface is the first yet proposed that provides a means of checking its validity, by predicting the temperature variation of adsorption. The method also provides a new way to obtain the monolayer capacity of a surface, which has hitherto been obtained almost universally by the B.E.T. method.

The heterogeneity of a solid surface must be reflected in the distribution of adsorptive potential energies that it offers to an adsorbate; and, since the measurement of adsorption is now a common technique, the hope has been entertained in recent years that the adsorption isotherm would be the ready means by which some information about this elusive property of a surface could be brought to light.

The immediate problem is to determine the form of the adsorption isotherm for a surface that has a distribution of adsorptive energies (U_0). In its most general form this problem can be expressed as the solution of the equation

$$\theta = \int_e^g \phi\,(U_0)\Psi(p,U_0)\,\mathrm{d}U_0 \qquad (1)$$

where θ is the relative surface concentration of the adsorbate. The fraction, $\mathrm{d}\delta_i$, of the total surface Σ that has a potential energy for adsorption U_{0i} is $\phi(U_0)\,\mathrm{d}U_0$: in other words, $\phi(U_0)\mathrm{d}U_0$ describes the distribution of the adsorptive energies that exists for a given adsorbate–adsorbent pair. The amount of surface having an adsorptive energy U_{0i} is $\Sigma\mathrm{d}\delta_i$; this patch of surface is treated as homotattic[2] for adsorption and the whole surface is considered as composed of a number of such patches, each with its own adsorptive energy. The fraction θ_i of a given patch that is occupied by adsorbate molecules at a pressure p is given by the function $\psi(p,U_0)$: in other words, $\psi(p,U_0)$ describes the adsorption isotherm for a homotattic patch of adsorptive energy U_{0i}.

Equation 1 is a general expression for the adsorption isotherm; it becomes a specific description only when a choice has been made for the functions $\phi(U_0)dU_0$ and $\psi(p,U_0)$. This choice will be determined by the nature of the model that we select; and the selection will be determined by what is considered to be the description nearest to physical reality.

A number of previous writers[3] on this subject have solved equation 1 analytically to obtain either the distribution function $\phi(U_0)dU_0$ or an expression for θ as a function of p. Their choice of model has almost invariably been a localized monolayer obeying the Langmuir equation, in which lateral interactions are ignored. The popularity of this treatment seems to have its source in its mathematical convenience: the Langmuir equation provides an explicit relation for θ_i as a function of p and U_{0i}, which is a mathematical requirement for the analytical integration of equation 1, whereas other adsorption isotherm equations that might be more attractive on physical grounds lack this necessary feature. The choice of distribution function is also limited by a similar mathematical requirement in that it must not lead to an intractable integral. Because of these restrictions, no analytic solution has yet been successfully completed of equation 1 that describes a model of a mobile adsorbed film on a solid surface, taking into account both lateral (or adsorbate–adsorbate)interactions and heterogeneity of the substrate. The theoretical description of such a model would be very desirable nevertheless, as evidence has now accumulated of its relevance to physical reality: de Boer[4] has shown the many implications to be derived from a theoretical model of a mobile, two-dimensional non-ideal gaseous adsorbed film on a homotattic surface; and the experimental findings of Ross and his coworkers,[5] who have selected as substrates for physical adsorption such near-homotattic solid surfaces as those of cube crystals of sodium chloride or highly graphitized carbon blacks, have shown how closely de Boer's prognostications came to describing these systems. These findings clearly demonstrate, with a series of increasingly more graphitic carbon blacks, that the more uniform the surface the more closely can its adsorption

(1) Based on a Thesis presented by J. P. Olivier to the faculty of Rensselaer Polytechnic Institute, January, 1960, in partial fulfillment of the requirements for the degree of Doctor of Philosophy. Copies of the thesis containing the computed Tables referred to in this paper may be obtained from University Microfilms, Ann Arbor, Mich.

(2) The term "homotattic" was introduced by Sanford and Ross, *J. Phys. Chem.*, **58**, 288 (1954), who defined a homotattic surface as the surface of a sub-microscopic patch or region, part of a larger surface, which acts as if its structure were uniform and homogeneous.

(3) An excellent historical survey (with 155 references) of adsorbent–adsorbate interactions and surface heterogeneity in physical adsorption has been published by J. M. Honig, *Ann. N. Y. Acad. Sci.*, **58**, 741 (1954).

(4) J. H. de Boer, "The Dynamical Character of Adsorption," Clarendon Press, Oxford, 1953.

(5) (a) S. Ross and H. Clark, *J. Am. Chem. Soc.*, **76**, 4291, 4297 (1954); (b) S. Ross and W. Winkler, *ibid.*, **76**, 2637 (1954); (c) *J. Colloid Sci.*, **10**, 319, 330 (1955); (d) S. Ross and W. W. Pultz, *ibid.*, **13**, 397 (1958).

isotherm be described by an equation based on a two-dimensional van der Waals equation of state. Toward the real problem, however, this work, both in theory and in experiment, is but the first step: it does not take us beyond the consideration of completely homotattic surfaces, which are actually of rare occurrence: each of the common solid materials that we employ daily offers a distribution of adsorption potentials. For the measurement of this distribution, no adequate methods have yet been developed.

Writers who have discussed the theory of adsorption[3,6] have noted and deplored the absence of explicit calculations for the model of a mobile adsorbed film on a heterogeneous substrate, while admitting the difficulties that beset such an undertaking. Thus Everett[6] points out that surface heterogeneity plays an important part in determining the adsorptive behavior of a surface, and is then constrained to add: "No explicit calculation of the behavior of a two-dimensional gas on a heterogeneous surface has, however, been made. For localized adsorption the problem is more tractable ...." The idea underlying the present development is, therefore, not novel: this work is an attempt to fill a long-recognized gap in the theory of adsorption, namely, the description of the behavior of a significant model hitherto unexplored.

The present paper reports the results obtained by applying a digital computer to the problem: by this means, instead of an analytic expression for the adsorption isotherm we obtain a series of computed isotherms for different values of the parameters, which, although less convenient to use, can be obtained without the constraint of the mathematical restrictions that would otherwise limit the forms of the functions $\phi(U_0)$ and $\psi(p,U_0)$.

A large number of mathematical formulations for the adsorption isotherm based on different two-dimensional equations of state, and for different distribution functions are available. While it would be naive to assume that our choice of expressions for $\phi(U_0)$ and $\psi(p,U_0)$ are necessarily precise, we offer them as probable formulations, valid as a first approximation if the adsorbed film is indeed a two-dimensional gas on a heterogeneous substrate.

As a description of the adsorbed film on each homotattic surface patch we follow de Boer in using an isotherm equation derived from the two-dimensional van der Waals equation of state, namely

$$p = K_i \frac{\theta_i}{1-\theta_i} \exp\left[\frac{\theta_i}{1-\theta_i} - \frac{2\alpha\theta_i}{RT\beta}\right] \qquad (2)$$

where α and β are the two-dimensional van der Waals' constants, which, for isotropic molecules that are negligibly polarized on adsorption, can be obtained from the familiar (three-dimensional) constants a and b by the relation $2\alpha/\beta = a/b$. K_i is a function of U_{0i}, hence descriptive solely of adsorbate–adsorbent interaction, and does not include lateral interaction energies; the latter are explicitly given by the exponential factor $2\alpha\theta_i/RT\beta$. It is assumed that α and β do not depend in any way on surface heterogeneity. The relative surface concentration θ is here defined by V/V_β where V_β is, ideally, the amount adsorbed at infinite pressure when the area available per molecule equals β.

If the adsorbed molecules are polarized by the electric field of the surface, or if they otherwise interact with the surface, as for example by a charge-transfer no-bond resonance,[6a] parallel-oriented dipoles are formed that would reduce the intermolecular forces of attraction between the adsorbate molecules; and hence also reduce the two-dimensional van der Waals constant α which measures these forces. De Boer[4] gives the relation:

$$\Delta\alpha = \pi\mu^2/d$$

where $\Delta\alpha$ is the decrease of the value of α from its theoretical value, d is the diameter of the adsorbed molecule, and μ is its dipole moment perpendicular to the surface. These dipoles produce another effect: namely, a change in the work function of the interface, which is observed as a surface potential and may be expressed as $\Delta\varphi = 4\pi\mu/\beta$, where $\Delta\varphi$ is the surface potential.

Unfortunately no experimental results have yet been obtained for surface potentials at graphite–adsorbate interfaces. Mignolet[7] found 0.03 volt for the surface potential of argon on nickel. If the same value is assumed for the graphite–argon interface, the surface-provoked dipole of argon would amount to 0.01 debye, and the lowering of α would be only 0.025%. Even if the surface potential were ten times greater, the lowering of α would amount to 2.5%. It therefore seems quite reasonable to suppose that for argon, nitrogen and other gases of low polarizability, the constants α and β can be derived from their three-dimensional van der Waals constants without serious error. Undoubtedly this assumption would not be reasonable for an adsorbate such as benzene, where there would enter not only high polarizability but a possible geometric factor as well.

For the distribution of adsorptive potentials of the whole surface we have selected the Gaussian probability function, *viz.*

$$f_i = d\delta_i = \phi(U_0)\,dU_0 = \frac{1}{n}\exp -[\gamma(U_{0i} - U_0')^2\,dU_0] \qquad (3)$$

where U_0 is the average adsorptive energy and γ determines the width of the distribution; n is the normalizing factor required to make $\int_e^g d\delta_i = 1$.

For purposes of theory an adsorption energy function that is characteristic of the system and independent of temperature is desirable: such a quantity, which we term U_0, is conveniently defined by the potential energy difference between the lowest energy state of a molecule in the gas phase and its lowest energy state in the adsorbed phase, both at infinite dilutions. The consideration of potential energy changes on adsorption is not required for a thermodynamic description of the process; but in this way we do obtain a quantity that is independent of the kinetic states of the molecule in either phase and that measures most directly the adsorptive potential of the system.[8]

(6) D. H. Everett, *Proc. Chem. Soc.*, 38 (1957).

(6a) R. S. Mulliken, *J. Am. Chem. Soc.*, **74**, 811 (1952); P. M Gundry and F. C. Tompkins, *Trans. Faraday Soc.*, **56**, 846 (1960).

(7) J. C. P. Mignolet, "Chemsorption," ed. W. E. Garner, Butterworths, London 1957, p. 118.

(8) For flexibility and clarity we have adopted the following system of symbols: the four positions around a letter-symbol, corresponding to the anterior and posterior superscripts and subscripts, are reserved, respectively, for designations of concentration, quality, phase and temperature (°K.), as

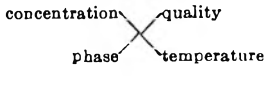

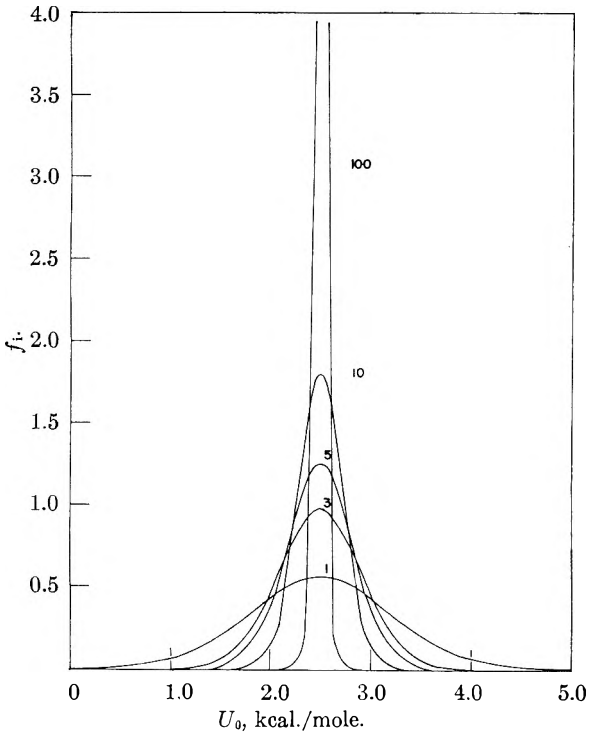

Fig. 1.—Gaussian adsorptive energy distribution curves for several values of γ (equation 3).

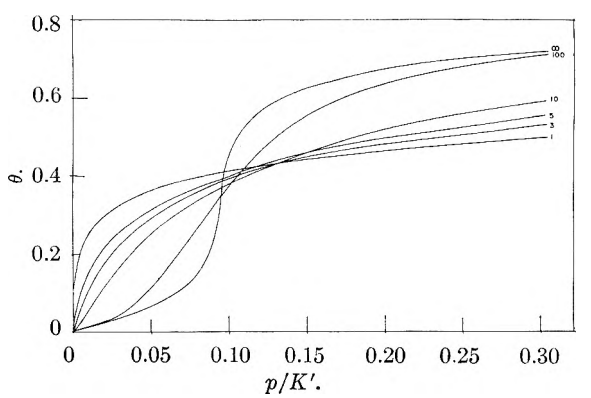

Fig. 2.—Computed isotherms for argon adsorbed as a mobile film at 77.5°K., corresponding to the distribution curves shown in Fig. 1.

To develop this function, let ${}_gP^{ads}$ be the potential energy per mole for adsorption of a molecule in the gas phase; then, for an ideal gas, the total energy per mole, kinetic and potential, of a molecule in the gas phase, ${}_g{}^0E$, is given by

$$ {}_g{}^0E = {}_gP^{ads} + {}_gE^{kin} $$

where ${}_gE^{kin}$ is the total kinetic energy per mole of a molecule in a gas: thus, ${}_gE^{kin} = {}^3/_2RT$ for an ideal monatomic gas. Let ${}_a\bar{E}^{vib}$ be the average vibrational energy per mole of a molecule in an adsorbed film; then for a mobile adsorbed film, the total energy (excluding interaction) per mole of a molecule in the surface film, ${}_a{}^0E$, is given by

$$ {}_a{}^0E = {}_a\bar{E}^{vib} + {}_aE^{kin} $$

where ${}_aE^{kin}$ is the kinetic energy of translation and rotation of the adsorbed molecule. The total energy change on adsorption is

$$ {}_g{}^0E - {}_a{}^0E = ({}_gP^{ads} - {}_a\bar{E}^{vib}) - \Delta E^{kin} $$

where

$$ \Delta E^{kin} = {}_aE^{kin} - {}_gE^{kin} $$

then

$$ {}_g{}^0E - {}_a{}^0E = ({}_gP^{ads} - {}_aE_0{}^{vib}) - ({}_a\bar{E}^{vib} - {}_aE_0{}^{vib}) - \Delta E^{kin} $$

where ${}_aE_0{}^{vib}$ is the zero-point vibrational energy of the adsorbed molecule, equivalent to ${}^1/_2\ Nh\nu$ where ν is the vibrational frequency of the adsorbed molecule with respect to the surface. We defined U_0 as the difference in energy of a molecule in its lowest energy state in the gas, *i.e.*, when ${}_gE^{kin} = 0$, and its zero-point vibrational level, ${}_a\bar{E}_0{}^{vib}$ on the surface; therefore

$$ U_0 = {}_gP^{ads} - {}_aE_0{}^{vib}; $$

and

$$ {}_g{}^0E - {}_a{}^0E = U_0 - ({}_a\bar{E}^{vib} - {}_aE_0{}^{vib}) + \Delta E^{kin} \quad (4) $$

For use in the computer, equation 1 is treated as a summation of finite terms: the infinitesimal dU_0 becomes the finite interval ΔU_0; hence, the infinitesimal fraction $d\delta_i$ becomes the finite fraction $\Delta\delta_i$ with an adsorptive energy U_{0i}; the whole surface is considered to be the sum of 50 homotattic patches. Equation 1 then becomes

$$ \theta = \sum_{i=1}^{50} \Delta\delta_i\theta_i \quad (5) $$

To get the computed isotherm, each finite surface patch is treated as an individual homotattic surface of adsorptive energy U_{0i} for which the amount adsorbed, θ_i at a pressure p, can be calculated by equation 2 using

$$ K_i = A^0 \exp(-U_{0i}/RT) \quad (6) $$

The quantity A^0 introduced in equation 6 is defined later in equation 17. A number of Gaussian adsorptive energy distribution curves, calculated by equation 3, for several values of γ, are shown in Fig. 1. In Fig. 2 we report a number of computed isotherms for argon adsorbed as a mobile film at 77.5°K. ($2\alpha/RT\beta = 6.51$), corresponding to the distribution curves shown in Fig. 1. The shape of the adsorption isotherms shown in Fig. 2 can be seen to depend on the following parameters: V_β, which defines θ; γ, which determines the width of the distribution curve; and K', defined by

$$ K' = A^0 e^{-U_0'/RT} \quad (6a) $$

where U_0' fixes the location of the maximum of the distribution curve. The family of curves shown in Fig. 2 vary in shape from the sigmoidal-type that is characteristic of near-homotattic surfaces to the convex-type usually associated with the Langmuir equation, but which now can be seen to arise as a possible description of a mobile adsorbed film on a heterogeneous surface. Almost any experimental isotherm can be expected to match one of these curves; the real test of the theory, therefore, is not so much the fitting of the data alone but also the reasonableness of the constants: (a) as determined by their ability to predict the variation of adsorption with temperature; (b) as revealed by the value of V_β, the monolayer capacity, compared with other estimates; and (c) as compared with other known characteristics of the surface, such as the magnitude of the heat of adsorption or the degree of heterogeneity, which may be known qualitatively as a result of purposeful efforts to obtain a uniform surface, as illustrated by the series of increasingly graphitic carbon blacks (P-33), quoted below.

The computed isotherms differ from experimentally obtained isotherms in that they record the variation of p/K' with θ rather than the experimentally observed p *vs.* V. The purpose of matching experimental with model isotherms is to obtain the appropriate values of K', V_β and γ that will bring the experimental isotherm into coincidence with one of the model isotherms. The process of matching is purely one of trial and error, although by the adoption of simple graphical techniques much labor is avoided.

We are obliged to add to this rule the well-established mathematical convention of the running index in the lower-right postion; *e.g.*, x_i for the *i*th value of x, and extend it to include particular values of a variable, *e.g.*, p_c for critical pressure.

TABLE I

PARAMETERS DERIVED FROM COMPARISONS OF EXPERIMENTAL DATA WITH THE MODEL OF A MOBILE ADSORBED FILM

Adsorbent	Adsorbate	Temp., °K.	$V\beta$ cc. (STP)/g.	V_m reported	Ref. to V_m reported	Method of V_m reported	γ	K'	U' calcd.	U' obsd.	d, e.u.
MT(3100)	Argon	77.5	2.3	.....	...	.....	240	1.89	2.12	2.02	1.2
MT(3100)	Argon	90.1	2.2	.....	...	.....	240	14.8	2.14	2.02	1.4
P-33(2700)	Argon	77.5	3.68	3.60	5(d)	Point B	170	1.90	2.12	2.01	1.3
P-33(2700)	Argon	90.1	3.68	3.46	5(d)	Point B	170	14.8	2.14	2.01	1.5
P-33(2700)	Nitrogen	77.5	3.15	2.86	5(d)	Point B	120	1.30	2.13	2.03	1.2
P-33(2700)	Nitrogen	90.1	3.15	2.72	5(d)	Point B	120	10.3	2.15	2.03	1.4
P-33(2700)	Krypton	90.1	3.41	2.94	5(c)	Langmuir	330	0.45	2.82	3.50	−7.5
P-33(2000)	Argon	77.5	3.65	3.60	9	Point B	100	1.92	2.12	2.13	−0.1
P-33(2000)	Argon	90.1	3.70	.....	...	.....	100	15.7	2.13	2.13	0
P-33(2000)	Nitrogen	77.5	3.10	2.90	9	Point B	70	1.13	2.15	2.09	0.7
P-33(2000)	Nitrogen	90.1	3.05	.....	...	.....	70	9.62	2.17	2.09	.9
P-33(1500)	Argon	77.5	3.7	3.50	5(d)	Point B	30	2.28	2.09	2.05	.5
P-33(1500)	Argon	90.1	3.6	.....	...	.....	30	17.8	2.11	2.05	.7
P-33(1500)	Nitrogen	77.5	3.1	2.95	5(d)	Point B	20	1.39	2.12	2.07	.6
P-33(1500)	Nitrogen	90.1	2.9	.....	...	.....	20	10.2	2.15	2.07	.9
P-33(1000)	Argon	77.5	3.60	3.50	5(d)	Point B	8.5	2.88	2.06	2.13	− .8
P-33(1000)	Argon	90.1	3.60	3.36	5(d)	Point B	8.5	25.0	2.05	2.13	− .9
P-33(1000)	Nitrogen	77.5	3.15	3.00	5(d)	Point B	6.0	1.96	2.06	2.12	− .7
P-33(1000)	Nitrogen	90.1	3.15	2.85	5(d)	Point B	6.0	16.9	2.06	2.12	− .7
P-33(1000)	Krypton	90.1	3.12	2.83	8	Point B	16	0.50	2.80	..	...
BN(Pultz)	Argon	77.5	5.86	5.06	5(d)	Langmuir	310	8.86	1.88	1.85	.4
BN(Pultz)	Argon	90.1	5.11	4.26	5(d)	Langmuir	310	60.0	1.89	1.85	.5
BN(Pultz)	Nitrogen	77.5	4.85	4.23	5(d)	Langmuir	220	7.18	1.86	1.84	.2
BN(Pultz)	Nitrogen	90.1	4.70	3.70	5(d)	Langmuir	220	48.0	1.87	1.84	.4
BN(Winkler)	Nitrogen	77.5	3.12	2.78	10	Langmuir	70	7.18	1.86	1.84	.2
BN(Winkler)	Nitrogen	90.1	3.12	.....	...	.....	70	48.0	1.87	1.84	.4
Linde 13X	Argon	77.5	196	185	11	B.E.T.	22	0.223	2 46	2.24	2.8
Linde 13X	Argon	90.1	196	.....	12, 13	.....	22	2.18	2.48	2.24	2.8
Diamond	Argon	77.2	0.95	0.327	14	B.E.T.	3	330	1.32	..	...
Diamond	Argon	90.0	1.00	.....	...	.....	3	1500	1.32	..	...
Diamond	Nitrogen	77.2	0.86	.350	14	B.E.T.	2	480	1.21	..	...
Diamond	Nitrogen	90.0	0.86	.....	...	.....	2	1850	1.22	..	...
Rutile	Argon	85	33.3	19.4	15	B.E.T.	2	63.5	1.76	1.72	0.5
Rutile	Oxygen	100	34.1	20.6	15	B.E.T.	2	325	1.77	1.91	−1.4
Anatase	Argon	77.5	4.16	.....	...	.....	2	33.0	1.68	..	...

The model isotherms corresponding to the given value of $2\alpha/RT\beta$ chosen for the adsorbate and temperature required are plotted on a large sheet of rectangular coördinate paper as ln p/K' *vs.* ln θ for the series of γ values. The experimental isotherm is plotted with the same scale on a separate sheet of paper as ln p *vs.* ln V. The two sheets of graph paper are superimposed so that the axes are parallel and the curve for the experimental points is interpolated within the family of model isotherms. The positioning of the curve is done by eye. The regularity and closeness of the points of intersection of the model isotherms near θ = 0.4 provides an additional aid to the proper positioning. One usually finds an unambiguous location for the experimental curve. In Fig. 3 is shown a number of these plots of the model isotherms and a superimposed experimental isotherm in its proper interpolated position. The X-Y displacement of the origin of the experimental graph relative to that of the graph of the models measures the scale factors that are required to bring the two sets of axes into coincidence. Thus the distance between the ln p axis and the ln p/K' axis, which is the displacement in the Y direction of the two graphs, is equal to ln $V\beta$; similarly, the distance between the ln V axis and the ln θ axis, which is the displacement in the X direction, is equal to ln K'. The third parameter γ is obtained by the interpolated position of the experimental curve within the family of model isotherms.

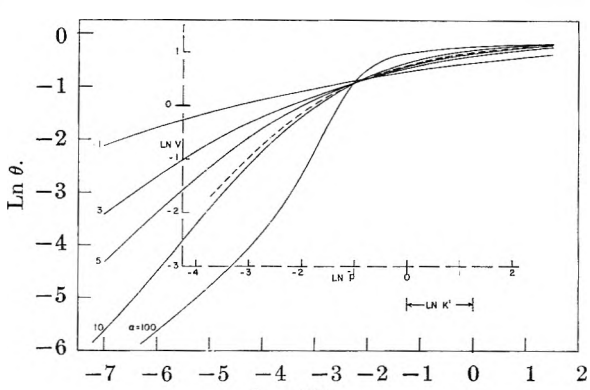

Fig. 3.—Model isotherms (solid lines) and a superposed experimental isotherm (dashed line) in its proper interpolated position.

The parameters γ, $V\beta$ and K', derived from comparisons of experimental data with the model of mobile adsorption, by fitting each particular isotherm separately within the appropriate family of model isotherms, are reported in Table I. The adsorbent designated MT(3100) is a carbon black graphitized at 3100°; the designation P-33 refers to another carbon black graphitized at centigrade temperatures indicated in parentheses. The designation BN refers to boron nitride, of which two different samples have been investigated. Linde 13X is a synthetic zeolite "molecular sieve',

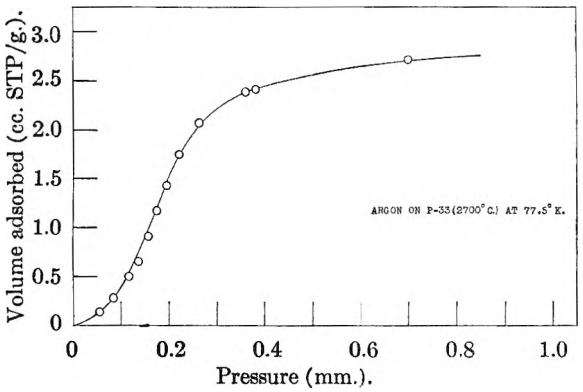

Fig. 4.—Comparison of experimental adsorption isotherms (individual points) with the theoretical description of a mobile adsorbed film (solid line). The parameters used for the calculated curve are reported in Table I.

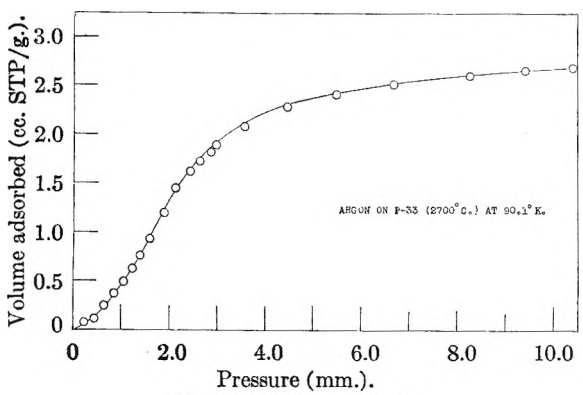

Fig. 5.—Same as Fig. 4.

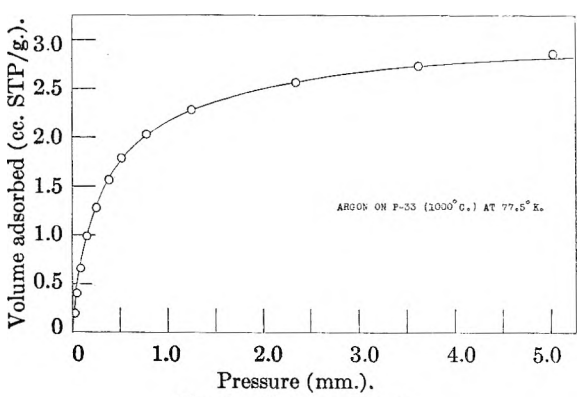

Fig. 6.—Same as Fig. 4.

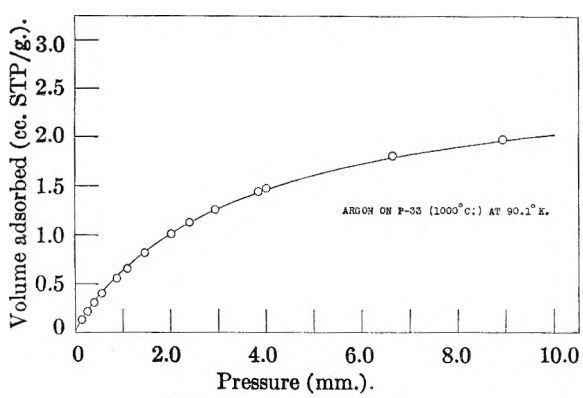

Fig. 7.—Same as Fig. 4.

manufactured by Linde Co. As illustrations of the precision of the theoretical description we submit Figs. 4 to 10. In these diagrams the solid curve is derived from model isotherms that were specially computed for the determined parameters, which are listed in Table I. The circles represent experimental points.

Comparisons between experiment and theory are illustrated by means of two isotherms at different temperatures, which are computed specially for the values of γ, K' and V_β already obtained by the graphical interpolation method described above. The invariance of γ, V_β and U'_0 over the short temperature range of the experiments is a requirement of the theory; and, when actually confirmed on comparison of the experimental and computed isotherms, creates confidence in the values obtained. In Table I we include for this comparison 16 different pairs of isotherms, each pair being isotherms at 77.5 and 90.1°K. for either argon or nitrogen as adsorbate on a given adsorbent. The agreement of the constants γ, V_β and U'(calculated) for each pair is seen to be excellent. Also included in Table I are a few isotherms that are of interest chiefly because they refer to adsorbents that have received attention in important papers by other workers, although suitable data are not available at two temperatures.

The values of V_β for the various adsorbents that are reported in Table I usually differ by less than 20% from estimates of "V_m" that have been derived for the same samples by other methods such as the point B method[16] or the B.E.T. equation.[17] This comparison is included in Table I. The present method of deriving V_β is free from the rather erratic changes with the temperature of adsorption that are occasionally so distressing in the determination of "V_m." Both V_β and "V_m" measure the surface area of an adsorbent; their use to determine this quantity requires different values for the cross-sectional area of the adsorbed molecules: thus, for example, for argon β = 13.6 Å.^{2}; σ_0, as used for the B.E.T. measurement, is 14.6 Å.^{2} at 77°K. and 15.5 Å.^{2} at 90°K.

The monolayer capacity of a solid surface, as determined by the present theory, would not be expected to show a large temperature coefficient since it is dependent on the two-dimensional van der Waals' β, hence on the collision diameters of the adsorbate molecules. In the temperature interval of 12 degrees, between 78 and 90°K., the change in V_β (probably less than 1%) would be unmeasurable. Nothing in the present theory links V_β with the liquid density: the temperature dependence of the distance of closest approach of adsorbed molecules at infinite pressure is much less than would be inferred from the temperature dependence of the density of the liquid.

We can demonstrate, by using the model isotherms as though they represented actual experimental data, that an application of the Langmuir equation yields a value of "V_m" that is smaller than the value of V_β used to generate

(9) W. W. Pultz, Ph.D. Thesis, Rensselaer Polytechnic Institute, 1958.

(10) W. Winkler, Ph.D. Thesis, Rensselaer Polytechnic Institute, 1955.

(11) R. M. Barrer and W. I. Stuart, *Proc. Roy. Soc.* (*London*), **249A**, 464, 484 (1959).

(12) E. S. Chen, unpublished results, R.P.I. laboratory.

(13) E. W. Albers, unpublished results, R.P.I. laboratory.

(14) V. R. Deitz, unpublished results, National Bureau of Standards.

(15) J. A. Morrison, J. M. Los and L. E. Drain, *Trans. Faraday Soc.*, **47**, 1023 (1951); L. E. Drain and J. A. Morrison, *ibid.*, **48**, 840 (1952); **49**, 654 (1953).

(16) S. Brunauer and P. H. Emmett, *J. Am. Chem. Soc.*, **57**, 1754 (1935); P. H. Emmett and S. Brunauer, *ibid.*, **59**, 1553 (1937).

(17) S. Brunauer, P. H. Emmett and E. Teller, *ibid.*, **60**, 309 (1938).

the curves; and that the discrepancy becomes greater as the surface is more heterogeneous (*i.e.*, lower values of γ). The model isotherms will give a straight Langmuir plot (p/V *vs.* p) above 0.4 coverage: the values of "V_m," however, derived from the straight lines are always too low, ranging from about 88% of the correct value for the less heterogeneous substrates down to 75% of the correct value for the most heterogeneous substrate. These findings are of value to future investigators as they reveal the disquieting fact that the Langmuir equation can be used to describe isotherms derived from a totally different model, and that the constants thereby determined, which include the important one of monolayer coverage, V_m, are always seriously in error. Nothing could be further removed from the present model than the Langmuir model: the former postulates interaction, heterogeneity of substrate and a mobile adsorbed film; whereas the latter postulates no interaction, homogeneity of substrate and a localized adsorbed film. We have here the clearest possible proof that merely to find data that fit the Langmuir equation cannot be accepted as any indication that the Langmuir model is a description of the physical situation. Since the B.E.T. theory is based on the Langmuir equation, we expect to find, as indeed in all instances we do find, that the B.E.T.-derived value of "V_m" is lower than our V_β; and that this discrepancy is the greater with the more heterogeneous substrates.

The adsorptive energy distribution of a solid surface has been mentioned by previous authors and a number of such distribution curves, based on one method or another, have been published.[13] Where these distributions of potential energies have been determined for the same surface at different temperatures the answers that were proffered were not constant: this is a sure indication of an error inherent in the method. In no case, moreover, has any means been provided that would furnish an independent check of the proposed distribution. The present method offers the possibility of such an independent check, as the distribution curve derived from one adsorption isotherm can be used to predict adsorption isotherms at other temperatures. These predictions are confirmed in so many experimental systems that the distributions assigned can be claimed with a high degree of probability to represent a real physical property of the adsorbent surfaces.

We cannot offer any external or independent comparison of the values of γ assigned to the adsorbents in Table I, since this is the first time that surface heterogeneity has been measured in terms of a Gaussian distribution; nevertheless the values of γ give reasonable widths to the distribution curves, as measured by the relation

$$r = 477\sqrt{1/\gamma}$$

where one-half of the surface is within $\pm$ r calories of the mean value U'_0. In addition, the sequence of the values of γ for the graphitized carbon blacks shows the expected trend toward surface uniformity with increasing temperature of graphitization.

We shall now relate U_0 to the more familiar heats of adsorption: q^{diff}, the differential heat of adsorption, and q^{st}, the isosteric heat of adsorption; which have been defined and discussed by Hill.[19]

$$q^{diff} = {}_\theta{}^pE - {}_a{}^\theta E - \theta\left[\frac{\partial({}_a{}^\theta E)}{\partial\theta}\right]_{T,\Sigma}$$

and

$$q^{st} = q^{diff} + RT \qquad (7)$$

For the particular case of a two-dimensional van der Waals' gas as the adsorbed phase, and a homotattic substrate

$$\left[\frac{\partial({}_a{}^\theta E)}{\partial\theta}\right]_{T,\Sigma} = -\frac{\alpha}{\beta} \qquad (8)$$

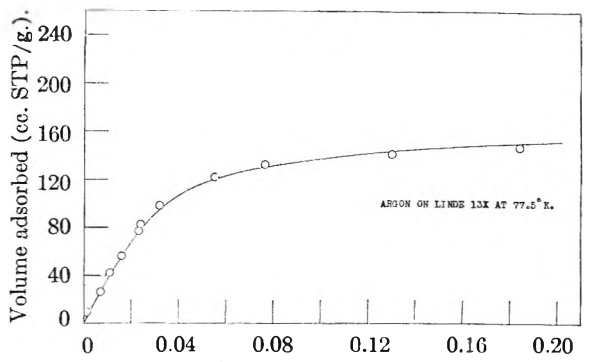

Fig. 8.—Same as Fig. 4.

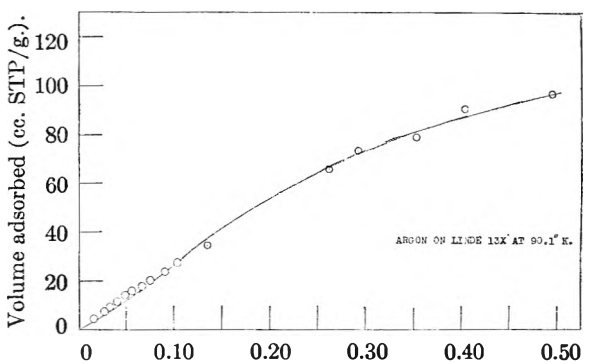

Fig. 9.—Same as Fig. 4.

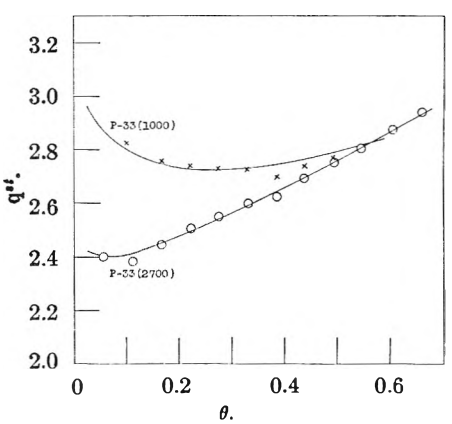

Fig. 10.—Isosteric heat curves for argon adsorbed on carbon blacks, as calculated by the computer from values of γ, v_β and K' (reported in Table I) by the present theory (solid line), compared with the isosteric heats calculated by the Clausius–Clapeyron equation from the experimental isotherms (individual points).

(18) (a) W. D. Harkins and R. S. Stearns, *J. Phys. Chem.*, **58**, 292 (1954); (b) Ref. 15 above; (c) J. J. Chessick and A. C. Zettlemoyer, *J. Phys. Chem.*, **62**, 1217 (1958); (d) J. P. Olivier and S. Ross, "Second International Congress of Surface Activity," Vol. 2, Academic Press, Inc., New York, N. Y., 1957, pp. 46–53 and p. 206; (e) S. Umeda, S. Teranishi and K. Tarama, *Bull. Inst. Chem. Research, Kyoto Univ.*, **32**, 109 (1954); (f) J. M. Honig and L. H. Reyerson, *J. Phys. Chem.*, **56**, 140 (1952).

(19) T. L. Hill, *J. Chem. Phys.*, **17**, 520 (1949).

hence

$$q^{\mathrm{diff}} = {}_{g}{}^{p}E - {}_{a}{}^{\theta}E + \frac{\alpha\theta}{\beta} \qquad (9)$$

Integrating equation 8 between limits

$$\int_{{}_{a}{}^{0}E}^{{}_{a}{}^{\theta}E} \mathrm{d}({}_{a}{}^{\theta}E) = -\frac{\alpha}{\beta}\int_{0}^{\theta} \mathrm{d}\theta$$

hence

$${}_{a}{}^{\theta}E = {}_{a}{}^{0}E - \frac{\alpha\theta}{\beta} \qquad (10)$$

Combining equation 10 with equations 4, 7 and 9 gives

$$q^{\mathrm{diff}} = {}_{g}{}^{p}E - {}_{a}{}^{0}E + \frac{2\alpha\theta}{\beta} = U_0 - ({}_{a}\bar{E}^{\mathrm{vib}} - {}_{a}E_0{}^{\mathrm{vib}}) - \Delta E^{\mathrm{kin}} + \frac{2\alpha\theta}{\beta} \qquad (11)$$

and

$$q^{\mathrm{st}} = q^{\mathrm{diff}} + RT = U_0 - ({}_{a}\bar{E}^{\mathrm{vib}} - {}_{a}E_0{}^{\mathrm{vib}}) - \Delta E^{\mathrm{kin}} + RT + \frac{2\alpha\theta}{\beta} \qquad (12)$$

if we assume that ${}_{g}{}^{p}E = {}_{g}{}^{0}E$ (true for most gases).

Considering now heterogeneous surfaces as defined by the computed model, by use of the relations

$$\mathbf{U}_0{}^{\mathrm{int}} = \sum \Delta\, \delta_i\theta_i U_{0i}$$

and

$$\mathbf{U}_0 = \Delta\mathbf{U}_0{}^{\mathrm{int}}/\Delta\theta$$

the computer can produce both integral and differential adsorptive energies, $\mathbf{U}_0{}^{\mathrm{int}}$ and $\mathbf{U}_0$, respectively, as a function of θ. Similarly, the differential heat of lateral (adsorbate–adsorbate) interaction on an heterogeneous surface is given by

$$\sum \Delta\delta_i\theta_i \frac{2\alpha}{\beta} = \frac{2\alpha\theta}{\beta}$$

For the heterogeneous surface, therefore, the definitions give by equations 11 and 12 become

$$\mathbf{q}^{\mathrm{diff}} = \mathbf{U}_0 - ({}_{a}\bar{E}^{\mathrm{vib}} - {}_{a}E_0{}^{\mathrm{vib}}) - \Delta E^{\mathrm{kin}} + \frac{2\alpha\theta}{\beta} \qquad (11\mathrm{A})$$

and

$$\mathbf{q}^{\mathrm{st}} = \mathbf{U}_0 - ({}_{a}\bar{E}^{\mathrm{vib}} - {}_{a}E_0{}^{\mathrm{vib}}) - \Delta E^{\mathrm{kin}} + RT + \frac{2\alpha\theta}{\beta} \qquad (12\mathrm{A})$$

Our experience with the computed isotherms has shown us a useful mathematical approximation: namely, that at $\theta = 0.4$, $\mathbf{U}_0 = U'_0$ (see Fig. 2). If experimental isotherms are measured at two temperatures not too far apart, the isosteric heat corresponding to U'_0, which we designate $\mathbf{q}^{\mathrm{st}}$ at $\theta = 0.4$, then can be determined with sufficient accuracy by the Clausius–Clapeyron equation

$$\mathbf{q}^{\mathrm{st}}(\mathrm{at}\,\theta = 0.4) = \left[R\left(\frac{T_2 - T_1}{T_2T_1}\right)\left(\ln\frac{p_2}{p_1}\right)\right]$$

Then, by equation 12A

$$U'_0 = \mathbf{q}^{\mathrm{st}}(\mathrm{at}\,\theta = 0.4) - R\left(\frac{2T_1T_2}{T_2 + T_1}\right) + ({}_{a}\bar{E}^{\mathrm{vib}} - {}_{a}E_0{}^{\mathrm{vib}}) + \Delta E^{\mathrm{kin}} - \frac{0.8\alpha}{\beta} \qquad (13)$$

We do not at present, for the adsorption systems listed in Table I, have sufficient information to calculate U'_0 exactly by the above equation. For our present purpose, therefore, we shall make the following assumptions: (a) at the low temperatures referred to in Table I the adsorbed molecules are mostly in their ground state of vibration; hence

$${}_{a}\bar{E}^{\mathrm{vib}} = {}_{a}E_0{}^{\mathrm{vib}} \qquad (14)$$

(b) the translational energy per mole of a molecule in the gas phase is given by $^3/_2RT$, and in the adsorbed phase by $^2/_2RT$; that is, the adsorbed phase behaves as a two-dimensional gas: further, for argon, nitrogen and oxygen we make the reasonable assumption that no change takes place in the rotational energy on adsorption; therefore

$$\Delta E^{\mathrm{kin}} = -\frac{1}{2}RT \qquad (15)$$

Equation 13 then becomes

$$U'_0 = \mathbf{q}^{\mathrm{st}}(\mathrm{at}\,\theta = 0.4) - \frac{3}{2}R\left(\frac{2T_1T_2}{T_1 + T_2}\right) - \frac{0.8\alpha}{\beta} \qquad (16)$$

These approximate values of U_0', calculated by equation 16, are listed in Table I, where available, as U'(observed).

Using the values of γ, V_β and U'(observed) determined for argon on P-33 (2700°) and P-33 (1000°), reported in Table I, the computer gives us $\mathbf{U}_0$, and hence, by equations 12A, 14 and 15, gives us $\mathbf{q}^{\mathrm{st}}$ as a function of θ. These computed isosteric heats are shown in Fig. 10 by the solid lines; the observed isosteric heats determined from the adsorption isotherms are shown in the same diagram as individual points. The agreement between the heat curves predicted by our model and those observed is again striking, and shows that the parameters obtained by our method of curve-fitting are not merely empirical quantities but quantitative measurements of physical constants of the system.

For further comparisons, the theory will provide us with a U'_0 from the determined value of K' only if we have a correct value of A^0 to insert in equation 6A. For the mobile adsorbed film of isometric molecules adsorbed on any homotattic patch of the surface, as described by equation 2, A^0 is given by the relation

$$\ln A^0 = -\frac{\Delta S_s}{R} + \frac{\Delta E^{\mathrm{kin}}}{RT} - \ln\frac{\theta_s}{1 - \theta_s} - \frac{\theta_s}{1 - \theta_s} + \ln p_s \qquad (17)$$

In this equation, ΔS_s is the standard differential entropy change between the gas molecules in their standard state (p_s) and the adsorbate in its standard state (θ_s). For these standard states we follow de Boer and Kruyer[20] in putting $\theta_s = \beta/4.08T$ and $p_s = 1$ atm. ΔE^{kin} is the kinetic energy change of the adsorbate molecules on transferring from the gas to the adsorbed state; we shall again assume $\Delta E^{\mathrm{kin}} = -{}^1/_2RT$.

ΔS_s also should take into account the loss of translational and rotational degrees of freedom, as well as any vibrational entropy in the adsorbed state; *i.e.*

$$\Delta S_s = \Delta S_s{}^{\mathrm{tr}} + \Delta S_s{}^{\mathrm{rot}} + {}_{a}S^{\mathrm{vib}}$$

For the systems and temperatures we consider here $\Delta S_s{}^{\mathrm{rot}}$ and ${}_{a}S^{\mathrm{vib}}$ are neglected by analogy with

(20) J. H. de Boer and S. Kruyer, *Koninkle. Ned. Akad. Wetenschap. Proc.*, **55B**, 451 (1952); **56B**, 67, 236, 415 (1953); **57B**, 92 (1954); **58B**, 61 (1955).

the energy terms, as a good approximation; ΔS_s^{tr} is calculated by the application of the Sackur–Tetrode equation to give[4]

$$-\Delta S_s^{tr} = \ln M + \ln T + 2.31$$

For argon at 77.5°K., $\Delta S_s = \Delta S_s^{tr} = -10.3$ e.u.; hence, by equation 17, $A^0 = 1.67 \times 10^6$ mm.; the corresponding calculation for nitrogen at 77.5°K. yields $A^0 = 1.40 \times 10^6$ mm. By means of these idealized values of A^0 and the experimentally determined values of K' we can use equation 6A to obtain an approximate value of U_0', which is listed in Table I as U'(calculated).

The difference between the values of U', calculated and observed, measures the departure of the behavior of the actual adsorbed film from the idealized concept of the kinetic state of the adsorbed molecule. We express this deviation in Table I, for the systems where the requisite data are available, as

$$d = \frac{U'_{(calcd)}}{T} - \frac{U'_{(obsd)}}{T} = \Delta S_{s(obsd)} - \Delta S_{s(model)}$$

Where $-\Delta S_s$(obsd) is less than $-\Delta S_s$(model) the difference can be ascribed to entropy of vibration of the adsorbate molecule with respect to the surface, although other factors exist that influence the entropy. The limited temperature range of the data considered in Table I does not allow our pressing too rigorously the significance of these relatively slight deviations of entropy. The closeness of ΔS_s(obsd) to ΔS_s(model) is, however, a reflection once more of the validity of the present model as a description of these systems.

The adsorptive energy distribution may not have a form that is symmetrical about a mean; it could possess enough asymmetry to defy description by means of the Gaussian equation 4. Examples of this type have been discovered[21] and will be reported later.

Acknowledgment.—The authors gratefully acknowledge a grant-in-aid of this research from Esso Research and Engineering Company, Linden, N. J.

(21) J. P. Olivier, Ph.D. Thesis, Rensselaer Polytech. Inst., 1960.

HIGH TEMPERATURE MAGNETIC SUSCEPTIBILITIES Of MnO, MnSe AND MnTe[1]

By John J. Banewicz, Robert F. Heidelberg and Allan H. Luxem

Southern Methodist University, Dallas, Texas

Received August 22, 1960

The magnetic susceptibilities of specimens of MnO, MnSe and MnTe were measured by a Faraday method at temperatures from 300 to above 1200°K. Using only the data above 600°K., the values of C_m and θ in the Weiss–Curie relationship were obtained. The Curie constants for both MnO and MnSe were less than the theoretical spin only value of 4.38. It is suggested that the low value of C_m is due to the overlap of 3d electrons on adjacent Mn^{++} ions with partially compensating spins.

I. Introduction

A recent determination of the high temperature magnetic susceptibility of sintered MnS has given a value of the Curie constant of 3.94 in the region between 675 and 1244°K.[2] This is considerably below the 4.38 expected for five unpaired electrons. An examination of the published data for the other antiferromagnetic compounds of manganese and the Group VI elements indicated a possible downward trend in the value of C_m for the members of this series with increasing chalkogen atomic weight.

However, in most cases the susceptibility measurements on these compounds were made at temperatures less than 500°K. There is some doubt as to whether the results were sufficiently far above the Néel temperature to validly fit the Weiss–Curie equation. It seemed worthwhile, therefore, to determine the magnetic susceptibilities of this family in the region above 600°K. to obtain values of C_m to compare with that recently determined for MnS.

II. Experimental

A. Measurement of Susceptibilities.—Susceptibilities were determined by a Faraday method[3] using a Sartorious balance as previously described. Instead of using sintered specimens, powder samples ranging from 60 to 120 mg. were sealed in evacuated Vycor capsules in the shape of miniature Florence flasks. The diamagnetic susceptibilities of several empty capsules were determined to evaluate the magnitude of the capsule corrections to be applied. In all cases the corrections were less than 1%. Measurements were made at field strengths of approximately 800 and 1500 Oersteds corresponding to values of $H(dH/dx)$ from 1 to 5×10^6.

B. Preparation of Samples.—$MnCO_3$ has been reported to decompose to form MnO at around 500° in the absence of air. Either because of traces of moisture in the $MnCO_3$ or the reduction of CO_2 to CO by the MnO_2,[4] the green oxide formed in this fashion was visibly contaminated by traces of brown higher oxides. Therefore the decomposition of $MnCO_3$ was caused to take place at around 600 in a stream of oxygen-free hydrogen. The resulting compound was a fine powder, greyish green in color. An analysis of two different batches gave 77.1 and 77.4 as the % Mn present, as compared with 77.4% theoretical. The active oxygen in both batches was found to be less than 0.1%. It is interesting to note that after twelve months storage in a stoppered test-tube the per cent. active oxygen in one of the batches was only about 0.2%. The MnO was found to have the NaCl type structure with "*a*" equal to 4.446 Å., in good agreement with the value reported in the literature.[5]

MnSe was made by the reaction of stoichiometric amounts o

(1) Assisted by a grant by the National Science Foundation.

(2) J. J. Banewicz, R. F. Heidelberg and R. Lindsay, *Phys. Rev.*, **117**, 736 (1960).

(3) P. W. Selwood, "Magnetochemistry," Interscience Publishers, New York, N. Y., 1956.

(4) N. V. Sidgwick, "Chemical Elements and their Compounds," Oxford, 1950, Vol. II, p. 1284.

(5) Swanson, *et al.*, NBS Circular 539, **5**, 45 (1955), ASTM Card 7-230.

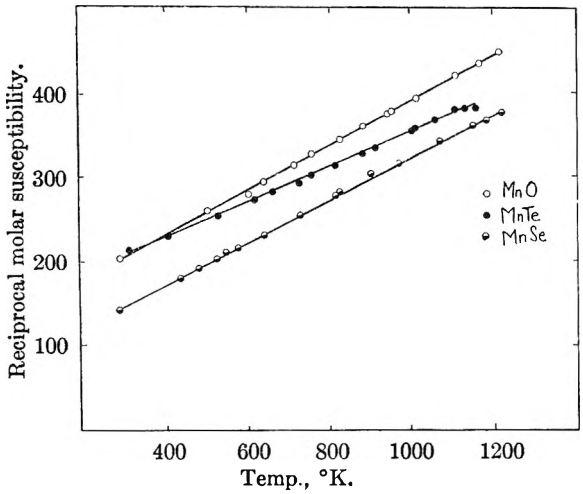

Fig. 1.—Reciprocal molar susceptibilities of MnO, MnSe and MnTe as functions of temperature.

Mn sponge (99.9%) and ground Se (99.999%) sealed in an evacuated Vycor capsule. The reaction vessel was heated slowly in a Bunsen burner flame to initiate the reaction. The MnSe was then further heated in an electric furnace at 900° for several days. The contents of the Vycor capsule were removed, ground and again heated at 900°. The analysis of the final MnSe gave 40.9% Mn as compared with 41.0% theoretical. The powder X-ray diffraction pattern showed it had a NaCl structure, as previously reported,[6] with "*a*" equal to 5.457 Å.

The procedure followed for the synthesis of MnTe was the same as for MnSe with the substitution of Te (99.99%) for Se. Some difficulty was experienced with the Vycor reaction vessel being attacked, in the first preparation to such an extent that rupture occurred and the contents had to be discarded. The final preparation was made in a partial helium atmosphere in a double walled Vycor vessel. The % Mn found was 30.0% as compared with the theoretical 30.1 %. MnTe was found to have the NiAs structure with "*a*" equal to 4.14 A., "*c*" equal to 6.70 Å.[7]

III. Results

The reciprocal molar susceptibilities *versus* temperature results are shown in Fig. 1.

The susceptibility of MnSe was field dependent up to about 400°. The points shown in this region have been extrapolated to infinite field strength. The molar susceptibilities were corrected for the diamagnetism of the constituent ions before Fig. 1 was plotted. The gram ion corrections applied were 26×10^{-6} for MnO, 62×10^{-6} for MnSe and 84×10^{-6} for MnTe.[2] Two different batches of MnO were prepared and measured; only one of these is represented in Fig. 1.

A summary of the Weiss–Curie constants obtained from the data above 600°K. is given in Table I. The data were fitted to the Weiss–Curie law by a least squares method using a Univac Scientific 1153 computer.

IV. Discussion

In the case of MnO, the Curie constant found is considerably lower than that reported by Johnston and Heikes[8] or Bhatnagar.[9] However, lower values have been reported previously.[10] Bhatnagar's room temperature value for the gram susceptibility of MnO is considerably higher than that reported by other workers and his results therefore are questionable.

TABLE I

THE WEISS–CURIE CONSTANTS C_m AND θ CALCULATED FROM THE EXPERIMENTAL DATA ABOVE 600°K.

Substance	% Mn Found	% Mn Theoretical	C_m	θ	Δ[a]
MnO (1)	77.4	77.4	3.78	461	1.3
MnO (2)	77.1	77.4	3.68	430	1.0
MnS[1]	62.9	63.1	3.94	397	..
MnSe	40.9	41.0	4.02	297	1.9
MnTe	30.0	30.1	4.46	584	1.3

[a] Δ is the standard deviation of the experimental points from the fitted line in the reciprocal molar susceptibility *versus* temperature plot.

The value of C_m for MnSe is in good agreement with that reported by Serres.[11]

The constants for MnTe are between the values obtained by Serres[11] and Uchida.[12] The value of C_m is close to that expected for 5 unpaired electrons. At around 830° the susceptibility of MnTe levels off abruptly probably because of some sort of phase transformation.

The data reported here indicate that, contrary to the results in reference 2, as the ionic character decreases, the value of C_M becomes closer to that expected for 5 unpaired electrons. There are several explanations which might be offered for this. It has been suggested previously[13] that, due to the persistence of short range order, the value of C_M for antiferromagnetics is to some extent a function of temperature being largest close to the Néel temperature, and becoming smaller as the temperature increases. In this case, the value of C_m observed for a particular family of compounds in the same temperature region should increase with increasing Néel temperature. This is the case for the manganese Group VI family.

The first three members of the family, MnO, MnS and MnSe, have the NaCl type structure. The distance of separation of the closest Mn^{++} ions increases over 20% as the size of the negative ion increases from O^{--} to Se^{--}. Therefore any overlap of 3d electrons which might result in partially compensating spins would also decrease with increasing negative ion size.

It is possible to analyze the data on MnO, MnS and MnSe in terms of the molecular field theory of antiferromagnetism and estimate the exchange energies corresponding to first and second nearest neighbor interactions. For these substances, which crystallize in the NaCl type structure and have antiferromagnetic ordering of the second kind, the exchange energies are given by[14]

$$J_{nn}/k(°K.) = \frac{(\theta - Tn)}{8S_0(S_0 + 1)} \qquad (1)$$

(6) E. Broch, *Z. physik. Chem.*, **127**, 446 (1927).

(7) I. Oftedal, *ibid.*, **128**, 135 (1927).

(8) W. D. Johnston and R. R. Heikes, *J. Am. Chem. Soc.*, **78**, 3255 (1956).

(9) Bhatnagar, Cameron, Harboard, Kapur, King and Prakash, *J. Chem. Soc.*, II, 1433 (1939).

(10) (a) Theodorides, *Compt. rend.*, **171**, 948 (1920); (b) Tyler, *Phys. Rev.*, **44**, 776 (1933).

(11) A. Serres, *J. phys. radium*, **8**, 146 (1947).

(12) Uchida, Kondoh and Fukuoka, *J. Phys. Soc. Japan*, **11**, 27 (1956).

(13) R. Lindsay and J. Banewicz, *Phys. Rev.*, **110**, 634 (1958).

(14) P. W. Anderson, *ibid.*, **79**, 705 (1950); J. S. Smart, *ibid.*, **86**, 968 (1952).

$$J_{nnn}/k(°K.) = \frac{T_n}{4S_0(S_0 + 1)} \quad (2)$$

where J_{nn} is the exchange interaction between nearest neighbors, J_{nnn} is the exchange interaction between next nearest neighbors, k is the Boltzmann constant, θ is the Curie–Weiss constant, T_n is the Néel temperature, and S_0 is the spin quantum number of the magnetic atom. It can be seen easily that the ratio of J_{nn} to J_{nnn} depends only on the ratio of θ to T_n.

$$\frac{J_{nn}}{J_{nnn}} = \frac{1}{2}\left(\frac{\theta}{T_n} - 1\right) \quad (3)$$

Table II gives the results obtained for J_{nn}/k, J_{nnn}/k and J_{nn}/J_{nnn} when available experimental data on θ and T_n are substituted.

TABLE II

Compound	S_0	θ (°K.)	T_n (°K.)	θ/T_n	J_{nn}/k (°K.)	J_{nnn}/k (°K.)	J_{nn}/J_{nnn}
MnO	5/2	461[a]	116[b]	3.78	4.9	3.3	1.4
MnS	5/2	397[c]	154[c]	2.58	3.5	4.4	0.8
MnSe[f]	5/2	297[a]	247[d]	1.20	0.7	7.0	0.1
	5/2	297[a]	130[e]	2.29	2.4	3.7	0.6

[a] This work. [b] H. Bizette, C. Squire, C. Tsai and B. Tsai, *Compt rend.*, 207, 449 (1938). [c] Ref. 2. [d] K. K. Kelley, *J. Am. Chem. Soc.*, 61, 203 (1939). [e] Average of values taken from cooling curves by: H. Bizette and B. Tsai, *Compt rend.*, 212, 75 (1941); R. Lindsay, *Phys. Rev.*, 84, 569 (1951). [f] A thermal hysteresis in the susceptibility *versus* temperature relation complicates the situation in MnSe. T_n on the first line of data is obtained from specific heat data on a warming curve from 54°K. T_n on the second line is estimated from magnetic susceptibility data on cooling curves down from room temperature. See ref. *e* for further description of this phenomenon.

The molecular field theory is the simplest approximation of the Heisenberg–Dirac model for coöperative magnetic phenomena and does not take into account short range ordering effects. There is probably considerable uncertainty in the absolute values of the J's derived by this method because it does overestimate the Néel temperature in comparison with other more rigorous approximations of the Heisenberg–Dirac model.[15] Despite the uncertainty, however, it is felt that the ratios of these J's are a meaningful measure of the relative strengths of the interactions in the compounds listed. In this connection it is interesting to note that a recent theoretical calculation by Casselman and Keffer[16] of the overlap integral between anion p^3 orbitals and cation 3d oribitals (at right angles) leads to a ratio of J_{nn}/J_{nnn} 1.5 for MnO which agrees quite well with the value reported in Table II.

MnTe has the NiAs structure, on the other hand, so perhaps it should be discussed separately. Pearson[17] already has discussed the abnormally high resistivity of MnTe as compared with other compounds of NiAs group. He has suggested that the explanation for this is the lack of overlap of the 3d subshells of the Mn^{++} ions in this compound which would cause it to be semiconducting instead of metallic in its properties. It is worth noting that he has proposed a structure for MnTe in which Mn^- and Te^+ ions exist involving resonating p^3 bonds with the 3d electrons of the manganese not concerned in the chemical bonding.

Acknowledgment.—The authors wish to express their appreciation to Dr. Paul D. Minton of the Southern Methodist University Computing Laboratory for carrying out the least squares calculations, and to Dr. Robert Lindsay of Trinity College, Hartford, Connecticut, to whom we are indebted for the section on Molecular Field Theory.

(15) J. S. Smart, *J. Phys. Chem. Solids*, **11**, 97 (1959).

(16) T. N. Casselman and F. Keffer, *Phys. Rev. Letters*, **4**, 498 (1960).

(17) W. B. Pearson, *Can. J. Phys.*, **35**, 886 (1957).

INFRARED STUDIES OF CARBON MONOXIDE CHEMISORBED ON NICKEL AND ON MERCURY-POISONED NICKEL SURFACES[1]

BY J. T. YATES, JR., AND C. W. GARLAND

Department of Chemistry and Spectroscopy Laboratory, Massachusetts Institute of Technology, Cambridge 39, Massachusetts

Received September 24, 1960

The infrared spectrum of CO chemisorbed on alumina-supported Ni surfaces has been investigated in the region from 1700 to 2400 cm.$^{-1}$. Full coverage spectra clearly show that the character of the Ni surface is a function of the Ni concentration; Ni surfaces ranging from a compact crystalline type to a dispersed type have been observed. Adsorption of CO on crystalline Ni sites occurs initially at very low pressures giving two surface species—a bridged CO between two adjacent Ni atoms, and a linear CO bonded to one surface Ni atom. At higher pressures it is proposed that CO is adsorbed as a bridged CO species between Ni atoms already having adsorbed linear CO species. On more dispersed Ni sites, CO is weakly adsorbed as a single linear species and the strength of adsorption decreases as the Ni atoms become less compactly arranged. The effect of Hg poisoning of a Ni surface on the chemisorption of CO has been investigated also.

I. Introduction

An infrared spectrum of CO chemisorbed on a silica-supported Ni sample has been reported by Eischens, Francis and Pliskin,[2] and Garland[3] has studied the effect of CS_2 poisoning on the infrared spectrum of CO adsorbed on alumina-supported Ni samples. A more extensive infrared study of CO chemisorbed at room temperature on finely divided Ni is reported below. The Ni was supported on a high-area alumina and the concentration of Ni in the samples was varied over a wide range (1.5–25% Ni by weight).

(1) Taken from the thesis of John T. Yates, Jr., Department of Chemistry, M.I.T., in partial fulfillment of the requirements for the degree of Doctor of Philosophy.

(2) R. P. Eischens, S. A. Francis and W. A. Pliskin, *J. Phys. Chem.*, **60**, 194 (1956).

(3) C. W. Garland, *ibid.*, **63**, 1453 (1959).

II. Experimental

Instrumental.—The infrared cell used in this work has been described in detail previously.[4] In essence it is a cylin-

drical Pyrex cell of 150-cc. volume with CaF_2 windows. The sample is supported on a 30 mm. diameter CaF_2 plate which is mounted at the center of the cell.

The modified Perkin–Elmer 12C spectrometer described by Yang and Garland[4] has been further modified so as to use the CaF_2 prism in combination with a 150 lines/mm. grating (blazed at 4.5 μ in the first order) mounted in the Littrow mirror position. Small shifts in the frequency of the absorption bands are more easily observed as a result of the increased dispersion obtained with this arrangement. Also, slit widths larger than those employed with a prism alone can be used with no sacrifice in resolution. Thus it becomes feasible to study weaker bands by using thicker samples. A Kodak 230 filter (40% transmission at 5 μ opaque at 3 μ) was placed over the exit slit to remove higher orders of the grating.

Sample Preparation.—Supported Ni samples were prepared as follows: A weighed amount of $Ni(NO_3)_2 \cdot 6H_2O$, Mallinckrodt A. R. Grade, was dissolved in a small volume of distilled water. Reagent grade acetone was added to the solution and a weighed amount of Alon C (a non-porous alumina[5]) was added with shaking. The final slurry contained about 4 g. of Alon C per 100 cc. of solution, and the solvent was between 20 and 22% distilled water by volume. The slurry was shaken for a few minutes and then transferred to an atomizer-spraying apparatus. Here the slurry was continuously mixed to prevent sedimentation. A fine spray was directed toward several weighed CaF_2 plates which were heated to 60–80° on a micro hot plate. A uniform coherent deposit was produced by adjusting the pressure of the carrying gas so that most of the water and acetone evaporated in the spray before it reached the heated plates.

A sample plate was then transferred to the infrared cell and the sample was dried by heating *in vacuo* at 150° for one hour. The temperature was then raised to 300° (at this point the sample becomes black due to the formation of nickel oxide). The sample was reduced at 300° using hydrogen gas at 150 mm. pressure. After one hour of reduction the cell was degassed for 0.25 hour. A second hydrogen reduction was then carried out for several hours followed by degassing for several hours. Finally the sample was treated for 12–18 hours more with hydrogen. It was then degassed for 3 hours at 300° and allowed to cool to room temperature.

The "density" of the Ni-alumina deposits used in this work ranged from about 15 to 50 mg./cm.^{2} after reduction.

Recording of Spectra.—After the sample had been reduced a background spectrum was recorded over the spectral region from 1700 to 2400 cm.$^{-1}$. All spectra have been plotted as absorbance values, $-\ln I/I_0$, where I_0 is the recorder deflection from 0% transmission to the background curve, and I is the deflection from 0% transmission to the spectral curve produced by adsorption of CO.

X-Ray Studies.—In order to determine the extent of crystallinity existing in the Ni samples used in this work, X-ray powder photographs were obtained for a 25% Ni sample, a 10% Ni sample and the Alon C support alone. Only the 25% Ni sample gave any evidence of containing crystalline Ni particles; this sample gave broad lines corresponding to the three most intense lines observed for bulk Ni samples (d = 2.034, 1.762, 1.246 Å.). From an examination of the line widths obtained, we estimate that the average Ni crystallite size is 38 Å. for the 25% Ni sample.[6,7]

III. Results and Discussion

It is convenient for the presentation of results and discussion to divide the spectral region investigated into five frequency regions which are defined in Table I. We shall show that a CO adsorption band is found to occur in each region for the higher concentration Ni samples. Therefore, the approximate band centers are also shown at this time in Table I.

(4) A. C. Yang and C. W. Garland, *J. Phys. Chem.*, **61**, 1504 (1957).

(5) Alon C is a product of Godfrey L. Cabot, Inc., Boston 10, Mass. We wish to thank Mr. K. A. Loftman for providing a sample with a B.E.T. area of 90 m.^{2} g.$^{-1}$.

(6) W. H. Bragg and W. L. Bragg, "The Crystalline State," Vol. 1, G. Bell and Sons, Ltd., London, 1955, p. 189.

(7) B. E. Warren and J. Biscoe, *J. Am. Ceramic Soc.*, **21**, 49 (1938).

TABLE I

FIVE FREQUENCY REGIONS DEFINED FOR CONVENIENCE IN DISCUSSING THE INFRARED SPECTRUM OF CO CHEMISORBED ON NICKEL AT ROOM TEMPERATURE

For 10 and 25% Ni samples a band is observed in each region; the approximate centers of these bands are shown in the last column

Region	Frequency interval, cm.$^{-1}$	Band center, cm.$^{-1}$
A	1850–1940	1915
B	1940–1990	1963
C	1990–2050	2035
D	2050–2070	2057
E	2070–2110	2082

Bands which lie above 2000 cm.$^{-1}$ have been assigned by Eischens, *et al.*,[2] to CO species with the CO bonded to a single Ni atom, as in $Ni(CO)_4$, and this type of bonding is designated as *linear*. Bands below 2000 cm.$^{-1}$ were assigned to CO species with the CO bonded between two Ni atoms in a bridge fashion. This generalized assignment is made on the basis that the linear carbonyl groups of metal carbonyls[8] and their derivatives[9] absorb in the region 1988–2080 cm.$^{-1}$, while metal carbonyls containing bridging CO groups have carbon–oxygen stretching frequencies below 2000 cm.$^{-1}$ (1828–1860 cm.$^{-1}$).

It should be noted that the analogy in frequencies between metal carbonyls and chemisorbed CO is good for linear CO species (bands in regions C, D and E lie at 2035, 2057 and 2082 cm.$^{-1}$, respectively) but poor for bridge CO species (bands in regions A and B lie at 1915 and 1963 cm.$^{-1}$, respectively). This discrepancy is to be expected since the frequency of bridge carbonyl groups is a function of the angle between the carbon–metal bonds[10]; the frequency of the bridge species should therefore be sensitive to the interatomic distance of the Ni atoms, and this distance would not be expected to be the same as the metal–metal distance in metal carbonyls.

A 25% Ni sample supported on *silica* (Cabosil) and prepared in the same fashion as our alumina-supported samples showed excellent agreement at full coverage with the band center frequencies given in Table I for regions B, C, D and E. Comparison of the frequency of the weak broad band in region A is difficult due to the presence of a broad background band in this region for silica-supported Ni samples. However, it seems that the band produced in region A by adsorption of CO on silica-supported Ni samples may occur initially at a somewhat lower frequency than that observed with alumina-supported Ni samples. Thus differences between the frequencies given in Table I and those observed by Eischens, *et al.*,[2] are primarily due to different sample *preparation* rather than any effect of a different supporting medium.

A. Addition of CO to Supported Ni Samples

1.5% Ni Samples.—Small known quantities of CO gas were added in a stepwise fashion to an infrared cell containing a reduced Ni sample. The CO pressure within the cell was measured at

(8) J. W. Cable and R. K. Sheline, *Chem. Revs.*, **56**, 1 (1956).

(9) T. S. Piper, F. A. Cotton and G. Wilkinson, *J. Inorg. and Nuclear Chem.*, **1**, 165 (1955).

(10) J. O. Halford, *J. Chem. Phys.*, **24**, 830 (1956).

equilibrium with a calibrated thermocouple gauge or with a McLeod gauge at low pressures. The isotherm obtained for a 1.5% Ni sample at room temperature is shown in Fig. 1. Above 5×10^{-2} mm. CO pressure the dead space correction became excessive and readings were therefore discontinued.

CO was added to another 1.5% Ni sample in two steps and the spectrum of the adsorbed CO was recorded after each addition (see Fig. 2). It is apparent from the spectrum that adsorption continues to occur at pressures considerably above the highest pressure which could be measured on the adsorption isotherm. Spectrum 2 in Fig. 2 was recorded immediately after 30 seconds of pumping to remove excess CO gas plus a small amount of $Ni(CO)_4$ vapor which was produced in the cell at this high pressure. This rapid removal of gases from the cell does not affect the intensity of the bands due to adsorbed CO. Above 2000 $cm.^{-1}$ the spectra shown in Fig. 2 are typical of several 1.5% Ni samples studied. However, not all 1.5% samples showed the weak band below 2000 $cm.^{-1}$; this band appears to be quite sensitive to sample preparation.

10% Ni Samples.—Figure 3 shows CO adsorption isotherms for three representative 10% Ni samples at room temperature. Figure 4 shows spectra for increasing coverage of CO on a typical 10% Ni sample. Here the intensity of bands A, B and C is much greater than in the 1.5% Ni sample shown previously. The infrared absorbance observed in regions A and C corresponds to CO adsorbed at pressures below 1×10^{-3} mm. (pressure range labeled A + C in Fig. 3). Between 10^{-3} and 2×10^{-2} mm. CO pressure (range labeled B + D in Fig. 3) the major change in the spectrum is an increase in absorbance in regions B and D. Above 2×10^{-2} mm. of CO, a band grows in region E. The spectra shown in Fig. 4 are typical of several 10% Ni samples studied although variations in the total absorbance for different samples were observed (note also the variation in the isotherms shown in Fig. 3).

The fact that $Ni(CO)_4$ gas is observed to form when a sample is treated with CO at a pressure above about 5 mm. afforded a convenient method of decreasing the concentration of Ni within a given sample while maintaining full coverage of CO. This treatment was applied to a sample which was initially 10% Ni and had a full-coverage spectrum like that shown in Fig. 4. The $Ni(CO)_4$ gas produced was sublimed into a cold trap at 77°K. as soon as it was formed thereby causing a continual removal of Ni from the sample. After 3 days treatment at a CO pressure of about 59 mm., the cell was pumped out for 30 seconds and a spectrum was recorded. This showed a marked decrease in absorbance in regions A, B and C but little change in regions D and E. After an additional treatment of 2.5 days with CO at a pressure of 117 mm., the cell was pumped out and another spectrum was recorded. This showed only weak absorption in regions D and E and the band shape was very similar to spectrum 1 of Fig. 2.

Although the measurement was difficult to make and not of high precision, we were able to determine

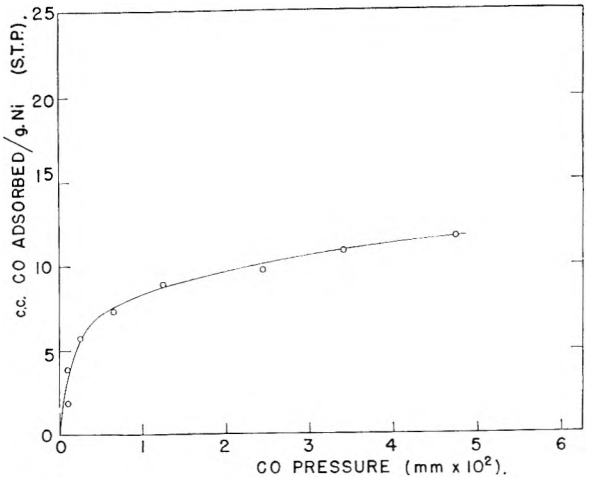

Fig. 1.—1.5% Ni sample. Typical CO adsorption isotherm at room temperature.

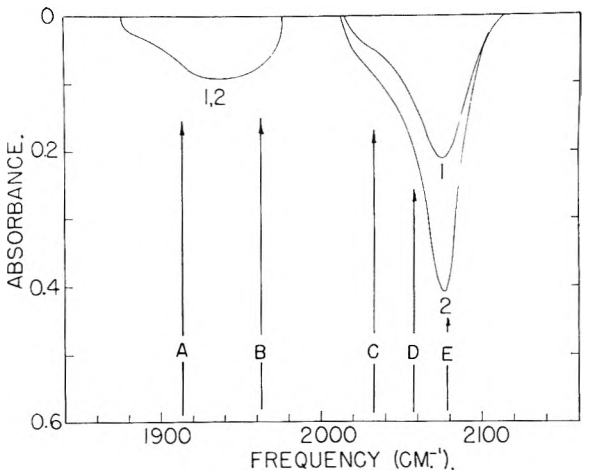

Fig. 2.—1.5% Ni sample. Spectrum 1, 1.5 mm. CO pressure; spectrum 2, 11.5 mm. CO pressure, then pumped 30 seconds.

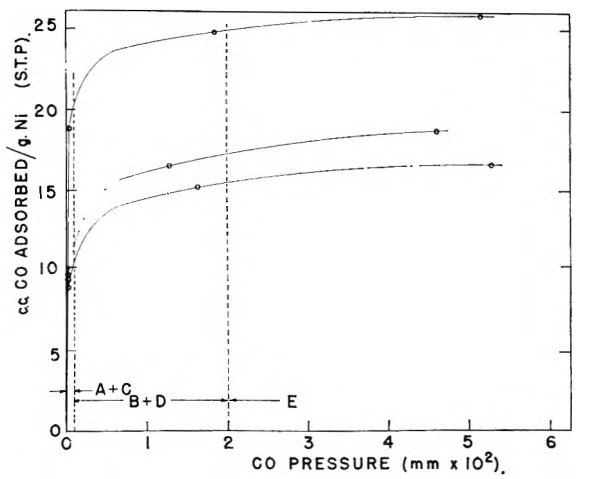

Fig. 3.—10% Ni samples. Typical CO adsorption isotherms at room temperature.

that more than half of the nickel originally in this 10% sample was removed as $Ni(CO)_4$ gas. Our best estimate of the final sample composition after treatment with excess CO is 3–4% Ni by weight.

25% Ni Sample.—Since the relative intensities of the various infrared bands differ between 1.5

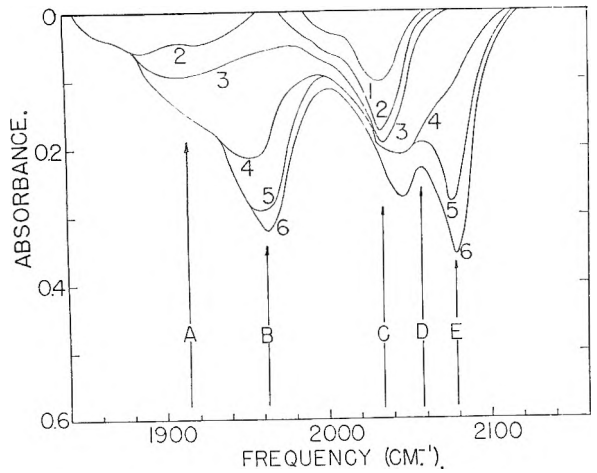

Fig. 4.—10% Ni sample. Spectrum 1, 1.7×10^{-4} mm. CO pressure; spectrum 2, 2.0×10^{-4} mm.; spectrum 3, 3.5×10^{-4} mm.; spectrum 4, 2.3×10^{-2} mm.; spectrum 5, 1.2 mm.; spectrum 6, 1.2 mm. after 12 hours.

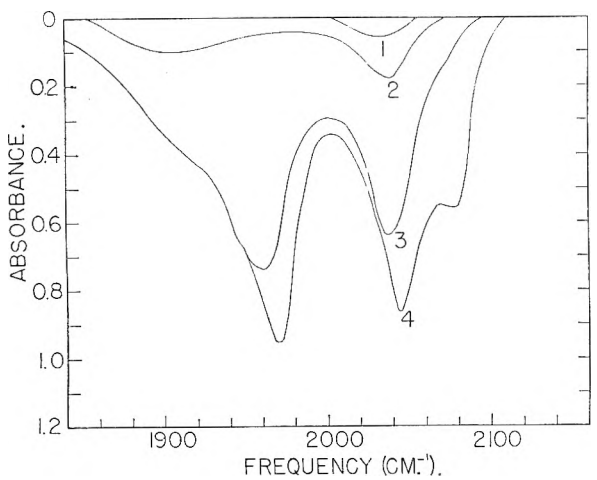

Fig. 5.—25% Ni sample. Spectrum 1, 4×10^{-4} mm. CO pressure; spectrum 2, 5×10^{-4} mm.; spectrum 3, 2.4×10^{-3} mm.; spectrum 4, 5.3 mm. after 6 hours then pumped 30 seconds.

and 10% Ni samples at full CO coverage, an experiment was performed on a 25% Ni sample. The spectra obtained on stepwise addition of CO are shown in Fig. 5. The trend of increasing relative intensity of bands in regions A, B and C as the Ni concentration is raised was substantiated by this experiment and the full-coverage spectrum shows comparatively slight absorbance in region E, relative to the strong absorbance in regions A, B and C.

CO was desorbed at room temperature from the full-coverage 25% Ni sample of Fig. 5 by pumping the cell at 10^{-5}–10^{-6} mm. The infrared absorption bands disappeared in essentially the reverse order of appearance on the initial stepwise adsorption. After approximately 30 minutes of desorption the band in region E disappeared completely and a small loss of absorbance occurred on the high frequency side of the band in region B. After this initial 30 minute period, changes occurred very slowly. Thus, in 40 hours desorption, the absorbance in region D disappeared by continued loss of intensity from the high frequency side and one-half of the absorbance in region B has been removed. Desorption was continued for 200 hours, during which time the absorbance in region B disappeared and a small loss of intensity in region C occurred. After 200 hours of desorption, a band in region A and a band in region C still remained.

CO was readsorbed on the sample by adding sufficient CO gas to bring the CO pressure up to that pressure at which full coverage was originally achieved (5.0 mm.). This readsorption caused the spectrum to return to its original full-coverage intensity of absorbance in all regions. Thus extensive desorption at room temperature does not seem to alter the character of the Ni surface; *i.e.*, there has been no decomposition of CO to form surface carbides.

Interpretation.—The full-coverage spectra of CO adsorbed on surfaces containing supported Ni at various concentrations clearly show that the character of the Ni surface is a function of the Ni concentration. On a 1.5% Ni surface at full coverage, the bands in regions A, B and C are of low intensity relative to the bands in regions D and E. When the concentration of Ni is increased to 10%, the bands in regions A, B and C become pronounced. On a 25% Ni sample at full coverage the bands in regions A, B and C are developed still more while the relative intensity in region E is decreased. The Ni stripping experiment confirms the observation that Ni concentration effects the full coverage spectra. Bands A, B and C seem to disappear simultaneously when Ni atoms are slowly removed from the 10% Ni surface as $Ni(CO)_4$ gas, and the final spectrum resembles that obtained with 1.5% Ni samples at full CO coverage.

This fact that the bands in regions A, B and C are strongest on the higher concentration Ni samples suggests that these bands represent CO molecular species adsorbed on compact Ni sites. These sites will be designated "crystalline." Thus band A is assigned to a bridge CO species on crystalline Ni while band C is assigned to a strongly adsorbed linear CO species on crystalline Ni. The presence of crystalline sites on a 25% Ni sample is supported by the X-ray diffraction results which indicate Ni crystals approximately 40 Å. in size. The fact that no X-ray lines were evident on a 10% Ni sample may be caused by a reduction of the average crystal size to an undetectable value.

Bands A and C both develop at very low equilibrium pressures. With increasing coverage band C seems to intensify at constant frequency (2035 $cm.^{-1}$), indicating that interaction between adsorbed linear CO's of this type at low CO coverage is small.

On the 1.5% Ni samples it is reasonable that the Ni should be of a more dispersed character. The predominance of the bands in regions D and E at full coverage on these samples suggests that these bands correspond to linear CO's bonded to Ni atoms which are more dispersed than those in crystalline sites. It is proposed that 10 and 25% Ni surfaces have a partial crystalline character indicated by the presence of bands A, B and C and a partial dispersed character corresponding to bands D and E. This conclusion is verified by the

adsorption isotherms studied on 10 and 1.5% samples. The isotherms obtained for 10% Ni samples show that about $^3/_4$ of the CO adsorbed up to 5×10^{-2} mm. pressure is adsorbed below 1×10^{-3} mm. (giving only bands A and C in the spectra) while on a 1.5% sample very little adsorption occurs below 1×10^{-3} mm.

By superimposing the 1.5% Ni isotherm and a 10% Ni isotherm in such a way that the "plateau" portions of the isotherms coincide, it may be seen that the 10% Ni surface seems to have a dual nature—a large portion adsorbing CO at a low equilibrium pressure and a smaller fraction displaying the adsorptive character of a 1.5% Ni sample. Thus the crystalline sites chemisorb CO at a low equilibrium pressure while adsorption on dispersed sites takes place at higher pressure.

Note that one cannot judge the degree of dispersion of the nickel on 1.5 and 10% samples by a comparison of the amount of CO adsorbed per g. of Ni as shown in Figs. 1 and 3 since the maximum pressure shown on these isotherms is 0.05 mm. and considerable adsorption occurs on dispersed Ni sites at higher pressures (see Figs. 2 and 4). Also only a small fraction of the Ni atoms present even in the 1.5% samples adsorb CO.

One might expect that the removal (as $Ni(CO)_4$ gas) of nickel from the 10% sample would have selectively removed dispersed Ni atoms and made the spectrum look more like that of a 25% Ni sample. However, it appears that both the dispersed and the crystalline Ni sites are attacked at a comparable rate and that as crystalline patches of nickel are eaten away new dispersed sites are formed. Thus as stripping of the 10% sample proceeds, the net effect is to remove crystalline sites more rapidly than dispersed sites.

Band B develops on 10 and 25% Ni samples at CO pressures higher than that necessary to completely form bands A and C. Also, some of the 1.5% Ni samples studied show a weak band in the A–B region; but, the absorbance in region B (and also in region C) is markedly less than that observed for 10 and 25% Ni samples. A possible surface bridge species corresponding to band B would be

This species would form only on crystalline sites during the later stages of adsorption of linear species (band C), agreeing with the order of appearance of band B.

The fact that band E is a single band indicates that it is probably not associated with a multiple CO species. Two or more CO's per Ni atom in a non-centrosymmetric species should produce an observable double band due to symmetric and antisymmetric CO stretching vibrations. The interpretation of the single band E is substantiated by the fact that the frequency of this band (2082 $cm.^{-1}$) lies between the antisymmetric and symmetric vibrational frequencies (2057 and 2128 $cm.^{-1}$) for $Ni(CO)_4$ gas.[11] In addition, the compound $(CO)_3NO$ which is isoelectronic with $Ni(CO)_4$ gives two infrared bands in the gas phase (2047 and 2108 $cm.^{-1}$) due to the antisymmetric and symmetric CO stretch.[12] This assignment of band E will be discussed further in the next section.

Band D is the most difficult band to observe accurately because of its position between bands C and E. Both its frequency (2057 $cm.^{-1}$) and order of appearance on stepwise adsorption of CO on both 10 and 1.5% Ni samples suggest that it corresponds to a linear CO adsorbed on a Ni site which is intermediate in character between crystalline and dispersed sites. This particular intermediate type of surface is designated as "semi-crystalline." It will be discussed further in the section devoted to Hg poisoning studies.

A summary of the assignments of infrared bands to surface species is presented in Table II.

TABLE II

ASSIGNMENT OF INFRARED BANDS TO SURFACE SPECIES FOR CO CHEMISORBED ON SUPPORTED Ni SAMPLES AT ROOM TEMPERATURE

Band	Frequency, $cm.^{-1}$	Species	Site	Strength of adsorption
A	1915	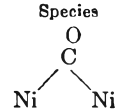	Crystalline Ni	Very strong
C	2035	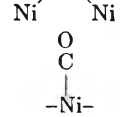	Crystalline Ni	Very strong
B	1963	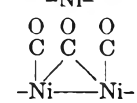	Crystalline Ni	Moderately strong
D	2057	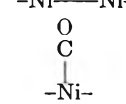	Semi-crystalline Ni	Moderately strong
E	2082	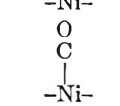	Dispersed Ni	Weak

An unreduced NiO sample showed no adsorption of CO at room temperature, and no infrared bands due to adsorbed CO species could be detected in the region 1800–2200 $cm.^{-1}$, so that it is certain that the adsorbed species reported are really on a Ni surface. (This is further supported by the fact that band E may be produced by the decomposition of $Ni(CO)_4$ gas, as discussed below.) In addition, any significant amounts of CO_2 produced by a carbiding reaction between the Ni sample and chemisorbed CO should have been detectable in the gas phase at 2349 $cm.^{-1}$. Since this band was never observed (even in the presence of excess CO), we assume that surface carbides did not form to any appreciable extent.

B. Addition of $Ni(CO)_4$ to Ni Samples.—A 10% Ni sample, freshly reduced, was treated with $Ni(CO)_4$ in an attempt to observe differences which might exist in approaching the equilibrium surface situation from the $Ni(CO)_4$ side. Small quantities of $Ni(CO)_4$ gas were admitted to the cell at room temperature and a spectrum was recorded

(11) L. H. Jones, *J. Chem. Phys.*, **28**, 1215 (1958).

(12) R. S. McDowell, W. D. Horrocks, Jr., and J. T. Yates *ibid.*, **34**, 530 (1961).

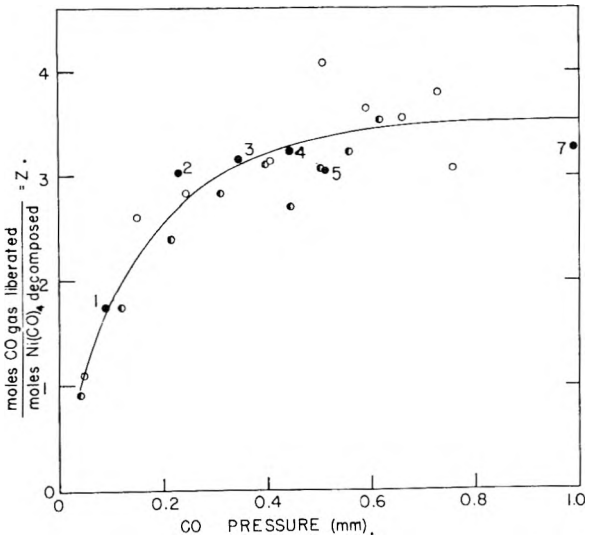

Fig. 6.—1.5% Ni sample. Quantitative stepwise addition of $Ni(CO)_4$ gas.

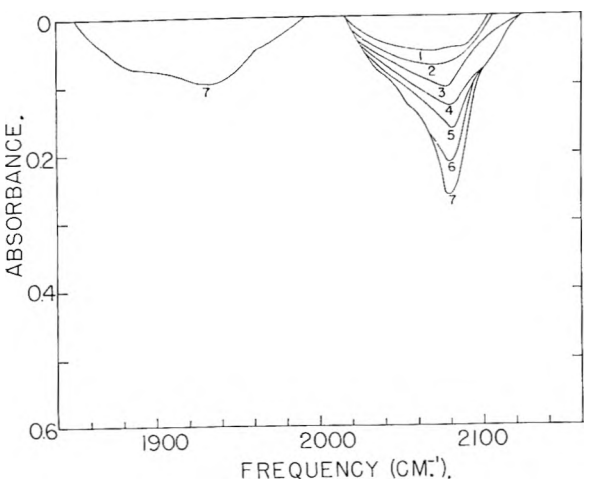

Fig. 7.—1.5% Ni sample. Quantitative stepwise addition of $Ni(CO)_4$ gas. Spectra 1 to 5 each after the addition of 0.0098 cc. $Ni(CO)_4$ gas; spectra 6 and 7 each after the addition of 0.0167 cc. $Ni(CO)_4$ gas (STP).

after each addition until a total of 0.15 cc.(STP) of $Ni(CO)_4$ had been added. Since the strong 2058 cm.$^{-1}$ band of $Ni(CO)_4$ was absent, we may assume that all this $Ni(CO)_4$ was decomposed. (In a blank run, $Ni(CO)_4$ gas was admitted to a cell containing a pure alumina sample and the spectrum was observed to be identical to that of the gaseous carbonyl at all pressures. A minimum of 10^{-3} cc. (STP) of carbonyl, which corresponds to a pressure of $\sim 5 \times 10^{-3}$ mm., could be definitely detected in the cell. Thus, the absence of a band at 2058 cm.$^{-1}$ indicates that neither $Ni(CO)_4$ gas nor physically adsorbed $Ni(CO)_4$ are present.) The spectra observed were in complete agreement with those obtained on addition of CO to a 10% Ni sample (Fig. 4). The sample was then allowed to stand overnight in the presence of about 2.3 mm. pressure of $Ni(CO)_4$ gas. Another spectrum was recorded after pumping for 30 seconds to remove the excess $Ni(CO)_4$ gas. In addition to a slight over-all increase in absorbance, this final spectrum showed abnormally strong absorbance in region E (absorbance $\cong 0.8$).

Apparently, when Ni is added to the surface by decomposition of $Ni(CO)_4$, the formation of dispersed adsorbing sites is favored, and the only major change in relative intensity is seen in region E.

The sharp band observed in region E on supported Ni samples might represent the presence of a molecular species which is the precursor to the formation of $Ni(CO)_4$ gas within the cell. This possibility is supported by the fact that on stepwise adsorption of CO, band E is the last band to form before $Ni(CO)_4$ gas begins to form and also that band E can be made abnormally intense by decomposing $Ni(CO)_4$ gas on fresh 10% Ni samples. Thus it seemed possible that band E might represent a surface species containing more than one CO molecule per active Ni (as suggested by Eischens, *et al.*[2]) in spite of the fact that such a species should give two active and resolvable infrared bands instead of the single band which is observed.

Because only a small fraction of the Ni within any given sample adsorbs CO under the conditions employed in this work, quantitative measurements of CO uptake per gram of Ni do not allow any estimate to be made of multiple adsorption of more than one CO per Ni atom. To test for this possibility, measured quantities of $Ni(CO)_4$ gas were decomposed on 1.5% Ni samples. By measuring the increase in CO pressure within the cell after each $Ni(CO)_4$ addition it was possible to calculate the ratio of the number of moles of CO gas liberated to the number of moles of $Ni(CO)_4$ gas decomposed. This ratio, called Z, is plotted *vs.* the equilibrium CO pressure in Fig. 6 for three 1.5% Ni samples. The resulting stepwise spectra for one of these samples is shown in Fig. 7 where the numbering of the spectra corresponds to the numbering of the solid points in Fig. 6. The Z *vs.* pressure data were obtained using a thermocouple gauge to measure CO pressures by multiple expansion in a system composed of known volumes. Since these measurements are quite difficult, the rather large scatter in Fig. 6 is not surprising.

Measurements of Z and of the spectra were made up to the point where the presence of undecomposed $Ni(CO)_4$ was indicated by the spectra. It may be seen that the spectra resemble those obtained on stepwise adsorption of CO on a 1.5% Ni sample (Fig. 2). Initially, when $Z < 3$, spectra 1 and 2 show absorption in region D. As coverage was increased, the sharp band in region E developed and Z became approximately 3. At an equilibrium CO pressure greater than 1 mm., undecomposed $Ni(CO)_4$ gas was detected within the cell.

Spectrum 7 shows a broad band in region A. Spectra were not recorded in region A before this particular spectrum so we do not have a stepwise picture of developments in this region. In all probability the band in region A formed during the early stages of the $Ni(CO)_4$ addition. The fact that approximately 3 CO gas molecules are generated for each $Ni(CO)_4$ molecule decomposed, as band E grows, indicates that band E in its early stages of development corresponds to a *single*

linear CO adsorbed on a Ni atom which exists in a dispersed environment. The fact that the frequency of band E did not change appreciably when large amounts of $Ni(CO)_4$ gas were decomposed on the 10% Ni sample suggests that band E corresponds to a single linear CO bonded to a dispersed Ni at all stages of its growth.

C. The Effect of Mercury Poisoning on the Infrared Spectrum of CO Adsorbed on Ni.—Hg vapor was accidentally found to cause major changes in the spectrum of CO adsorbed on Ni. During the course of some room temperature desorption studies, several 10% Ni samples were desorbed in a system connected to an untrapped McLeod gauge. Instead of displaying the normal desorption behavior (disappearance of bands in the reverse order of their appearance on adsorption), these samples exhibited intensification of a sharp band in region D as CO was desorbed. Also, after lengthy desorption plus accompanying Hg poisoning, it was observed that these samples lost their ability to readsorb CO as bridge species A and B and as linear species E.

In a separate experiment a 10% Ni surface fully covered with CO, was exposed for 9.5 hours to Hg vapor (0.27 mm. pressure), originating from a clean droplet of Hg contained in a side arm in the vacuum system. The bands attributed to bridge CO species (A and B) disappeared as the Hg treatment was carried out, and simultaneously the sharp band in region D appeared. (No change in the spectrum occurs when the cell is merely closed off and a Ni sample with adsorbed CO is allowed to stand under vacuum for more than 12 hours; thus, any possibility that the effect is due to leaks in the cell was completely eliminated.)

These studies indicate that Hg poisoning causes crystalline Ni sites to lose their ability to chemisorb bridged CO. It is also evident that Hg poisoning effects dispersed Ni sites causing them to be unable to adsorb CO (as band E).

To investigate this phenomenon more thoroughly, a 1.5% Ni sample was treated with CO up to a pressure corresponding roughly to completion of the band in region D, but at a pressure too low for extensive development of band E. In spectrum 1 of Fig. 8, band D, which corresponds to linear CO adsorbed on semicrystalline sites, is shown to best advantage since interference from absorbance in regions C and E is essentially absent. The sample was then exposed to Hg vapor. The temperature of the side arm containing the liquid Hg was controlled so that the Hg vapor pressure was 2×10^{-3} mm. Figure 8 shows the intensification of the new band (2060 $cm.^{-1}$), which will be referred to as band D*, as the length of exposure to Hg vapor increases. After about 2 hours of poisoning under these conditions, major changes in the absorbance of band D* cease. This sample was desorbed (10^{-5}–10^{-6} mm.) at room temperature, and spectra were recorded periodically. After 2 hours, band D* has shifted to 2052 $cm.^{-1}$ with slight decrease in over-all intensity. After 24 hours desorption, the peak absorbance has decreased from 0.71 to 0.55; the frequency of D* was constant at 2052 $cm.^{-1}$ during this desorption.

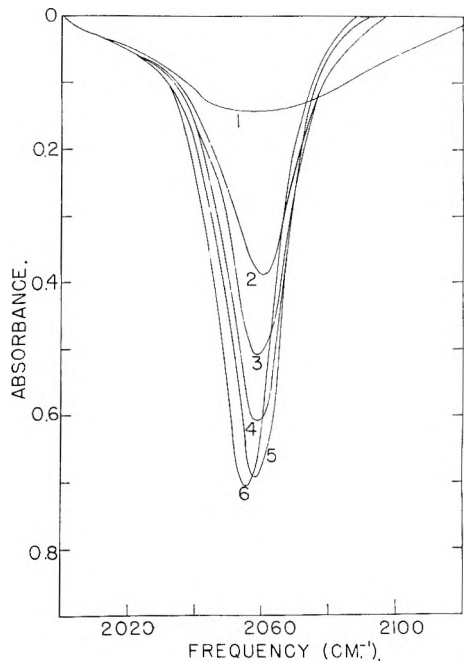

Fig. 8.—1.5% Ni sample. Addition of Hg to sample at partial CO coverage. Spectrum 1, 4.75×10^{-2} mm. CO pressure; spectrum 2, sample exposed to Hg vapor for 28 minutes; spectrum 3, for 47 minutes; spectrum 4, for 71 minutes; spectrum 5, for 112 minutes; spectrum 6, for 14 hours.

A second 1.5% Ni sample of identical weight to the previous sample was treated with CO up to the same pressure as the sample in Fig. 8; a spectrum identical to spectrum 1 in Fig. 8 was obtained. This partially covered sample was treated with Hg in the same fashion as before and band D* was observed to intensify at the same rate as before. After 29 minutes poisoning, band D* (2060 $cm.^{-1}$, absorbance = 0.34) was similar to spectrum 2, Fig. 8. Hg poisoning was then stopped and the desorption of this partially poisoned sample was carried out under the same conditions as in the previous sample. In 19 hours desorption, D* has decreased in intensity (absorbance = 0.21) and has shifted to 2056 $cm.^{-1}$. Thus these two experiments illustrate that qualitatively the initial rate at which D* absorbance disappears on desorption is independent of the extent of Hg poisoning. Exposure of the partially desorbed sample to Hg vapor for 2 hours produced no change in the spectrum, indicating that all of the CO now present on the Ni surface is completely influenced by the Hg added at the start of the experiment. This indicates that the adsorbed CO molecules which are on semicrystalline sites affected by Hg are more strongly held on the surface than those on unpoisoned semicrystalline Ni sites. Desorption rate measurements support this conclusion; *viz.*, some Hg poisoned samples exhibit a strong D* band even after 200 hours of desorption.

It may be argued that if the effect of each Hg atom was to influence a large area of semicrystalline Ni surface (as in an explanation based on a band theory of metals) *all* adsorbed CO molecules would be equivalent and would uniformly become more strongly held and more intensely infrared

absorbing as more Hg was added. Then at an intermediate stage of poisoning, band D* should disappear on desorption more rapidly than it does after complete poisoning; *this is not observed.* Also, after a period of desorption of a partially poisoned sample, further poisoning should continue to make band D* grow; *this is not observed.* But if the effect of a Hg atom is local, then at an intermediate stage of poisoning some adsorbed CO molecules are affected (converted to a new species which is more strongly held and has a greater absorbancy) while other CO's are not affected. Then one predicts that band D* should disappear at the same rate for all stages of poisoning, as is observed. Also a period of desorption on a sample which has been partially poisoned will remove most of the weaker-held CO species which had not been affected by Hg (band D species). Then further poisoning cannot cause band D* to grow, again in agreement with observation.

Thus the effect of the Hg seems to be of a local nature, and extensive poisoning does not seem to cause a situation which is very different from that caused by slight poisoning, with the exception that the intensity of band D* (and also the number of CO's on sites affected by Hg) is proportional to the extent of poisoning.

It has been shown in a further experiment that the Hg poisoning effect does not depend on the preadsorption of CO on the semicrystalline Ni sites; initial poisoning with Hg followed by CO adsorption produces the same strong band at 2060 cm.$^{-1}$. Thus the Hg poisoning of semicrystalline sites may be visualized as a local alloying process in which the Hg enters into the semicrystalline Ni lattice, perhaps at vacancies which are certainly very prevalent in the semicrystalline surface. In this connection, Eischens[13] has reported a spectrum of CO adsorbed on a Cu–Ni alloy (10% Cu) which shows a band in the linear CO region which has a greater relative intensity compared to the bridge CO bands than the linear CO band on a pure Ni surface.

(13) R. P. Eischens, *Z. Elektrochem.*, 60, 782 (1956).

It is impossible to advance more than a conjecture as to the theoretical nature of the Hg poisoning effect. Two experimental facts are prominent: (1) Hg adsorbed on semicrystalline Ni causes the Ni–C bond strength in adsorbed linear CO species to increase markedly as judged by the rate of desorption; (2) the extinction coefficient for the CO stretching vibration in adsorbed linear CO species on semicrystalline Ni sites is increased several fold when Hg poisoning of the Ni surface takes place. It is possible that the first of the two effects is caused by an increase in the number of metallic bonding orbitals which are utilized by a Ni atom in a semicrystalline site when Hg poisoning takes place. This view is supported by the existence of various Hg-metal carbonyl complexes which are much more stable than their parent carbonyls.[8] At this time we have no explanation for the increase in the carbonyl extinction coefficient of D* species when Hg poisoning takes place.

IV. Summary

The adsorption of CO on crystalline Ni sites occurs at very low pressure and is typical of chemisorption. Adsorption of CO on semicrystalline and dispersed sites occurs at pressures higher than normally associated with chemisorption, and such CO is more weakly held. The sequence of appearance and disappearance of linear CO bands on adsorption and desorption indicates that the carbon–oxygen stretching frequency becomes higher as the strength of bonding of the CO to the Ni surface decreases. The correspondence between infrared absorption bands and adsorbed species proposed for CO adsorbed on alumina-supported nickel samples is shown in Table II.

Mercury poisoning of a Ni surface containing adsorbed CO results in the formation of an intense band at 2060 cm.$^{-1}$. This band is associated with a linear CO species strongly adsorbed on a semicrystalline site "alloyed" with Hg. The effect of Hg is of a local nature as far as its influence on chemisorbed CO is concerned.

INFRARED STUDIES ON PYRROLES. THE STRUCTURE OF 2,5-DIPHENYLPYRROLE-3-DIAZONIUM CHLORIDE

BY ALFRED KREUTZBERGER[1] AND PAUL A. KALTER

Scientific Laboratory, Ford Motor Company, Dearborn, Michigan

Received September 26, 1960

For the purpose of structure determinations in the pyrrole series, the infrared spectra of pyrrole (III) and four of its simple non-functional derivatives, *viz.*, 2,5-dimethylpyrrole (IV), 2,5-diphenylpyrrole (V), 1-methylpyrrole (VI) and 1-phenylpyrrole (VII) have been measured from 4000–670 cm.$^{-1}$, and correlations of absorption bands to vibrational elements have been established. On the basis of these investigations, the nature of 3-diazo-2,5-diphenylpyrrole has been found to be that of resonance hybrid (I). The structure of the "hydrochloride of 3-diazo-2,5-diphenylpyrrole" has been elucidated by these infrared studies to be 2,5-diphenylpyrrole-3-diazonium chloride (II).

Introduction

In connection with attempts at synthesizing the as-yet-unknown azopyrroles, the azo coupling reaction, being the most important method for the preparation of azo compounds in general, was considered one of the most promising routes toward the contemplated new compound class. Investigation of this route would require avail-

(1) Presented at the 138th National Meeting of the American Chemical Society in New York, N. Y., September, 1960.

ability of a possibly simple pyrrolediazonium salt as a model substance. However, neither the parent compound of any pyrrolediazonium salt, nor any derivative thereof carrying only non-functional substituents, was known hitherto. Theoretically, such a model substance should be accessible through the reaction of an aminopyrrole with sodium nitrite. Unfortunately, the simplest aminopyrroles, *e.g.*, aminopyrrole itself or the amino C-methyl or C-phenyl pyrroles, are not known either.

Thus the simplest known aminopyrrole model substance appeared to be 3-amino-2,5-diphenylpyrrole (IX). As a matter of fact, this compound does react with sodium nitrite in concentrated acetic acid but, instead of a diazonium salt, furnishes a free diazopyrrole, $C_{16}H_{11}N_3$ (I).[2] Angelico[2] assigned to it structure IA or IB.

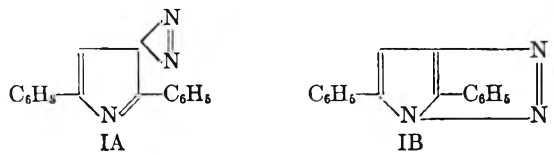

IA IB

As a diazo compound, this substance was expected to undergo coupling reactions with suitable agents under proper conditions. However, difficulties were encountered in preliminary experiments. To overcome these, the structure of the diazo compound was reinvestigated. Surprisingly, the infrared spectrum was not one expected of a structure IA or IB. The elucidation of this structure was rendered even more difficult by the fact that not much was known about the chemistry of this compound. The only two facts known with certainty were that it is so stable as to remain unchanged even under the action of concentrated sulfuric acid, and that it gives a hydrochloride (II).[2] This hydrochloride (II) has neither been ever analyzed nor any structure been assigned. One could reasonably speculate, however, that this hydrochloride might have the structure of a diazonium salt. To obtain an insight into the structure, an infrared study was deemed to be most promising.

A requirement for this investigation was the availability of a general frequency scheme of the pyrrole nucleus and particularly the combination of pyrrole and benzene nuclei. Although infrared spectra of several pyrrole derivatives are scattered throughout the literature, no comprehensive interpretation can be found which would facilitate elucidation of obscure pyrrole structures. While the strictly organic part of this problem is dealt with elsewhere,[3] this paper discusses the physical-chemical aspects pertaining to the structure elucidation of I and II.

Experimental

The infrared spectra were recorded with a Perkin–Elmer double beam spectrophotometer, Model 137. In the case of solid substances, the measurements were made on pressed disks of pure potassium bromide in which the compounds were dispersed. Liquid substances were measured undiluted. No compensation plates were used in the reference beam. The spectra were taken from 4000–670 cm.$^{-1}$ as plots of percentage transmittance against wave number or wave length, respectively.

Liquid substances were purified by vacuum-fractionation under nitrogen, and the following fractions were used for the infrared measurements: pyrrole (III) b.p. 45° (30 mm.), $n^{20}D$ 1.5094; 2,5-dimethylpyrrole (IV) b.p. 83° (30 mm.), $n^{20}D$ 1.4958; 1-methylpyrrole (VI) b.p. 110–111° (760 mm.), $n^{20}D$ 1.4866. 2,5-Diphenylpyrrole (V) was prepared[4] from *trans*-1,4-diphenyl-2-butene-1,4-dione and purified by recrystallization from ethyl alcohol–water; m.p. 143–144°. 1-Phenylpyrrole (VII) was purified by sublimation; m.p. 61–62°. 3-Diazo-2,5-diphenylpyrrole (I) and its hydrochloride (II) were prepared by known procedures starting with 2,5-diphenylpyrrole (V)[4] and converting this *via* 3-nitroso-2,5-diphenylpyrrole (VIII) to the 3-amino-2,5-diphenylpyrrole (IX).

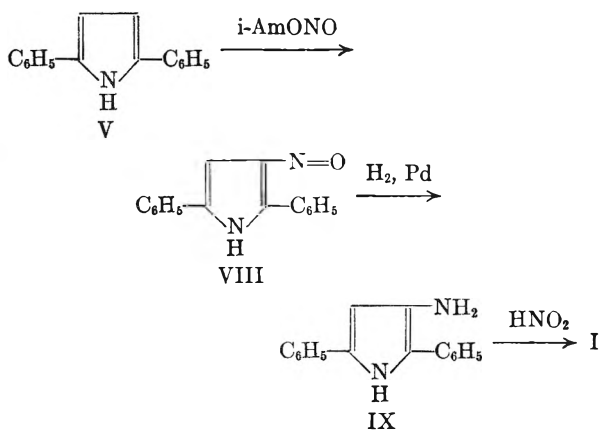

V VIII IX

In order to overcome Angelico's difficulties[2] in obtaining sufficient material, the methods used in all intermediate steps were improved such as to give more satisfactory yields. Because of the organic nature of these investigations, details are described in a separate publication.[3]

Results and Discussion

The behavior of the pyrrole ring is best described in terms of a resonating benzenoid system. It has thus no fixed double bonds and therefore does neither undergo additive reactions typical of olefins nor act as a diene in the Diels–Alder reaction. Moreover, its aromatic behavior is manifested in the ease with which it undergoes substitution reactions, as nitration, halogenation, Gattermann, Hoesch and Reimer–Tiemann reactions. Quantitatively, the degree of aromatization in the pyrrole nucleus is expressed by the amount of 31 kcal./mole.[5]

By analogy one might then expect the vibrational spectra of pyrroles to resemble those of carbocyclic aromatic compounds but modified by the NH group of the pyrrole ring. To study the fundamental vibrations of the pyrrole nucleus in 2,5-diphenylpyrrole (V), the infrared spectrum of this compound has been lined up with those of pyrrole (III), 2,5-dimethylpyrrole (IV), 1-methylpryrole (VI) and 1-phenylpyrrole (VII) (Fig. 1).

Criteria of a resonating system are skeletal vibrations of semi-unsaturated carbon–carbon and, in addition to these in the case of pyrroles, carbon–nitrogen bonds. On the basis of the fundamental studies in the benzene series,[6] on thiophenes,[7] furans[8] and s-triazine,[9] the characteristic skeletal

(2) F. Angelico, *Atti reale accad. Lincei*, [5] **14**, II, 167 (1905).

(3) A. Kreutzberger and P. A. Kalter, *J. Org. Chem.*, **26**, in press (1961).

(4) A. Kreutzberger and P. A. Kalter, *J. Org. Chem.*, **25**, 554 (1960).

(5) V. Schomaker and L. Pauling, *J. Am. Chem. Soc.*, **61**, 1769 (1939).

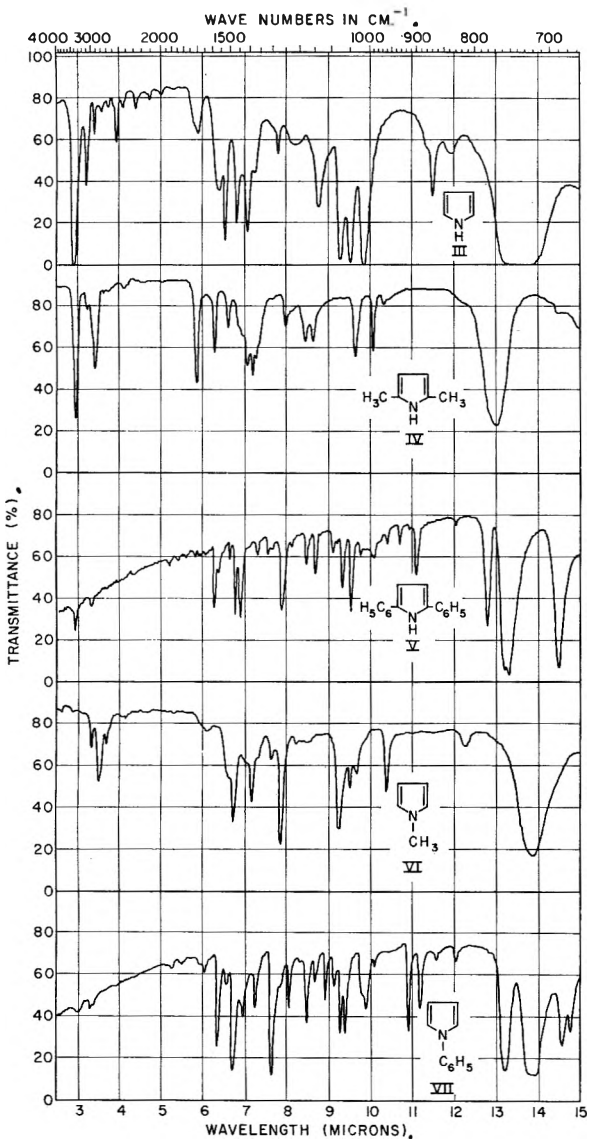

Fig. 1.—Infrared absorption spectra of pyrrole (III), 2,5-dimethylpyrrole (IV), 2,5-diphenylpyrrole (V), 1-methylpyrrole (VI) and 1-phenylpyrrole (VII).

stretching modes of pyrroles must be assigned to the 1700–1350 cm.$^{-1}$ region in which a group of three to four bands appears. For 2,5-diphenyl pyrrole, they may be found at 1590, 1480 and 1450 cm.$^{-1}$.

Of other skeletal modes, a ring-breathing frequency may be expected in the 1000–800 cm.$^{-1}$ range. The bands at 870, 990, 900, 960 and 920 cm.$^{-1}$ for, respectively, III, IV, V, VI and VII may be assigned to this cause.

In addition to these skeletal vibrations, aromatic-type structures exhibit as another characteristic those frequencies caused by vibrations of hydrogen atoms directly attached to the ring. These can be divided into =C—H stretching in the 3000 cm.$^{-1}$ region,[10] =C—H in-plane deformation[11] between 1300 and 950 cm.$^{-1}$, and out-of-plane bending[12] at 1000–650 cm.$^{-1}$. Particularly, the =C—H stretching vibration is a safe means of recognizing a resonating ring system. It occurs in all pyrrole derivatives III through VII at 3020–2920 cm.$^{-1}$. Mention must be made of the fact that on the low wave length side of the infrared spectrum of pyrrole (III), three absorption bands appear, *viz.*, at 3420, 3100 and 2940 cm.$^{-1}$, of which the latter is being assigned to the =C—H stretching mode. Coblentz, who measured the infrared spectrum of pyrrole for the first time,[13] did not find this band because the technique he used did not enable him to resolve the one broad band he found into the existing three bands. Subsequent investigators in infrared spectroscopy of pyrrole (III)[14,15] only considered the range up to 1500 and 1900 cm.$^{-1}$, respectively.

The =C—H stretching mode has also been found in other resonating heterocyclic nuclei, *e.g.*, thiophene,[16] pyridine,[17] pyrimidine.[18,19]

Another type of vibrations expected of hydrogen atoms attached to an aromatic ring results from the =C—H in-plane deformation mode. This gives cause to the appearance of a series of bands whose position is largely determined by the position of hydrogen and other substituents. In analogy to benzene and its derivatives,[11] the region between 1320–1010 cm.$^{-1}$ may be assigned to the =C—H in-plane deformation vibrations in pyrrole and its non-functional derivatives. The outstanding absorptions in this region of pyrrole (III) are at 1280, 1140, 1080, 1050 and 1020 cm.$^{-1}$, while those of 2,5-diphenylpyrrole (V) can be found at 1260, 1180, 1150, 1070 and 1050 cm.$^{-1}$. It is noteworthy that the band at the high frequency side of this region is particularly marked in the N-substituted pyrroles, *i.e.*, with 1-methylpyrrole (VI) (1280 cm.$^{-1}$) and 1-phenylpyrrole VII (1320 cm.$^{-1}$).

A third series of bands shown by carboxyclic aromatic compounds stems from =C—H out-of-plane deformation vibrations.[12] The positions of these bands have been shown to be characteristic of the number and position of C–H bonds and to be largely independent of the nature of the substituents.[20] On the basis of these findings, the absorption bands at, respectively, 740, 770, 750, 720 and 720 cm.$^{-1}$ in III, IV, V, VI and VII may be as-

(6) W. R. Angus, C. R. Bailey, J. B. Hale, C. K. Ingold, A. H. Leckie, C. G. Raisin, J. W. Thompson and C. L. Wilson, *J. Chem. Soc.*, 966, 971 (1936); K. S. Pitzer and D. W. Scott, *J. Am. Chem. Soc.*, **65**, 803 (1943).

(7) A. R. Katritzky and A. J. Boulton, *J. Chem. Soc.*, 3500 (1959).

(8) A. R. Katritzky and J. M. Lagowski, *ibid.*, 657 (1959).

(9) J. Goubeau, E. L. Jahn, A. Kreutzberger and Ch. Grundmann, *J. Phys. Chem.*, **58**, 1078 (1954).

(10) J. J. Fox and A. E. Martin, *Proc. Roy. Soc.* (*London*), **A167**, 257 (1938).

(11) R. R. Randle and D. H. Whiffen, *Trans. Faraday Soc.*, **52**, 9 (1956).

(12) N. B. Colthup, *J. Opt. Soc. Am.*, **40**, 397 (1950).

(13) W. W. Coblentz, "Investigations of Infra-Red Spectra," Carnegie Institute of Washington, Washington, D. C., 1905, 99, 143. 278.

(14) R. Manzoni-Ansidei and M. Rolla, *Atti reale accad. naz. Lincei*, [6] **27**, 410 (1938).

(15) R. C. Lord, Jr., and F. A. Miller, *J. Chem. Phys.*, **10**, 328 (1942).

(16) G. Waddington, J. W. Knowlton, D. W. Scott, G. D. Oliver, S. S. Todd, W. N. Hubbard, J. C. Smith and H. M. Huffmann, *J. Am. Chem. Soc.*, **71**, 797 (1949).

(17) C. H. Kline, Jr., and J. Turkevich, *J. Chem. Phys.*, **12**, 300 (1944).

(18) L. N. Short and H. W. Thompson, *J. Chem. Soc.*, 168 (1952).

(19) A. Kreutzberger, *Z. physik. Chem.* (*Frankfurt*), **24**, 368 (1960).

(20) D. A. McCaulay, A. P. Lien and P. J. Launer, *J. Am. Chem. Soc.*, **76**, 2354 (1954).

signed to the =C—H out-of-plane deformation mode in pyrroles. The remaining bands of this region in 2,5-diphenylpyrrole (V) (780 and 690 cm.$^{-1}$) and in 1-phenylpyrrole (VII) (760 and 690 cm.$^{-1}$) are to be considered due to =C—H out-of-plane vibrations of the benzene ring[21] mono-substituted by the pyrrole nucleus.

The NH group as the unique pyrrole feature among resonating systems would cause one to expect a single vibration in the NH stretching region typical of secondary amines. This is indeed the case with all pyrroles unsubstituted in 1-position as demonstrated on III, IV and V, the NH stretching absorptions being found at 3410, 3360 and 3410 cm.$^{-1}$, respectively. In this range, the parent compound III, and it alone, shows a second absorption at 3110 cm.$^{-1}$. In view of the fact that even the relatively low position of the main NH absorption at 3410 cm.$^{-1}$ has been shown to be due to hydrogen bonding effects,[22] it is reasonable to consider the band at 3110 cm.$^{-1}$ to be due to this cause also. In agreement with this assignment is the fact that other secondary amines also show a second absorption at higher concentrations. As is to be expected, no absorption in this region is found with pyrroles bearing substituents in 1-position like 1-methylpyrrole (VI) and 1-phenylpyrrole (VII).

This general vibration scheme of the pyrrole nucleus is only little changed upon entering of a substituent other than hydrogen. If, for example, an amino group is attached to the pyrrole ring of 2,5-diphenylpyrrole (V), the absorption bands in the infrared spectrum of 3-amino-2,5-diphenylpyrrole (IX) (Fig. 2) are essentially the same as in V, but the additional NH_2 group in IX shows up clearly through its pronounced N–H stretching vibration at 3310 cm.$^{-1}$ and the C–N stretching mode at 1300 cm.$^{-1}$, the latter hardly influencing the original nearby 1260 cm.$^{-1}$ =C—H in-plane deformation mode of V at all.

Introduction of the diazo group into 2,5-diphenylpyrrole (V) also leaves absorptions stemming from skeletal and =C—H vibrations largely untouched. However, the most outstanding feature in the infrared spectrum of 3-diazo-2,5-diphenylpyrrole (I) (Fig. 3) is a very strong band in the triple bond region at 2040 cm.$^{-1}$ which can only be interpreted as belonging to the diazo group. With regard to the fact that the fifth valence of the nitrogen atom in a structure IC in reality is an ionic bond

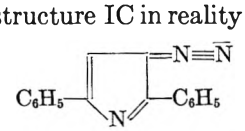

IC

3-diazo-2,5-diphenylpyrrole may best be represented as the resonance hybrid I

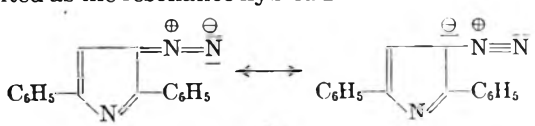

I

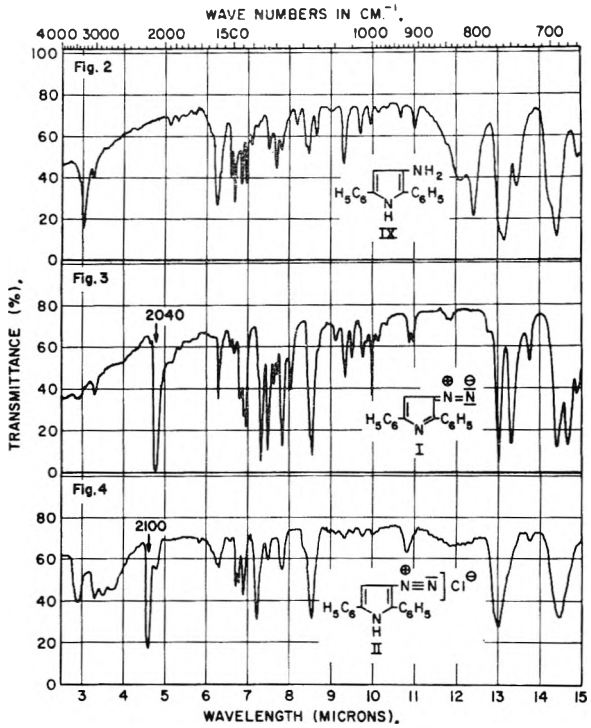

Figs. 2, 3 and 4.—Infrared absorption spectra of 3-amino-2,5-diphenylpyrrole (IX), 3-diazo-2,5-diphenylpyrrole (I) and 2,5-diphenylpyrrole-3-diazonium chloride (II).

The two mesomeric species of I are void of the original secondary amino function of the pyrrole nucleus. This situation is borne out by the fact that the infrared spectrum of I shows no absorption band in the N–H stretching region. Instead, the nitrogen atom of the pyrrole ring in I is present as a tertiary amino group. This feature is manifested in the strong bands at 1350 and 1330 cm.$^{-1}$ typical of C–N stretching vibrations of tertiary amines.[12]

The infrared spectrum of the hydrochloride II of 3-diazo-2,5-diphenylpyrrole (I) still exhibits the strongest absorption in the triple bond range (Fig. 4), but the position is shifted from 2040 cm.$^{-1}$ in I to 2100 cm.$^{-1}$ in II. Although the vibrational relationship between diazo compounds and the corresponding diazonium salts has never been studied, a comparison of diazo triple bond structures[23] with diazonium salt triple bonds[24] reveals that there is generally a shift toward higher frequencies when proceeding from the former to the latter. On the basis of this relationship, the hydrochloride II of I may then be assigned the structure of 2,5-diphenylpyrrole-3-diazonium chloride as represented by structure II

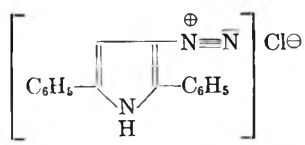

II

In structure II, the normal pyrrole ring con-

(21) M. Josien and J. Lebas, *Bull. soc. chim. France*, 53 (1956).

(22) N. Fuson, M. Josien, R. L. Powell and E. Utterback, *J. Chem. Phys.*, **20**, 145 (1952).

(23) J. H. Boyer, *J. Am. Chem. Soc.*, **73**, 5248 (1951).

(24) K. B. Whetsel, G. F. Hawkins and F. E. Johnson, *ibid.*, **78**, 3360 (1956).

taining the secondary amino group has been re-established. This would require the NH stretching band to appear again, an expectation which is fulfilled in the infrared spectrum of II. Chemical proof for the correctness of assigning compound II the structure of 2,5-diphenylpyrrole-3-diazonium chloride is its capability of undergoing coupling reactions with suitable coupling components. Diazo coupling with other pyrrole derivatives has thus led to the new compound class of azopyrroles.[3]

RADIATION CHEMISTRY OF IONIC SOLIDS. I. DIFFUSION-CONTROLLED MECHANISM FOR RADIOLYSIS OF IONIC NITRATES[1]

BY J. CUNNINGHAM

Argonne National Laboratory, Argonne, Illinois

Received September 29, 1960

The $G_{NO_3^-}$ values for the radiolysis of alkali-metal nitrates have been determined at temperatures from −110° to 340°. The accuracy of the method was adequate to definitely detect a kinetic isotope effect in the rate of radiolysis of $KN^{14}O_3^{18}$ relative to $KN^{14}O_3^{16}$ at 25°. The ratio of the *G*-values of these isotopic KNO_3 materials was 1.03 ± 0.03 at −110° but 1.12 ± 0.02 at 25°. A model which identifies the rate-determining process in the radiolysis of the various nitrates as the jump probability for escape of the oxygen fragment from an excited NO_3^-, gives consistent results when treated by a theory developed for diffusion in metals.

Several factors of possible importance in the mechanisms of radiation-induced decomposition of ionic solids arise from their rigidity, order and defect structure. These include: (1) greatly decreased probability of rapid diffusion of product species away from the reaction sites; (2) ease of propagation of exciton waves through the ordered lattices and the existence of stable trapping centers for excitons and electrons; (3) Existence of preferred directions for dissociation and product orientation. The relative importance of these factors is being studied in various solids. The alkali-metal nitrates form the first sequence of salts investigated.

Large differences have been reported between the rates of radiation-induced decomposition of various solid nitrates under either ultraviolet,[2] γ-ray,[3] or X-ray[4] irradiation. While there is general agreement that the primary process is unimolecular dissociation of an NO_3 species producing nitrite and oxygen,[2-7] the varying sensitivities have been attributed to (A) different polarizing power of the cations,[2] (B) to competition between nitrate ions and oxygen atoms for the oxygen fragments produced,[3] and (C) to differences in the closeness of packing of the crystal structures.[4] Factor (C) is related to ease of diffusion and the present paper reports further investigations of the importance of this "cage" effect in the γ-ray radiolysis of alkali-metal nitrates.

Experimental

Holders.—Samples for irradiation were weighed to ±0.005 mg. into numbered Pyrex holders(H) accurately ground to 0.455 ± 0.025 cm. o.d. (See Fig. 1.) Care was taken that samples always occupied ~2 mm. length at the bottom of the 1 mm. bore of the holders. They were compacted down and stray grains removed from the inside walls with a polished tungsten rod.

Irradiation Vessel.—The principal features of the stainless steel vessel, designed to give exactly reproducible positioning of the sample holders, are diagrammatically represented in Fig. 1. The holders were pressed tightly into numbered slots in the copper block A by retaining bands. Their vertical positioning was made exact by the heat-radiation shield S, and lateral changes in the position of A relative to D were prevented by four clamping screws, F. The 4500 curie Co^{60} γ-ray source rod seated reproducibly into cup D, and the outer vessel E seated immovable into holes in a fixed stand in the radiation chamber.

Temperature Control.—Temperatures of 25 and −110° were registered by thermocouples embedded in sample holders at normal positions during irradiation, when tap water or liquid N_2 was supplied to can B. Pressure was normally $\sim 10^{-3}$ mm. under continuous pumping during irradiation. Temperatures up to 350° were obtained using cartridge heaters embedded in A.

Dosimetry.—Absolute dosimetry at the sample positions was difficult because of the small sample-holder volumes. Reproducible values were obtained with $FeSO_4/CuSO_4$ dosimeter solutions[8] by combining, for each reading of optical density, equal aliquots from 4 quartz holders of i.d. 0.3 cm. and o.d. 0.455 ± 0.025 cm. They agreed to within 6% with a dose rate of 2.7×10^{21} e.v./l./min. determined by the Fricke dosimeter at the same distance as the samples. Absorbed doses were calculated using, true mass-absorption coefficients reported in the literature,[8] the above value of flux, values of the relative intensity at each position determined by KNO_3, and correction factors for source decay.

Internal Dosimetry.—Several calibration runs were made over the duration of the experiments with KNO_3 in all 16 positions. At 25 and −110° the reproducibility of the relative decompositions at the various positions in any run was better than ±1%. The decomposition at the reference positions in several standard runs at 25° did not differ by more than 2% from that calculated from the decay of source intensity, and the average difference was less than 1%. In all irradiations several normal KNO_3 samples were used to check that the relative intensities did not change and to check the actual dose rate. Only above 130° was it found necessary to apply a small correction for the intensity in the outer positions due to expansion of the copper block.

Preparation of Samples.—All normal nitrates were recrystallized and the middle fractions dried *in vacuo* at 120°. They were ground in an agate mortar but not sieved.

Nitrates with high enrichment in stable isotopes N^{15} and O^{18} were obtained from Isomet Corp. and the Weizmann Institute Israel, respectively. $KN^{15}O_3$ and $NaN^{15}O_3$ in the text refer to materials supplied as being 99.6% enriched in N^{15}, and $KN^{14}O_3^{18}$ refers, mainly, to a batch of quoted en-

(1) Based on work performed under the auspices of the U. S. Atomic Energy Commission.

(2) P. Doigan and T. W. Davis, *J. Phys. Chem.*, **56**, 704 (1952).

(3) C. J. Hochanadel and T. W. Davis, *J. Chem. Phys.*, **27**, 333 (1957).

(4) J. Cunningham and H. G. Heal, *Trans. Faraday Soc.*, **54**, 1355 (1958).

(5) A. O. Allen and J. A. Ghormley, *J. Chem. Phys.*, **15**, 208 (1947).

(6) L. K. Narayanswamy, *Trans. Faraday Soc.*, **31**, 1411 (1935).

(7) G. Hennig, R. Lees and M. S. Matheson, *J. Chem. Phys.*, **21** 664 (1953).

(8) E. Hart, *Radiation Research*, **2**, 33 (1955).

richment in O^{18} of 84%. However a separately prepared batch of $KN^{14}O_3{}^{18}$ was supplied as being 87% enriched in O^{18} and its behavior was identical with that of the 84% enriched material. The quoted enrichment on $KN^{15}O_3$ was verified by studies of its infrared spectra.

The O^{18}/O^{16} ratio in oxygen evolved from $KN^{14}O_3{}^{18}$ by slow thermal decomposition agreed within ±10% with the quoted enrichment.

These isotopically enriched samples were recrystallized by micro-techniques. Fractional recrystallization and subsequent irradiation were used to determine if the additional recrystallization produced changes in G-values but no such changes were detected.

Analysis.—The irradiated samples were washed out of the containers and analyzed for nitrite within three hours after the end of irradiation. This precaution was taken because of reported annealing effects in nitrates after irradiation.[9,10]

Results

Isotope Effects at 25°.—Several detailed intercomparisons between $KN^{14}O_3{}^{18}$ and $KN^{14}O_3{}^{16}$ were made in alternate positions during an irradiation and a ratio of 0.88 was constantly found in the fractional decomposition to nitrite between the O^{18} and O^{16} containing salt. Similar exact comparison for $KN^{15}O_3$ with $KN^{14}O_3$ and $NaN^{15}O_3$ with $NaN^{14}O_3$ failed to detect any measurable difference in fractional decomposition.

Previous studies[4] of X-ray radiolysis of $KN^{14}O_3{}^{16}$ have shown that the data for nitrite formation can be represented up to 0.015 fraction of the nitrate ions decomposed to nitrite by the relationship $y = b_1X$, where y = log (fraction of NO_3^- undecomposed) and X = dose. Above this fractional decomposition the data were represented up to the highest decomposition attained (0.3 fractional decomposition) by $y = a + b_2X$, where a was a constant and the slope, b_2, was only 0.7 of b_1. This change to a linear section of lower slope above ~0.02 fractional decomposition was detected in the X-ray studies at all temperatures except those close to the transition point of KNO_3, and below −30°.

The data here obtained were in exact agreement with the X-ray results, when plotted as log (fraction NO_3^- undecomposed) *vs.* dose. Figures 2 and 3 show the graphs thus obtained for $KN^{14}O_3{}^{16}$ and $KN^{14}O_3{}^{18}$ irradiated at 25°. The data were treated by the method of least squares to derive the best values of b. For $KN^{14}O_3{}^{16}$ the standard deviation for 22 values before the break in the plot was only ±0.8%, and, for $KN^{14}O_3{}^{18}$ 11 values before the break had a deviation of ±1.3%. Since excessively long times were required to attain sufficiently high decomposition to delineate the $y = a + b_2X$ section above ~0.02 fraction decomposed, fewer points are available in this region and the standard deviations are less significant. From the least squares values of b_1 and b_2 initial $G_{NO_3^-}$ values corresponding to the rate of nitrite formation for energy absorbed in the pure nitrate, were readily calculated and are listed in Table I. The points of particular interest are that, within the small standard deviation derived by the least-squares method, and relative to the rate of production of $(N^{14}O_2{}^{16})^-$ from $KN^{14}O_3{}^{16}$ as a standard: (a) No kinetic isotope effect is detected in the production of $(N^{15}O_2{}^{16})^-$ from $KN^{15}O_3{}^{16}$, since the ratio of initial G-values is

(9) A. G. Maddock, *Nature*, **182**, 1797 (1958).

(10) A. S. Baberkin, Proc. All-Union Conference Moscow, March 1957. "Chemical Action of Co^{60} γ-Radiation on Solid Crystalline Salts."

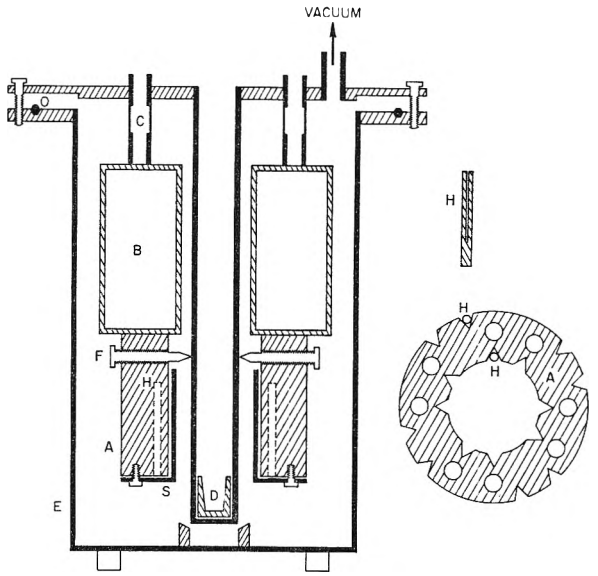

Fig. 1.—Irradiation vessel: A, copper block; B, coolant can; C, thin-wall leads into B; D, positioning cup for source; E, outer metal container; F, positioning screws; H, sample holder; S, heat shield.

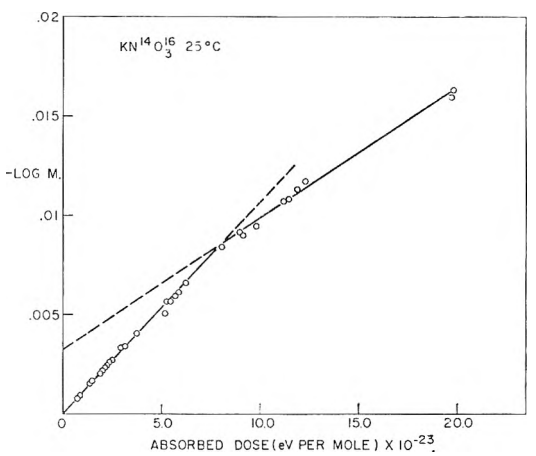

Fig. 2.—First-order plot for the decomposition of normal KNO_3 at 25° up to ~0.035 fraction decomposed.

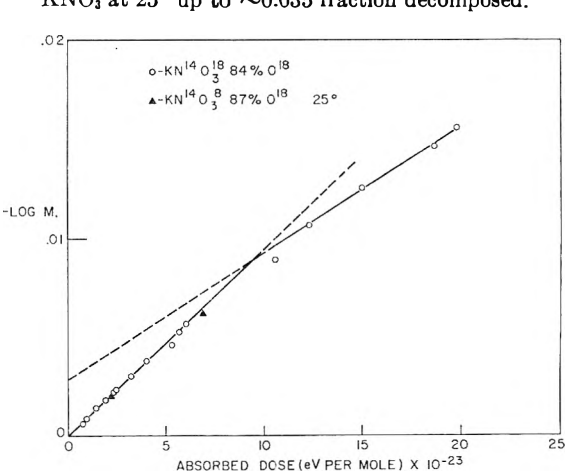

Fig. 3.—First-order plot for the decomposition of KNO_3 enriched to 84% in O^{18}. Values for 87% enriched material do not differ significantly.

1.015 ± 0.021; (b) An anomalously large kinetic isotope effect exists at 25° in the formation of $(N^{14}$-

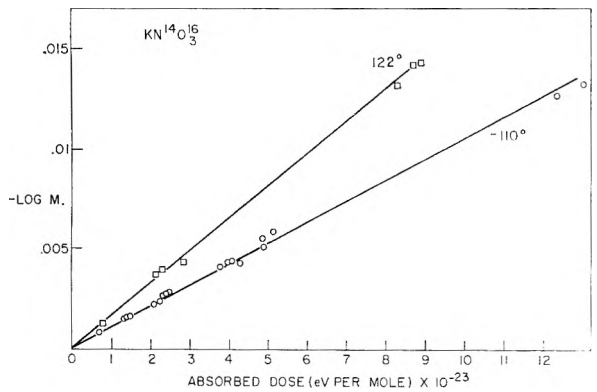

Fig. 4.—Decomposition of normal KNO_3 up to 0.035 fraction decomposed, at 122 and −110°.

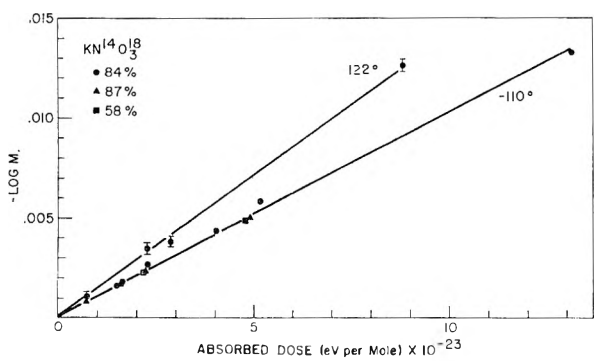

Fig. 5.—Decomposition up to 0.035 fraction decomposed for KNO_3 enriched in O^{18}: (a) at 122° all points refer to 84% enriched KNO_3. (b) at −110° points for various enrichments fall upon the same line.

$O_2^{18})^-$ from $KN^{14}O_3^{18}$, up to 0.015 fraction decomposed, the ratio of initial G-values being 1.122 ± 0.024; (c) This latter isotope effect is greatly reduced after the change to the $y = a + b_2X$ region, since the ratio of the slopes is then 1.02 ± 0.07.

TABLE I

Salt	Initial process $G_{NO_2^-} = b_1$	Second process $G_{NO_2^-} = b_2$	b_2/b_1
$KN^{14}O_3^{16}$	1.456 ± 0.011 (22)[a]	0.902 ± 0.029 (11)[a]	0.63
$KN^{14}O_3^{18}$	1.298 ± 0.017 (11)[a]	0.888 ± 0.037 (4)[a]	.68
$KN^{15}O_3^{16}$	1.435 ± 0.019 (10)[a]	.....	
$KN^{14}O_3^{16}$ (X-rays)	1.89 ± 0.019	1.32	.70

[a] Numbers in brackets indicate number of experimental determinations from which the mean square values and standard deviations were calculated.

Isotope Effects in KNO_3 at Other Temperatures.—The complication of a change in slope was not encountered in the X-ray data[4] below −30° nor within 10° of the transition point at 127°. Data for the γ-radiolysis of KNO_3 at −110 and 122° likewise show no change in slope (Fig. 4 and Fig. 5). The graphs are accurately linear up to 0.05 fractional decomposition, and $G_{NO_2^-}$ values calculated from the least-squares slopes, with their standard deviations, are shown in Table II.

Again relative to production of $(N^{14}O_2^{16})^-$ from $KN^{14}O_3^{16}$ as a standard at each temperature, it is seen that: (a) At −110° the rate of production of $(N^{15}O_2^{16})^-$ from $KN^{15}O_3^{16}$ and that of production of

TABLE II

VALUES UP TO 0.05 FRACTION DECOMPOSED, ACCURATELY REPRESENTED BY $y = bX$

Salt	Temp., °C.	$G_{NO_2^-} = b$	Ratio of G-values
$KN^{14}O_3^{18}$	−110	1.428 ± 0.023	$\frac{G(O^{16})}{G(O^{18})} = 1.030 \pm 0.033$
$KN^{14}O_3^{16}$	−110	1.472 ± .020	
$KN^{15}O_3^{16}$	−110	1.518 ± .024	$\frac{G(N^{14})}{G(N^{15})} = 0.970 \pm .04$
$KN^{14}O_3^{16}$	122	2.250 ± .023	$\frac{G(O^{16})}{G(O^{18})} = 1.06 \pm .027$
$KN^{14}O_3^{18}$	122	2.130 ± .04	

$(N^{14}O_2^{18})^-$ from $KN^{14}O_3^{18}$ do not differ by more than the combined standard deviations from the reference. In consequence no kinetic isotope effect greater than 3% is detected at −110°, and this result provides important evidence that the isotope effects detected at 25 and 122° do not arise from some unknown factor in the method, since it seems improbable that an experimental procedure giving this agreement at −110° would give rise to a difference of 12% when only the temperature during irradiation was changed; (b) At 122° a large kinetic isotope effect still exists in the production of $(N^{14}O_2^{18})^-$ from $KN^{14}O_3^{18}$.

Kinetics Studies of NO_2^- Production in Other Nitrates at 25°.—The explanation previously advanced[4] for the occurrence of the change in slope for KNO_3 at ~0.015 fraction decomposed was that this point corresponded to the appearance of interstitial oxygen molecules in the lattice. Evidence was sought in the present work for the occurrence of such a "break" in the first-order plots for other nitrates, since the interstitial molecules should likewise build up in them under irradiation. In all these other nitrates the initial values accurately obeyed the [log (fraction of NO_3^- undecomposed) = $b \times$ Dose] relation, and accurate initial $G_{NO_2^-}$ values derived from the values of the slope b, are compared in Table III with previous data. Con-

TABLE III

COMPARISON OF $G_{NO_2^-}$ VALUES DERIVED BY LEAST-SQUARES (COLUMN 2), WITH PREVIOUSLY REPORTED $G_{NO_2^-}$ VALUES

Temp., °C.	25°	−110°	24°	15°
$NaNO_3$	0.200 ± 0.004[a]	0.341 ± 0.013	0.25	0.37
KNO_3	1.456 ± .011	1.472 ± .017	1.57	1.96
$RbNO_3$	0.60 ± .10	0.79 ± .05	..	0.64
$CsNO_3$	1.72 ± .10	1.364 ± .043	1.68	1.37
$Ba(NO_3)_2$	1.80 ± .10	1.462 ± .020	1.88	1.75
Ref.	This work	This work	(3)	(4)

[a] The errors quoted are exact relative to that method of determination, but errors in *absolute* dosimetry of ~ ±5% are possible from one work to another. Errors in the calculated continuous spectrum from an X-ray tube are believed responsible for the substantially different values for ref. 4.

sidering the uncertainty of ±5% in the absolute dosimetry, agreement with previous γ-ray data is good. When the fractional decomposition at 25° exceeded 0.015 for $RbNO_3$, $CsNO_3$ and $Ba(NO_3)_2$ the values fell greatly below the extrapolation of the initial line but only for $CsNO_3$ were sufficient data obtained to delineate clearly a section of lower slope (Fig. 6). For $NaN^{14}O_3$ the highest fractional decomposition attained was 0.008 and values lay accurately upon a straight line. Values for $NaN^{15}O_3$

TABLE IV

Temp., °C.	$NaNO_3$	$KN^{14}O_3{}^{16}$	$KN^{14}O_3{}^{18}$	$RbNO_3$	$CsNO_3$	$Ba(NO_3)_2$	$LiNO_3$
60	0.308 ± 0.02	1.46 ± 0.04	1.40 ± 0.04	0.78 ± 0.05	1.66 ± 0.05	1.78 ± 0.06	..
81	.47 ± .03	1.62 ± .03	1.40 ± .04	0.95 ± .05	1.62 ± .06	1.73 ± .06	..
122	.67 ± .02	2.25 ± .03	2.13 ± .04	1.11 ± .05	2.12 ± .08	1.89 ± .06	..
190	1.04 ± .10	2.84 ± .20	2.98 ± .20	2.54 ± .10	3.13 ± .15	1.81 ± .08	..
330	5.1 (L)[a]	5.8 (L)[a]	6.9 (L)[a]	4.5 (L)[a]	7.0 (L)[a]	0.8 (s)	0.07 (L)[a]

[a] L for liquid.

did not depart significantly from this line indicating the absence of any (N^{14}/N^{15}) isotope effect in the radiolysis of $NaNO_3$. (Fig. 6.) Results obtained for $CsNO_3$ and $Ba(NO_3)_2$ at $-110°$ are shown in Fig. 6 to lie accurately upon a single line with no evidence for the change in slope found at 25°.

Initial $G_{NO_2^-}$ Values at Temperatures 25–350°.—For the range up to 0.01 fraction decomposed the formation of nitrite was accurately first order at 60, 80, 122, 190 and 240° for all the nitrates studied. $G_{NO_2^-}$ values corresponding to the slopes are given in Table IV. The temperature dependence of the $G_{NO_2^-}$ values of the solids is referred to in detail in the discussion. However, each $G_{NO_2^-}$ value quoted at 330° was determined by an experiment giving only 2 values for each nitrate. For this irradiation of molten nitrates the samples were first melted *in vacuo* in quartz holders and pumped down to $<10^{-5}$ mm. at which pressure they were sealed off, and irradiated at 330 ± 10°. The $G_{NO_2^-}$ values can be in error by ~ ±10% owing to creepage of the molten nitrates but have the same magnitude as that ($G = 6$) reported[11] for decomposition of KNO_3 by fission recoil, where the environment of the spur is essentially molten. The small $G_{NO_2^-}$ value found for $LiNO_3$ does not fit the behavior noted in the other alkali-metal nitrates at 330°. This is attributed to further decomposition of the nitrite to produce oxides of nitrogen which were detected in the quartz holder after irradiation.

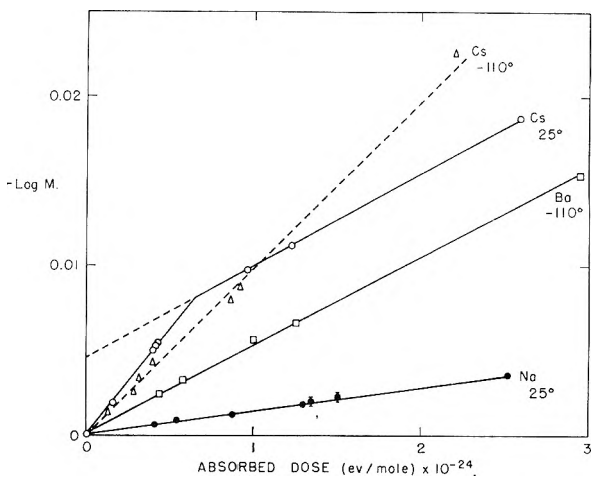

Fig. 6.—Decomposition of various nitrates at the temperature shown, up to ~0.03 fraction decomposed.

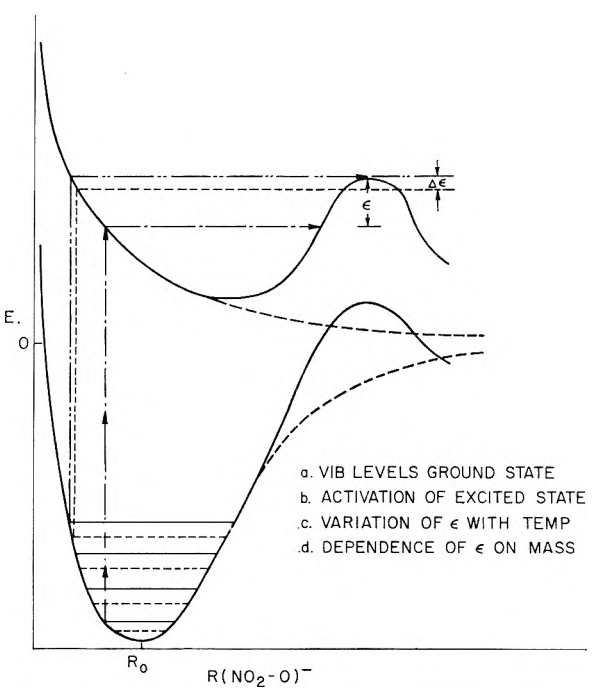

Fig. 7.—Approximate P energy diagram illustrating the relevance of considerations a-d to the dissociation of NO_3^- in an ionic lattice.

Discussion

In terms of the model proposed to account for the great differences in $G_{NO_2^-}$ values under X-ray irradiation,[4] the probability of dissociation of excited nitrate ions is determined in each nitrate by the closeness of packing of the surrounding ions. The free-space of each crystal, which is simply the average volume per ion pair minus the combined volume of cation and anion, is an inverse measure of the closeness of packing. On a crude P. Energy diagram representation this "free-space" determines the height of the barrier which the oxygen fragment of a dissociating excited nitrate ion has to surmount to achieve (Fig. 7) minimum critical separation from the nitrite fragment (Fig. 7). Although activation energies calculated by two independent methods for the different nitrates between 15 and 150° (and then thought to correspond to temperature effects on factors a, b and c in Fig. 7) were in fair agreement,[4] it is not certain that transition-state methods are strictly applicable to this case of a dissociating excited ion in a solid. The availability of the isotopically enriched KNO_3 materials provides the opportunity of specific study of possible contributory factors a,b,c and d in the model in Fig. 7. Corresponding to factor a, the dotted vibrational energy levels are lower because of the lower zero-point energy of an N^{14}–O^{18} or N^{15}–O^{16} bond relative to N^{14}–O^{16}. From the results with $KN^{15}O_3$ and $NaN^{15}O_3$ such lowering of the zero point energy alone does not contribute any

(11) D. Hall and G. N. Walton, *J. Inorg. Nucl. Chem.*, **10**, 215 (1959).

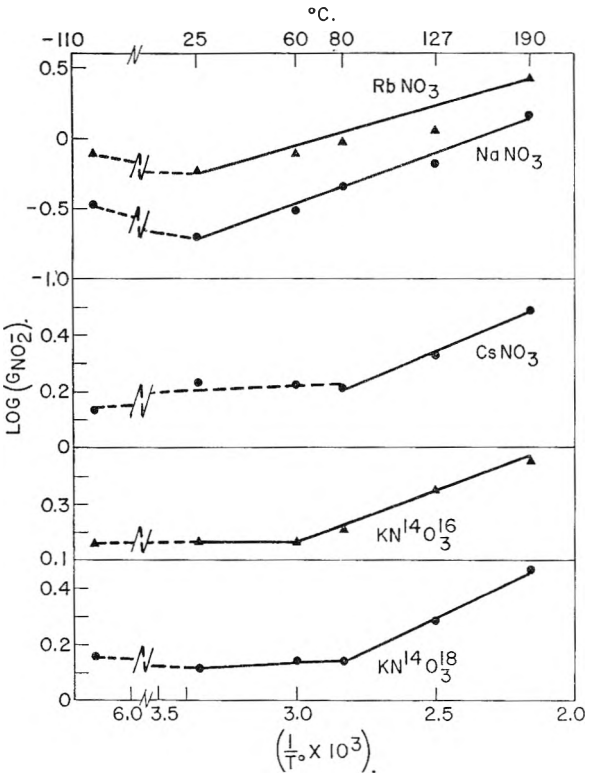

Fig. 8.—Temperature dependence of $G_{NO_2^-}$ values of alkali metal nitrates.

detectable isotope effect in this case. A maximum change of 33 cm.$^{-1}$ in the vibrational levels of KNO_3 by N^{15} substitution has been measured[12] and similar changes are expected for O^{18} substitution. The contribution to the isotope effects in $KN^{14}O_3{}^{18}$ due to zero point energy changes are therefore expected to be small. Additional factors must be taken into consideration for the O^{18} substituted salt. The nature of these factors can be understood by analogy with the results of Lampe and Noyes[13] for the photolysis of iodine in inert solvents. They found the quantum yield decreased with increasing mass of the surrounding solvent particles; for the case of $KNO_3{}^{18}$, the mass of the surrounding oxygen atoms has been increased and a similar decreased probability of dissociation is possible (factor d in Fig. 7).

Since the rate-determining factor is essentially the jump probability for an oxygen atom away from the nitrite fragment, *i.e.*, diffusion, the approximate treatment which follows is based upon that recently developed by S. A. Rice for diffusion in metals.[14,15]

Rice considers the jump probability Γ of an atom in a metal lattice to reach the nearest stable configuration. The basic assumptions of the model are: (1) The amplitude of thermal vibration of the diffusing atom must be sufficient to carry it from one stable configuration to another; (2) The neighboring atoms tend to obstruct the motion of the diffusing atom, and so for a successful jump they must move a sufficient distance away from the path of the diffusing atom that a hole is opened for its motion. Then Γ_m is given by $\sum_i \sum_j P(k_{ij},\delta)$ where the summation extends over all nearest neighbors and $P(k_{ij}, \delta)$ defines (1 and 2) as the occurrence of a configuration in which the diffusing atom has the correct amplitude in the proper direction, and there is out of phase motion of the surrounding atom such that a path is opened for it.

From consideration of crystal dynamics Rice has shown $P(k_{ij},\delta)$ to be of the form

$$P(k_{ij}, \delta) = \bar{\nu} \exp(-V_0/kT) \prod_j \exp(-V_j/kT) \prod_{k>l} g_{kl}$$

For the restricted case of harmonically bound atoms, in which the critical amplitude required by the diffusing atom is assumed to be one-half that to a neighboring lattice site. Rice has obtained the form

$$\Gamma_m = n\bar{\nu} \exp - \left[\left(V_0 + \sum_j V_j + \sum_{k>l} W_{kl}\right)/kT\right]$$

where n is the number of independent paths

$\bar{\nu}$ is a weighted mean frequency for the lattice vibrations
V_0 is the energy to give the atom its critical amplitude
V_j is the energy required to hold the neighboring atom from the path of diffusion
W_{kl} is the potential of the mean force between pairs of atoms, and formally replaces the correlation term $\prod_{k>l} g_{kl}$

Since the diffusion coefficient is given by

$$D = {}^1/_2\Gamma(\Delta x)^2, \ \Delta x = \text{jump length}$$

Then

$$D = {}^1/_2 n\bar{\nu}(\Delta x)^2 \exp\left[-\left(V_0 + \sum_j V_j + \sum_{k>l} W_{kl}\right)/kT\right]$$

As a working approximation, let us apply this equation to the diffusion of oxygen fragments of excited NO_3^- through the cage of surrounding ions. V_0 is here supplied by the excitation into a repulsive state and so

$$G_{NO_2^-} \propto D = {}^1/_2 n\bar{\nu}(\Delta x)^2 \exp\left[-\left(\sum_j V_j + \sum_{k>l} W_{kl}\right)/kT\right]$$

Nitrate crystals expand on heating, therefore $\sum_j V_j$ is not temperature independent as would be true for ideal harmonic oscillations.

Graphs of ln $G_{NO_2^-}$ *vs.* $1/T$ should then give values of

$$\sum_j V_j + \sum_{k>l} W_{kl}$$

The data for various nitrates in this form are shown in Fig. 8.

The graphs are characterized by a high temperature region where an activation energy is indicated, and by apparently slight, or zero, dependence on temperature at lower temperatures.

The temperatures at which this change occurs together with activation energies from the slopes of the temperature dependent regions are presented in Table V.

Exponential plots of diffusion or conductivity data *vs.* $1/T$ for ionic solids, likewise consist of low temperature linear sections in which diffusion proc-

(12) E. V. Sayre, *J. Chem. Phys.*, **31**, 72 (1959).
(13) F. E. Lampe and R. M. Noyes, *J. Am. Chem. Soc.*, **76**, 2140 (1954).
(14) S. A. Rice, *Phys. Rev.*, **112**, 804 (1958).
(15) A. W. Lawson, S. A. Rice and R. D. Corneliussen, Report NP-207, pg. 1-20.

TABLE V

Salt	Onset temp., °K. T_D	0.5 T_m, °K.	Activation energy, kcal./mole	Free space, cm.^{3} × 10^{23}
$NaNO_3$	<298	290	2.77 ± 0.17	4.5
$RbNO_3$	<298	291	2.47 ± .43	5.1
$CsNO_3$	~360	344	1.95 ± .19	5.4
$KN^{14}O_3{}^{16}$	330	303	1.63 ± .11	5.7
$KN^{14}O_3{}^{18}$	340		2.23 ± .16	5.7[a]
$Ba(NO_3)_2$	~470	433	.....	4.5

[a] X-Ray powder diffraction patterns of $KN^{14}O_3{}^{18}$ were identical with those of $KN^{14}O_3{}^{16}$, showing that no change in lattice parameter accompanied isotopic substitution.

esses proceed *via* impurity and imperfection mechanisms. Diffusion through the crystalline lattice onsets more or less sharply at temperatures dependent on crystal treatment and results in rapid enhancement of total diffusion and a high-temperature linear section of greater slope.[16] The temperatures T_D, at which rapid enhancement of diffusion occur in various solids have been summarized by Pimental[23] and generally $T_D \cong (0.5 \pm 0.1)\ T_m$, where $T_m = MPt_1$, for the release and reaction of trapped free radicals. It is interesting, therefore, to observe that the temperature at which the $G_{NO_2^-}$ value for a nitrate begins to show normal thermal enhancement (called T_D in Table V) corresponds closely with 0.5 T_m for that salt. It is proposed that these temperatures correspond, approximately, with significant occurrence of additional diffusion of oxygen fragments through the cage of surrounding ions. The additional diffusion arises, on this model, from the occurrence of favorable configurations of the cage which, in turn, appear because of increased vibrational amplitude of the units of the cage. An alternative statement of the case would be that below the temperature $T_D{}^0$ the units of the cage are frozen-in, and only above this can they be displaced sufficiently to permit the passage of an oxygen fragment.

The activation energies above $T_D{}^0$ correspond to $\sum_j V_j + \sum W$, and the $\sum_j V_j$ term, which is the sum of the energies required to cause the surrounding lattice units to have a configuration favorable to diffusion, should be greater for tightly packed lattices than for lattices of high free-space. This is true in Table V, where the activation energy is seen to decrease with increasing free-space.

For $NaNO_3$, the activation energy has a reasonable value, as shown by an approximate calculation. Consideration of the packing diagram for this crystal shows a favorable direction for dissociation along an N-O bond direction. Regarding atoms as hard spheres, separation of the oxygen from the nitrite fragment to an interstitial position, requires the tilting by ~0.15 Å. of four NO_3^- groups and more serious tilt by ~0.3 Å. of another NO_3^- group. Force constants of 0.03×10^5 dynes/cm. have been used successfully in accounting for the lattice vibrations of ~70 $cm.^{-1}$ for $NaNO_3$[17] and, using this value, an energy of ~1.5 kcal. per mole is required for these displacements. The force constant for movement of the Na^+ ion is 0.35×10^5 dynes/cm. and movement of ~0.1 Å. of two Na^+ corresponds to another 1 kcal./mole.

The experimental activation energy is supported by this rather approximate calculation of ΣV_j and according to the derivation it should also be less than diffusion activation energies measured by normal methods. The measured energy of lattice diffusion in $NaNO_3$ is ~5 kcal. per mole.[18]

The term $\sum_{k>l} W_{kl}$ has not been evaluated for metals and its magnitude is not evident from the theory. This is unfortunate since these arguments lead to the conclusion that when the lattice becomes "frozen-in" the $G_{NO_2^-}$ values should be dependent on D, where, with ΣV_j inoperative

$$D \propto {}^1/_2 n\bar{\nu}(\Delta\bar{x})^2 \exp(-\Sigma W/kT)$$

As an approximation, $\sum_{k>l} W_{kl}$ may be assumed equal in all nitrates (since many atom-atom interactions do not change with cation) and

$$G_{NO_2^-} \cong D \cong {}^1/_2 n\bar{\nu}(\Delta\bar{x})^2 \times \text{constant}$$

at one temperature. At −110° the lattices are all frozen-in according to the data, and the $G_{NO_2^-}$ values should be dependent on the variable $(\Delta\bar{x})^2$ where $\Delta\bar{x}$ is the distance of jump. For excited nitrate ions the jump may occur in several directions, especially if the excited ion acquires rotational energy, and so $(\Delta\bar{x})$ may occur in any direction into the spherical volume around the nitrate ion. The free-space is a measure of this spherical volume, which is unoccupied, and so of the probability that an oxygen fragment can achieve the necessary separation ($\cong \Delta\bar{x}$) for a complete dissociation. It follows that $G_{NO_2^-}$ should be proportional to $(\text{Free-Space})^{2/3}$, if the assumptions are valid. Within the errors of the experimental $G_{NO_2^-}$ values, such dependence is consistent with the data as shown in Fig. 9.

Isotope Effects.—The physical implication of the dependence on free-space at low temperatures is not clear, but it appears that in some directions (whose occurrence is related to free space) the oxygen and nitrite fragments of a dissociating ion can separate to a sufficient distance for completed dissociations. There are two distinct treatments for such dissociations of excited states.

I. Franck-Condon type treatment where excitation is regarded as vertical with dissociation occurring in times equal to the period of 1 vibration. In such cases the dissociation is dependent upon the configuration of the ground state upon excitation. Schaeffer has calculated the relative probabilities of bond rupture in CO_2 enriched in O^{18} and verified them experimentally.[19] His data, stated as the probability of bond rupture relative to rupture of a $C\text{-}O^{16}$ bond in $CO_2{}^{16}$ are

$O^{18}\text{—}C\text{—}O^{18} \longrightarrow O^{18}$	0.946
$O^{18}\text{—}C\text{—}O^{16} \longrightarrow O^{18}$	0.960
$O^{16}\text{—}C\text{—}O^{16} \longrightarrow O^{16}$	1.000

II. Statistical approach in which the excited species passes through several states until dissociation takes place in times of several vibrations.[20] In

(16) A. B. Lidiard, Ionic Conductivity, "Encyclopedia of Physics," Vol. XX, Berlin, 1957, p. 246.

(17) B. S. Rao, *Proc. Indian Acad. Sci.*, **19A**, 93 (1944).

(18) Ling Yang, *J. Chem. Phys.*, **27**, 601 (1957).

(19) O. A. Schaeffer, *J. Chem. Phys.*, **23**, 1309 (1955).

(20) N. B. Slater, *Proc. Roy. Soc.* (*London*), **A194**, 112 (1948).

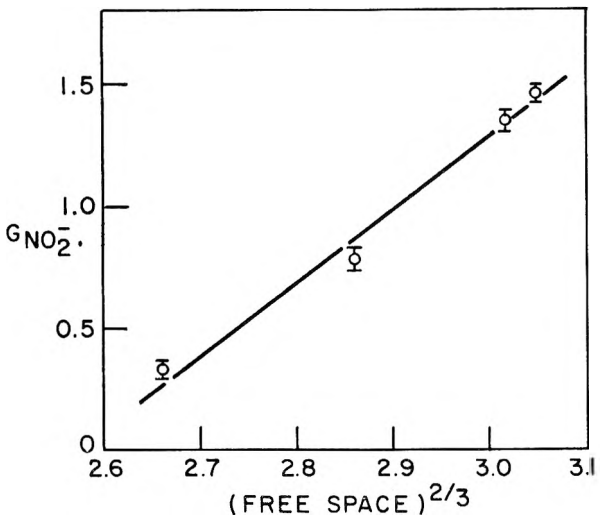

Fig. 9.—Dependence of $G_{NO_2^-}$ at $-110°$ on (Free-Space)$^{2/3}$.

this case, the excited state is not in thermal equilibrium with the system and several treatments of this quasi-equilibrium have been given.[21]

An approximate application to the relative rates of rupture of $(NO_3^{18})^*$ and $(NO_3^{16})^*$ gives

$$\frac{k_{16}}{k_{18}} = \frac{\pi_{16}\pi_{18}^*}{\pi_{16}^*\pi_{18}}\left(\frac{E-\epsilon_{16}}{E-\epsilon_{18}}\right)^{3n-7}$$

where π and π^* are partition functions of the ground and excited states, respectively, and E is the energy given to the ion and ϵ_n is the activation energy for the dissociation of the nitrate ion containing the oxygen isotope n. Values of E are unknown for the complex energy dissipation process of γ-rays, but may be approximated to by 10 e.v. Then using values of ϵ_{16} and ϵ_{18} from Table V, the second term has the value 1.013. The partition functions have not been evaluated but, from application of the theory of absolute reaction rates to the thermal dissociation of NH_4NO_3, a value of 1.026 has been calculated for the ratio of the partition functions in the ruptures of the O_2N-O^{16} and O_2N-O^{18} bond.[22] An isotope effect of about 4% is thus crudely estimated from the statistical approach. The experimental value was $O^{16}\ G_{NO_2^-}/O^{18}G_{NO_2^-} = 1.03 \pm 0.03$ at $-110°$ which agrees with the values approximately calculated from the nature of the proposed model, for either approach I or II.

The details of the temperature dependence between $-110°$ were studied with X-rays[4] and showed regions over which $G_{NO_2^-}$ decreased with increasing T, leading to a minimum G about 15°. Further evidence for the operation of opposing factors comes from the -110 and 25° $G_{NO_2^-}$ values for the nitrates under γ-irradiation (see Table III). For nitrates of small free space such as $NaNO_3$ and $RbNO_3$ the G-value is greater at $-110°$ while with higher free-space nitrates, $Ba(NO_3)_2$, $CsNO_3$ the values at 25° are greater. Deactivation of the excited species by lattice collisions, which could be more extensive in closely packed lattices, is a probable factor contributing to a decrease in G from $-110 \rightarrow 25°$. The thermal expansion of the lattices should increase $\Delta\bar{x}$ and so $G_{NO_2^-}$ and, according to the diffusion model proposed here, significant occurrence of additional paths for dissociation through the surrounding lattice cage provides another temperature-enhanced factor. Recent results of free radical diffusion have shown diffusion often to start in solids at $\sim 0.4\ T_m$.[23]

With the appearance of the additional dissociative paths at $\sim 0.4 T_m$ ($= -30°$ in KNO_3) two new isotopically sensitive processes can be distinguished on the diffusion model.

(a) The jump rate of two isotopes across the same energy barrier is theoretically expected to favor the light isotope by the inverse root of the masses.[24] For the relative jump rates of the oxygen fragments this ratio is 1.06, *i.e.*, an isotope effect of 6%. The jump rates of Fe^{55} and Fe^{59} in silver and copper crystals have been experimentally shown to be in this inverse ratio of the square root of the masses. Similar mass dependence has been found for the diffusion of Li^6 and Li^7 interstitials in silicon,[25] and in tungsten.[26] (b) The amplitude of lattice vibrations for $N^{16}O_3^-$ and $N^{18}O_3^-$ should vary, according to classical theory, by the inverse square root of the masses. This consideration is important because the model represents as a necessary condition for additional dissociations above $\sim 0.4\ T_m$, the displacement of surrounding units from the path of the oxygen. Because of its lower vibrational amplitude at any temperature the displacement of $N^{18}O_3^-$ to a minimum necessary distance from the path of the oxygen, should require greater energy than for $N^{16}O_3^-$, *i.e.*

$$\sum_j V_j(N^{16}O_3^-) < \sum_j V_j(N^{18}O_3^-)$$

The activation energies for $KN^{16}O_3$ and $KN^{18}O_3$ were in fact 1.6 and 2.2 kcal./mole. This isotope effect has resemblances to the Franck-Rabinowitch "cage" effect in solution. Since it arises from differences in vibrational amplitude an estimate of its magnitude would be that

$$\frac{\nu(N^{16}O_3^-)}{\nu(N^{18}O_3^-)} \cong \sqrt{\frac{m(N^{18}O_3^-)}{m(N^{16}O_3^-)}} \cong 1.05$$

No studies have been reported by which the validity of this "cage" isotope effect can be justified. Some such effect is indicated by the magnitude of the room temperature (O^{16}/O^{18}) isotope effect in KNO_3, and in conjunction with the isotope effect upon the jump frequency, would provide a reasonable explanation for the appearance of a larger isotope effect at 25 than at $-110°$. Above 25° the magnitude of the isotope effect decreases with temperature as predicted by theory for isotope effects resulting from differences, in zero-point energy.[27]

The diffusion-controlled model for the γ-radiolysis is thus seen to be consistent with the observed initial isotope effects. Operation of the effects of the

(21) A. L. Wahrhaftig, Chapter in "Advances in Mass Spectrometry," New York, N. Y., 1959.

(22) L. Friedman and J. Bigeleisen, *J. Chem. Phys.*, **18**, 1325 (1950).

(23) A. M. Bass and H. P. Broida, editors, "Formation and Trapping of Free Radicals," Academic Press, New York, N. Y., 1960.

(24) D. Lazarus, Paper to be presented at IAEA Conference Sept. 1960.

(25) D. Lazarus, private communication, 1960.

(26) G. M. McCracken and H. M. Love, *Phys. Rev. Letters*, **5**, 201 (1960).

(27) H. C. Urey, *J. Chem. Soc.*, 562 (1947).

lattice cage would obviously cease at the melting point. The similarity of the $G_{NO_2^-}$ values for the molten salts where the dissociating excited species is surrounded in all nitrates by a relatively easily ruptured liquid envelope agrees well with the behavior expected from the model.[27]

The initial difference of 12% in the rate of radiolysis of $KN^{14}O^{18}O_3$ apparently disappeared above the "break" at 0.015 fraction decomposed. A previous explanation of the KNO_3 "break" attributed it to the build-up of oxygen molecules interstitially in the lattice and consequent 30% reduction of probability of dissociation due to decreased "free space." The result above conflicts with this simple explanation, since a substantially unaltered isotope effect would be predicted by it.

Recent results by Johnson and Forten[28] have shown that the change in slope of the kinetic plot for KNO_3 is accompanied by: (a) sharp increase in the heat of solution (H) of the irradiated material. The plot of H *vs.* dose shows a sudden sharp rise just before that dose corresponding to the "break" and these anomalously high H-values are obtained only for a small range of doses, after which the plot regains a slow gradual increase slightly greater than that before the anomalous rise. Samples having the anomalously high H-values regained normal values when annealed at 150°; (b) an abrupt decrease in density of ~1% with density values constant to with 0.1% before and after this change.

These workers associate the additional H to strain energy of the lattice generated by the misfit of the oxygen molecules, and possibly nitrite. They also found additional H for irradiated $NaNO_3$ and $CsNO_3$ at the same decompositions at which inflections occurred in the kinetic plots. In agreement with the ideas here developed for the relevance of free-space to the diffusion of oxygen, the additional strain energy was found to be five times greater for $NaNO_3$, than for KNO_3 which has a much larger free-space. Johnson discusses evidence favoring the view that this strain energy causes the change to a crystal lattice of more open structure in which increased vibration–rotation of the nitrate ions occurs. The decrease in $G_{NO_2^-}$ value is attributed to increased vibration–rotation of the nitrate ions in the new structure resulting in added dissipation of energy.[28] Since this postulate would not change the nature of the dissociation event, it does not appear probable that it can account for the disappearance of the isotope effect. There seems little doubt, in view of Johnson's results, and the persistence to high decomposition of a large isotope effect when the oxygen escapes continuously from the crystal under irradiation at 122°. (Table II), that oxygen molecules are intimately involved in the occurrence of the "break." Furthermore, Johnson's data indicate that interstitial molecules are not present in large numbers above the break because the anomalously high H attributed to their strain energy does not persist after the inflection. There is other evidence that the oxygen is present in gas pockets at pressures up to 1400 atmospheres. Participation of the gas in these pockets in the reaction path could occur by any of several mechanisms, but the evidence available is insufficient to decide between them. To be acceptable any mechanism must (a) account for the absence of any large isotope effect, (b) explain why the inhibiting effect in KNO_3 apparently does not occur til the lattice expands, and (c) why the decomposition continues to be 1st order in [nitrate] above the break. While reaction schemes involving the participation of gas pockets in the dissociative event can account for (a) by replacing the isotopically sensitive diffusion-controlled dissociative event by an equilibrium-type step, possibly with ozone molecules as intermediates, it does not appear profitable at this stage to advance unsupported mechanisms for the dissociation above the break. Experiments are in preparation to study the nature of the occluded oxygen product by measurements of static magnetic susceptibility, which may provide the information needed to clarify the mechanism in this region.

(28) E. R. Johnson and J. Forten, Prog. Rept., June 1960, AEC AT(30-1 1824).

Conclusions

The representation of the dissociation of nitrate ions in terms of a diffusion-based model gives a satisfactory and consistent account of the relationship of the free-space to the rate of dissociation of the alkali metal nitrates at high and low temperatures. The kinetic isotope effects observed, which are anomalous on normal theories of isotope effects, are also accounted for by this model, but only for decompositions below the inflection in the kinetic plots. Further information is needed to clarify the nature of the dissociation process at higher decomposition.

Acknowledgment.—The author wishes to thank A. Hrobar for her assistance with the many colorimetric analyses for nitrite, and is indebted to Dr. M. Matheson and Dr. G. Montet for helpful discussion.

REACTION KINETICS OF NEEDLE-SHAPED PARTICLES WITH A GAS: THE 1,1-DIPHENYLUREA–HYDROGEN BROMIDE SYSTEM[1]

BY F. E. MASSOTH AND W. E. HENSEL, JR.

Department of Chemistry and Chemical Engineering, Southwest Research Institute, 8500 Culebra Road, San Antonio, Texas

Received September 30, 1960

The kinetics of the reaction between hydrogen bromide and 1,1-diphenylurea needles has been studied from −3 to 50° and 50 to 300 mm. pressure by means of a weight change method. The reaction followed parabolic law kinetics derived for rod-like particles. Rate constants were proportional to the pressure to the 1.7 power. An Arrhenius plot was obtained for the temperature variation of the reaction constants; the activation energy was found to be 7.3 kcal. per mole. The rate constant is given by the expression $k = 2.4 \times 10^{-3} P^{1.7} e^{-7,300/RT}$ sec.$^{-1}$, where P is in mm. and T in °K. The rate-determining step is interpreted as diffusion of hydrogen bromide from the surface to the reaction interface under a concentration gradient, the surface concentration being pressure dependent. A qualitative particle size effect was noted.

Introduction

The basic kinetic laws for gas–metal reactions have been well established. Evans,[2] Gulbranson[3] and Mott[4] have pioneered studies on the oxidation of metals. Their results were interpreted in terms of weight change or film thickness measurements. Since they were dealing with flat surfaces, particle geometry was not a factor.

More recently, gas–solid reactions involving powdered materials have been studied. The basic kinetic laws evolved from studies with metals were modified to take into account the changing surface area of the unreacted particle during reaction. Previous investigators have derived kinetic expressions for spherical particles,[5] cubic particles,[6] and disc-like particles.[7] In the present investigation this concept is extended to rod-like particle shapes.

Reaction of gaseous hydrogen bromide with 1,1-diphenylurea forms a salt-like product having the formula, $(C_6H_5)_2$ $NCONH_2 \cdot HBr$. Since this reaction results in an increase in weight due to the solid product formed, the kinetics may be studied conveniently by a weight-change method. The melting point of the reactant is 189°, and thus its loss in weight due to volatilization is negligible under the experimental conditions. Although the reaction product decomposes at about 145°, preliminary tests indicated no loss due to decomposition below 50°.

Theory

The parabolic law is most often followed in gas–solid reactions; this law is defined as

$$\frac{dx}{dt} = \frac{a}{x} \text{ or } at = \frac{x^2}{2} \qquad (1)$$

where x is the film thickness of product at time t and a is a proportionality constant. The film thickness of product is not easily measurable, but can be related to the fraction converted, F. The latter quantity can be determined experimentally from weight-gain measurements taken during the course of the reaction. Equation 2 expresses this relationship

$$F = \frac{W_t - W_0}{W_0\left[\left(\frac{M_p}{M_0}\right) - 1\right]} \qquad (2)$$

where W_t is the weight of sample at time t, W_0 is the initial weight of sample, M_0 is the molecular weight of the solid reactant, and M_p is the molecular weight of the product.

The relationship between F and x is dependent upon particle geometry. In order to derive the relationship, the following assumptions are made: (1) the solid reactant consists of needle or rod-like particles; (2) the length of a particle is much greater than its radius; (3) the product film is uniform in thickness.

Consider a partially reacted cylindrical particle consisting of an inner core of unreacted material and an outer shell of reaction product. The volume of reactant, v_u, left at any time is related to the fraction converted and the initial particle volume, v_0, for an average particle by

$$v_u = (1 - F)v_0 \qquad (3)$$

Since the volume of a cylinder is proportional to the square of its radius times its length, and since the length is essentially constant during the reaction, the above expression becomes

$$r_u = (1 - F)^{1/2} r_0 \qquad (4)$$

where r_u and r_0 are the radii of unreacted and initial particles, respectively.

The particle volume v at any time t is equal to the sum of the unreacted volume and the reacted volume v_r. However, $v_r = (v_0 - v_u)\beta$ where β is the ratio of the molar volumes of product to reactant. Hence

$$v = v_u + v_0\beta - v_u\beta \qquad (5)$$

Substitution of equation 3 into equation 5 yields

$$v = v_0[1 - F + \beta F]$$

or in terms of radius, r, of the particle at time t

$$r = r_0[1 - F + \beta F]^{1/2} \qquad (6)$$

The thickness of product layer, x, is

$$x = r - r_u \qquad (7)$$

Substituting equations 4 and 6 into equation 7 and defining $c = -(1 - \beta)$, one obtains

$$\frac{x}{r_0} = (1 + cF)^{1/2} - (1 - F)^{1/2} \qquad (8)$$

Substitution for x into the integrated parabolic expression, equation 1, yields

(1) Paper presented at the Spring 1960 American Chemical Society National Meeting, Cleveland, Ohio.

(2) U. R. Evans, *Trans. Electrochem. Soc.*, **91**, 547 (1947); **83**, 335 (1943).

(3) E. A. Gulbransen, *ibid.*, **83**, 301 (1943); **91**, 573 (1947).

(4) N. F. Mott, *Trans. Faraday Soc.*, **36**, 472 (1940).

(5) R. L. Farrar, Jr., and H. A. Smith, *J. Phys. Chem.*, **59**, 763 (1955).

(6) F. E. Massoth and W. E. Hensel, Jr., *ibid.*, **63**, 697 (1959).

(7) F. E. Massoth and W. E. Hensel, Jr., *ibid.*, **64**, 414 (1960).

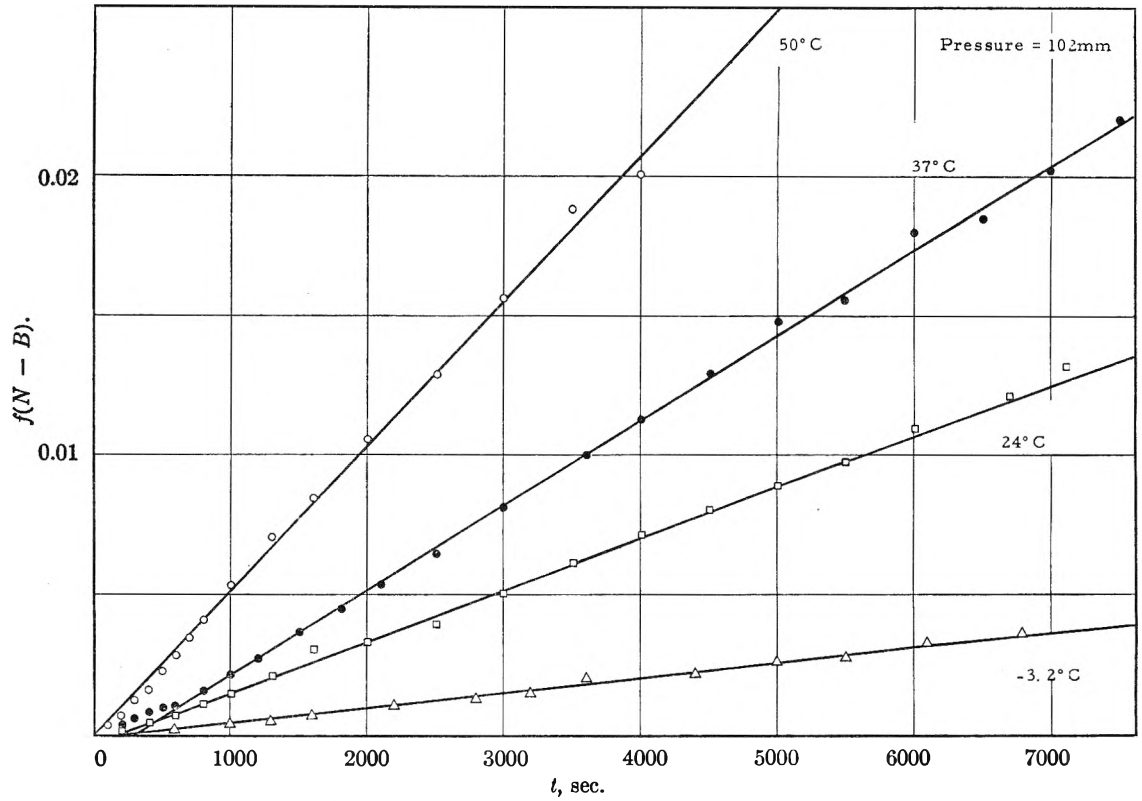

Fig. 1.—Temperature variation at constant pressure.

$$kt = \tfrac{1}{2}[(1 + cF)^{1/3} - (1 - F)^{1/3}]^2 = f'(N - B) \quad (9)$$

where k is the parabolic rate constant $= a/r_0^2$. Now, if the assumption is made that the external particle dimension remains constant throughout the reaction (c = 0), then a much simpler expression results

$$kt = \tfrac{1}{2}[1 - (1 - F)^{1/3}]^2 = f(N - B) \quad (10)$$

Hence, the function of $f(N - B)$ can be calculated from the F values obtained experimentally. A plot of $f(N - B)$ *vs.* t should give a straight line if the rate of reaction follows the parabolic law.

Variation of the rate constant with temperature is usually treated by the Arrhenius equation. In most cases when a diffusion mechanism prevails, the activation energy is that for the diffusion process. On the other hand, the effect of pressure upon the rate of reaction for gas–solid reactions, is generally not predictable from theoretical considerations. The rate constant can sometimes be related to the pressure P at constant temperature by a power term in P, *viz.*

$$k = KP^n \quad (11)$$

where K is the diffusion rate constant and n is a constant. If the product exhibits an appreciable dissociation pressure, a plot of k *vs.* P^n will not go through the origin, and equation 11 would have to be corrected to include a dissociation pressure term.

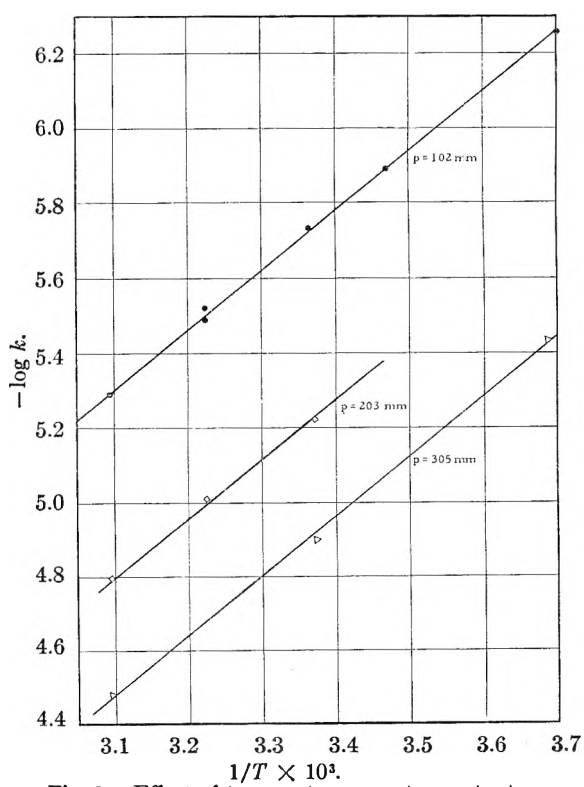

Fig. 2.—Effect of temperature on rate constant.

Experimental

Highest purity 1,1-diphenylurea was obtained from the Fisher Scientific Company as small crystalline plates. This material was recrystallized as needles from methanol. The crystals were screened three times, retaining the portion through 20 mesh and held on 40 mesh as the sample. One large batch of material was used for the runs which constitute the basic data. Anhydrous hydrogen bromide, minimum purity 99.8%, was procured from The Matheson Company, Inc. and was not further purified. The reaction product, 1,1-diphenylurea hydrobromide, had a needle-like form and a tan-orange appearance. It decomposed about 145°, was very slightly hygroscopic and had a density of 1.47 and refractive index of 1.641.

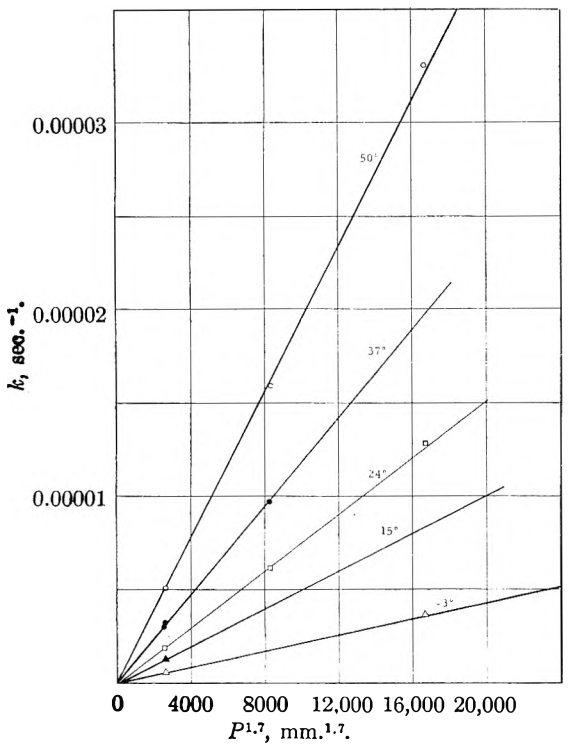

Fig. 3.—k *vs.* $P^{1.7}$.

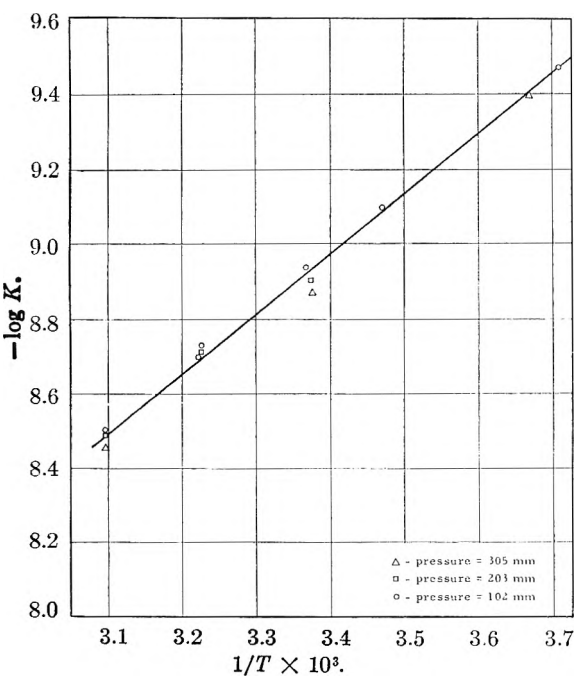

Fig. 4.—Arrhenius plot—pressure independent.

A quartz helix spring, having a maximum load capacity of 500 mg., was employed for the weight-change measurements. Spring displacement was measured with a 12 mm. vernier attached to a cathetometer. A small Pyrex bucket held the sample. Analytical weights were used for calibration of the spring extension *versus* load, linear displacement being assumed over the range measured. No change in spring constant was observed upon recalibration after numerous runs. The helix spring was supported in a Pyrex reactor having an over-all length of 36 cm., and an outside diameter of 3 cm. A ground glass joint permitted disassembly of the reactor and a side-arm for gas entry was located about two-thirds from the bottom. A standard glass vacuum system provided for introduction and removal of gas. Pressure was measured by means of a mercury manometer to ±1 mm. A thermostated water-bath maintained constant reactor temperature. Reactor temperatures were measured to ±0.25° with a thermometer suspended inside the reactor.

A total of twelve runs were made at five temperatures and three pressures. Approximately 75 mg. of 1,1-diphenylurea was used for each run. Spring extension was measured at various time intervals with the cathetometer. Three readings were taken at each interval and averaged; the deviation of the average was ± 0.02 mm., which corresponded to a weight deviation of ±0.2 mg. A blank run with hydrogen bromide resulted in no weight change in the bucket indicating negligible reaction of this gas with Pyrex.

Results

The basic data in terms of mole fraction converted, F, were calculated from weight change measurements.[8] Using the values of F, values for $f(N - B)$ were computed at each time. In Fig. 1, linear plots of $f(N - B)$ *vs.* t for several typical runs clearly show the parabolic dependence of the reaction. The slope of each line is equal to the reaction rate constant k at the given conditions of temperature and pressure. All runs showed similar straight-line $f(N - B)$ plots, thus establishing a parabolic mechanism for the reaction.

Figure 1 also shows that increase in temperature at constant pressure resulted in an increase in reaction rate. The variation of the reaction rate constant with temperature is shown in Fig. 2, where log k is plotted against the reciprocal of the absolute temperature at three levels of pressure. The straight lines obtained show conformance to a normal Arrhenius temperature dependency of the reaction at each isobar.

The data obtained for the variation of pressure at constant temperature showed that pressure had an accelerating effect upon the reaction. In order to determine the pressure dependency of the reaction, log k was plotted *vs.* log P (not shown). At each isotherm, a straightline was obtained, indicating that k is proportional to some power of pressure, the power being the slope of the line. The average of the three slopes gave a value of 1.7. To determine whether the reaction product exhibits a dissociation pressure in the temperature range studied, k was plotted against $P^{1.7}$. As shown in Fig. 3, the straight lines pass through the origin, therefore indicating no dissociation pressure and also that the following relationship obtains between the rate constant and pressure

$$k = KP^{1.7}$$

In accordance with the pressure relationship given above, parabolic rate constants, independent of pressure, were calculated. These new rate constants K now fall on a single line in an Arrhenius plot, as illustrated in Fig. 4. The least squares slopes of this plot yields an activation energy of 7.3 ± 0.2 kcal./mole, and the intercept a frequency factor of (2.4 ± 0.1) × 10^{-3} sec.$^{-1}$ (mm.)$^{-1.7}$. Thus, the rate constant in the temperature range

(8) A more detailed form of this paper (or extended version, or material supplementary to this article) has been deposited as Document number 6518 with the ADI Auxiliary Publications Project, Photoduplication Service, Library of Congress, Washington 25, D. C. A copy may be secured by citing the Document number and by remitting $1.25 for photoprints, or $1.25 for 35 mm. microfilm. Advance payment is required. Make checks or money orders payable to: Chief, Photoduplication Service, Library of Congress.

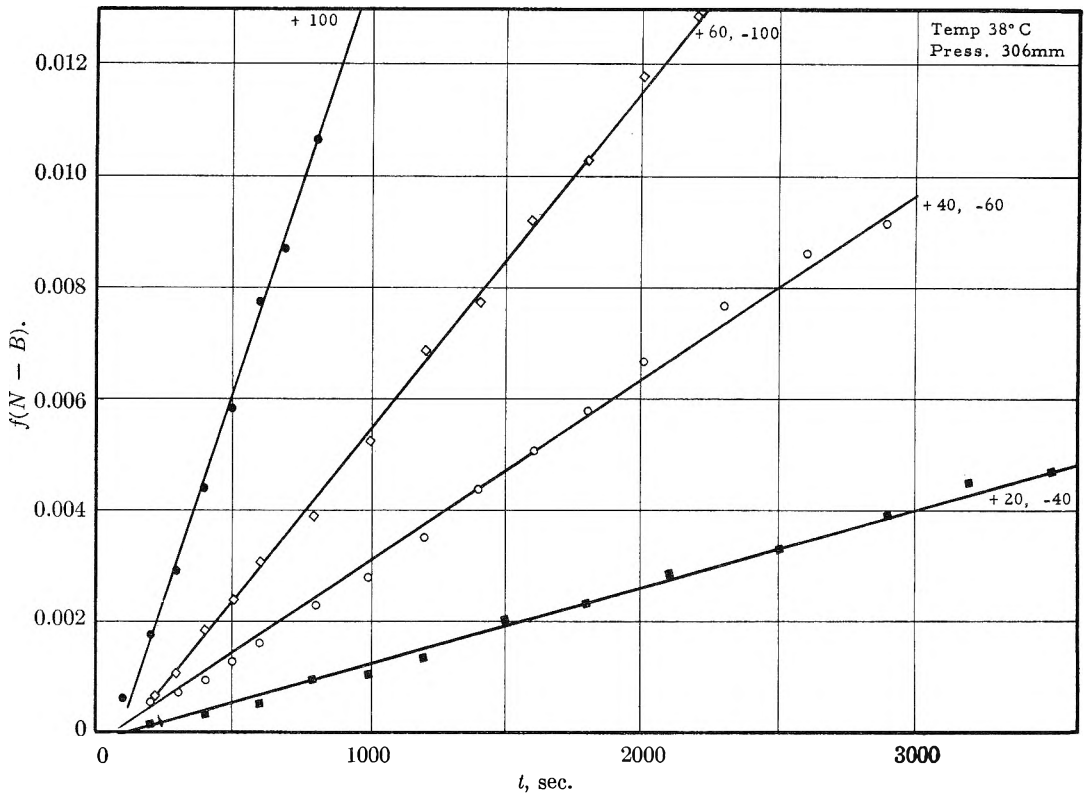

Fig. 5.—Variation of particle size at constant temperature and pressure.

−3 to 50° and for pressures up to 300 mm. is given by the expression

$$k = 2.4 \times 10^{-3} P^{1.7} e^{-7,300/RT} \text{ sec.}^{-1}$$

where P is in mm. and T is in degrees absolute.

Although not shown in the rate expression presented, particle size is another variable in correlating reaction rates. A particle size effect in the reaction rate is expected since the rate constant is inversely proportional to the square of the initial radius of the particles. The effect of particle size upon the reaction rate was studied by screening the recrystallized needles into four sieve sizes. The relative rates of reaction of these four batches are shown in Fig. 5. A general increase was noted in rate of reaction as the particle size decreased. It was not possible to develop a quantitative correlation between the rate constant and the average particle size because screening was found to be only partially effective.

Discussion

Reaction of a solid and a gas, where only a solid product is formed, proceeds at the interface between the two solids.[9] The over-all rate of reaction is generally the rate at which reactants can reach the interface. Where parabolic kinetics are found, the rate of build-up of film is proportional to the inverse of the film thickness, and it is usually assumed that the reaction is controlled by volume diffusion of gaseous reactant through the product film. In this case, the film is considered protective. The formation of a protective film can be attributed to the fact that the product molecules which are formed on the surface have a diameter slightly greater than that of the original reactant molecules. If the product molecules are smaller or much larger than the original molecules, cracking of the film results and the film is not protective.[4] In the latter case, the parabolic law will not be followed.

In using the parabolic expression, $f(N - B)$, the assumption is made that the external dimensions of the particle remain constant throughout the reaction. It is recognized that expansion is not always negligible. In our case the molar volume expansion is 1.25. For this expansion factor, $f(N - B)$ can be shown to be proportional to $f'(N - B)$, within experimental error for values of F up to 0.85; hence, the effect of expansion is negligible over most of the reaction range studied. The elimination of the expansion term greatly simplifies the kinetic laws, and as such, the shorter forms are most generally used in correlating rate data.

Deviations from the parabolic law were encountered in some instances in the early stages of the reaction, particularly at high temperatures and high pressures. A faster rate occurred than would be predicted by this law. This is attributed to a localized, heat effect caused by the rapid initial exothermic reaction on the surface of the unreacted particles. The heat, not being dissipated fast enough due to the low thermal conductivity of the material, raises the surface temperature of the mixture and results in a more rapid reaction rate. After the initial product layer is formed, this situation does not obtain; the temperature falls to ambient temperature and the rate approaches that predicted by the parabolic law. This heat effect was proved in a separate experiment in which ground glass was added to the diphenylurea, so

(9) S. J. Gregg, "Surface Chemistry of Solids," Reinhold Publ. Corp., Inc., New York, N. Y., 1951.

that the surface heat might be better dissipated. The initial deviation in this case was markedly less, resulting in a better parabolic fit. It should be pointed out that the slopes of the linear portions in the $f(N - B)$ plots with and without heat effects are the same; therefore, the rate constant k can still be obtained even though an initial deviation occurs.

In most cases, the reaction followed the parabolic law until approximately 75% of the reactant was converted to product, after which the reaction practically stopped. Additional slow reaction was noted on letting the partially reacted material stand for prolonged periods in the presence of hydrogen bromide gas. In one run, material was removed from the reactor, ground and re-reacted several times, whereupon complete conversion was finally attained. Thus, the reaction proceeds to completion according to stoichiometry. However, the latter phase is extremely slow under reaction conditions and is probably governed by a different mechanism. It is interesting to speculate that there may be a critical thickness of film product, beyond which the parabolic growth is no longer obeyed. Qualitatively, it was found that smaller particles gave larger conversions before cut-out and *vice versa*, in line with such a supposition. A shift of mechanism at a definite thickness of product has been noted for the reaction of sodium fluoride with uranium hexafluoride.[6]

Many earlier workers had not studied the effect of pressure upon reaction rates. If the product formed is volatile or it is a semi-conductor, pressure would have a negative or slight positive effect, respectively, upon the reaction rate.[10] Neither case applies to our reaction. The reaction of diphenylurea with hydrogen bromide is markedly dependent upon pressure. Since diffusion is the rate-determining process, the rate of reaction is proportional to the migration of gas molecules across the boundary layer; this diffusion will be dependent upon the concentration gradient from the gas–product interface to the reactant–product interface. As pressure increases, the concentration gradient increases, since the surface concentration is higher while the reaction interface concentration remains constant. Thus, since the transport of gas across the product film is rate determining, we have a parabolic process whose magnitude is pressure dependent.[11]

The above picture should be clearly distinguished from the case where the rate of reaction is controlled by the rate of adsorption, under which condition we would not be dealing with a parabolic mechanism. If adsorption were rate controlling, the rate of reaction would be expected to be proportional to the external surface area of the particle. Since there is a swelling of the particle upon reaction, an appropriate increase in surface area would be expected. Hence, the rate of adsorption should increase proportionally during reaction. However, the rate of reaction, experimentally observed, constantly decreased during reaction.

A further argument against adsorption being rate determining is as follows: The rate of simple adsorption is proportional to the product of the pressure and the uncovered surface minus the rate of evaporation times the surface coverage. In our case, surface coverage is expected to be very low since the pressures employed were small compared to saturation pressure (50–300 mm. *vs.* 25 atm.). Therefore, the rate of adsorption should be proportional to P^1, and since it was found experimentally that the reaction rate was proportional to $P^{1.7}$, adsorption is not rate controlling.

For the sake of completeness, it should be pointed out that neither diffusion in the gas phase nor chemical reaction at the reactant–product interface can be rate determining. Reaction control by the former would require the rate of conversion to be constant with time, while control by the latter would require the rate to follow a linear law, *i.e.*, reaction decreases directly with decrease of surface area of reactant.

The reaction of diphenylurea with hydrogen bromide follows a normal Arrhenius dependency. Since the rate of reaction is diffusion controlled, the activation energy is that for the diffusion process. The experimental rate constant is a function of the concentration gradient across the boundary layer as well as the temperature, whereas the true diffusion rate constant is dependent on temperature alone. Since the concentration gradient is a function of the system pressure, an Arrhenius relationship at each isobar is obtained (Fig. 2). The activation energy at each pressure is the same and therefore the effect of pressure shows up only in the pre-exponential factor. When pressure is taken into account, the resulting diffusion rate constants yield a single straight line Arrhenius plot (Fig. 4). That the rate process is determined by the same factor throughout the temperature range investigated is confirmed by the consistency of the activation energy over this range.

Several runs were made at higher temperatures. Good parabolic fits were not obtained. At 80°, the data seemed to fit best a logarithmic law.[2,6] It might be that a shift in mechanism with temperature occurred; such a phenomenon is not uncommon in gas–solid reactions.[12,13] Another explanation for the apparent divergence from parabolic kinetics could be weight loss *via* volatilization at this temperature.

The parabolic rate constant should be proportional to the inverse of the square of the particle radius. It was not possible to test this relationship due to inability to reproduce particle sizes from one recrystallized batch of material to another. However, as was shown in a qualitative way, the rate of reaction increased with decreasing particle size. The major factors which affect reproducibility between batches of material are recrystallization and sieving. In recrystallizing diphenylurea from methanol, the size of the crystals formed depended on concentration, recrystallization time and agitation, among other things. It was difficult to reproduce these conditions from one batch to another. It was hoped that screening the material

(10) J. T. Law, *J. Phys. Chem.*, **61**, 1200 (1957).
(11) D. Perchanski, *Ann. Chim.*, [12] **2**, 601 (1947).
(12) J. Waber, *et al.*, *J. Electrochem. Soc.*, **99**, 121 (1952).
(13) D. J. Cubicciotti, *J. Am. Chem. Soc.*, **74**, 1200 (1952).

would produce particles of uniform size so that particle radius could be determined. Photomicrographs of screened material showed sieving to be ineffective. The material collected from any sieve contained particles of the expected size plus many small particles and some larger ones. The small particles were held to other needles, probably by an electrostatic force. The large particles must have passed through the sieve pores in a vertical manner. Although sieving was ineffective, the relative number of particles of a given dimension varied from one sieve to another. Thus, the effect of particle size on reaction rate could only be determined in a qualitative manner.

Acknowledgment.—The authors wish to express their gratitude to the Southwest Research Institute Associate Fund, whose financial support made this work possible.

COMPLETE SET EXPANSIONS FOR MOLECULAR WAVE FUNCTIONS

BY H. O. PRITCHARD AND F. H. SUMNER

University of Manchester, Manchester 13, England

Received October 5, 1960

The wave functions for the $1s\sigma_g$, $2s\sigma_g$ and $3d\sigma_g$ states of H_2^+ have been expanded in terms of two complete sets of spherical functions, one centered on each atom. No serious difficulty was caused by overcompleteness, and excellent representations of the energies and wave functions were obtained.

Before it is possible to perform accurate calculations on small molecules, it will be necessary to find quick and efficient methods for the representation of electron–nucleus and electron–electron distribution functions. Such progress can only be expected if the basic functions used for the representation are members of a suitable complete set. Several complete sets of spherical functions are known which might be suitable for the representation of electron–nucleus distribution functions, but the simple substitution of one of these sets for, say, the hydrogen-like set in the normal l.c.a.o. treatment of H_2^+ can be expected to lead to difficulties due to overcompleteness. In principle, the wave function for H_2^+ can be expanded using only one complete set: if two complete sets are used, one of them is superfluous and the system of secular equations becomes insoluble.[1] However, the expansion of the wave function of H_2^+ in terms of only one set is very disappointing,[2] largely because it is difficult to reproduce the singularities at the two nuclei in terms of sums of smooth functions. On the other hand, using only the first two members of a complete set centered on each nucleus, a far better representation of H_2^+ is obtained[3] than the equivalent treatment using the first ten hydrogen atom functions.[4] It will be shown in this paper that by generalizing this treatment, an almost exact description of the H_2^+ system can be obtained before overcompleteness becomes a serious handicap.

The L.C.M.O. Method Using Epstein Functions.—The general method of calculation is essentially that used by us before[4] in which a tenth order secular determinant was constructed by a program written for the Manchester University Mark I Computer. The substitution of the functions

$$\phi_i = \chi_{nl}(x)Y_l(\vartheta) = \left[\frac{(n-l-1)!}{2n\,[(n+l)!]^3}\cdot\left(\frac{2Z}{a_0}\right)^3\cdot\frac{2l+1}{2}\cdot\frac{1}{2\pi}\right]^{1/2}\left(\frac{2Zr}{a_0}\right)^l L_{n+l}^{2l+1}\left(\frac{2Zr}{a_0}\right)P_l^0(\cos\theta)\cdot e^{-\frac{Zr}{a_0}}$$

$$[n = 1,2,3,4;\ l = 0 \ldots (n-1);\ (m = 0)]$$

for the hydrogen-like set was actually a considerable simplification of the original program. There is, however, one slight complication in that, while any member of the set is orthogonal to most of the other members, it is not orthogonal to adjacent functions having the same value of l; the relevant relations were given by Hylleraas[5] as follows (with $x = 2Zr/a_0$)

$$\int_0^\infty \chi_{nl}^2(x)\,x^2\,dx = 1 \qquad \text{(a)}$$

$$\int_0^\infty \chi_{nl}(x)\,\chi_{(n+j)l}(x)\,x^2\,dx = 0 \text{ for } j = 2,3,4 \ldots\ldots \qquad \text{(b)}$$

$$\int_0^\infty \chi_{nl}(x)\,\chi_{(n+1)l}(x)\,x^2\,dx = -\frac{1}{2}\left[\left(1-\frac{l}{n}\right)\left(1+\frac{l}{n+1}\right)\right]^{1/2} \qquad \text{(c)}$$

$$\int_0^\infty \chi_{nl}^2(x)\,x\,dx = 1/2n \qquad \text{(d)}$$

$$\int_0^\infty \chi_{nl}(x)\,\chi_{(n+j)l}(x)\,x\,dx = 0 \text{ for all } j \neq 0 \qquad \text{(e)}$$

As before, we define ten molecular orbitals as

$$\Phi_i = (2 + 2\xi_{ii})^{-1/2}(\phi_i^a + p_i\phi_i^b),\ i = 0, 1 \ldots 9$$

where p_i is the parity (± 1) of the wave function ϕ_i and ξ_{ii} is the overlap integral between ϕ_i^a centered on atom A and $p_i\phi_i^b$ centered on atom B. We then write the total wave function for the system as

$$\Psi = \sum_{i=0}^{9} c_i\Phi_i = \sum_{i=0}^{9} c_i\,(2 + 2\xi_{ii})^{-1/2}\,(\phi_i^a + p_i\phi_i^b)$$

Minimizing the energy with respect to the coefficients c_i leads to the tenth order secular determinant $|H_{ij} - S_{ij}E| = 0$. The matrix ele-

(1) P.-O. Lowdin, *Advances in Phys.*, **5**, 1 (1956); *Advances in Chem. Phys.*, **2**, 207 (1959); *Ann. Rev. Phys. Chem.*, **11**, 107 (1960).

(2) K. M. Howell and H. Shull, *J. Chem. Phys.*, **30**, 627 (1959).

(3) B. F. Gray, Ph.D. Thesis, Manchester, 1957.

(4) B. F. Gray, H. O. Pritchard and F. H. Sumner, *J. Chem. Soc.*, 2631 (1956).

(5) E. A. Hylleraas, *Z. Physik*, **48**, 469 (1928).

ments H_{ij} and S_{ij} may then be obtained, remembering that the ϕ_i are not eigenfunctions of a hydrogen-like Hamiltonian, but satisfy the equation

$$\mathcal{H}'\phi_i = \epsilon_i'\phi_i \text{ where } \mathcal{H}' = -\frac{1}{2}\nabla^2 - \frac{nZe^2}{r}$$

Thus

$$S_{ij} = 2(2 + 2\xi_{ii})^{-1/2}(2 + 2\xi_{jj})^{-1/2}(\xi_{ij} + \omega_{ij})$$

and

$$H_{ij} = 2(2 + 2\xi_{ii})^{-1/2}(2 + 2\xi_{jj})^{-1/2}[(\xi_{ij} + \omega_{ij})(\epsilon_j' + e^2/R) - e^2(J_{ij} + K_{ij}) + (Zn_j - 1)e^2(L_{ij} + K_{ji})]$$

where e is the electronic charge, R is the internuclear separation, ϵ_j' is the eigenvalue of ϕ_j for the Hamiltonian $\mathcal{H}'$, $\xi_{ij} = p_j \int \phi_i^a \phi_j^b \, d\tau$

$\omega_{ij} = \int \phi_i^a \phi_j^a \, d\tau$, $J_{ij} = \int \phi_i^a \phi_j^a r_b^{-1} \, d\tau$,
$K_{ij} = p_j \int \phi_i^a \phi_j^b r_a^{-1} \, d\tau$ and $L_{ij} = \int \phi_i^a \phi_j^a r_a^{-1} \, d\tau$

From the relations d and e given above $L_{ij} = Z/n_j$ atomic units if $i = j$ and zero otherwise; similarly, ω_{ij} may be written down from relations a, b and c. A further simplification is possible because $\epsilon_j' = Z^2 n_j^2 \epsilon_j$ where ϵ_j is the eigenvalue of ϕ_j with $Zn_j = 1$, and since ϵ_j is $(n_j)^{-2}$ times the ionization potential of hydrogen, $\epsilon_j' = -Z^2/2$ atomic units. This makes the relation between K_{ij} and K_{ji} very simple, *i.e.*

$$K_{ji} = \frac{n_i}{n_j} K_{ij}$$

Solution of the Secular Equations.—The calculations were performed initially for $Z = 1.0$ and $Z = 1.25$, at an internuclear separation of $R = 2a_0$, but because of the approach to overcompleteness, we were unable to solve either of the resulting secular determinants with the programs which then existed for dealing with this problem.[6] Furthermore, as it was only a matter of weeks before the Mark I computer was to be dismantled, we decided to construct secular determinants for as large a range of Z as possible, and evaluate them later on the Mercury machine with which it was replaced. Unfortunately, we thought that the energy maximum of the 1s hydrogen-like function at $Z = 1.228$ would probably dominate throughout the calculation, with the result that we covered the range $Z = 1.0$ to $Z = 1.4$; however, although excellent representations of $1s\sigma_g$, $2s\sigma_g$ and $3d\sigma_g$ states were obtained, our chosen range of Z did not span the best value for any of these three states.

The first solutions were obtained by substituting trial values of E in the secular determinant, until a value was found for which the determinant vanished; the determinants were well-behaved functions of E and there was no difficulty. The coefficients c_i were then found by solving sets of simultaneous equations; this will be called method 1.

Subsequently, a more accurate version of our original Mark I matrix program became available. (The set of equations $|H - SE| = 0$ was transformed to a new set $|S^{-1}H - IE| = 0$ by inverting the matrix $\mathbf{S}$; $\mathbf{S^{-1}H}$, being unsymmetrical, was solved by the Lanczos procedure—method 2a). The eigenvalues for the bound states obtained using this program were identical with those from method 1, but the corresponding eigenvectors looked significantly different. Nevertheless, both sets of vectors were found to be equally acceptable solutions for the problem, and both corresponded to wave functions of equal numerical magnitude. There are two reasons why this might happen. One is that the system is so nearly overcomplete that a whole range of wave functions is more or less equally acceptable and the one found is that most favored by the particular combination of rounding errors. The other is that our original basic set of functions is not an orthogonal set, and again depending on the accumulation of rounding errors, the wave function can be equally well represented to within the accuracy of the calculation by several different combinations of these non-orthogonal functions; in a sense, this also is overcompleteness. This point will be discussed further below.

Overcompleteness causes the determinant of the overlap matrix to vanish.[7] In the present calculations the magnitude of these determinants is about 10^{-6}; we have therefore written a new program (method 2b) which is not only faster, but minimizes the difficulties caused by the overlap matrices being nearly singular. A real symmetric matrix $\mathbf{S}$ can be resolved into the product of two triangular matrices,[8] *i.e.*, $\mathbf{S} = \mathbf{LU}$ where $\mathbf{L}$ is the transpose of $\mathbf{U}$; the determinants of $\mathbf{L}$ and $\mathbf{U}$ are now of the order 10^{-3}. Using this fact, the set of equations $(H - SE)c_i = 0$ can be transformed into $(L^{-1}HU^{-1} - IE_i)\,x_i = 0$ where $\mathbf{x}_i = \mathbf{U}\mathbf{c}_i$ (the c_i of course being normalized such that $\mathbf{c}_i\mathbf{S}\mathbf{c}_i = 1$); the new matrix is symmetric and can be solved by the very much faster Givens method. Unfortunately, in the formation of the matrix product $\mathbf{L^{-1}HU^{-1}}$ there is severe cancellation which necessitates the use of double-length arithmetic, not only in the formation of this product, but also in the formation of $\mathbf{L}$ and $\mathbf{L^{-1}}$. This limitation was unexpected, but even so method 2b is still considerably faster than method 2a, *e.g.*, for these tenth order sets, the computing times are 1.5 and 8 minutes, respectively. The new method is also more accurate, for although both methods produced identical values for the negative roots (these are accurate solutions of $|H - SE| = 0$ to 8 significant figures), it gives better values for the largest positive roots.

Numerical Results

Table I compares the energies of the $1s\sigma_g$ state of H_2^+ given by various approximations (also listed are the exact solution, two sets of data for hydrogen-like functions, and results obtained using orthogonalized orbitals). It can be seen that as soon as the function $n = 2$, $l = 0$ is included, the energy becomes almost independent of Z, but there is a general tendency for the energy to improve as Z increases. The tenth order approximation for

(6) H. O. Pritchard and F. H. Sumner, *Proc. Roy. Soc.* (*London*) **A235**, 136 (1956).

(7) H. Margenau and G. M. Murphy, "Mathematics of Physics and Chemistry," D. Van Nostrand, New York, N. Y., 1943, p. 130.

(8) (a) R. A. Brooker, *Brit. J. Appl. Phys.*, **4**, 321 (1953); V. N. Faddeeva, "Computational Methods of Linear Algebra," Dover, New York, N. Y., 1959, p. 81. (b) Provided that the elements on the main diagonal are large compared to the other elements, as is always so in these calculations, the triangular matrices will always be real.

TABLE I

(−)TOTAL ELECTRONIC ENERGY OF THE $1s\sigma_g$ STATE OF H_2^+ IN RYDBERG UNITS AT $R = 2a_0$

	Last function added									
Z	$n = 1$, $l = 0$	$n = 2$, $l = 0$	$n = 2$, $l = 1$	$n = 3$, $l = 0$	$n = 3$, $l = 1$	$n = 3$, $l = 2$	$n = 4$, $l = 0$	$n = 4$, $l = 1$	$n = 4$, $l = 2$	$n = 4$, $l = 3$
	Hydrogen-like set									
1.0	2.107543	2.127838	2.127951	2.132933	2.133715	2.135466	2.136267	2.137636	2.140021	2.140098
1.25	2.172865	2.174286	2.182012	2.182826	2.183068	2.192879	2.193007	2.193952	1.197533	2.197661
	Complete set									
1.0	2.107543	2.178321	2.196446	2.196875	2.202938	2.203073	2.203549	2.204534	2.204699	2.204700
1.05	2.132135	2.177150	2.197983	2.197999	2.203221	2.203397	2.204029	2.204710	2.204857	2.204857
1.10	2.150932	2.175539	2.198626	2.199177	2.203499	2.203723	2.204389	2.204819	2.204977	2.204978
1.15	2.163978	2.174109	2.198902	2.200326	2.203763	2.204042	2.204638	2.204896	2.205064	2.205065
1.20	2.171290	2.173223	2.199157	2.201376	2.203994	2.204334	2.204817	2.204951	2.205122	2.205123
1.25	2.172865	2.173029	2.199579	2.202279	2.204176	2.204582	2.204928	2.204989	2.205160	2.205162
1.30	2.168677	2.173510	2.200229	2.203009	2.204301	2.204775	2.204996	2.205018	2.205184	2.205_g87
1.35	2.158688	2.174540	2.201080	2.203564	2.204373	2.204913	2.205038	2.205042	2.205200	2.205203
1.40	2.142849	2.175932	2.202044	2.203955	2.204401	2.205005	2.205065	2.205065	2.205210	2.205214
	Orthogonalized orbitals									
	1 term	2 terms	3 terms	4 terms	5 terms	6 terms	7 terms	8 terms	9 terms	10 terms
1.40	1.199633	1.253628	1.972751	1.984449	2.086714	2.088267	2.095059	2.181467	2.205164	2.205214
	Exact soln.									2.20525

$Z = 1.4$ is within $0.00004I_H$ of the correct solution, and it seems likely that with a higher value of Z, this discrepancy might easily be halved. It is noted in passing that the best energy for a $1s(Z)$ function is about $2.173I_H$, not $2.166I_H$ as given by Finkelstein and Horowitz[9]; their derivation of the optimal value of Z is correct, but they did not carry sufficient terms in their energy expansion.

As soon as two or three functions (depending on the value of Z) are included, approximations to the $2s\sigma_g$ state begin to appear, and after a further two functions are added, the $3d\sigma_g$ state appears; the tenth order solutions for the energies of these two states are given in Table II. In both these sets of

TABLE II

(−) TOTAL ELECTRONIC ENERGY OF THE $2s\sigma_g$ AND $3d\sigma_g$ STATES OF H_2^+ IN RYDBERG UNITS AT $R = 2a_0$

Z	$2s\sigma_g$	$3d\sigma_g$
	Hydrogen-like set	
1.0	0.65734	0.45198
1.25	0.71034	0.45781
	Complete set	
1.40	0.69935	0.40390
1.35	.70591	.41602
1.30	.71105	.42683
1.25	.71494	.43634
1.20	.71770	.44458
1.15	.71955	.45160
1.10	.72067	.45749
1.05	.72125	.46208
1.0	.72151	.46566
	Exact solution	
	0.72173	0.47155

results, the trend with Z is opposite to that for the ground state; the energy of the higher of the two states is varying more rapidly and clearly the best value of Z for this state is considerably less than 1.

(9) B. N. Finkelstein and G. E. Horowitz, *Z. Physik*, **48**, 118 (1928).

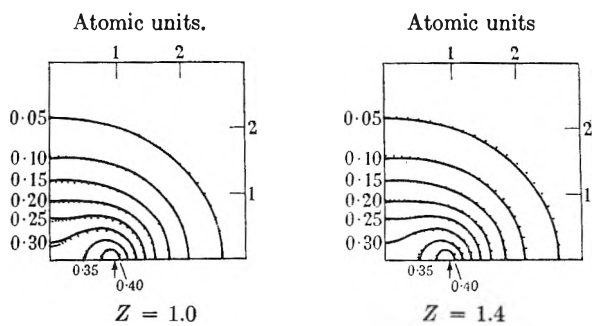

Fig. 1.—Comparison of the exact wave function for the $1s\sigma_g$ state of H_2^+ (taken from Bates, Ledsham and Stewart[10]) with the $Z = 1.0$ and $Z = 1.4$ complete-set approximations. (The exact wave function is reproduced by kind permission of the Royal Society.)

It would appear, therefore, that for an intermediate number of functions, the proper value of Z to use in these calculations is near η/n where η is the effective charge of the united atom and n is the quantum number of the corresponding united atom state: thus we should use $Z \approx 2$ for $1s\sigma_g$, $Z \approx 1$ for $2s\sigma_g$ and $Z \approx 2/3$ for $3d\sigma_g$.

Two alternative forms of truncation of the set were investigated to see if simpler calculations are likely to be of any value. In one case, only the $l = 0$ functions were taken: the results for $n = 1$ and $n = 1,2$ are given in the first two columns of Table I; for $n = 1,2,3$ and $n = 1,2,3,4$, the energy values were $2.180 \pm 0.001I_H$ and $2.1812 \pm 0.0002I_H$, respectively, virtually independent of Z. In the other case, only the functions without radial nodes were considered, *i.e.*, $l = (n - 1)$; here, the maximum near $Z = 1.25$ was maintained, and for $n = 1,2,3,4$, the energy value was $2.2040I_H$, which is about as good as the best 4-function representation in Table I. This form of truncation is equivalent to the use of Slater orbitals, but omitting the quantum number from the exponent, and as it would involve a great deal less labor, the convergence properties would merit further investigation, especially for approximate treatments.

TABLE III

COMPLETE-SET EXPANSIONS FOR H_2^+ WAVE FUNCTIONS

	$n=1$, $l=0$	$n=2$, $l=0$	$n=2$, $l=1$	$n=3$ $l=0$	$n=3$, $l=1$	$n=3$, $l=2$	$n=4$, $l=0$	$n=4$, $l=1$	$n=4$, $l=2$	$n=4$, $l=3$
					$1s\sigma_g$ state, $Z = 1.4$					
$(1+\xi_{ii})$	1.389995	1.639177	1.100740	1.609275	0.703473	1.063676	1.601595	0.660456	1.358266	1.016951
c_i (method 2b)	0.841401	−0.120382	0.128523	−0.014904	−0.009119	0.034439	−0.002295	−0.003538	0.005239	0.008172
					$2s\sigma_g$ state, $Z = 1.0$					
$(1+\xi_{ii})$	1.586453	1.730811	0.774441	1.737685	0.547593	1.321797	1.729284	0.474727	1.492124	0.705623
c_i (method 2b)	0.131117	0.693794	0.229268	−0.404426	0.012573	0.073721	0.066110	−0.008898	0.016481	0.011170
					$3d\sigma_g$ state, $Z = 1.0$					
c_i (method 2b)	0.644444	−0.167654	−1.086649	−0.179637	0.651507	0.120453	0.120182	−0.196341	−0.070844	0.005729

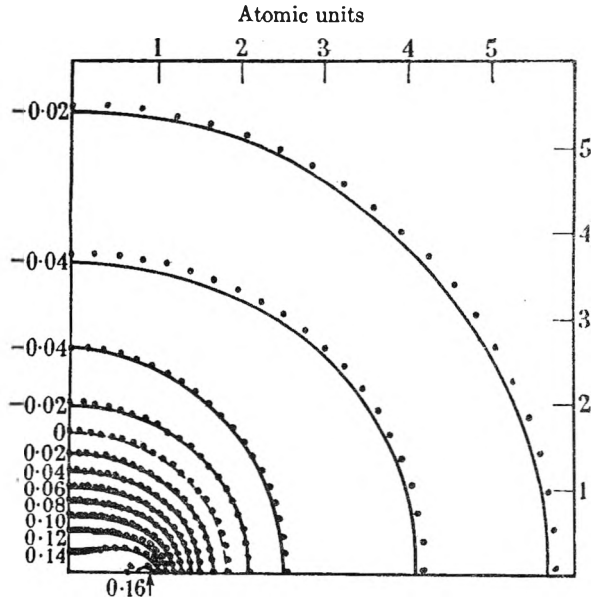

Fig. 2.—Comparison of the exact wave function for the $2s\sigma_g$ state of H_2^+ (taken from Bates, Ledsham and Stewart[10]) with the $Z = 1.0$ complete-set approximation. (The exact wave function is reproduced by kind permission of the Royal Society.)

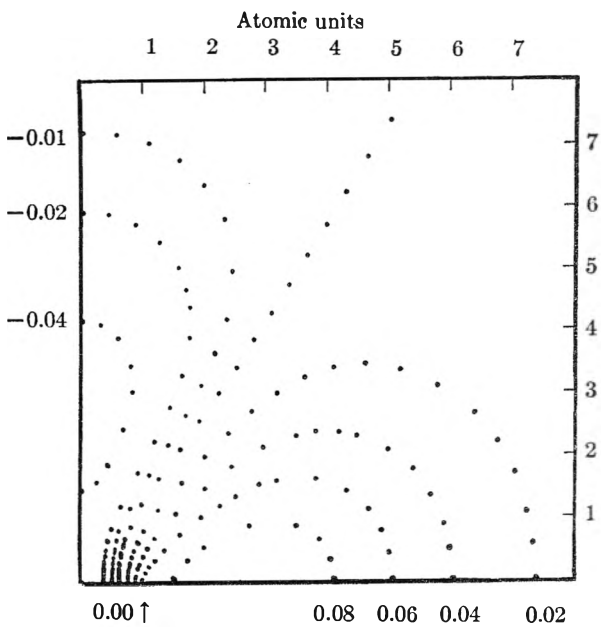

Fig. 3.—$Z = 1.0$ complete-set approximation to the wave function of the $3d\sigma_g$ state of H_2^+.

The wave functions obtained for the $1s\sigma_g$ ($Z = 1.4$), $2s\sigma_g$ ($Z = 1$) and $3d\sigma_g$ ($Z = 1$) approximations are given in Table III; they were also plotted out in the form of contour diagrams using the Manchester University Graphical Output, and are shown in Figs. 1, 2 and 3, respectively. Diagrams of the exact wave functions for the $1s\sigma_g$ and $2s\sigma_g$ states have been given already by Bates, Ledsham and Stewart[10] and as our approximate wave functions are very similar, we have superimposed our own contour maps on photographs of their exact functions. In Fig. 1, both the approximations for $Z = 1$ and $Z = 1.4$ are compared with the exact function. It can be seen that whilst the $Z = 1.4$ function agrees reasonably with the exact function over the whole region of space, the $Z = 1$ function differs significantly near the center of the bond, despite the fact that it corresponds to an energy which is only $0.00055I_H$ in error. It appears that if an unsuitable value of Z is chosen, then the truncated function cannot be made to fit satisfactorily over the whole of space, and as the more remote regions are more heavily weighted in the calculation, the function is forced to fit best at large distances. If, however, Z is chosen to be near η/n, the function automatically behaves correctly at large distances, and therefore stands a much better chance of spanning the central regions satisfactorily.

The Problem of Overcompleteness.—The question as to whether or not the ill-conditioning of our system of equations is due to overcompleteness was decided in the following way. The eigenvalues λ_k and eigenvectors $\mathbf{x}_k$ of the overlap matrix S were first obtained. A matrix K was then constructed such that each row consisted of an eigenvector $\mathbf{x}_k$ of S, the rows being written from top to bottom in descending order of the eigenvalues λ_k. The secular determinant was then transformed from $(H - SE)$ to $(KH\tilde{K} - KS\tilde{K}E) \equiv (KH\tilde{K} - \lambda E)$ and the eigenvalues of this set of equations were determined for all orders from one to ten. The ground-state eigenvalues are listed in Table I under the heading of orthogonalized orbitals; at least five orbitals are needed before the system is bonding, and eight are required before the energy is better than a simple 1s function of the same value of Z. It is found that the difference in energy between the use of the nine functions ($\mathbf{x}_0 \ldots \mathbf{x}_8$) and the ten functions ($\mathbf{x}_0 \ldots \mathbf{x}_9$) is an order of magnitude greater than the difference between the original ninth and tenth order approximations: the same is true for the

(10) D. R. Bates, K. Ledsham and A. L. Stewart, *Phil. Trans. Roy. Soc. (London)*, **A246**, 215 (1953).

$2s\sigma_g$ state, and for the $3d\sigma_g$ state, the discrepancy is more than two orders of magnitude. Thus it is clear that when only the first ten members of the set are used, there is no redundancy, even though each member of the set is used twice.

We conclude that using the simple l.c.m.o. procedure, as we have done, overcompleteness is likely to become troublesome if many more than ten functions are used. However, by that time, with a suitable choice of Z for each individual state, it is possible to reproduce both the energy and the wave function to a degree of accuracy which will be sufficient for most purposes, and the wave functions obtained in this way will certainly be easier to manipulate than the exact functions. Should greater accuracy be required, we can see no obvious reason why a few more members of the set should not be included and any resulting redundancy removed by an orthogonalization procedure such as that just described; it may however be necessary to compute the basic integrals to an accuracy of better than the 1 part in 10^8 which we have used.

We wish to acknowledge our indebtedness to Dr. B. F. Gray for his collaboration in the early stages of this work and to Mr. W. B. Brown and Mr. D. J. Evans for many discussions; also to Professor D. R. Bates, F. R. S. for permission to use his published contour maps in the construction of Fig. 1 and 2.

Appendix

The matrix elements for the hydrogen-like set, arbitrary Z, are given below. The functions are eigenfunctions of the operator

$$\mathcal{H}'' = -\frac{1}{2}\nabla^2 - \frac{Ze^2}{r}$$

with $\epsilon_i'' = Z^2\epsilon_i$ where ϵ_i corresponds to $Z =$ Thus

$$S_{ij} = 2(2 + 2\xi_{ii})^{-1/2}(2 + 2\xi_{jj})^{-1/2}(\xi_{ij} + \delta_{ij})$$

and

$$H_{ij} = 2(2 + 2\xi_{ii})^{-1/2}(2 + 2\xi_{jj})^{-1/2}[(\xi_{ij} + \delta_{ij})(\epsilon_j'' + e^2/R) - e^2(J_{ij} + K_{ij}) + (Z - 1)e^2(L_{ij} + K_{ji})]$$

where $\delta_{ij} = 1$ if $i = j$, or $= 0$ if $i \neq j$, and the other symbols have their previous meaning; the relation between K_{ij} and K_{ji} is

$$Ze^2K_{ji} = Ze^2K_{ij} + (\xi_{ij} + \delta_{ij})(\epsilon_i'' - \epsilon_j'')$$

L_{ij} now occurs between all pairs of ϕ_i and ϕ_j having the same l-quantum number.

THE DEHYDRATION OF SODIUM TRIPHOSPHATE HEXAHYDRATE

BY WARREN O. GROVES AND JAMES W. EDWARDS

Monsanto Chemical Company, Research and Engineering Division, Dayton, Ohio

Received October 8, 1960

The mechanism of the dehydration of sodium triphosphate hexahydrate has been investigated. Two routes for the dehydration have been found, the second, in the presence of water vapor, leads to direct formation of anhydrous sodium triphosphate, a reaction commercially important in the spray-drying of synthetic detergents. The most significant result is the influence of water vapor on the course of reaction. In the range of 100 to 150°, by controlling the pressure of water vapor, the reaction can be changed from a complete degradation to ortho- and pyrophosphates to an essentially pure dehydration to anhydrous sodium triphosphate, form II. Under certain conditions a new crystalline orthophosphate, a second modification of the double salt, $NaH_2PO_4 \cdot Na_2HPO_4$, appears. Other variables affecting the course of the reaction are particle size, sample purity, amount of grinding and previous history of the sample. It is concluded that two competing types of dehydration, a direct dehydration and a hydrolytic degradation, follow two fundamentally different mechanisms. The predominance of one or the other is controlled principally by the pressure of water vapor over the system.

Introduction

The dehydration of sodium triphosphate hexahydrate has been studied by a number of investigators[1-8] both because of its importance commercially and because of interest in the unusual behavior of this hydrate. Although the triphosphate ion is normally only metastable in the presence of water,[6] undergoing more or less rapid reversion to ortho- and pyrophosphates, the hexahydrate of sodium triphosphate is remarkably stable. It may be stored for years under ordinary conditions without undergoing appreciable decomposition. Only when an attempt is made to separate the water from the crystalline hydrate does degradation of the triphosphate ion by water occur.

Previous workers have shown that hydrolytic degradation occurs on either thermal or vacuum decomposition of the hydrate at temperatures below about 150°. Below about 80°, water can only be removed under vacuum and with difficulty. The mechanism of this low temperature vacuum dehydration involves initially an amorphous phase containing triphosphate ions.[8] These triphosphate ions subsequently degrade with the crystallization of tetrasodium pyrophosphate, the only crystalline product detectable by X-ray diffraction. The products obtained on thermal dehydration between 80 and 120° are similar to those from vacuum dehydration,[7] suggesting a similar mechanism; however, an alternative mechanism involving primary cleavage of a triphosphate ion by the water with which it is associated in the hexahydrate lattice

(1) P. Bonneman-Bemia, *Ann. Chim.*, **16**, 395 (1941).
(2) J. R. Mills, Thesis, University of Illinois, 1952.
(3) B. Raistrick, *Roy. Coll. Sci.*, **19**, 9 (1949).
(4) E. Thilo and H. Seeman, *Z. anorg. allgem. Chem.*, **267**, 65 (1951).
(5) O. T. Quimby, *Chem. Revs.*, **40**, 141 (1947).
(6) O. T. Quimby, *J. Phys. Chem.*, **58**, 603 (1954).
(7) A. E. Zettlemoyer, C. H. Schneider, H. V. Anderson and R. J. Fuchs, *ibid.*, **61**, 991 (1957).
(8) C. Y. Shen, J. S. Metcalf and E. V. O'Grady, *Ind. Eng. Chem.*, **51**, 717 (1959).

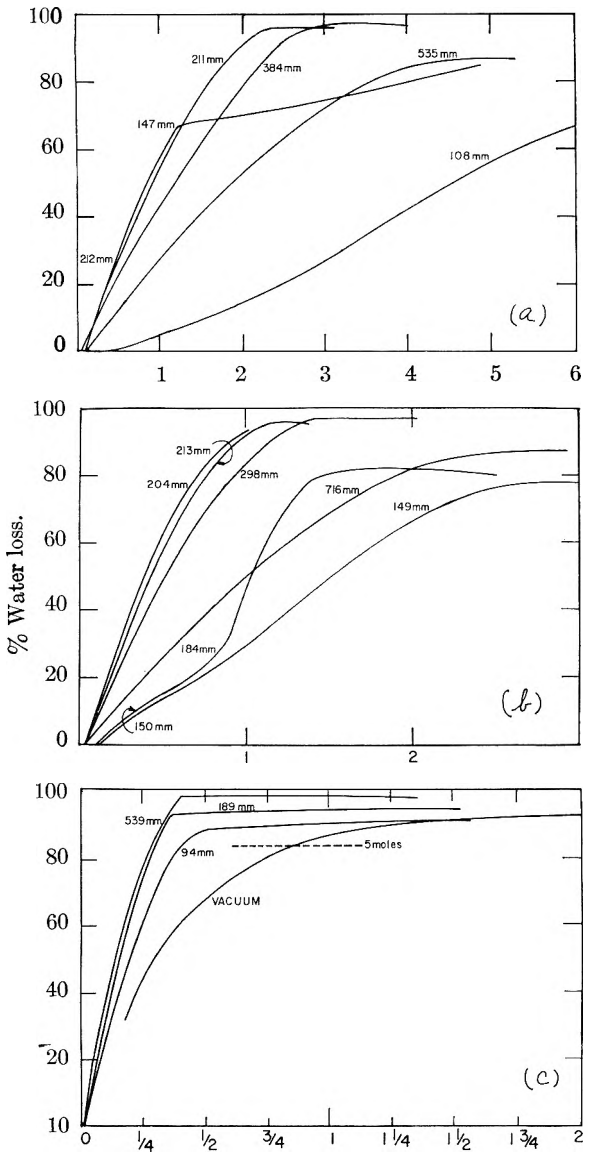

Fig. 1.—Rate of water loss of $Na_5P_3O_{10}\cdot 6H_2O$ at: (a) 110°; (b) 120°; (c) 150°.

might also explain the results. Above about 120° the increasing amounts of crystalline anhydrous sodium triphosphate found in the dehydration products raise the question of direct dehydration *vs.* recombination of initial degradation products.

In an attempt to answer some of these unresolved questions we undertook to study the effect of water vapor pressure on the rates of dehydration. This investigation very shortly led to a very surprising and unexpected result. By maintaining a certain pressure of water vapor over the dehydrating system, nearly pure anhydrous crystalline sodium triphosphate could be obtained. This paper is a report on the results of this study.

Experimental

Materials.—Sodium triphosphate hexahydrate was prepared from commercial sodium triphosphate by recrystallization several times from the aqueous solution by slow addition of ethyl alcohol. Analysis: 19.8% P; *p*H of 1% solution, 10.02; % of P as triphosphate, 99.1%; as pyrophosphate, 0.9%; ignition loss, 22.71%.

Several experiments were conducted using large crystals, and also with samples deliberately contaminated with either excess acidic or basic components. Details of these experiments are included in the section on Results and Discussion following.

Analyses.—Semiquantitative X-ray diffraction analyses were carried out using the General Electric XRD-3 X-ray Spectrogoniometer. Quantitative analyses by paper chromatography using the technique of Karl-Kroupa[9] were carried out in the research laboratories of the Inorganic Chemicals Division of Monsanto Chemical Company.

Apparatus.—For the rate studies sample weights were obtained continuously under vacuum, or controlled pressure of water vapor, by utilizing a quartz spiral spring. To avoid condensation of water vapor within the system all exposed tubing was wound with nichrome heating ribbon, and insulated; the Pyrex tube serving as the spring housing was contained within a larger heated tube. The sample tube, long enough to accommodate the maximum spring extension under full load and attached to the spring housing tube with a standard taper joint, was immersed in a bath of "Fischer Bath Wax" whose temperature was controlled automatically to ±0.05°. Attached to the sample tube just below the bath surface was a mercury "U-tube" manometer, the other arm of which was attached by rubber tubing to a conventional manometer system. The water vapor reservoir consisted of a bulb loosely packed with glass wool on which water was condensed, immersed in a small heated water-bath whose temperature was controlled manually.

The quartz spring, obtained from the Houston Technical Laboratories, was calibrated at a series of temperatures from 25 to 175° for loads of 0.7 to 1.0 g. Weights calculated from the observed extension were accurate to ±0.5 mg.

The sample, 0.8 g., was contained in a small aluminum foil bucket suspended by a fine platinum wire from the quartz spring. Two aluminum foil radiation shields threaded on the wire minimized radiation to or from the upper parts of the apparatus.

In a typical run the sample was weighed into the bucket, the bucket suspended in the system, and the system evacuated to 10^{-5} mm. of Hg. In the meanwhile the water vapor reservoir bath was brought to temperature and the wax-bath (removed from the system) heated to a temperature 3 or 4° higher than that of the run. After closing the main stopcock to the vacuum system, the stopcock to the water vapor reservoir was opened slightly and the bath quickly raised around the sample tube. Equilibrium was attained within two to five minutes; weight readings were made at convenient intervals, usually of five minutes.

Results and Discussion

The most significant result of this work has been the discovery of the influence of water vapor pressure on the course of the dehydration of sodium triphosphate hexahydrate. In the range from 100 to 150°, by controlling the pressure of water vapor, the reaction can be changed from a complete degradation to ortho- and pyrophosphate to an essentially pure dehydration to anhydrous sodium triphosphate. That at least two distinctly different routes with radically different mechanisms are involved in these reactions is established by the experimental results here described. The routes will be designated as degradative dehydration and direct dehydration, respectively.

The rates of water loss of the hexahydrate at different temperatures and under various pressures of water vapor are shown in Figs. 1 (a)–(c). At 110° and 108 mm., Fig. 1a, the degradative dehydration yielded principally crystalline tetrasodium pyrophosphate. The runs at 211 and 384 mm. are examples of direct dehydration, 87 and 92% triphosphate being obtained. The principal differences to be noted are: (1) difference in the

(9) E. Karl-Kroupa, *Anal. Chem.*, **28**, 1091 (1956).

induction period, and (2) difference in the shape of the curve. The degradative reaction starts slowly after an induction period of about 20 minutes, while the direct dehydrations set in abruptly after a period of 3 to 7 minutes. The degradative dehydrations show a long acceleration period following induction and before a gradual decay. The direct dehydrations start abruptly and decay slowly, actually following very closely fractional order rate equations. Orders have been found to range between 0.31 and 0.58 and hold from 0 to 90% completion based on final total water loss. The reaction during the run at 535 mm. may be classed as a direct dehydration based on the short induction period and adherence to the fractional order rate law. However, the low final weight loss and analysis of product show that extensive degradation has taken place. The effect of excessive water pressure is threefold. It slows the dehydration by tending to reverse the reaction; it causes hydrolytic degradation of the initially formed anhydrous triphosphate; and it induces the crystallization of trisodium acid pyrophosphate monohydrate.

In Fig. 1b similar data for runs at 120° are presented. Here the degradative dehydration at 149 mm. produced a crystalline orthophosphate double salt as well as tetrasodium pyrophosphate. The slight inflection in the curve is real and probably corresponds to initiation of formation of the crystalline orthophosphate. Degradation of triphosphate and pyrophosphate ions to form the orthophosphate ions consumes water which would otherwise be evolved. The difference between induction periods for the two reactions is less than at 110° but still evident. The run at 716 mm. again shows the effect of excessive water vapor pressure.

The sharp difference between degradative and direct dehydration in this temperature region is further emphasized by the very critical dependence on water vapor pressure. The effect of decreasing water vapor pressure is illustrated in Fig. 1a. After initiating a direct dehydration at 212 mm., the pressure was gradually reduced. The water loss proceeded at the normal rate for a direct dehydration until a pressure of 147 mm. was reached. At this point as evidenced by the sharp break in the curve, direct dehydration abruptly ceased and the independent degradative dehydration with its long acceleration period took over. The effect of increasing water vapor pressure is illustrated in Fig. 1b. A degradative dehydration initiated at 150 mm. increased slightly in rate as the pressure was increased until at 194 mm. there was an abrupt rise in rate as direct dehydration commenced.

At 150°, Fig. 1c, the rates of water loss at 94, 189 and 539 mm. are almost equal but a gradual transition from degradative to direct dehydration is shown by the increase in total water loss. These results indicate that at this high temperature the degradative and direct mechanisms can operate simultaneously over a range of water vapor pressures, or that some anhydrous triphosphate may be formed by the mechanism of the degradative dehydrations.

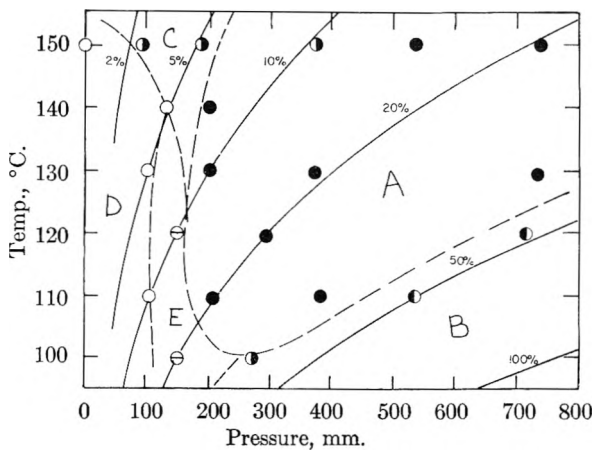

Fig. 2.—Products of $Na_5P_3O_{10}\cdot 6H_2O$ dehydration as function of temperature and water vapor pressure. ● $Na_5P_3O_{10}$-II, only crystalline component (region A); ◑ $Na_5P_3O_{10}$-II, major component with $Na_4P_2O_7$ (region C); ◐ $Na_5P_3O_{10}$-II, major component with $Na_4P_2O_7$ and $Na_3HP_2O_7\cdot H_2O$ (region B); ○ $Na_4P_2O_7$, only major crystalline component (region D); ⊖ $Na_4P_2O_7$, major component with $Na_2HPO_4\cdot NaH_2PO_4$* (region E).

The most convincing proof of the radically different nature of the two routes of dehydration comes from experiments using large crystals in which sites of initiation and growth of reaction zone in the two types of reaction were observed to differ completely.

The crystals, about 10 × 15 × 2 mm., were prepared by allowing acetone to diffuse slowly into a nearly saturated aqueous solution of the hexahydrate.[8] Two runs were made at 120°, one at 175, the other at 230 mm. of water vapor pressure.

At 175 mm., after a long induction period during which the surface of the crystal remained clear, small opaque spots began to appear, concentrated at first at the corners and edges of the crystal. Simultaneously with the appearance of the spots, weight loss began. The spots, probably corresponding to slowly growing dehydration nuclei, spread diffusely over the surface of the crystal until it was completely covered. At this time, two hours after the start of the run, only one mole of hydration water had been evolved.

In contrast, at 230 mm., change was first observed after a much shorter time as a white line approximately bisecting the crystal. This line may have corresponded to a twinning plane of the crystal. Later another line appeared roughly perpendicular to the first. The dense opaque regions spread slowly through the crystal, maintaining sharp boundaries. Disappearance of the last trace of clear surface area coincided with cessation of weight loss indicating completion of the reaction.

The products of the run at 175 mm., as determined by semiquantitative XRD analysis, included about 22% $Na_4P_2O_7$ and a large amount of orthophosphate double salt while those of the run at higher pressure contained 70–80% triphosphate and only 3–7% $Na_4P_2O_7$.

The results on the effect of water vapor pressure on the course of the reaction are summarized in Fig. 2. Here, the temperature of each run is plotted as ordinate, the water vapor pressure as abscissa. Lines of constant per cent. saturated

TABLE I

ANALYSIS OF PRODUCTS OF DEHYDRATION OF $Na_5P_3O_{10}\cdot 6H_2O$

No.	Temp., °C.	Pressure, mm.	XRD analysis			Chromatographic analysis, % of P as		
			% $Na_5P_3O_{10}$(II)	$Na_4P_2O_7$	Other	tri-	pyro-	ortho
31	100	153	~5	17–27	$Na_3H_3(PO_4)_2$*[a] major	..	..	..
20	100	273	60–75	8–13	.....	71.0	24.5	4.5
24	110	108	....	20–30	$Na_3H_3(PO_4)_2$*[a] trace, $Na_5P_3O_{10}\cdot 6H_2O$	..	..	..
29	110	211	65–80	...	.....	86.8	12.2	1.0
21	110	384	65–80	...	.....	92.3	6.8	0.9
32	110	535	50–65	13–23	$Na_3HP_2O_7\cdot H_2O$, 9–19%	..	..	..
27	120	149	.....	17–27	$Na_3H_3(PO_4)_2$*[a] major	8.9	37.2	53.8
28	120	298	65–80	...	.....	..	..	..
17	120	716	38–48	15–20	$Na_3HP_2O_7\cdot H_2O$, 10–30%	52.8	33.8	13.4
26	130	102	<8	26–36	$Na_3H_3(PO_4)_2$*[a] small amount	..	..	..
25	130	206	68–83	...	.....	79.3	18.7	2.0
22	130	374	65–80	...	.....	93.4	5.3	1.2
18	130	734	~100	...	.....	92.7	3.4	4.0
33	140	135	8–18	29–39	$Na_3H_3(PO_4)_2$*[a] small amount	14.2	61.3	24.5
30	140	204	65–80	...	.....	84.3	14.0	1.7
2	150	0	Trace	45–55	.....	24.9	70.1	3.7
14	150	94	12–22	20–30	.....	24.7	69.1	6.2
15	150	189	50–60	7–11	.....	56.8	41.6	1.6
16	150	376	64–78	3–7	.....	77.4	18.8	3.9
23	150	539	65–80	...	.....	94.4	2.1	3.5
13	149	740	~100	...	.....	95.8	2.0	2.2

[a] $Na_2H_3(PO_4)$*$_2$—previously unreported modification of double salt, $NaH_2PO_4\cdot Na_2HPO_4$.

water vapor pressure are included for reference. The final products as determined by semiquantitative X-ray analysis are indicated by code; the actual analyses by X-ray diffraction and by paper chromatography are listed in Table I. The approximate boundaries of the regions in which the different reactions predominate are sketched in as dashed lines. Thus, in region A the reaction is direct dehydration, anhydrous sodium triphosphate being the only crystalline product. The triphosphate ion content by paper chromatography ranges from about 80% at the left to 96% at the upper right.

In region B the primary reaction is direct dehydration though excessive water vapor pressure, as noted above, causes secondary reversion of the triphosphate. Crystalline products include $Na_5P_3O_{10}$-II, $Na_4P_2O_7$ and $Na_3HP_2O_7\cdot H_2O$.

In region D, degradative dehydration is the predominant reaction. The principal crystalline product is $Na_4P_2O_7$.

In region C apparently neither reaction predominates. Anhydrous sodium triphosphate, $Na_5P_3O_{10}$-II and $Na_4P_2O_7$ are both found in the products. Either the two competing reactions occur simultaneously or crystalline sodium triphosphate is formed *via* the degradative route, *i.e.*, by crystallization from the initially formed amorphous phase.

In region E a new species has been discovered. This phase is the only crystalline orthophosphate to be found among the dehydration products of $Na_5P_3O_{16}\cdot 6H_2O$ and is probably a second modification of the double salt of di- and monosodium orthophosphate, $Na_2HPO_4\cdot NaH_2PO_4$. It has been observed in the products from a variety of samples and is well characterized by its X-ray pattern. The X-ray pattern is similar to, but distinctly different from, that of Na_2HPO_4. The structures are probably closely related.

The identity of this material appearing on dehydration at temperatures between 100 and 140°, and under pressures of water vapor between 100 and 175 mm., is established by total weight loss, X-ray analysis and paper chromatography. The water loss of 4.56 moles during a reaction virtually completed in five hours at 120° under 148 mm., is close to that required for the reaction

$$Na_5P_3O_{10}\cdot 6H_2O \longrightarrow {}^1/_2Na_4P_2O_7 + Na_3H_3(PO_4)_2 + 4^1/_2H_2O$$

X-Ray analysis of the essentially crystalline product, 23–39% $Na_4P_2O_7$ (theoretical 33.7%) confirms that the only other crystalline material must have a ratio Na_2O/P_2O_5 close to 1.5. Chromatographic analysis, 60.9% of P as ortho-, 37.2% as pyro- and 1.9% as triphosphate, confirms the major constituent as an orthophosphate and therefore as the double salt $Na_3H_3(PO_4)_2$.

The results reported above have been obtained on one recrystallized and unground sample. Variables other than temperature and water vapor pressure which modify the course of the dehydration may be related to surface conditions of the hexahydrate crystals and include: particle size, sample purity, amount of grinding and previous history of the sample. An example of the effect of crystal size has been cited in the case of the very large single crystals. Several runs using hexahydrate samples deliberately contaminated by rapid precipitation form solutions containing either orthophosphoric acid or sodium hydroxide show that contamination of the hexahydrate favors the degradative route to dehydration, higher water pressures being required to catalyze the direct route. Grinding of the hexahydrate crystals,

as might be expected, increases the rate of their dehydration and also favors the degradative route. Neither of these effects, however, can be separated from those of particle size. The effect of previous history is also closely related to sample purity. As may be seen in Fig. 1b, and has also been observed in the experiments with contaminated samples, if degradation products are introduced by preliminary degradation or by direct addition, the water vapor pressure required to effect direct dehydration is increased. However, if direct dehydration is then initiated, the rate of water loss is more rapid than from pure samples under similar conditions.

Conclusions and Summary

It is concluded that the dehydration of sodium triphosphate hexahydrate may follow one of two fundamentally different routes. The first, the one usually encountered, involves formation of an amorphous triphosphate phase and leads to degradation of the triphosphate ion. The second, requiring the catalytic effect of water vapor leads to direct formation of anhydrous crystalline sodium triphosphate.

These two routes, aside from the differences in final products obtained, differ in: (1) initiation site, (2) method of propagation through the crystal, (3) length of induction time, (4) rate, and (5) shape of the rate curve or rate law.

The mechanisms for the two routes to dehydration may be summarized as follows: For degradative dehydration the reaction is initiated at the surface of the crystal where it is nucleated by some residual surface decomposition, impurity or other defect. The primary step following loss of water is the collapse of the hexahydrate lattice. The triphosphate ion in the hydrous amorphous phase formed tends to be hydrolytically degraded and one or more species from the resulting mixture may crystallize depending on the particular conditions of temperature, water vapor pressure and composition.

For direct dehydration, requiring the catalytic effect of water vapor pressure, the primary step is the direct transformation from the hexahydrate lattice to the anhydrous triphosphate lattice with the simultaneous loss of six moles of water. The role of water vapor is obscure but such a role in aiding crystallization of a dehydration product is not uncommon.[10-11] The direct dehydration is nucleated along lines perhaps corresponding to twinning planes (or protected edges of the crystal) rather than at random points in the surface. Evidence cited above indicates that preliminary degradation inhibits the initiation of direct dehydration, possibly by modifying nucleation sites. However, following a rapid nucleation, the reaction proceeds rapidly with no apparent impedance to diffusion of water from the reaction zone. Meanwhile, decomposition by the degradative mechanism may take place but, because of its long induction period and slow acceleration, does not contribute significantly to the reaction, at least 130°.

Acknowledgment.—The authors are indebted to Mr. R. R. Ferguson for the X-ray diffraction analyses and to Mr. R. L. Liss and Mr. B. R. Pierson for the paper chromatographic analyses.

(10) W. E. Garner, "Chemistry of the Solid State," Academic Press, Inc., New York, N. Y., 1955, p. 213 ff.

(11) G. B. Frost and R. A. Campbell, *Can. J. Chem.*, **31**, 107 (1953).

THE SOLUBILITIES AND DIFFUSION COEFFICIENTS OF ISOBUTYLENE IN DINONYL PHTHALATE

BY G. HOUGHTON, A. S. KESTEN, J. E. FUNK AND J. COULL

Chemical Engineering Department, Division of Engineering Research, University of Pittsburgh, Pittsburgh, Pennsylvania

Received October 17, 1960

The solubilities of isobutylene in dinonyl phthalate have been measured at 0–100° for isobutylene pressures in the range 72.6–740 mm. The non-ideality of the solutions is discussed in relation to Raoult's law, and the heat of solution was found to be 4.56 kcal./g.-mole. The diffusion coefficients of isobutylene in dinonyl phthalate have been measured at low concentrations of dissolved isobutylene using the square root law. The diffusion coefficients in cm.²/sec. are given by $D_L = 0.64 \exp(-8000/RT)$. The experimental data are interpreted on the basis of various models for diffusion in the liquid phase.

Introduction

The solubilities and diffusion coefficients of isobutylene in dinonyl phthalate are of interest since this system is typical of hydrocarbon systems found in separations by gas–liquid partition chromatography. The most widely used method of determining diffusion coefficients of dissolved gases is to measure the rate of volumetric uptake of gas through a gas–liquid interface. The diffusion coefficient is then obtained from the data by applying the square-root law, first used by Stefan[1]

$$V = m\sqrt{t} \qquad (1)$$

and

$$D_L = \pi \left[\frac{mP}{2RTA(c^* - c_i)}\right]^2 \qquad (2)$$

In order to calculate the diffusion coefficient D_L from the slope m of the plot of volume absorbed V *vs.* $\sqrt{t}$, where t is time, it is first necessary to know the solubility c^* of the gas in the liquid at the pressure P. T is the absolute gas temperature. The surface area of the gas–liquid interface is A and c_i is the initial uniform concentration of the gas in the liquid phase before exposing the interface to the diffusing gas. R is the universal gas constant. In the derivation of equations 1 and 2 from

(1) J. Stefan, *Sitzber. Wien. Akad.*, **79**, Abt II, 179 (1879).

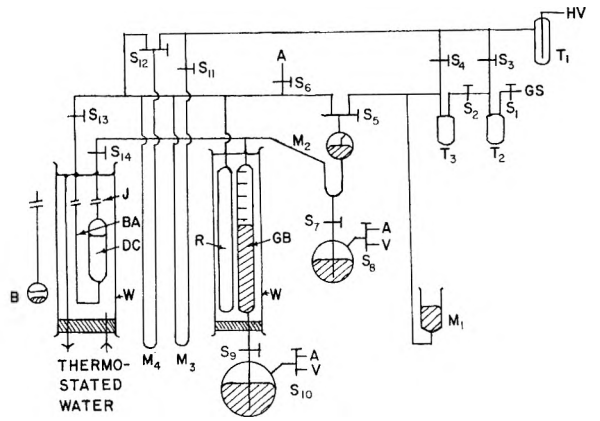

Fig. 1.—Apparatus: A, compressed air; B, solubility bulb; BA, balancing arm; DC, diffusion cell; GB, gas buret; GS, gas supply; HV, high vacuum pumps; J, glass blown joint; M_1, M_3, mercury manometers; M_2, inclined tube manometer with levelling pointer; M_4, dibutyl phthalate manometer; R, reference volume; S, stopcocks; T, cold traps; V, vacuum line; W, water-bath.

Fick's law, it has been assumed that the liquid is of infinite depth, the diffusion coefficient is independent of concentration, there is no change in volume of the liquid phase on solution and there is no gas film resistance at the interface. The experimental methods described in the literature differ mainly in the geometry of the gas–liquid interface. Plane surfaces have been used by Pomeroy and coworkers,[2] Hill and Lacey[3] and also Reamer, Opfell and Sage[4] to measure diffusion coefficients in hydrocarbon systems under pressure. Curved surfaces have been used by Ringbom,[5] Gertz and Loeschcke,[6] Groothius and Kramers,[7] Davidson and Cullen[8] and Houghton, *et al.*[9]

The present work is concerned with an apparatus for the measurement of both solubilities and diffusion coefficients. The diffusion coefficients are determined at low gas pressures in such a way that the assumptions inherent in the square root law are virtually satisfied.

Experimental

The apparatus for the measurement of both solubilities c^* and diffusion coefficients D_L is shown in Fig. 1. To determine solubilities it is only necessary to glass-blow the solubility bulb B in place of the diffusion cell DC and close stopcock S_{13}.

The isobutylene used in these experiments was Matheson C.P. grade (99.0% minimum purity) and was introduced into the evacuated system at the gas supply point GS. The gas entering the system was condensed in the trap T_2 by a mixture of Dry Ice and ethanol at −78°. By alternately warming, cooling and evacuating, it was possible to remove air and other light gases from the isobutylene. The remaining liquid was then fractionally distilled by warming trap T_2 to 0° and placing a Dry Ice–ethanol mixture around T_3 to condense the vapor. The middle one-third fraction was collected in T_3. The purity of the isobutylene could be checked by measuring its vapor pressure at 0° on mercury manometer M_1.

To make a solubility measurement, about 0.5–1.5 g. of dinonyl phthalate (National Research Corporation, specially refined Narcoil-40) was weighed into the bulb B, which was then joined onto the system at point J. A small amount of mercury (about 1 ml.) was also introduced into the bulb to facilitate agitation during absorption. The dead space between the bulb B and stopcock S_{14} was first determined by expanding air from the gas buret GB into the evacuated dead space. The dead space was determined at several temperatures in the range 0–100°. To continue the solubility measurement, the system was again evacuated and S_{14} closed. Purified isobutylene was then allowed to fill the gas buret through S_6 until the desired pressure was reached. The gas in the mercury-filled buret was then isolated from the rest of the system by raising the mercury in the cut-off M_2, which also served as an inclined tube manometer. Stopcock S_{14} was lubricated with a glycerol–bentonite mixture that does not dissolve hydrocarbons. On opening S_5 to the manometers M_3 and M_4 the pressure in the gas buret could be balanced with an equal pressure of air, by opening S_6 until the inclined tube manometer M_2 registered no differential pressure. The inclined tube manometer was sensitive to 0.05 mm. Pressures below 50 mm. were measured to 0.05 mm. on the dibutyl phthalate manometer M_4, while pressures above 50 mm. were read on the mercury manometer M_3 to 0.2 mm. On opening S_{14} and agitating the bulb B it was possible to measure the volume of gas taken up by a known weight of Narcoil at the pressure in the system. Before reading the gas volume on the buret, it was always necessary to balance the inclined tube manometer M_2. It was the practice to first measure the solubility at 100° and then lower the temperature in steps of about 25° until 0° was reached. In this way a complete solubility isobar was obtained. The water circulating around the bulb was provided from a thermostated bath which could be held at any temperature in the range 0–100° to within ±0.05° The 100 ml. gas buret GB could be read to within ±0.1 ml.

The diffusion cell DC in Fig. 1, used to measure the diffusion coefficients, consisted of a glass tube 15 cm. long, whose cross-sectional area was found to be 5.16 cm.², and a balancing arm BA. During a measurement dinonyl phthalate filled part of the diffusion cell and the balancing arm to a depth of 12 cm. The position of the dinonyl phthalate meniscus in the balancing arm was used to follow the absorption of the gas and balance the pressure in the system. To make a measurement the system was pumped out and stopcocks S_{13} and S_{14} were closed. The gas buret was then filled with isobutylene as before at a low pressure in the range 20–30 mm. and the equivalent balancing air pressure was measured on the manometer M_4. By simultaneously opening S_{13} and S_{14} the diffusion run was started. During a run the reading of the gas buret GB was recorded as a function of time, such that the meniscus on the balancing arm BA was maintained at the constant zero level. Finally the dinonyl phthalate used in the diffusion measurements was degassed at 50° *in vacuo* for a period of 10 hours before making a determination.

In order to calculate c^*, the solubility in g.-mole/cm.³, it is necessary to know the density of the sample of dinonyl phthalate. The density was therefore determined pyknometrically at five temperatures about evenly spaced in the region 0–100°. The results are fitted to within 0.2% by the relationship

$$\rho = 0.980 - 0.00071(T - 273) \qquad (3)$$

where ρ is the density of dinonyl phthalate in g./ml. and T is the absolute temperature in °K.

The viscosities of dinonyl phthalate used in the diffusion theory were determined in the range 0–100° by a series of calibrated Ostwald–Fenske viscometers.

Results and Discussion

In order to calculate the diffusion coefficients D_L it is necessary to have the solubilities c^* as a function of temperature and pressure so that the solubility data will be discussed first.

Solubilities.—The experimental solubilities of isobutylene in dinonyl phthalate were obtained in the region 0–100° in the form of isobars at 72.6, 96.0, 164.0, 299.0, 444.0, 606.0 and 740.0 mm.

(2) R. D. Pomeroy, W. N. Lacey, N. F. Scudder and F. P. Stapp, *Ind. Eng. Chem.*, **25**, 1014 (1933).

(3) E. S. Hill and W. N. Lacey, *ibid.*, **26**, 1324 (1934).

(4) H. H. Reamer, J. B. Opfell and B. H. Sage, *ibid.*, **48**, 275 (1956).

(5) Von A. Ringbom, *Z. anorg. allgem. Chem.*, **238**, 94 (1938).

(6) K. H. Gertz and H. H. Loeschcke, *Z. Naturforsch.*, **9b**, 1 (1954).

(7) H. Groothuis and H. Kramers, *Chem. Eng. Sci.*, **4**, 17 (1955).

(8) J. F. Davidson and E. T. Cullen, *Trans. Brit. Inst. Chem. Eng.*, **35**, 51 (1957).

(9) G. Houghton, P. D. Ritchie and J. A. Thomson, to be published.

The volumes absorbed under the particular experimental conditions were converted to mole fractions, x, of isobutylene, so that the following modified form of Henry's law could be used

$$P = Kx \tag{4}$$

where

$$K = Be^{-\Delta H/RT} \tag{5}$$

If the system obeys Raoult's law then the empirical constant K will be equal to the vapor pressure p^0 of isobutylene at the absolute temperature T. At the temperatures in the present experiments, dinonyl phthalate can be considered as an involatile solvent since its vapor pressure is less than 10^{-3} mm. Combining equations 4 and 5

$$\ln x = \frac{\Delta H}{RT} + \ln\left(\frac{P}{B}\right) \tag{6}$$

Since the measurements were obtained at a constant total pressure P, and B is assumed to be a constant, then a plot of log x *vs.* $1/T$ will be a straight line of slope $\Delta H/2.303R$, where ΔH is the heat of solution. Figure 2 shows that the experimental data, when plotted in this way, give good straight lines with a deviation less than $\pm 2\%$. From these graphs it is possible to obtain isothermal plots at 0, 15, 25, 50, 75 and 100° which are shown in Fig. 3 as smooth curves of x *vs.* P. From the smoothed data of Fig. 2 it is then possible to construct Table I showing the mole fraction of isobutylene in the liquid phase at even increments in temperature and pressure. In keeping with the accuracy of most solubility data obtained in this way (*cf.* Houghton, *et al.*[10]) the tabulated data have an estimated accuracy of $\pm 3\%$. According to Henry's law the volume of gas absorbed is relatively independent of pressure, so that the data reported in Table I will have a roughly constant percentage error even for the smallest solubilities. The most common source of error in solubilities determined by volumetric absorption is the difficulty of reaching true equilibrium. In the present work, supersaturation was avoided by always starting at the highest temperature and reducing the temperature in steps, while undersaturation was minimized by waiting until no further changes in volume absorbed were noted.

TABLE I

SOLUBILITIES OF ISOBUTYLENE IN DINONYL PHTHALATE

P, mm.	Mole fraction isobutylene in liquid phase, x							
t, °C.	100	200	300	400	500	600	700	740
0	0.110	0.209	0.30	0.38	0.47	0.55	0.60	0.62
15	.070	.135	.194	.25	.31	.36	.40	.42
25	.054	.104	.149	.195	.24	.28	.31	.33
50	.030	.057	.083	.108	.133	.157	.181	.191
75	.0179	.035	.051	.067	.082	.098	.113	.119
100	.0111	.022	.033	.043	.054	.065	.075	.079

Figure 3 also shows the nature of the fit of the experimental data to Raoult's law using the vapor pressures of Coffin and Maass.[11] Since these latter authors only list vapor pressures of isobutylene for temperatures in the range −79 to 22°, it was found most convenient to make comparisons at 0 and 15°.

(10) G. Houghton, A. M. McLean and P. D. Ritchie, *Chem. Eng. Sci.*, **6**, 132 (1957).

(11) C. C. Coffin and O. Maass, *Trans. Roy. Soc. (Canada)*, **21**, 33 (1927).

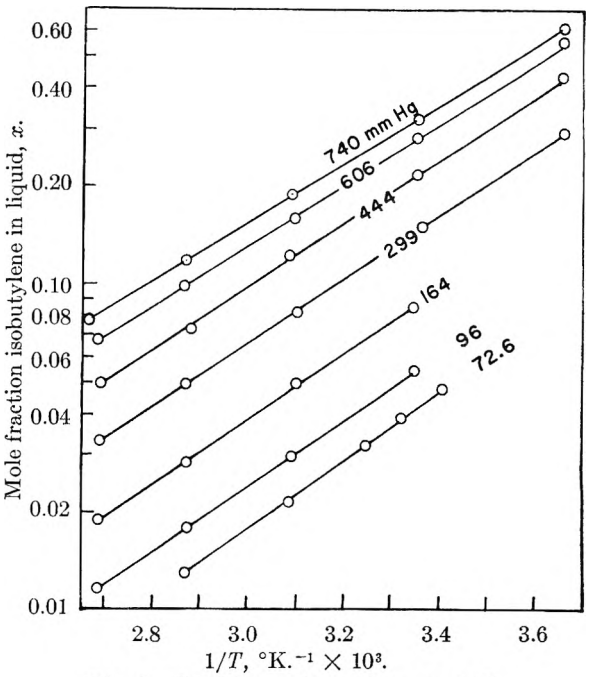

Fig. 2.—Solubility isobars—log x *vs.* $1/T$.

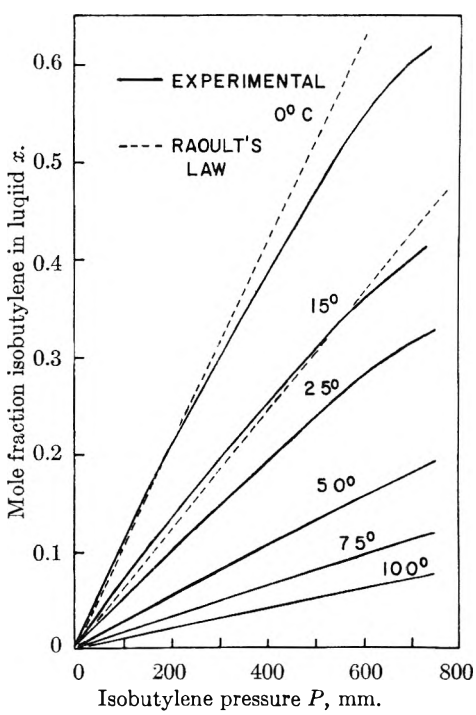

Fig. 3.—Solubility isotherms and Raoult's law—x *vs.* P.

It is evident that below 25°, plots of x *vs.* P are curved and that deviations from Raoult's law may be as much as 20% at the higher pressures. However, at 50, 75 and 100° the isotherms are linear within the 3% experimental error, but in this range there are no vapor pressure data for comparison with Raoult's law. At pressures below 200 mm. plots of x *vs.* P were found to be linear within 5% for temperatures in the range 0–25° and linear to within 3% for temperatures in the range 25–100°.

Since the isotherms are relatively linear below 200 mm. the average heats of solution, ΔH, of

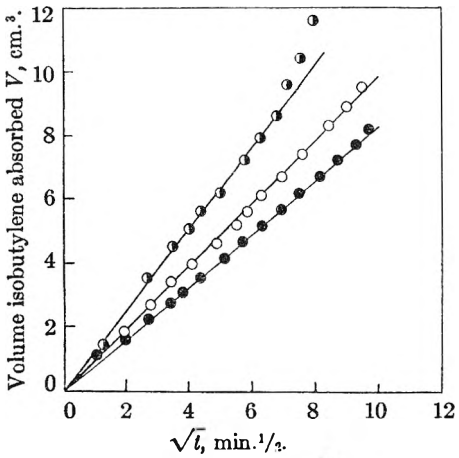

Fig. 4.—Square root law plots—V *vs.* $\sqrt{t}$: ◑, 0.0°, 19.6 mm.; ○, 50.0°, 21.9 mm.; ●, 75.0°, 25.8 mm.

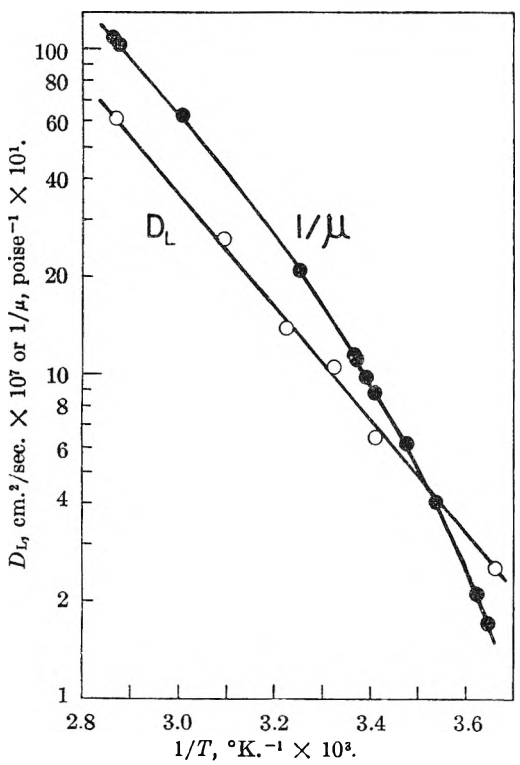

Fig. 5.—Diffusion coefficients and viscosities as a function of temperature—log D_L and log $(1/\mu)$ *vs.* T^{-1}.

isobutylene in dinonyl phthalate were calculated from the slopes of the isobars in Fig. 2 at the pressures of 72.6, 96.0 and 164.0 mm. and were found to be 4.54, 4.57 and 4.56 kcal./g.-mole, respectively for the temperature range 0–100°. The average heat of solution is 4.56 ± 0.02 kcal./g.-mole, compared with a value of 5.4 ± 0.2 kcal./g.-mole for the heat of vaporization of isobutylene calculated from the vapor pressure data of Coffin and Maass[11] in the temperature range 0–22°. It is evident from this comparison that even though the isotherms are relatively linear below 200 mm., Raoult's law is still not applicable to the solutions. Furthermore these observations perhaps lead to the general conclusion that linear chromatography will be a rare occurrence even for the simplest hydrocarbon systems.

Diffusion Coefficients.—The diffusion coefficients were obtained by plotting the volume absorbed V *vs.* $\sqrt{t}$ at constant temperature T and pressure P. Typical plots are shown in Fig. 4. The diffusivities D_L were calculated from the slopes m using equation 2. In the present work the initial concentration c_i in the liquid is zero before admitting the gas. The solubility c^* in equilibrium with a pressure P of isobutylene was calculated by using the observation that below 200 mm., the isotherms are linear and obey equation 4 within the error of the measurements. The densities of liquid dinonyl phthalate were calculated from equation 3. Since all the diffusion measurements were made at low pressures in the range 20–30 mm., the solubilities of isobutylene were so low (less than 2 mole %) that the volume change on solution was negligible compared with the ± 3% error in the solubility measurements. As a consequence it was unnecessary to determine the densities of isobutylene–dinonyl phthalate solutions.

By repeating diffusion coefficient measurements under similar conditions, it was found that the precision of the determination was within ±5% As with most diffusion measurements of this kind, the above deviation is largely due to the presence of convection currents in the liquid phase caused by temperature and concentration differences. However, the presence of convection is often easy to detect since its onset produces a rapid change in slope of the plot of V *vs.* $\sqrt{t}$ as shown by the later part of the isotherm at 0° in Fig. 4. To avoid convection due to temperature gradients, a period of 3 hours was allowed for the liquid temperature to become uniform before starting a run.

The effect of dissolved isobutylene concentration on the diffusion is likely to be negligible compared with the experimental precision of ±5% since the dissolved gas never exceeds 2 mole % for all the diffusion measurements.

The possibility of error in the diffusion measurements incurred by the presence of an inert gas film resistance is eliminated in these experiments by the use of pure isobutylene.

With respect to the effect of liquid depth on the diffusion rates, the average diffusion length, $\sqrt{D_L t}$, for a relatively high diffusion coefficient of 10^{-5} cm.²/sec. and a run lasting 100 min. is about 0.25 mm. Hence the depth of penetration into the liquid of 0.25 mm. is negligible compared with the total depth of liquid of 120 mm. Further, Pomeroy[2] has shown experimentally that the depth of the liquid phase has a negligible effect so long as the liquid contains less than half the gas required for its saturation at the prevalent temperature and pressure. This criterion is satisfied in the present experiments when, at the end of a typical run, less than 0.2% of the gas required for saturation is dissolved in the liquid.

It is evident from the above discussion that the assumptions involved in the use of the square-root law lead to errors negligible compared with the precision of the determination, namely ±5%. As a consequence, it may be expected that the diffusion coefficients will also have good absolute accuracy, also of the order of ±5%.

Figure 5 shows a plot of log D_L *vs.* $1/T$. The least squares line through the experimental data is given by the equation

$$D_L = 0.64 \exp\left(-\frac{8000}{RT}\right) \quad (7)$$

where the units of D_L are cm.^{2}/sec. Equation 7 has been used to calculate the observed values of D_L in Table II for comparison with values calculated by various theoretical and empirical approaches which will now be discussed.

TABLE II

DIFFUSION COEFFICIENTS AND VISCOSITIES

	Obsd. values			Theor. values		
				$D_L \times 10^7$, cm.^{2}/sec.		
°C.	μ, poise	$D_L \times 10^7$, cm.^{2}/sec.	$\frac{D_L\mu}{kT} \times 10^7$, cm.$^{-1}$	Eyring[15]	Wilke[14]	Longuet-Higgins[22]
0	6.82	2.6	4.7	0.023	0.059	76
15	1.54	5.5	2.1	.049	.27	83
25	0.813	8.8	1.7	.077	.53	87
50	.234	25	1.3	.21	1.96	99
75	.0927	61	1.2	.51	5.3	112

The temperature dependence of the diffusion coefficient D_L and the solvent viscosity μ can be compared by using the following equation obtained by Taylor[12] from Eyring's[13] results

$$\frac{D_L\mu}{kT} = \frac{\lambda_1}{\lambda_2\lambda_3} \quad (8)$$

where λ_1, λ_2 and λ_3 are the dimensions of the cell occupied by the molecule, so that the product $\lambda_1\lambda_2\lambda_3 = \lambda^3$ represents the volume of the cell with λ as the average distance between two successive equilibrium positions of a diffusing molecule. Equation 8 arises from Eyring's theory of absolute reaction rates by assuming that binary diffusion is a special case of self-diffusion of solvent molecules. Table II shows that $D_L\mu/kT$ is not constant as predicted by (8), but varies markedly with temperature. It is further evident from Fig. 5 that the slope of the log $(1/\mu)$ *vs.* $1/T$ plot only approaches that of the log (D_L) *vs.* $1/T$ plot at temperatures above 35°, indicating that at low temperatures the mechanism of isobutylene diffusion is different from that of self-diffusion of dinonyl phthalate. Additional evidence that the rate of diffusion of isobutylene in dinonyl phthalate is much faster than the self-diffusion of dinonyl phthalate is obtained by estimating D_L from the equations

$$\frac{D_L\mu}{kT} = 5.4 \times 10^6 \frac{M^{0.5}}{V^{0.6}} \quad (9)$$

$$D_L = \frac{\lambda^2}{V_f^{1/3}}\left(\frac{RT}{2\pi M}\right)^{1/2} \exp\left(-\frac{\Delta E_v}{nRT}\right) \quad (10)$$

Equation 9 is an empirical modification of (8) for unassociated liquids due to Chang and Wilke[14] and equation 10 is due to Eyring and co-workers.[15] M and V are the molecular weight and molecular volume of the solvent, respectively, while V_f is the free volume of the cell not occupied by the solvent molecule. The following approximations due to Eyring and Hirschfelder[16] were used for λ and V_f

$$\lambda = (V/N)^{1/3} \text{ and } V_f = (2RT/\Delta E_v)(V/N)^{1/3} \quad (11)$$

N is Avogadro's number, ΔE_v is the latent heat of vaporization and n is a parameter equal to the ratio of the latent heat of vaporization of the solvent to the activation energy for diffusion. In the present work the latent heat of vaporization of dinonyl phthalate has been calculated to be 24.1 kcal./g.-mole from its vapor pressure data,[17] while the energy of activation from equation 7 is 8.0 kcal./g.-mole, giving a ratio of 3.0. Taylor[12] has quoted a value of $n = 3.0$ for the diffusion of tetrabromoethane in tetrachloroethane using the data of Cohen and Bruins[18]; Ewell and Eyring[19] have found $n = 3.0$ for viscous flow of benzene and $n = 2.4$ for diffusion in aqueous solutions, while Fishman[20] gives values of 3.6 and 3.7, respectively, for the self-diffusion of pentane and heptane. It is evident from Table II that values of D_L calculated from equations 9 and 10 are a factor of 20–100 smaller than the experimental values. This result is not surprising since Eyring's approach assumes that the solute and solvent are the same molecular size, when in this case the volume of an isobutylene molecule[21] is 1.5×10^{-22} cm.^{3} at 0° compared with a value of 7.1×10^{-22} cm.^{3} for a dinonyl phthalate molecule. Since $n = 3.0$ the average hole size will be about one-third the size of a dinonyl phthalate molecule, or 2.4×10^{-22} cm.^{3}, which is still somewhat larger than an isobutylene molecule. Steric effects may also be important since the long chain nonyl groups may hinder the self-diffusion of dinonyl phthalate and yet provide interstices through which isobutylene molecules may readily pass.

A further method of estimating the diffusion coefficients is the equation of Longuet-Higgins and Pople,[22] derived on the assumption that the molecules of the liquid are closely packed hard spheres of diameter σ with no interaction

$$D_L = \left(\frac{\sigma}{4}\right)\left(\frac{\pi RT}{M}\right)^{1/2}\left(\frac{PV}{RT} - 1\right)^{-1} \quad (12)$$

Following McCall, Douglass and Anderson[23] the cohesive pressure P and the molecular diameter σ can be estimated from

$$P = \Delta E_v/V \text{ and } \sigma = (2.37V)^{1/3} \times 10^{-8} \quad (13)$$

The equation for σ assumes that the molecules are spherical and fill 75% of the available space. It is evident from Table II that values of D_L calculated from equation 12 are somewhat higher than the experimental values and that the temperature dependence is not as great as that observed experimentally. This is further indication that molecular

(12) H. S. Taylor, *J. Chem. Phys.*, **6**, 331 (1938).
(13) H. Eyring, *ibid.*, **4**, 283 (1936).
(14) P. Chang and C. R. Wilke, *J. Phys. Chem.*, **59**, 592 (1955).
(15) A. E. Stearn, E. M. Irish and H. Eyring, *ibid.*, **44**, 981 (1940).
(16) H. Eyring and J. Hirschfelder, *ibid.*, **41**, 249 (1937).
(17) Private communication from National Research Corporation, Newton Highlands, Massachusetts.
(18) E. Cohen and H. R. Bruins, *Z. physik. Chem.*, **103**, 404 (1923).
(19) R. H. Ewell and H. Eyring, *J. Chem. Phys.*, **5**, 726 (1937).
(20) E. Fishman, *J. Phys. Chem.*, **59**, 469 (1955).
(21) The density of liquid isobutylene is 0.620 g./cm.^{3} from the data of Coffin and Maass.[11]
(22) H. C. Longuet-Higgins and J. A. Pople, *J. Chem. Phys.*, **25**, 884 (1956).
(23) D. W. McCall, D. C. Douglass and E. W. Anderson, *ibid.*, **31**, 1555 (1959).

interactions in the liquid phase cannot be neglected and that the diffusion of isobutylene in dinonyl phthalate is an activated process.

Acknowledgments.—The authors thank Mr. R. C. Szafranski for measuring some of the diffusion coefficients used in this paper, and two of us (J. E. F. and A. S. K.) are indebted to the Westinghouse Corporation for Graduate Fellowships.

GENERAL CONSIDERATIONS FOR THE FORMATION OF MOLECULAR COMPLEXES IN SOLUTION

BY MILTON TAMRES

The Chemistry Department of the University of Michigan, Ann Arbor, Mich.

Received October 24, 1960

The formation of 1:1 complexes in solution has been considered from the standpoint of (a) solvent competition, (b) various concentration ratios of electron donor to electron acceptor, and (c) the effect on the equilibrium constant when concentration terms are neglected in the equilibrium constant expression. The general views developed are applied to several examples for iodine complexes.

Introduction

The work of Benesi and Hildebrand[1] on the interaction of iodine with aromatic hydrocarbons has led to an increasing number of investigations to determine the properties of such complexes. A commonly employed technique for these studies is the spectrophotometric method because, apart from convenience, the spectral data are in themselves of theoretical interest.[2] The progression of studies has led simultaneously to modifications of the Benesi–Hildebrand equation[1] in order to handle a variety of specific experimental conditions. Many of these modifications have been reviewed recently by Drago and Rose,[3,4] and will not be restated here.

The effect of solvent on the equilibrium constants of complexes dissolved in different solvents also has received some attention. Merrifield and Phillips[5] have proposed that, for their study, the differences in the constants found in various solvents could be accounted for by considering a second equilibrium between solvent and the electron acceptor in addition to the normal electron donor–acceptor interaction. The equation employed by these investigators is essentially the same as that formulated by Corkill, Foster and Hammick[6] for the case of a single electron acceptor interacting with two electron donor species. This treatment is limited to the case where both electron donor species are in large excess, so that the equilibrium and initial concentrations are taken as being equal. The re-evaluation by Drago and Rose[3,4] has shown that, in some cases, appreciable error can be introduced by neglecting the correction for the small change in concentration of the electron donor species.

It is the purpose of this paper to show that, omitting the factor of activity coefficients, all aspects can conveniently be taken into account in studies on the formation of 1:1 molecular complexes. It is shown that if approximations are introduced in the equations commonly employed it is possible to estimate their effect on the results.

Mathematical Considerations

If an electron donor B and an electron acceptor Z are dissolved in a solvent S the simultaneous equilibria[7,8] are

$$B + Z \rightleftharpoons \text{Complex 1}$$
$$S + Z \rightleftharpoons \text{Complex 2}$$

and the corresponding constants are

$$K_1 = \frac{C_{C_1}}{(C_B - C_{C_1})(C_Z - C_{C_1} - C_{C_2})} \quad (1)$$

$$K_2 = \frac{C_{C_2}}{(C_S - C_{C_2})(C_Z - C_{C_1} - C_{C_2})} \quad (2)$$

where the concentration terms, in moles per liter, are self-evident.

Case 1.—$C_S \gg C_{C_2}$. This simplifies equation 2 to

$$K_2 = \frac{C_{C_2}}{(C_S)(C_Z - C_{C_1} - C_{C_2})} \quad (3)$$

From equation 1

$$C_Z - C_{C_1} - C_{C_2} = \frac{C_{C_1}}{K_1(C_B - C_{C_1})} \quad (4)$$

And from equation 3

$$C_{C_2} = \frac{(C_Z - C_C)K_2C_S}{1 + K_2C_S} \quad (5)$$

Substituting (5) in (4) and solving for K_1 gives

$$K_1 = \frac{C_{C_1}(1 + K_2C_S)}{(C_B - C_{C_1})(C_Z - C_{C_1})} \quad (6)$$

This equation is readily altered to that of (7)

$$K_1^{-1} = \frac{1}{(1 + K_2C_S)} \left\{ \frac{C_BC_Z}{C_C} - C_B - C_Z + C_{C_1} \right\} \quad (7)$$

(1) H. A. Benesi and J. H. Hildebrand, *J. Am. Chem. Soc.*, **71**, 2703 (1949); **70**, 2832 (1948).

(2) R. S. Mulliken, *ibid.*, **74**, 811 (1952); *J. Phys. Chem.*, **56**, 801 (1952).

(3) N. J. Rose and R. S. Drago, *J. Am. Chem. Soc.*, **81**, 6138 (1959).

(4) R. S. Drago and N. J. Rose, *ibid.*, **81**, 6141 (1959).

(5) R. E. Merrifield and W. D. Phillips, *ibid.*, **80**, 2778 (1958).

(6) J. M. Corkill, R. Foster and D. L. Hammick, *J. Chem. Soc.*, 1202 (1955).

(7) If the electron donor reacts with the electron acceptor to form a series of complexes from 1:1 to n:1, the equilibrium constant is

$$K_1 = \frac{C_{C_1}}{\left(C_B - \frac{C_{C_1}}{K_1}\sum_{i=1}^{n} nK_i\right)\left(C_Z - \frac{C_{C_1}}{K_1}\sum_{i=1}^{n} K_i - C_{C_2}\right)}$$

which, except for additional constants, is of the same form as equation 1.

(8) It is apparent that the same considerations are applicable if the solvent S is an electron acceptor rather than donor.

or it can be expanded to give[9]

$$K_1C^2_{C_1} - (1 + K_2C_S + K_1C_Z + K_1C_B)C_{C_1} + K_1C_ZC_B = 0 \quad (8)$$

Case 2.—$C_S \gg C_{C_2}$; $C_ZC_B \gg C^2_{C_1}$.—Equation 8 is thus reduced from a quadratic to a linear equation in C_{C_1}, the solution for which is

$$C_{C_1} = \frac{K_1C_BC_Z}{K_2C_S + K_1(C_B + C_Z) + 1} \quad (9)$$

This equation can be rearranged to (10)

$$K_1^{-1} = \frac{1}{(1 + K_2C_S)}\left\{\frac{C_BC_Z}{C_{C_1}} - C_B - C_Z\right\} \quad (10)$$

Case 3.—$C_S \gg C_{C_2}$; $C_ZC_B \gg C^2_{C_1}$; $C_B \gg C_Z$. For these conditions it follows directly from (9) and (10) that

$$C_{C_1} = \frac{K_1C_BC_Z}{K_2C_S + K_1C_B + 1} \quad (11)$$

and

$$K_1^{-1} = \frac{1}{(1 + K_2C_S)}\left\{\frac{C_BC_Z}{C_{C_1}} - C_F\right\} \quad (12)$$

Spectrophotometric Equations.[10]—From

$$A = a_{C_1}bC_{C_1} + b\sum_{i=1} a_iC_i \quad (13)$$

where A = absorbancy, C_{C_1} = equilibrium concentration of the electron donor–acceptor complex having a molar absorbancy index a_{C_1}, b = length of cell, and C_i = equilibrium concentration of the ith species having a molar absorbancy index a_i, it follows that equations 7, 10 and 12 can be written in the equivalent forms, respectively

$$K_1^{-1} = \frac{1}{(1 + K_2C_S)}\left\{\frac{C_BC_Za_{C_1}b}{A - b\sum_{i=1} a_iC_i} - C_B - C_Z + \frac{A - b\sum_{i=1} a_iC_i}{a_{C_1}b}\right\} \quad (14)$$

$$K_1^{-1} = \frac{1}{(1 + K_2C_S)}\left\{\frac{C_BC_Za_{C_1}b}{A - b\sum_{i=1} a_iC_i} - C_B - C_Z\right\} \quad (15)$$

$$K_1^{-1} = \frac{1}{(1 + K_2C_S)}\left\{\frac{C_BC_Za_{C_1}b}{A - b\sum_{i=1} a_iC_i} - C_B\right\} \quad (16)$$

Discussion

The simultaneous equations 1 and 2 involve no assumptions other than those of unity for the activity coefficients and the absence of higher complexes, these being the standard assumptions in reporting data on 1:1 complexes. Thus the thermodynamic equilibrium constant is not under consideration here, but rather K_C or K_X, where C and X refer to units of mole $l.^{-1}$ and mole fraction, respectively.

Case 1.—Simplification of equation 2 to 3 is quite justifiable, in all practical cases, since the concentration of solvent generally is in such great excess. The resulting equation 7 includes the solvent contribution in determining K_1, and thus has the special advantage of being applicable when using a "like" solvent in order to widen the range of study of difficultly soluble substances.

Equation 7 (or its equivalent, (14)) takes the form utilized by Rose and Drago[3] for the simple donor–acceptor interaction, *i.e.*, $K_2 = 0$. It is evident that the detailed analytical discussion presented by those authors is applicable here as well. In addition, however, observed curvature in K_1^{-1} as a function of solvent dilution could be related to the term $1 + K_2C_S$; thus permitting, in principle, an evaluation[11] of the magnitude of K_2. For example, the conclusion of Rose and Drago of the absence of a variation in K_1^{-1} as a function of solvent concentration for the benzene–iodine complex in carbon tetrachloride would be in accord with the assumption that K_2 is quite small.[12]

The quadratic equation 14 can be solved by an iterative procedure such as utilized by Kiefer and Andrews.[13] It can also be evaluated graphically, as shown by Rose and Drago,[3] giving at same time an indication of the precision. A related method, but one which is based on an algebraic procedure, has been reported by Briegleb and Czekalla.[14] The latter two procedures, by their nature, generally result in large error limits for the quantities evaluated. A preferable procedure, one based on the method of least squares, will be illustrated in the next section (Experimental Considerations).

Case 2.—One of the major features of equation 7 is that it enables the study to be carried out for all ratios of donor:acceptor concentrations. Hence, it overcomes the often used experimental restriction of working with a large excess of one reagent,

(9) By retaining the C_{C_2} term in equation 2 and equating this with (1) leads to

$$C^2_{C_2}(K_1 - K_2) - C_{C_1}(1 + K_2C_S + [K_1 - K_2]C_Z + K_1C_B) + K_1C_ZC_B - \frac{K_2C_{C_1}}{C_B - C_{C_1}} = 0$$

Unless one deliberately selects a system such that the last term becomes of importance, the above equation essentially reduces to that of equation 8.

(10) The evaluation of the equilibrium constant by use of spectrophotometric data involves certain assumptions regarding spectral characteristics. See, for example, W. G. Barb, *Trans. Faraday Soc.*, **49**, 143 (1953).

(11) It is possible also to determine K_2 independently by studying the S + Z interaction in some "inert" solvent, as was done by Merrifield and Phillips.[5] In principle, omitting activity factors, it is possible to determine the values for three equilibrium constants by studying each of the three pairs of systems separately. However, it is very doubtful that, except perhaps for very similar systems the activity coefficients can be neglected. At room temperature, the equilibrium constant, K_X, for the benzene–iodine complex in carbon tetrachloride is larger than that for the complex in *n*-heptane, being 1.73 and 1.15, respectively.[1] The same is found for the mesitylene–iodine complex in these two solvents, *i.e.*, 7.2 and 5.3, respectively, which is a change in the same direction and of a somewhat similar percentage magnitude as for the benzene–iodine case. On the other hand, for dioxane–iodine at 25°, K_X is smaller in carbon tetrachloride than in *n*-hexane (which should have properties similar to *n*-heptane), being 9.1 and 9.3, respectively.[15]

(12) If a 5% variation in K_1^{-1} between the region of low and of high concentration can be taken as significant, and if the value of 10.3 mole $l.^{-1}$ for the concentration of pure carbon tetrachloride at 25° is used, an upper limit for $K_2 \leq 0.005$ l. mole^{-1} can be set. The setting of these limits for cases where solvent interaction is weak should not be construed as implying the existence of a complex, nor can these limits be utilized in general in conjunction with observed absorbancies of solvent–electron acceptor solutions since, as has been proposed, these spectra can arise without the formation of a true complex [see S. P. McGlynn, *Chem. Revs.*, **58**, 1113 (1958), for a recent summary on contact charge transfer].

(13) R. M. Keefer and L. J. Andrews, *J. Am. Chem. Soc.*, **74**, 1891 (1952).

(14) G. Briegleb and J. Czekalla, *Z. Elektrochem.*, **58**, 249 (1954).

as is necessitated in employing the Benesi–Hildebrand equation or the Ketelaar[15] modification.

The approximation $C_Z C_B \gg C^2_{C_i}$ leads to equation 9 or 15 and puts the data in linear form, which makes it convenient for analysis.[16] At the same time, (9) or (15), which would be valid for most studies, still retains the feature of permitting varying the donor:acceptor ratio over the entire concentration range. The product $C_Z C_B$ must be greater than $C^2_{C_i}$, and the difference will be larger for the conditions of (1) a large excess either of C_Z or C_B, (2) dilute solutions, and (3) weak complexes.

Rearranging equation 15 gives

$$\frac{C_Z b C_B}{A - b\sum_{i=1} a_i C_i} = \frac{C_B + C_Z}{a_{C_i}} + \frac{1 + K_2 C_S}{K_1 a_{C_i}} \quad (17)$$

For very dilute solutions, where the solvent concentration C_S is essentially the same in all experiments, a plot of the left-hand term *vs.* $C_B + C_Z$ should give a straight line. For more concentrated solutions, where it is desirable to take into account differences in solvent concentration, the data may be plotted according to equation 18.

$$\frac{C_Z b C_B}{(1 + K_2 C_S)\left(A - b\sum_{i=1} a_i C_i\right)} = \frac{C_B + C_Z}{a_{C_i}(1 + K_2 C_S)} + \frac{1}{K_1 a_{C_i}} \quad (18)$$

Dropping the $K_2 C_S$ term in (17) or (18) gives an equation similar to that which has been employed by Andrews and Keefer[17] and also by Ross and Labes.[18] It differs only in that the role of slope and intercept are interchanged as in the form preferred by Scott.[19] In some cases considerations such as the formation of other than 1:1 complexes[18] and spectral interference of a reagent[20] have made working with an excess of one reagent less practical.

Case 3.—For the added condition $C_B \gg C_Z$, the equation 11 which is obtained is identical to that given by Corkill, Foster and Hammick,[6] and also by Merrifield and Phillips[5] (if mole fraction is employed, $N_B + N_S = 1$). Expansion of (16) would give an equation which is analogous to (18), and if now the $K_2 C_S$ term also is dropped the resulting equation becomes identical to that of Scott.[19] Actually, the omission of the above terms does little to reduce the work in the usual methods of analyzing the data whereas their inclusion permits considerable expansion in the range of experimental conditions, especially to those cases where factors of cost and availability, as well as solubility, of reagents are of importance.

Effect of Concentration Approximations.—The effect of dropping concentration terms can be considered more quantitatively. Since the general discussion regarding the effect of concentration approximations on the evaluation of K_1 is not altered by assumptions regarding solvent interaction, a value of $K_2 = 0$ will be taken for convenience. Hence, equation 7 can be written as[21]

$$K_{19}^{-1} = \left(\frac{C_B C_Z}{C_C} - C_B\right) - (C_Z - C_C) \quad (19)$$

where the subscript for the equilibrium constant has been introduced to coincide with the equation considered because the value determined for the equilibrium constant depends upon the approximations employed.

The first approximation which can be made is to neglect C_C. This, then, gives equation 20.

$$K_{20}^{-1} = \left(\frac{C_B C_Z}{C_C} - C_B\right) - C_Z \quad (20)$$

The second approximation is to neglect the entire second term in (19)

$$K_{21}^{-1} = \frac{C_B C_Z}{C_C} - C_B \quad (21)$$

This leads directly to equation 12, or the Benesi–Hildebrand[1] or Ketelaar[15] equation.

Drago and Rose[3,4] have pointed out, quite correctly, that introduction of approximations occasionally can lead to large errors. However, the effect of these approximations on evaluating K^{-1} can readily be estimated. Letting $\alpha = C_B/C_Z$ and letting $\beta = C_C/C_Z$ (*i.e.*, fraction of acceptor species converted to complex), equations 19, 20 and 21 reduce, respectively, to

$$\frac{K_{19}^{-1}}{C_Z} = \left(\frac{1 - \beta^*}{\beta^*}\right)\alpha^* - (1 - \beta^*) \quad (22)$$

$$\frac{K_{20}^{-1}}{C_Z} = \left(\frac{1 - \beta}{\beta}\right)\alpha - 1 \quad (23)$$

$$\frac{K_{21}^{-1}}{C_Z} = \left(\frac{1 - \beta}{\beta}\right)\alpha \quad (24)$$

The asterisk has been introduced in equation 22 to point out that, in general, $\beta \neq \beta^*$ and $\alpha \neq \alpha^*$. The left side of equation 23 or 24 is independent of the value of α or β because the product $[(1 - \beta)/\beta]\alpha$ is a constant and, thus, K_{20} may be calculated if K_{21} is known, and *vice versa*. This is not true of equation 22 where the term on the left is a function of β (or α). Therefore, it is not possible to substitute (23) or (24) into (22) without first knowing the one value for β (or α) which satisfies all three equations simultaneously. This value cannot be selected *a priori*, but since β must be between 0 and 1, K_{20} and K_{21} represent the upper and lower limit, respectively, to K_{19}. In the above forms it is immediately apparent that whether (23) or (24) is a better approximation to (22) depends upon whether β is less or greater than $1/2$. This is illustrated in Fig. 1 which, at the same time, shows the errors to be expected by introducing the approximations. When $\alpha = 1$, large errors will result even in the region of small values for β if equation 21 is used, and for larger values of β the results get progressively worse for equation 20. But

(15) J. A. A. Ketelaar, C. van de Stolpe, A. Goudsmit and W. Dzcubas, *Rec. trav. chim.*, **71**, 1104 (1952).

(16) H. Margenau and G. S. Murphy, "The Mathematics of Physics and Chemistry," D. Van Nostrand and Co., New York, N. Y., 1943, Chapter 13.

(17) L. J. Andrews and R. M. Keefer, *J. Am. Chem. Soc.*, **75**, 3776 (1953).

(18) S. D. Ross and M. M. Labes, *ibid.*, **79**, 76 (1957).

(19) R. L. Scott, *Rec. trav. chim.*, **75**, 787 (1956).

(20) R. Foxter, *J. Chem. Soc.*, 5098 (1957).

(21) In this discussion it will be assumed that $C_Z < C_B$. Obviously, this does not limit the conclusions drawn since, for a reversal in concentrations, the two terms C_B and C_Z in equation 19 can be interchanged.

when $\alpha = 1000$, the conversion of C_z to complex must be well above 90% before appreciable differences arise among the various equations.

This does not mean that having a large excess of electron donor allows the form (20) or (21) to be used without caution, because it is just this condition which favors a large per cent. conversion of the electron acceptor. However, from the experimental conditions employed and from even a crude evaluation of the equilibrium constant by any of the standard methods, reference to Fig. 1 will give immediately a good indication of the error to be expected from (20) or (21).

Experimental Considerations

The effect on the equilibrium constants of concentration approximations and of methods of calculation will be illustrated by several pertinent experimental studies.

I. Benzene–Iodine.—The concentrations used by Benesi and Hildebrand[1] in studying this complex in carbon tetrachloride were such that even the smallest value for α is of the order of 2000. Hence a point for this system is not shown in Fig. 1. However, considering that at room temperature iodine dissolved in *pure* benzene is complexed to the extent of about 60 mole %,[1] there should be little significant dependence of the result on the method of analysis. The re-evaluation by Rose and Drago[3] gave $K_X = 1.78 \pm 0.05$; $a_C = 15{,}400 \pm 600$ l. mole^{-1} cm.$^{-1}$, which are similar to the values obtained by Benesi and Hildebrand $K_X = 1.73$; $a_C = 15{,}400$ l. mole^{-1} cm.$^{-1}$, entirely as expected.

The above remarks would be equally applicable, for example, to the mesitylene–iodine system in carbon tetrachloride where it has been reported[1] that iodine in *pure* mesitylene at room temperature is complexed to the extent of 85 mole %. Along the same lines, it is of interest that Briegleb, Czekalla and Hauser[22] recently have noted that application of the Benesi–Hildebrand equation to the data for the picric acid–anthracene complex gave the same value for the equilibrium constant as the one obtained by means of a procedure developed previously[14] in which all concentration terms are retained. It would be anticipated from the data that the Benesi–Hildebrand treatment would give a result which would fall within the 2% error limit reported for the equilibrium constant of this complex.

II. Pyrene–Iodine.—The study of a number of polynuclear aromatic hydrocarbon–iodine complexes in carbon tetrachloride has been reported in the literature[23] and the results have been redetermined by Drago and Rose.[4] The latter authors show that there exists considerable scatter in the data. Specific mention is made to the pyrene–iodine system where the re-evaluated result ($K_C = 43 \pm 7$ l. mole^{-1}; $a_C = 140$ l. mole^{-1} cm.$^{-1}$) is appreciably different from the original ($K_C = 36.5$ l. mole^{-1}; $a_C = 161$ l. mole^{-1} cm.$^{-1}$). The discrepancy seemed puzzling.

Replacing C_C in equation 19 by its spectrophotometric equivalent, A/ba_C (for the case where the complex is the only absorbing species, as seems applicable here), it is evident that greater caution must be exercised in omitting the C_C term for complexes whose molar absorbancy indices are low, as in the pyrene–iodine case. Experimentally, the net effect of a low molar absorbancy index is to necessitate using more concentrated solutions, thereby favoring complex formation. Thus the general considerations discussed earlier are equally applicable here, and reference can be made to Fig. 1 for estimating the effect of neglecting terms.

Using $\alpha = 100$ as an approximation to the range of concentrations employed[23] (C_Z was held constant at 3.24×10^{-4} mole l.$^{-1}$ and C_B ranged from 2.79×10^{-3} to 6.99×10^{-3} mole l.$^{-1}$), and using the reported value of $K_C = 36.5$ l. mole^{-1}, the point A plotted in Fig. 1 shows that use of equation 19 should not appreciably alter the results from those obtained from (21), the equation used by Bhattacharya and Basu.[23] The source of the discrepancy was found to lie in an error in the original report. A redetermination of K_C and a_C from the original data by employing equation 21 and using a least squares treatment to determine the slope and intercept gives results ($K_C = 43$ l. mole^{-1} and $a_C = 140$ l. mole^{-1} cm.$^{-1}$) in agreement with the values found by Drago and Rose.[4] Consequently, the comments of the latter authors reflect not so much the need for elimination of approximations as they do perhaps the need for including an error treatment. In the above case an appropriate treatment, following the procedure of Fieller,[24] gives for the 50% confidence interval $K_C = 43.6 \pm 5.6$ l. mole^{-1} and $a_C = 142 \pm 15$ l. mole^{-1} cm.$^{-1}$.

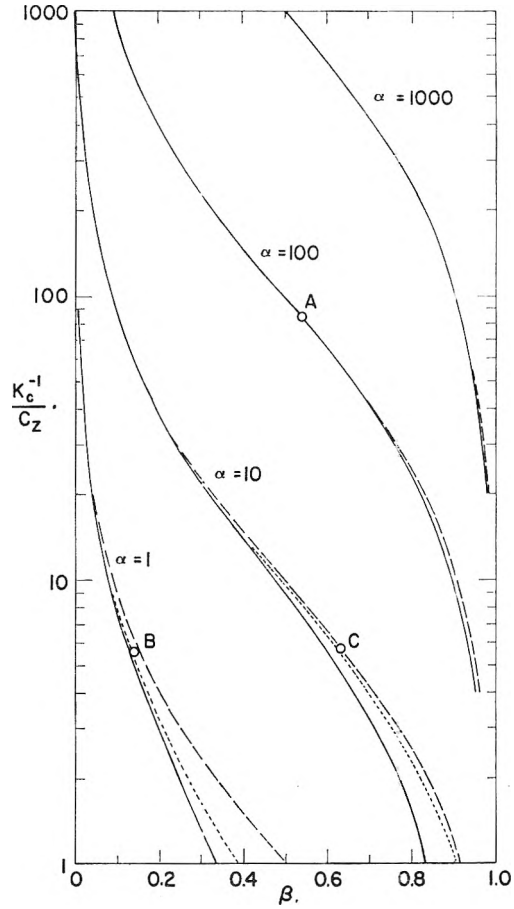

Fig. 1.—Logarithmic scale of K_c^{-1}/C as a function of β for various values of α: dotted line, equation 22; dashed line, equation 24; solid line, equation 23. The points A, B and C represent iodine complexes with pyrene (in CCl_4),[23] with trimethylene sulfide (in CCl_4)[25] and with triethylamine (in *n*-heptane),[30] respectively.

III. Trimethylene Sulfide–Iodine.—McCullough and Mulvey[25] have studied a number of cyclic sulfide–iodine complexes in carbon tetrachloride. The work is of special interest for consideration here because the detailed data for trimethylene sulfide–iodine show that the concentrations used are in the range of $\alpha = 1$ and also that complex formation is highly favored. Values for K_C and a_C were determined at a number of wave lengths using the iterative method of Keefer and Andrews.[13] One typical result, $K_C^{-1} = 11.7 \times 10^{-3}$ mole l.$^{-1}$ and $a_C = 1920$ l. mole^{-1} cm.$^{-1}$ at 440 mμ, was selected to see if the data could be treated more conveniently by use of equation 17. This approximation could introduce an error of a few per cent. as may be seen from point B in Fig. 1, the point having been evaluated from the typical data[25] $C_B = 2.060 \times 10^{-3}$ mole l.$^{-1}$, and $C_Z = 2.097 \times 10^{-3}$ mole l.$^{-1}$, using the reported value for K_C.

Considering first the more exact solution, the form of equation 19 which is applicable to this study is

(22) G. Briegleb, J. Czekalla and A. Hauser, *Z. physik. Chem.*, **21**, 99 (1959).

(23) R. B. Bhattacharya and S. Basu, *Trans. Faraday Soc.*, **24**, 1286 (1958).

(24) E. C. Fieller, *Appendix Suppl. J. Roy. Stat. Soc.*, **7**, 1 (1940).

(25) J. D. McCullough and D. Mulvey, *J. Am. Chem. Soc.*, **81**, 1291 (1959).

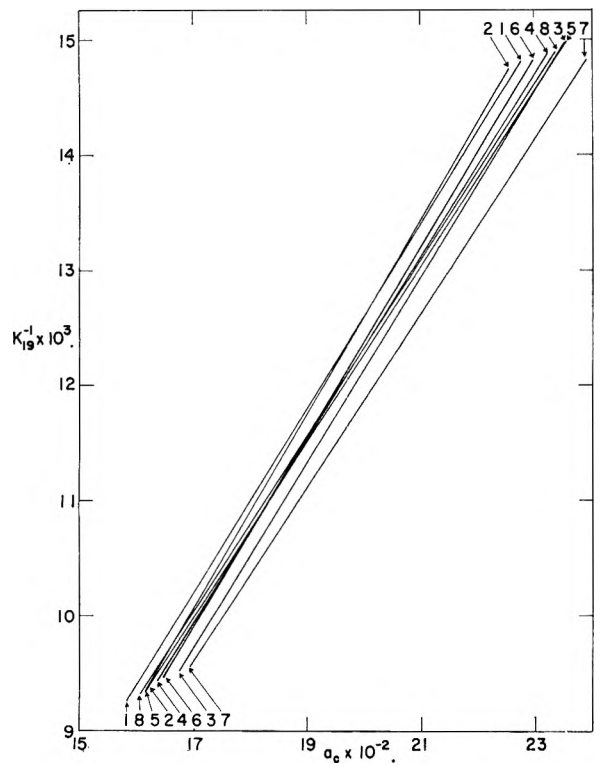

Fig. 2.—K_{19}^{-1} as a function of a_C for the trimethylene sulfide–iodine complex in carbon tetrachloride at room temperature. The points refer to the following concentrations in mole $l.^{-1} \times 10^3$ for trimethylene sulfide and for iodine, respectively[25]: (1) 1.443 and 1.590; (2) 1.164 and 1.282; (3) 2.060 and 2.097; (4) 0.825 and 0.840; (5) 2.836 and 0.599; (6) 2.294 and 0.484; (7) 2.151 and 1.048; (8) 1.604 and 0.782.

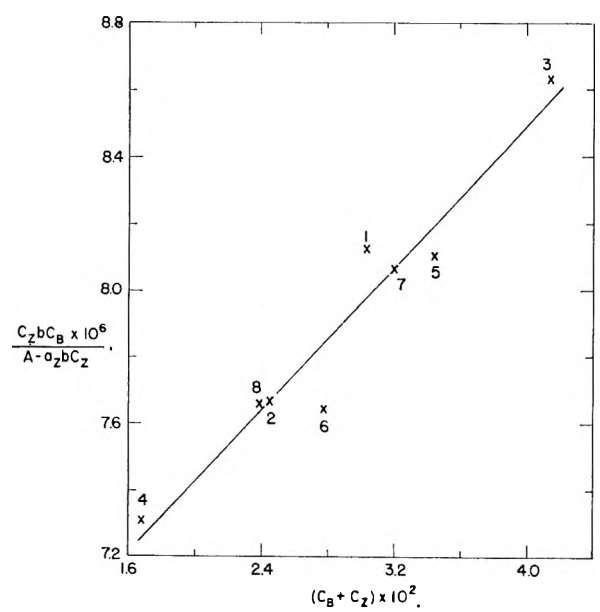

Fig. 3.—$C_Z bC_B/(A - a_Z bC_Z)$ *vs.* $C_B + C_Z$ for the system trimethylene sulfide–iodine in carbon tetrachloride at room temperature.[25] The points refer to the same concentrations as given in Fig. 2.

$$K_{19}^{-1} = \frac{C_B C_Z (a_C - a_Z) b}{A - b a_Z C_Z} - C_B - C_Z + \frac{A - b a_Z C_Z}{b(a_C - a_Z)} \quad (25)$$

where a_Z is the molar absorbancy index of free iodine in carbon tetrachloride. Taking a_Z = 89.0 l. mole^{-1} cm.$^{-1}$ at 440 mμ; the value employed by McCullough, *et al.*,[25,26] K_{19}^{-1} and a_C were evaluated by the technique suggested by Drago and Rose.[3,4] The series of lines thus obtained are shown in Fig. 2. It is seen that the lines intersect over a very wide range, with some lines being almost parallel, making a graphical analysis impractical. Therefore, the slope and intercept of each line were determined separately, and the points of intersection were calculated algebraically. A detailed listing of the 28 points of intersection will not be given, but they will be summarized as follows: 5 intersections with negative values for K_{19}^{-1}; 9 intersections with K_{19}^{-1} ranging from 0 to 0.01; 12 intersections with K_{19}^{-1} ranging from 0.01 to 0.023; 1 intersection with K_{19}^{-1} at about 0.036 and 1 at nearly 0.117. Averaging only the positive values for K_{19}^{-1} in the range 0 to 0.023 and averaging the corresponding a_C values gives, including the average error, $K_{19}^{-1} = 10.7 \pm 3.4 \times 10^{-3}$ mole $l.^{-1}$ and $a_C = 1800 \pm 440$ l. mole^{-1} cm.$^{-1}$.

Using the approximate equation 20, which for this system takes the form (26), permits convenient graphical repre-

$$\frac{C_Z bC_B}{A - b a_Z C_Z} = \frac{C_B + C_Z}{(a_C - a_Z)} + \frac{1}{K_{20}(a_C - a_Z)} \quad (26)$$

sentation of the data. These are given in Fig. 3. There is some deviation from the expected straight line. However, it should be noted that the coördinates do not cover a wide numerical range.

From the values of the slope and intercept as determined by the method of least squares, the results for the equilibrium constant and molar absorbancy index, for the 50% confidence interval,[24] are $K_{20}^{-1} = 12.2 \pm 1.3 \times 10^{-3}$ mole $l.^{-1}$ and $a_C = 2010 \pm 200$ l. mole^{-1} cm.$^{-1}$. Considering the error limits for the results obtained by the two analytical procedures, the use of the more convenient equation 26 certainly seems justified.

The apparently large scatter in the results from the first treatment is due primarily to the method of analysis, which is essentially that of taking all pairs of combinations of the data to solve for two unknowns, and does not signify extremely poor data. This may be seen in the work of Briegleb and Czekalla, *et al.*,[14,22] where comparatively large error limits appear in spite of the great precision in the data. From the second treatment it may be seen that a change in the absorbancy data of just a little more than 2%, which is not much beyond the normal error for the spectrophotometric method, would make even the farthest removed point in Fig. 3 fall on the line.

If equation 25 is to be used to determine the equilibrium constant and molar absorbancy index of the complex, it would perhaps be better to employ the method of least squares as was done for equation 26. The latter equation has the form

$$Y = sX + i \quad (27)$$

where $Y = C_Z bC_B/(A - b a_Z c_Z)$, $X = C_B + C_Z$, the slope $s = 1/(a_C - a_Z)$, and the intercept $i = 1/K_{20}(a_C - a_Z)$. Equation 25 can be put in the form

$$Y = sX + i^* - sW^2 \quad (28)$$

where $i^* = 1/K_{19}(a_C - a_Z)$ and $W = (A - b a_Z C_Z)/b$. A least squares evaluation of s and i^* leads to the results $K_{19}^{-1} = 11.4 \times 10^{-3}$ mole l^{-1} and a_C = 1870 l. mole^{-1} cm.$^{-1}$, which are close to the values obtained by McCullough and Mulvey[25] from their iterative procedure.

It should be mentioned that small errors in a_Z can have an appreciable effect on the calculated value for the equilibrium constant. For example, if instead of 89 a value of 93 l. mole^{-1} cm.$^{-1}$ were used for a_Z, as given by de Maine,[27] the results for K_{20}^{-1} and a_C, giving the 50% confidence interval,[24] as determined by the method of least squares applied to equation 26 are $14.2 \pm 1.7 \times 10^{-3}$ mole l^{-1} and 2200 ± 250 l. mole^{-1} cm.$^{-1}$, respectively.[28] The need for having an accurate determination for a_Z would have been minimized if an iodine–solvent solution had been used for the blank.[29]

(26) N. W. Tideswell and J. D. McCullough, *ibid.*, **79**, 1031 (1957).

(27) P. A. D. de Maine, *J. Chem. Phys.*, **26**, 1192 (1957).

(28) A comparably large dependence on a_Z is observed also when the Rose–Drago[3] technique is used.

(29) Sister M. Brandon O.P., M. Tamres and S. Searles, *J. Am. Chem. Soc.*, **82**, 2129 (1960).

IV. Triethylamine–Iodine.—Of the many iodine complexes reported in the literature, the one formed with triethylamine is the most stable.[30] It is not surprising, therefore, that use of approximate equations might result in appreciable error in the equilibrium constant, which for this system was found to be approximately 10% by Drago and Rose.[4] The point C in Fig. 1 was plotted using the Nagakura data[30] at 25° of $K_{21} = 4.69 \times 10^{-3}$ mole l.$^{-1}$, $C_B = 3.90 \times 10^{-4}$ mole l^{-1}, and $C_Z = 3.64 \times 10^{-5}$ mole l.$^{-1}$. It may be seen from the graph that an error of this magnitude is possible for K_{21} and more important, that the direction for correcting the error can be predicted. Equations 23 and 24 represent a lower and an upper limit to K^{-1}/C_Z. Thus substituting the Nagakura result for K_{21} into equation 23 gives the value $K_{20} = 5.66 \times 10^3$ l. mole^{-1}. This checks quite favorably with the value determined directly by the application of equation 17 to the original data, the result from a least squares treatment being 5.76×10^3 l. mole^{-1}. Comparison is not strictly valid because in equation 17 the role of the slope and intercept is interchanged from that of the Benesi–Hildebrand equation, which was the one employed by Nagakura. Different methods of plotting the same experimental data have been noted to give different results for the equilibrium constant.[19] This is to be expected when a least squares treatment of data is employed, the differences being nil only when the experimental data all lie on an exact line, a point which has recently been mentioned.[31] The prediction that K_{19}, as determined by using equation 22, should be larger than 4.69×10^3 l. mole^{-1} and smaller than 5.66×10^3 l. mole^{-1} is in accord with the result of 5.13 l. mole^{-1} reported by Drago and Rose.[4]

Only the constant at 25° could be re-evaluated by Drago and Rose because detailed experimental data were available at this temperature only.[30] In the absence of other information, a reasonable estimate may be made for the correction of K at the other temperatures, thus permitting a re-evaluation of ΔH and ΔS. It is clear that the correction will increase with decreasing temperature, thereby increasing ΔH and ΔS.

It was mentioned that it is not possible to select *a priori* that particular value of β between 0 and 1 which will permit proper conversion of equation 24 to 22. Using the Nagakura data and choosing a value of $\beta = 1/2$ gives $K_{19} = 5.13 \times 10^4$ l. mole^{-1}, exactly that obtained by Drago and Rose. Assuming that this value for β is also applicable at the other temperatures,[32] the K_{19} column in Table I is readily obtained. The last column establishes the expected upper limit, *i.e.*, for $\beta = 1$. At 40°, the percentage difference between the limits K_{21} and K_{20} has been reduced considerably, rendering less critical a proper selection for β.

The data for the corrected log K *vs.* $1/T$ lie on a straight line. A least squares treatment gives $\Delta H = -12.9$ kcal. mole^{-1} and $\Delta S = -26.3$ e.u., which may be compared to the Nagakura values $\Delta H = -12.0$ kcal. mole^{-1} and $\Delta S = -23.5$ e.u.

Acknowledgment.—The author wishes to acknowledge helpful discussions with Dr. M. Mayot, Dr. A. R. Bloemena, Dr. R. Albrecht and Miss C. Valdemoro during his stay at the University of Paris and at the University of Amsterdam. He wishes also to express his thanks to the John Simon Guggenheim Memorial Foundation for a Fellowship.

TABLE I

EQUILIBRIUM CONSTANT CORRECTIONS FOR THE SYSTEM TRIETHYLAMINE–IODINE IN *n*-HEPTANE

t, °C.	K_{21},[a] $\times 10^{-3}$ l. mole^{-1}	K_{19}, $\times 10^{-3}$ l. mole^{-1}	K_{20}, $\times 10^{-3}$ l. mole^{-1}
20.5	6.32	7.14	8.21
25.0	4.69	5.13	5.66
30.0	3.31	3.52	3.76
40.0	1.74	1.80	1.86

[a] Reference 30.

(30) S. Nagakura, *ibid.*, **80**, 520 (1953).

(31) M. Tamres and Sister M. Brandon O.P., *ibid.*, **82**, 2134 (1960), see Table I.

(32) For any given concentration of base to acid, the fraction of acid converted to complex will be greater at the lower temperature. But the β which is of concern here is the one value at each temperature which will satisfy equations 22, 23 and 24 simultaneously. In the triethylamine–iodine study where a constant concentration of C_Z was used, and assuming only minor variation of C_Z with temperature, the relation for β which applies at two temperatures T_1 and T_2 is

$$\frac{(\beta)_{T_1}}{(\beta)_{T_2}} = \left[\frac{(K_{20}K_{21})_{T_2}}{(K_{20}K_{21})_{T_1}}\right]\left[\frac{(K_{20} - K_{19})_{T_1}}{(K_{20} - K_{19})_{T_2}}\right]$$

where the first and second terms in brackets tend to compensate. However, appreciable and even random variation of β with temperature may be found for a given set of experimental results, especially when there is greater scatter in the data.

THE DECARBOXYLATION OF OXAMIC ACID IN QUINOLINE AND IN 8-METHYLQUINOLINE

BY LOUIS WATTS CLARK

Department of Chemistry, Western Carolina College, Cullowhee, North Carolina

Received November 4, 1960

Kinetic data are reported on the decarboxylation of oxamic acid in quinoline and in 8-methylquinoline. The parameters of the Eyring equation are evaluated and compared with those for oxalic acid, malonic acid and the trichloroacetate ion. The data support the transition-complex mechanism previously proposed for the reaction. An interesting parallel is pointed out between the decarboxylation of oxamic acid and the acid oxalate ion in 8-methylquinoline.

Kinetic studies on the decomposition of oxalic acid into carbon dioxide and formic acid have been made in the solvents dioxane,[1] glycerol,[2] dimethyl sulfoxide, triethyl phosphate, aniline, N-methylaniline, N,N-dimethylaniline, quinoline,[3] 6-methylquinoline and 8-methylquinoline.[4] In weakly basic solvents the rate-determining step of the reaction appears to be the formation of a transition complex, one of the carbonyl carbon atoms of the un-ionized diacid coördinating with an unshared pair of electrons on the nucleophilic atom of the solvent molecule.

The results of kinetic studies on the decomposition of oxamic acid into carbon dioxide and formamide in the solvents aniline and *o*-toluidine indicated that, in this case also, the rate-determining

(1) A. Dinglinger and E. Schöber, *Z. physik. Chem.*, **A179**, 401 (1937).

(2) L. W. Clark, *J. Am. Chem. Soc.* **77**, 6191 (1955).

(3) L. W. Clark, *J. Phys. Chem.*, **61**, 699 (1957).

(4) L. W. Clark, *ibid.*, **62**, 633 (1958).

step may be the formation of an intermediate compound between solute and solvent.[5] Since more information on this reaction was needed in order to more firmly establish the proposed mechanism further kinetic studies have been carried out in this Laboratory on the decarboxylation of oxamic acid in two additional polar solvents, quinoline and 8-methylquinoline. The results of this investigation are reported herein.

Experimental

Reagents.—(1) The oxamic acid used in this investigation was analytical reagent grade, 100.0% assay. See reference 5 for analytical procedures. (2) The solvents were reagent grade chemicals. Each sample of each solvent, before the beginning of each decarboxylation experiment, was distilled directly into the dried reaction flask at atmospheric pressure.

Apparatus and Technique.—The kinetic experiments were conducted in a constant temperature oil-bath by measuring the volume of CO_2 evolved at constant pressure, as described in a previous paper.[6] In each experiment a 0.1585-g. sample of oxamic acid (the amount required to produce 40.0 ml. of CO_2 at STP on complete reaction) was introduced in the usual manner into the reaction flask containing a weighed sample of solvent saturated with dry CO_2 gas.

Results

It was noted in the initial studies on the decarboxylation of oxamic acid in aniline and *o*-toluidine[5] that there was a tendency for the reverse reaction to take place, namely, formamide and carbon dioxide combining to give oxamic acid. In further studies of this phenomenon the following experiments were performed: (1) CO_2 was bubbled into formamide—no reaction; (2) CO_2 was bubbled into a mixture of formamide and aniline–oxamic acid was produced. Evidently aromatic amines act as a catalyst for the reaction, the nitrogen probably coördinating with the aldehydic hydrogen atom of the formamide facilitating CO_2 fixation.

It was found in the initial studies that the reverse reaction could be largely circumvented by employing a relatively large volume of solvent and using a gentle stirring action. Also no appreciable difference in the specific reaction velocity constant at constant temperature was detected when the volume of solvent was varied between 50 and 135 g. Similar results were obtained in the present studies. No significant difference in the velocity constant was observed on carrying out the experiment in quinoline at 153.45°, using 50, 100 and 135 g. of solvent. In the experiments in quinoline and 8-methylquinoline there was a tendency for the reverse reaction to take place. However, on using large volumes of solvent (100–135 g.) and gentle stirring the forward reaction in most cases was found to go to 99% completion before oxamic acid crystals began to collect in the condenser.

The rate of decarboxylation of oxamic acid was measured in quinoline and in 8-methylquinoline over a range of about 20°. The plot of $\log(V_\infty - V_t)$ *vs.* t was linear over nearly the entire experiment indicating that the reaction is first order. The average rate constants calculated in the usual manner from the slopes of the experimental logarithmic plots are shown in Table I. The parameters of the Eyring equation, based upon the data in Table I, are shown in Table II, along with corresponding data for oxalic acid, malonic acid and the trichloroacetate ion.

(5) L. W. Clark, *J. Phys. Chem.*, **65**, 180 (1961).
(6) L. W. Clark, *ibid.*, **60**, 1150 (1956).

TABLE I

APPARENT FIRST-ORDER RATE CONSTANTS FOR THE DECARBOXYLATION OF OXAMIC ACID IN QUINOLINE AND IN 8-METHYLQUINOLINE

Solvent	Temp., °C. cor.	No. of expts.	$k \times 10^4$, sec.$^{-1}$	Av. dev.
Quinoline	137.62	2	1.33	±0.01
	144.77	2	3.65	± .01
	153.45	3	12.08	± .01
8-Methylquinoline	127.73	2	1.27	± .01
	135.13	2	2.92	± .02
	145.74	3	9.21	± .02
	148.62	3	12.53	± .02

TABLE II

KINETIC DATA FOR THE DECARBOXYLATION OF OXAMIC ACID, OXALIC ACID, MALONIC ACID AND THE TRICHLOROACETATE ION IN QUINOLINE AND IN 8-METHYLQUINOLINE

Solvent	Quinoline		8-Methylquinoline	
Reactant	$\Delta H^\ddagger$, kcal.	$\Delta S^\ddagger$, e.u.	$\Delta H^\ddagger$, kcal.	$\Delta S^\ddagger$, e.u.
Oxamic acid	47.0	+37.5	36.0	+12.2
Oxalic acid[3,4]	38.9	+15.8	37.7	+13.7
Malonic acid[7]	26.7	− 2.3	24.4	−10.5
Trichloroacetate ion[8]	24.0	− 2.4	22.3	− 8.4

Discussion of Results

In the decarboxylations of malonic acid[9] and the trichloroactate ion,[8] as well as oxalic acid,[8] intermediate compound formation between solute and solvent has been shown to take place. That the same is true for the oxamic acid reaction is clearly demonstrated by the data in Table II.

It will be observed in column I of Table II that, for the reaction in quinoline, the $\Delta H^\ddagger$ of the reaction decreases on passing from oxamic acid to oxalic acid, from oxalic acid to malonic acid, and from malonic acid to the trichloroacetate ion. This is the order that would be predicted on the basis of the principle that an increase in the attraction between two reactants lowers the activation energy of the reaction.[10] The effective positive charge on the polarized carbonyl carbon atom of the reactant, involved in coördination with the solvent, increases on passing from oxamic acid to oxalic acid (since the +M effect of the amide group is greater than that of the hydroxyl),[11] from oxalic acid to malonic acid (since the methylene group tends to prevent the transmission of inductive effects between the two terminal carboxyl groups),[12] and from malonic acid to the trichloroacetate ion (due to the strong negative inductive effects of the three α-halogen atoms).

It is well known that oxalic acid and malonic acid associate through hydrogen bonding to some extent, past the dimer stage, to form "supermole-

(7) L. W. Clark, *ibid.*, **62**, 500 (1958).
(8) L. W. Clark, *ibid.*, **63**, 99 (1959).
(9) G. Fraenkel, R. Belford and P. E. Yankwich, *J. Am. Chem. Soc.*, **76**, 15 (1954).
(10) K. J. Laidler, "Chemical Kinetics," McGraw-Hill Book Co., Inc., New York, N. Y., 1950, p. 138.
(11) A. E. Remick, "Electronic Interpretations of Organic Chemistry," John Wiley and Sons, Inc., New York, N. Y., 2nd Ed., 1949, p. 57.
(12) R. Q. Brewster, "Organic Chemistry," 2nd. ed., Prentice–Hall, Inc., New York, N. Y., 1953, p. 581.

cules" composed of 3–4 single molecules each.[13] However, oxamic acid, being a very weak acid, and having only one carboxyl group, probably does not associate thus to any appreciable extent. Since there is very little difference in size between oxalic acid and oxamic acid the $\Delta S^{\ddagger}$ values for their reactions in quinoline would be expected to be approximately equal, provided the transition complex in each case were composed of the same number of units. It is seen, however, in Table II, column II, that the $\Delta S^{\ddagger}$ for the reaction in quinoline is considerably greater for oxamic acid than it is for oxalic acid. We have here additional evidence for the inference that a single molecule of oxamic acid is involved in the formation of the transition complex, whereas, in the case of oxalic acid, a "supermolecule" cluster composed of 3–4 single molecules is involved.[5]

The methyl group in 8-methylquinoline has two effects: (1) a positive inductive effect which releases electrons and increases the effective negative charge on the tertiary nitrogen atom, and (2) a steric effect which offers hindrance to the approach of an electrophilic agent to the nitrogen. If the rate-determining step of a reaction involves the coördination of an electrophilic agent with a nucleophilic agent, effect (1) will cause a decrease in the $\Delta H^{\ddagger}$ of the reaction, whereas effect (2) will cause a decrease in the $\Delta S^{\ddagger}$ of the reaction on going from quinoline to 8-methyl-quinoline. It will be seen in Table II that, on passing from quinoline to 8-methylquinoline, a considerable decrease in both $\Delta H^{\ddagger}$ and $\Delta S^{\ddagger}$ takes place for the decarboxylations of oxamic acid, malonic acid and the trichloroacetate ion. These results strongly substantiate the proposed transition-complex mechanism for the decarboxylation of oxamic acid in polar solvents.

In the case of oxalic acid the decrease in $\Delta H^{\ddagger}$ and $\Delta S^{\ddagger}$ is very slight in comparison with the behavior of the other three compounds. This anomaly has been explained as being the result of the circumstance that, in the reaction in quinoline, un-ionized oxalic acid is involved, whereas, in 8-methylquinoline, one of the acid hydrogens is ionized and the acid oxalate ion undergoes decarboxylation.[4]

If, in 8-methylquinoline, the acid oxalate ion suffers cleavage, it would be expected that the ion would form a transition complex with the solvent involving the un-ionized carboxyl group. Furthermore, having only one un-ionized carboxyl group, the ion would not be expected to form an association cluster or "supermolecule" through hydrogen bonding. The second ionization constant of oxalic acid being much smaller than the first, the effective positive charge on the carbonyl carbon atom of the ion involved in coördination with the solvent would be smaller than in the case of the diacid, resulting in the reaction's requiring a higher activation energy. A single molecule of oxamic acid will have approximately the same size as a single acid oxalate ion. Since oxygen is slightly smaller than nitrogen, the acid oxalate ion will be actually somewhat smaller than oxamic acid. This will mean that the $\Delta S^{\ddagger}$ values of the two reactions should be approximately equal, being somewhat larger for the acid oxalate ion than for the un-ionized oxamic acid.

It will be seen in Table II, lines 1 and 2, columns 3 and 4, that all these deductions are verified completely by the experimental data. The fact that the $\Delta H^{\ddagger}$ values of the two reactions are very nearly equal indicates that the two substances have very nearly the same acid strength, the oxamic acid being a slightly stronger acid than the acid oxalate ion.

On the basis of the results reported herein it appears highly probable that (1) oxamic acid forms a transition complex with nucleophilic solvents; (2) the complex consists of one molecule of solvent plus one molecule of un-ionized oxamic acid; (3) coördination takes place between the polarized, electrophilic, carbonyl carbon atom of the un-ionized oxamic acid and an unshared pair of electrons on the nucleophilic atom of the solvent molecule; (4) the acid oxalate ion, in 8-methylquinoline, behaves in a manner quite analogous to oxamic acid, and (5) oxalic acid and malonic acid, in weakly basic solvents, associate to form a cluster or "supermolecule" composed of 3–4 single molecules, one end of which coördinates with the nucleophilic agent.

Further work on this problem is contemplated.

Acknowledgment.—The support of this research by the National Science Foundation, Washington, D. C., is gratefully acknowledged.

(13) W. Hückel, "Theoretical Principles of Organic Chemistry," Vol. II, Elsevier Publishing Co., New York, N. Y., 1958, p. 329 *et seq.*

ACTIVITY COEFFICIENTS OF SODIUM CHLORIDE AND POTASSIUM CHLORIDE IN MIXED AQUEOUS SOLUTIONS AT 25°

BY R. A. ROBINSON

Chemistry Department of the University of New England, Armidale, N.S.W., Australia

Received November 10, 1960

Isopiestic vapor pressure measurements have been made at 25° of solutions of sodium chloride and potassium chloride mixtures. The activity coefficients of both components have been evaluated by the method of McKay and Perring. The logarithm of the activity coefficient of potassium chloride varies linearly with the sodium chloride concentration in solutions of constant total molality but there is a small departure from linearity for the logarithm of the activity coefficient of sodium chloride.

Symbols

γ_B = activity coefficient of electrolyte B in a soln. of total molality m, of which $m_B = xm$ is electrolyte B and $m_C = (1 - x)m$ is electrolyte C
γ_B^0 = activity coefficient of electrolyte B in a soln. containing B only at the same molality m
Γ_B = activity coefficient of electrolyte B in a soln. containing B only at a molality M', with the same solvent vapor pressure as the mixed solution of total molality m
γ_C = activity coefficient of electrolyte C in the mixed soln. of total molality m
γ_c^0 = activity coefficient of electrolyte C in a soln. containing C only at the same molality m
Γ_C = activity coefficient of electrolyte C in a soln. containing C only at a molality M, with the same solvent vapor pressure as the mixed soln. of total molality m
R = isopiestic ratio, M/m
φ = osmotic coefficient
α_B, α_C, β_B, β_C = parameters of eq. 1 and 2
a_W = water activity of a soln. of both electrolytes at a total molality m
$a_{W(C)}$ = water activity of a soln. of electrolyte C alone at a molality m
In this work, B = potassium chloride and C = sodium chloride

If, for a series of mixed aqueous solutions of two 1:1 electrolytes, at constant total molality, the activity coefficient of one is given by

$$\log \gamma_B = \log \gamma_B^0 - \alpha_B m_C - \beta_B m_C^2 \qquad (1)$$

and the activity coefficient of the other by

$$\log \gamma_C = \log \gamma_C^0 - \alpha_C m_B - \beta_C m^2{}_B \qquad (2)$$

then[1,2]

$$-55.51/(xm^2) \log a_W/a_{W(C)} = 4/3\, x^2 m(\beta_C - \beta_B) + x[(\alpha_B + \alpha_C) - 2m(\beta_C - \beta_B)] - 2\alpha_C \qquad (3)$$

and if $\beta_B = \beta_C$ (not necessarily $\beta_B = \beta_C = 0$)

$$-55.51/(xm^2) \log a_W/a_{W(C)} = x(\alpha_B - \alpha_C) - 2\alpha_C \qquad (4)$$

i.e., at constant total molality, log a_W is quadratic in x and from isopiestic vapor pressure measurements α_B and α_C can be evaluated. Owen and Cooke[3] were the first to use the method for lithium chloride–potassium chloride mixtures and later Robinson and Lim[4] made measurements on sodium chloride–potassium chloride mixtures. The defect of this method is that it is difficult to make isopiestic measurements on a series of a solutions of exactly the same total molality and recourse has often to be made to some form of graphical interpolation. McKay and Perring[5] proposed another relationship (equation 5) which is more suited to isopiestic measurements; this has been used[6] for potassium chloride–potassium bromide mixtures and Robinson[7] has recalculated his earlier data on sodium chloride–potassium chloride mixtures to test the method. This, however, involved considerable interpolation of data and it was thought worthwhile making a new set of very careful measurements to which the equation of McKay and Perring could be applied directly.

Their equation can be written

$$\ln \gamma_C = \ln \Gamma_C + \ln R + \int_0^{M\varphi} \left[\frac{1}{m^2}\left(\frac{dm}{d \ln x}\right)_{M\varphi} + \frac{R-1}{M}\right] d(M\varphi) \qquad (5)$$

In the event that, for any set of solutions of the same vapor pressure, R can be expressed as

$$R = 1 - ax - bx^2 \qquad (6)$$

where a and b are functions of m but not of x, the integral in (5) takes the simple form

$$\int_0^{M\varphi} = x^2 \int_0^{M\varphi} \frac{b}{M} d(M\varphi) \qquad (7)$$

If b/M can be expressed as a function of $(M\varphi)$

$$-b/M = j + 2k(M\varphi) + 3l(M\varphi)^2 \qquad (8)$$

then

$$-\int_0^{M\varphi} = x^2(M\varphi)[j + k(M\varphi) + l(M\varphi)^2] \qquad (9)$$

The experimental measurements reported in this paper relate to the isopiestic ratio, $R = M/m$, *i.e.*, the molality of a solution of sodium chloride alone of molality M and of a mixed solution of total molality m, each having the same solvent vapor pressure, are measured directly. The desiccator in which the measurements were made contained up to thirteen dishes, three of which were used to give triplicate measurements of the concentration of the sodium chloride solution and the remainder were used for duplicate measurements of the concentrations of mixtures. No result was accepted unless duplicates agreed within 0.05% in the isopiestic ratio or the mean deviation of the triplicates was 0.03% or less. In general the agreement was much better than this: over about one hun-

(1) H. S. Harned and B. B. Owen, "The Physical Chemistry of Electrolytic Solutions," Third Edition, Reinhold Publ. Corp., New York, N. Y., 1958, Chap. 14.

(2) R. A. Robinson and R. H. Stokes, "Electrolyte Solutions," Butterworths Scientific Publications, London, 1959, Chap. 15.

(3) B. B. Owen and T. F. Cooke, *J. Am. Chem. Soc.*, **59**, 2273 (1937).

(4) Reported in "Electrochemical Constants," NBS Circular 524, 171 (1953).

(5) H. A. C. McKay and J. K. Perring, *Trans. Faraday Soc.*, **49**, 163 (1953).

(6) H. W. McCoy and W. E. Wallace, *J. Am. Chem. Soc.*, **78**, 1830 (1956).

(7) R. A. Robinson, *Trans. Faraday Soc.*, **49**, 1411 (1953).

TABLE I

ISOPIESTIC MEASUREMENTS WITH REFERENCE SOLUTIONS OF SODIUM CHLORIDE APPROXIMATELY 4 M

M	x	m_C	m_B	$(m_B + m_C)$	R	R (cor.)	R (calcd.)	%Δ
3.9371	0.6359	1.5675	2.7382	4.3057	0.9144	0.9139	0.9138	−0.01
	.9307	0.3079	4.1354	4.4433	.8861	.8854	.8851	− .03
3.9684	.0892	3.6659	0.3591	4.0250	.9859	.9859	.9859	0
	.3907	2.5628	1.6436	4.2064	.9434	.9434	.9432	−0.02
	.8320	0.7455	3.6918	4.4373	.8943	.8943	.8939	− .04
	1.0	....	4.5111	4.5111	.8797	.8797	.8793	− .04
4.0043	0.1480	3.4918	0.6066	4.0984	.9770	.9771	.9770	− .01
	.2467	3.1340	1.0264	4.1604	.9625	.9627	.9627	0
	.4964	2.1700	2.1391	4.3091	.9293	.9297	.9300	+0.03
	.7563	1.0843	3.3652	4.4495	.8999	.9005	.9012	+ .07
	.8695	0.5875	3.9149	4.5024	.8894	.8901	.8904	+ .03

dred duplicates (or triplicates) the average deviation from the mean was 0.016%.

Some results are quoted in Table I to demonstrate that equation 6 is applicable. Eleven mixed solutions were measured, using three reference solutions close to 4 M in concentration. Figure 1 shows the change in the isopiestic ratio with x at this and some other concentrations of the reference solution; from this graph there can be read off the small correction necessary to give the isopiestic ratios of the eleven solutions in equilibrium with exactly 4 M NaCl. These are given as R(cor.) in Table I; the next column gives calculated values of the isopiestic ratio using equation 6 with $a = 0.1613$ and $b = -0.0406$; thefinal column gives the difference between R(cor.) and R(calcd.); the mean difference is 0.03%.

Table II gives the parameters of equation 6 calculated in this way for eleven reference solutions; the last column is again the difference between R(cor.) and R(calcd.), the overall mean difference being 0.03%. These parameters are plotted in Figs. 2 and 3, against M in the first case and against $(M\varphi)$ in the second. The b/M points plotted against $(M\varphi)$ lie close to a smooth curve except for the points corresponding to the two lower concentrations: the isopiestic ratio is so close to unity at these concentrations that a range of values of the parameters of equation 6 can be used with almost equal success. The curve show in Fig. 3 is the one which best fits all the points: it is the curve of equation 8 with $j = 0.01658$, $k = -0.00072$ and $l = 0.000009$. If the two points at the lower concentrations are neglected, the best values of the parameters are very different, $j = 0.01778$, $k = -0.00105$, $l = 0.000033$; nevertheless, the integral of equation 5, which is the area under the curve of Fig. 3, is almost the same. Thus at $(M\varphi) = 7$, about the highest value reached in this work, and $x = 0.4$, the integral contributes 0.0058 to log γ_C by the first set of parameters and 0.0059 by the second set.

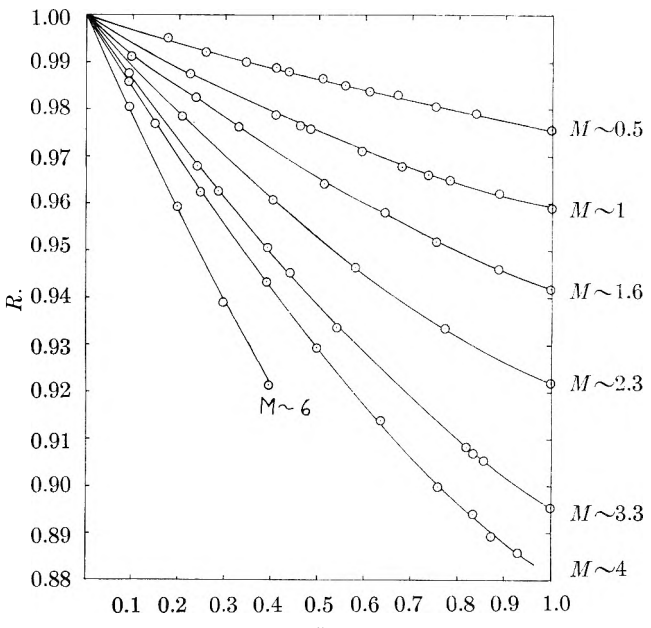

Fig. 1.—Isopiestic ratios as a function of x.

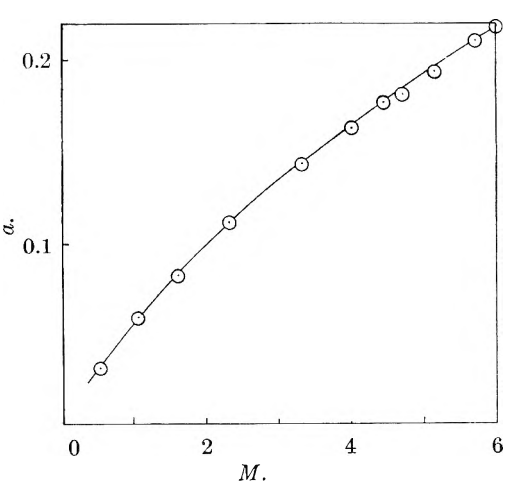

Fig. 2.—The a parameter of equation 6.

TABLE II

PARAMETERS OF EQUATION 6

M	a	$-b$	$-b/M$	%Δ
0.5	0.0304	0.0067	0.0135	0.03
1.032	.0593	.0184	.0178	.05
1.6	.0806	.0230	.0144	.02
2.325	.1111	.0332	.0143	.02
3.348	.1427	.0377	.0113	.02
4.0	.1613	.0406	.0102	.03
4.446	.1772	.0456	.0102	.04
4.7	.1803	.0412	.0088	.02
5.15	.1942	.0422	.0082	.06
5.7	.2108	.0485	.0085	.02
6.0	.2184	.0436	.0072	.03

TABLE III

CALCULATION OF α_B AND α_C AT $M \sim 4$

M	x	R	$M\varphi$	$-\log \Gamma_C$	$-\log R$	J	$-\log \gamma_C$	$-\log \gamma_C^0$	α_C	$-\alpha_B$	$\alpha_B + \alpha_C$
3.9371	0.6359	0.9144	4.375	0.1088	0.0389	0.0104	0.1581	0.0922	0.0241	0.0092	0.0149
	.9307	.8861			.0525	.0223	.1836	.0857	.0237	.0088	.0149
3.9684	.0892	.9859	4.419	.1075	.0062	.0002	.1139	.1050	.0248	.0089	.0159
	.3907	.9434			.0253	.0040	.1368	.0968	.0243	.0092	.0151
	.8320	.8943			.0485	.0180	.1740	.0860	.0238	.0095	.0143
4.0043	.1480	.9770	4.469	.1059	.0101	.0006	.1166	.1017	.0246	.0090	.0156
	.2467	.9625			.0166	.0016	.1241	.0989	.0246	.0091	.0155
	.4964	.9293			.0318	.0065	.1442	.0920	.0244	.0092	.0152
	.7563	.8999			.0458	.0150	.1667	.0854	.0242	.0089	.0153
	.8695	.8894			.0509	.0199	.1767	.0829	.0240	.0092	.0148
								Mean	.0243	.0091	.0152

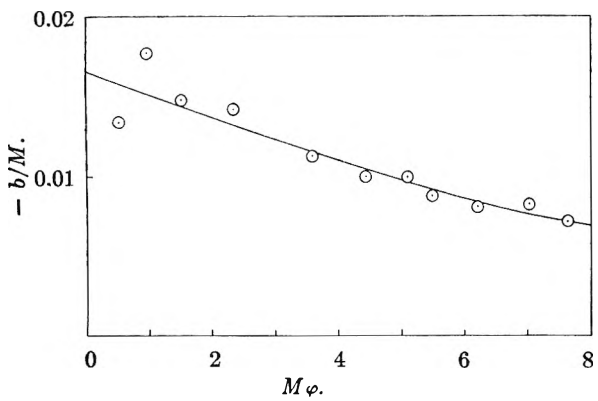

Fig. 3.—The b parameter of equation 6.

With $x = 1$, $(M\varphi) \sim 5$ was the highest value that could be reached (limited by the solubility of potassium chloride); the first set of parameters gave 0.0287 as the contribution to $\log \gamma_C$, the second set 0.0291. Thus the integral can be calculated with confidence for different values of M and x. Table III illustrates how the α_B and α_C coefficients of equations 1 and 2 are evaluated. The first three columns reproduce the experimental data in Table I; the fourth column gives the $(M\varphi)$ data needed to evaluate the integral; the next three columns give the three terms on the right of equation 5, those in the seventh column being 0.4343 times the integral of equation 5. The next two columns give the value of γ_C in the mixed solution at a total molality $m = M/R$ and of γ_C^0 the value at the *same* molality, m, but in the absence of potassium chloride. Γ_C, γ_C and γ_C^0 were interpolated from tables.[8] The coefficient α_C is now calculated as $(1/m_B) \log \gamma_C/\gamma_C^0$ where $m_B = xM/R$.

Corresponding to equation 5 we can write

$$\ln \gamma_B = \ln \Gamma_B + \ln R' + \int_0^{M\varphi} \left[\frac{1}{m^2}\left(\frac{dm}{d \ln (1-x)}\right)_{M\varphi} + \frac{R'-1}{M'}\right] d(M\varphi)$$

where M' is the molality of a potassium chloride solution of the same vapor pressure as a sodium chloride solution of molality M and $R' = M'/m$. The integral is now

$$(1-x)^2 \int_0^{M\varphi} \frac{b}{M}\, d(M\varphi)$$

Corresponding to any M, M' is known[9] so that γ_B and hence α_B can be calculated. α_B and $(\alpha_B + \alpha_C)$ are recorded in the last two columns of Table III. It will be noted that the α_C values show a degree of constancy; the variation is between 0.0237 and 0.0248 with a mean of 0.0243; the α_B values show less variation between 0.0088 and 0.0095; whether these variations are significant is a matter that will be discussed later.

The experimental results are collected in Table IV, grouped in eleven series, the M value being

TABLE IV

CALCULATION OF α_B AND α_C COEFFICIENTS

M	x	R	α_C	$-\alpha_B$	$(\alpha_B + \alpha_C)$
			Series 1		
0.49990	0.3404	0.9902	0.0256	0.0126	0.0130
	.5054	.9864	.0246	.0136	.0110
	.6679	.9832	.0247	.0142	.0105
.50118	.2527	.9923	.0266	.0119	.0147
	.4049	.9889	.0244	.0126	.0118
	.6083	.9839	.0252	.0175	.0077
	.7497	.9809	.0256	.0125	.0131
.51960	.1722	.9950	.0245	.0125	.0120
	.4330	.9881	.0242	.0128	.0114
	.5563	.9851	.0252	.0137	.0115
	.8362	.9789	.0248	.0138	.0110
		Mean	.0250	.0134	.0116
			Series 2		
1.0166	0.2280	0.9877	0.0239	0.0097	0.0142
	.4579	.9775	.0233	.0099	.0134
	.7355	.9672	.0230	.0101	.0129
1.0176	.6770	.9691	.0229	.0103	.0126
	.8787	.9617	.0233	.0078	.0155
1.0426	.2218	.9871	.0248	.0092	.0156
1.0493	.4061	.9783	.0239	.0093	.0146
	.4817	.9763	.0228	.0101	.0127
	.5925	.9713	.0230	.0100	.0130
	.7818	.9643	.0232	.0093	.0139
		Mean	.0234	.0096	.0138
			Series 3		
1.5001	0.2322	0.9833	0.0233	0.0086	0.0147
	.3225	.9776	.0226	.0086	.0140
	.6400	.9600	.0222	.0090	.0132
	.7573	.9544	.0226	.0087	.0139
1.6223	.0920	.9926	.0224	.0087	.0137
	.5100	.9642	.0222	.0089	.0133
	.8841	.9461	.0223	.0087	.0136
		Mean	.0225	.0087	.0138

(8) Ref. 2, p. 476.

(9) R. A. Robinson, *Trans. Roy. Soc. (New Zealand)*, **75**, 203 (1945).

		Series 4			
2.3248	0.2060	0.9785	0.0233	0.0084	0.0149
	.4010	.9610	.0230	.0084	.0146
	.5797	.9465	.0229	.0081	.0148
	.7739	.9337	.0225	.0076	.0149
		Mean	.0229	.0081	.0148
		Series 5			
3.3109	0.0892	0.9878	0.0237	0.0085	0.0152
	.3907	.9506	.0236	.0088	.0148
	.8320	.9083	.0232	.0090	.0142
3.3188	.2367	.9680	.0242	.0086	.0156
	.4366	.9453	.0237	.0088	.0149
	.8181	.9092	.0232	.0090	.0142
3.3477	.2835	.9627	.0238	.0088	.0150
	.5384	.9337	.0233	.0088	.0145
	.8559	.9052	.0239	.0084	.0155
		Mean	.0236	.0087	.0149
		Series 6 (See Table III)			
~4		Mean	0.0243	0.0091	0.0152
		Series 7			
4.4461	0.1716	0.9708	0.0257	0.0091	0.0168
	.3598	.9426	.0251	.0094	.0157
	.5567	.9157	.0249	.0095	.0154
	.6496	.9036	.0248	.0092	.0156
		Mean	.0251	.0093	.0156
		Series 8			
4.6857	0.1194	0.9785	0.0259	0.0092	0.0167
	.2161	.9629	.0253	.0093	.0160
	.3231	.9459	.0254	.0095	.0159
	.4257	.9308	.0252	.0096	.0156
4.7635	.0892	.9845	.0248	.0093	.0155
	.2643	.9550	.0253	.0095	.0158
	.4580	.9254	.0252	.0097	.0155
	.7481	.8874	.0249	.0098	.0151
		Mean	.0253	.0095	.0158
		Series 9			
5.1309	0.1945	0.9631	0.0267		
	.2950	.9460	.0263		
	.3938	.9298	.0262		
5.1572	.0991	.9816	.0258		
	.3558	.9365	.0260		
	.4489	.9217	.0259		
	.5314	.9094	.0257		
		Mean	.0261		
		Series 10			
5.6970	0.1194	0.9754	0.0272		
	.2161	.9565	.0270		
	.3231	.9372	.0267		
	.4257	.9194	.0265		
5.7722	.0580	.9879	.0270		
	.0739	.9848	.0271		
	.1628	.9668	.0271		
	.2645	.9472	.0269		
		Mean	.0269		
		Series 11			
5.9941	0.0920	0.9805	0.0272		
	.1945	.9592	.0274		
	.2950	.9389	.0275		
	.3938	.9213	.0274		
6.0839	.1945	.9583	.0278		
	.2950	.9385	.0275		
	.3938	.9206	.0271		
		Mean	.0274		

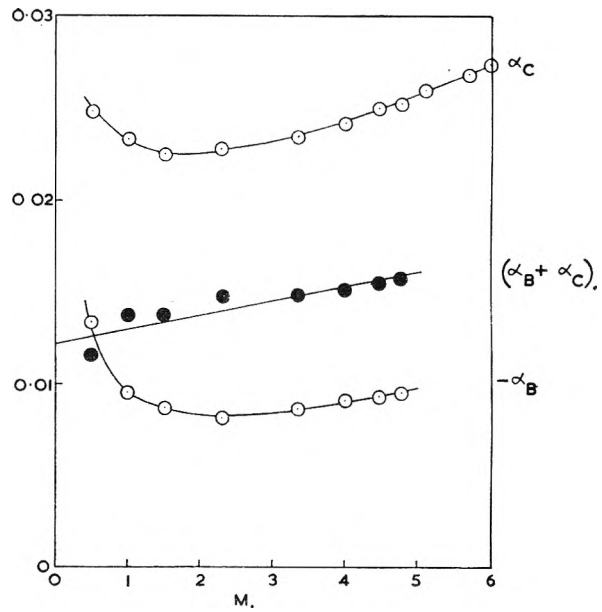

Fig. 4.—α_B, α_C and $(\alpha_B + \alpha_C)$ *vs.* M.

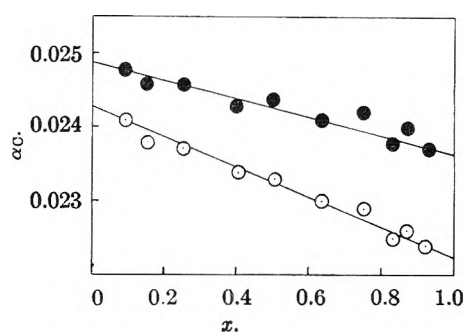

Fig. 5.—Variation of α_C with x. The points on the upper line correspond to the condition of nearly constant total molality. A small correction to a constant total molality of 4.25 gives the points on the lower line (the points are plotted lower by 0.001 in α_C). From the lower line $\alpha_C = 0.0253$ at $x = 0$ and $\beta_C = -0.0004$.

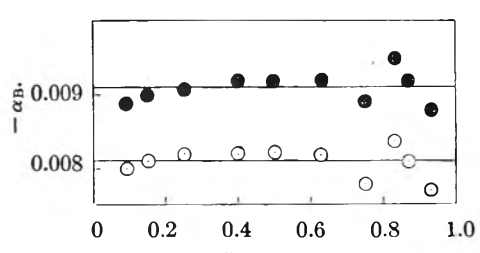

Fig. 6.—Variation of α_B with x. The points on the upper curve correspond to the condition of nearly constant total molality. A small correction to a constant total molality of 4.25 gives the points on the lower line (the points are plotted lower by 0.001 in $-\alpha_B$).

nearly the same for all results quoted in any one series. The corresponding values of α_B, α_C and $(\alpha_B + \alpha_C)$ have been calculated by the method described above and are recorded. In each series, the α_B and α_C coefficients show a considerable measure of constancy; they should be constant, within the limits of experimental accuracy, if equations 1 and 2 hold with $\beta_B = \beta_C = 0$. There is, however, no reason why α_B and α_C should not vary with M and Fig. 4 shows that there is a

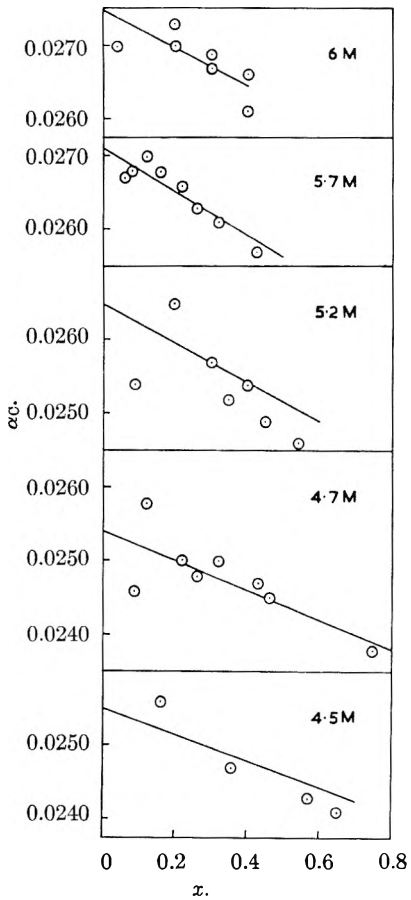

Fig. 7a.—Variation of α_C with x at constant total molality.

Molality =	α_C =	β_C =
4.5	0.0255	−0.0004
4.7	.0254	−0.0004
5.2	.0265	−0.0006
5.7	.0271	−0.0005
6	.0275	−0.0004

small change in both α_B and α_C with M. The α_B and α_C values calculated from the data at $M \sim 0.5$ do not have high accuracy but it is believed that they are accurate enough to confirm that the upward trend between $M = 1.5$ and $M = 1.0$ is enhanced in more dilute solutions. It is not uncommon for these α coefficients to be approximately constant in moderately concentrated solutions and exhibit considerable change in more dilute solutions, *e.g.*, the system: hydrochloric acid–cesium chloride.[10] What, however, is of more interest is the change, if any, of $(\alpha_B + \alpha_C)$ with concentration. Figure 4 shows that there is a small change: it is not believed that experimental error could explain even the small change to be noted in Fig. 4 and this change must be accepted as real. Again not much significance is to be given to the point at $M \sim 0.5$; if it is accepted, the slope of the line is 0.00078; if it is rejected the slope will be slightly less. It can be shown[11] as a necessary consequence of equations 1 and 2 that

$$(\alpha_B + \alpha_C) = \text{constant} - 2m(\beta_B + \beta_C) \quad (10)$$

Thus the slope of $(\alpha_B + \alpha_C)$ *vs.* M in Fig. 4 is $-2(\beta_B + \beta_C)$ so that $(\beta_B + \beta_C) = -0.0004$.

(10) Ref. 1, Fig. (14-6-2), p. 610.

(11) Ref. 2, p. 441; see also E. Glueckauf, H. A. C. McKay and A. R. Mathieson, *J. Chem. Soc.*, S299 (1949).

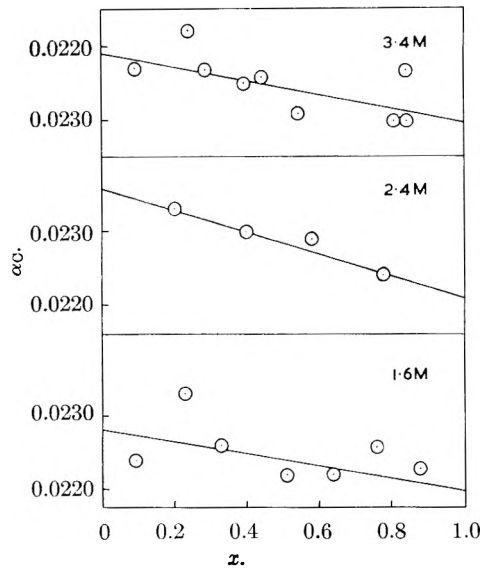

Fig. 7b.—Variation of α_C with x at constant total molality.

Molality =	α_C =	β_C =
1.6	0.0228	−0.0005
2.4	.0236	−0.0006
3.4	.0239	−0.0003

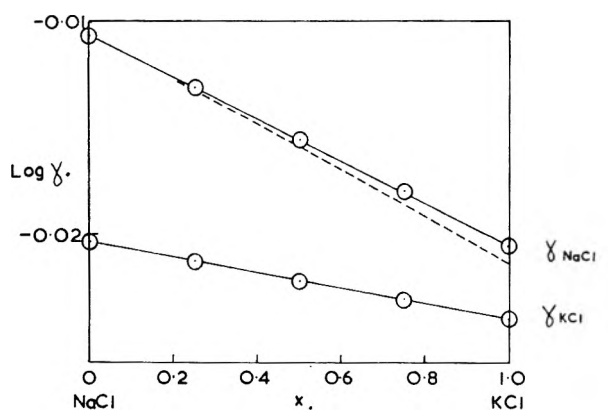

Fig. 8.—Variation of γNaCl and γKCl with composition of the mixture at constant total molality of 4. The upper curve for γNaCl assumes $\beta_C = 0$, the broken curve, $\beta_C = -0.0005$.

(To conform with equation 10, $(\alpha_B + \alpha_C)$ should be plotted against m and not against M but the difference is insignificant). If $\beta_B = 0$, then $\beta_C = 0.0004$ and such a term is by no means negligible; it would contribute 0.0064 to log γ_C for sodium chloride present in vanishingly small quantity in 4 M potassium chloride solution.

It is possible that either β_B or β_C is zero but both cannot be zero. There is therefore something wrong with any assumption that the α_B and α_C values in any one series in Table IV are really constant. The results must therefore be examined in more detail. The upper curve of Fig. 5 shows the results at $M \sim 4$ in the form of a plot of α_C against x; it can now be seen that the variation of α_C between 0.0237 and 0.0248, although small, is systematic, *i.e.*, there is a uniform downward trend with increasing x. There is no such trend with the α_B data (Fig. 6). The slope of the line in Fig. 5 is −0.0012 whence $\beta_C = -0.0003$ whereas from Fig. 6, $\beta_B = 0$.

It can be said that it is erroneous to plot the points in this way, for each α_C value in Table III corresponds not to a solution of constant total molality but to a solution whose total molality varies (see Table I) between 4.02 and 4.51 M. This is true but, as Fig. 4 shows, the variation of α_C with total molality is small and can be allowed for. At $M = 4$, α_C is increasing by 0.0015 for unit change in M. It is possible, therefore, to make a small correction to the ten values of α_C in Table III to give data corresponding to a constant total molality equal to the mean of the extremes, 4.25 M. The corrected values are plotted as the lower curve of Fig. 5; there is less scatter of the points but still a definite downward trend with slope -0.0019, giving $\beta_C = -0.0004$.

A similar correction applied to the α_B data (lower curve of Fig. 6) does not alter the constancy of α_B with changing x.

The downward trend of the α_C points in Fig. 5 with changing x at a constant total molality of 4.25 leading to $\beta_C = -0.0004$ is therefore fully consistent with the conclusion drawn from the variation of $(\alpha_B + \alpha_C)$ with changing M (Fig. 4) that $(\beta_B + \beta_C) = -0.0004$.

The data at $M \sim 4$ have been used because they are the most complete and reliable. At higher values of M, the limited solubility of potassium chloride restricts the range of x in which measurements can be made. At lower values of M, the effect of experimental error is enhanced. Nevertheless, by plotting α_C against x (Fig. 7) the same downward trend with increasing x is observed in all cases. β_C is certainly independent of m within limits of experimental error and the assumption of an average value of $\beta_C = -0.0005$ is sufficient to bring consistency into all the measurements made in this work.

TABLE V

SMOOTHED VALUES OF α_B AND α_C

m	0.5	1.0	2.0	3	4	5	6
$-\alpha_B$	(0.013)	0.0095	0.0084	0.0084	0.0090	0.0098	....
α_C	(0.025)	0.0235	0.0230	0.0235	0.0246	0.0260	0.0275

$\beta_B = 0$, $\beta_C = -0.0005$

Table V gives smoothed value of α_B and α_C at round values of the total molality. Finally, Fig. 8 shows how γ_B and γ_C vary with composition of the mixture at a constant total molality of 4. With $\beta_B = 0$, log γ_B is linear in x, increasing from -0.2390 when $x = 1$ to -0.2030 at the limit when $x = 0$. If the β_C term is neglected, log γ_C decreases linearly from -0.1061 when $x = 0$ to -0.2045 at $x = 1$; the introduction of the β_C term causes a slight downward curvature shown by the broken curve in Fig. 8, leading to a limiting value of -0.2125 at $x = 1$. It should be noted that these limiting values of log γ_B when $x = 0$ and of log γ_C when $x = 1$ are almost but not exactly the same and are much closer to log γ_B when $x = 1$ than they are to log γ_C when $x = 0$, in other words, on mixing both electrolytes tend to behave more like potassium chloride than sodium chloride.

DISSOCIATION CONSTANT OF THE PROTONATED ACID FORM OF 2-AMINO-2-(HYDROXYMETHYL)-1,3-PROPANEDIOL [TRIS-HYDROXYMETHYL)-AMINOMETHANE] AND RELATED THERMODYNAMIC QUANTITIES FROM 0 TO 50°

BY ROGER G. BATES AND HANNAH B. HETZER

Division of Chemistry, National Bureau of Standards, Washington 25, D. C.

Received November 17, 1960

The thermodynamic dissociation constant (K_{bh}) of the protonated form (BH^+) of 2-amino-2-(hydroxymethyl)-1,3 propanediol (tris-(hydroxymethyl)-aminomethane) has been determined at 11 temperatures from 0 to 50° by measurement of the electromotive force of hydrogen–silver chloride cells without liquid junction. The results are given by the equation $-\log K_{bh} = 2981.4/T - 3.5888 + 0.005571T$, where T is in °K. The changes of free energy, enthalpy, entropy and heat capacity were computed for the dissociation of the cation acid BH^+ in the standard state, as well as for the basic dissociation, $B + H_2O = BH^+ + OH^-$. For the acidic dissociation at 25°, ΔG^0 is 46,075 j. mole^{-1}, ΔH^0 is 47,600 j. mole^{-1}, $\Delta S^0 = 5.1$ j. deg.$^{-1}$ mole^{-1}, and ΔC_p^0 is -64 j. deg.$^{-1}$ mole^{-1}. The entropy changes for the isoelectric dissociation of cation acids (BH^+) appear to indicate restrictive orientation of solvent molecules about the ions and the attendant hindrance of free rotation about carbon–carbon bonds. This simple picture is, however, unable to account satisfactorily for the observed changes in heat capacity.

Introduction

Tris-(hydroxymethyl)-aminomethane, or 2-amino-2-(hydroxymethyl)-1,3-propanediol, is a solid, water-soluble organic base of considerable interest both as an acidimetric standard[1–3] and as a biological buffer.[4–6] For brevity, it is known variously as "tris" and "T.H.A.M." Fossum, Markunas and Riddick[1] found it to be easily purified, stable and suitable for standardizing aqueous solutions of strong acids. The hygroscopicity of

(1) J. H. Fossum, P. C. Markunas and J. A. Riddick, *Anal. Chem.*, **23**, 491 (1951).

(2) T. H. Whitehead, *J. Chem. Educ.*, **36**, 297 (1959).

(3) A. C. Holler, *Anal. Chem.*, **28**, 1359 (1956).

(4) G. Gomori, *Proc. Soc. Exptl. Biol. Med.*, **62**, 33 (1946).

(5) H. Stormorken and T. F. Newcomb, *Scand. J. Clin. and Lab. Invest.*, **8**, 237 (1956).

(6) G. G. Nahas and H. Rosen, *Federation Proc.*, **18**, 111 (1959); L. B. Berman, T. F. O'Connor, G. G. Nahas and P. C. Luchsinger, *Physiologist*, **2**, 10 (1959).

the base is comparable to that of potassium hydrogen phthalate. Furthermore, aqueous solutions of the free base are not strongly alkaline and display no pronounced tendency to absorb atmospheric carbon dioxide.[1,2]

The negative logarithm of the basic dissociation constant of tris is found by measurements of pH[7] and e.m.f.[8] to be approximately 5.9 at 25°. The base is thus about one-sixteenth as strong as ammonia. It is sufficiently strong, however, that the neutralization curve obtained by titrating the base with a strong acid shows a sharp break at the equivalence point, namely at pH 4.7 for a 0.05 M solution.[1,2] Buffer solutions formed by adding 5.7 to 47.7 ml. of 0.1 M hydrochloric acid to 50 ml. of a 0.1 M solution of the base, with dilution to a total volume of 100 ml., cover[9] the pH range 7.00 to 9.00 at 25°. Both a primary acidimetric standard grade and a buffer grade of the free base are now available from several commercial sources.

Tris has been used to a considerable extent as a buffer in biochemical experiments,[4,5] its relatively non-toxic character even permitting its use *in vivo*.[6] In studies of the heats of certain biological reactions in buffered media, the heat of ionization of the buffer acid must be known.[10,11] It was therefore considered desirable to extend the measurements of the dissociation constant at 20, 25 and 30° (made previously in this Laboratory[8]) to cover the temperature range 0 to 50°, in order to permit the changes in heat content, entropy and heat capacity accompanying the dissociation to be computed.

Method

The dissociation constant was determined by the measurement of the e.m.f. of hydrogen–silver chloride cells without liquid junction. The method used was essentially that of Harned and Ehlers,[12] and the procedures were the same in nearly all respects as those used extensively in the study of other bases in this Laboratory (see, for example, references 13–15). The cell is represented as

Pt; H_2(g., 1 atm.), $(CH_2OH)_3CNH_3Cl(m_1)$,
$(CH_2OH)_3CNH_2(m_2)$, AgCl; Ag

where m is molality.

The cell solutions contained tris and its hydrochloride in approximately equal molal amounts. The e.m.f. data yield directly the equilibrium constant for the dissociation process

$$BH^+ + H_2O \rightleftharpoons B + H_3O^+ \qquad (1)$$

or, since the activity of water is taken as unity in the infinitely dilute solution

$$BH^+ \rightleftharpoons B + H^+ \qquad (1a)$$

where B represents the base and BH^+ is its conjugate acid. The constant for the equilibria 1 and 1a (the acidic dissociation constant of BH^+) is given the symbol K_{bh}.

Tris reacts with silver ion to a sufficient extent to permit the base to be used as a complexing agent in the titration, with silver nitrate, of sulfhydryl groups in proteins.[16] Nevertheless, this reaction is not so extensive as to prohibit the use of the silver–silver chloride electrode in solutions of the concentrations employed here[8] or to require the application of corrections for a change in chloride molality. The equilibrium constant, K_f, for the formation of the diammine–silver complex, namely the process

$$Ag^+ + 2B \rightleftharpoons AgB_2^+$$

was found[8] to be 2.7×10^6 ($\log K_f = 6.43$) if the solubility product constant (K_{sp}) of silver chloride at 25° is taken[17] to be 1.78×10^{-10}. Benesch and Benesch[16] found $\log K_f$ to be 6.56 at 23° on the assumption that the formation of the diammine complex occurs in two steps.[18]

Combination of the e.m.f. equations with the mass-law expression for equation 1a and with the two-parameter form of the Debye–Hückel equation gives

$$-\log K_{bh}' = -\log K_{bh} - \beta m_1 = \frac{E - E^0}{2.3026RT/F} + 2\log m_1 - \log m_2 - \frac{2A\sqrt{m_1}}{1 + Ba^*\sqrt{m_1}} \qquad (2)$$

In equation 2, E is the e.m.f. corrected as usual to a partial pressure of 1 atm. of dry hydrogen, E^0 is the standard potential of the cell,[19] A and B are constants of the Debye–Hückel theory,[20] and a^* and β are adjustable parameters, the first being the "ion-size parameter."

Experimental

Hydrochloric acid of reagent grade was diluted to a concentration approximately 6 M and distilled twice, the middle third being collected each time. A stock solution, approximately 0.1 M, was prepared from the redistilled acid and was standardized by a gravimetric determination of chloride as silver chloride. The average difference among replicate determinations was ±0.03%.

Tris-(hydroxymethyl)-aminomethane of primary acidimetric-standard grade assayed 99.9 ± 0.1% when titrated under carbon dioxide-free conditions with the standard solution of hydrochloric acid. The end-point (pH 4.7) was detected by a pH measurement with the glass electrode. The base was powdered and stored in a desiccator over Drierite for at least 12 hours before use. The melting point was 171° when the heating rate was slightly less than 2 deg./min.

Three stock solutions containing approximately equimolal concentrations of the amine and its hydrochloride were prepared by mixing accurately-weighed portions of the base, of the standard hydrochloric acid, and, for one stock solution only, of carbon dioxide-free water. Each of the stock

(7) S. Glasstone and A. E. Schram, *J. Am. Chem. Soc.*, **69**, 1213 (1947).

(8) R. G. Bates and G. D. Pinching, *J. Research Natl. Bur. Standards*, **43**, 519 (1949).

(9) R. G. Bates and V. E. Bower, *Anal. Chem.*, **28**, 1322 (1956).

(10) J. M. Sturtevant, *J. Am. Chem. Soc.*, **77**, 1495 (1955).

(11) R. J. Podolsky and M. F. Morales, *J. Biol. Chem.*, **218**, 945 (1956).

(12) H. S. Harned and R. W. Ehlers, *J. Am. Chem. Soc.*, **54**, 1350 (1932).

(13) R. G. Bates and G. D. Pinching, *J. Research Natl. Bur. Standards*, **42**, 419 (1949).

(14) R. G. Bates and V. E. Bower, *ibid.*, **57**, 153 (1956).

(15) R. G. Bates and H. B. Hetzer, *ibid.*, **44**, 427 (1960).

(16) R. E. Benesch and R. Benesch, *J. Am. Chem. Soc.*, **77**, 2749 (1955); R. E. Benesch, H. A. Lardy and R. Benesch, *J. Biol. Chem.*, **216**, 663 (1955).

(17) B. B. Owen and S. R. Brinkley, Jr., *J. Am. Chem. Soc.*, **60**, 2233 (1938).

(18) J. Bjerrum, "Metal Ammine Formation in Aqueous Solutions," P. Haase and Son, Copenhagen, 1941.

(19) R. G. Bates and V. E. Bower, *J. Research Natl. Bur. Standards*, **53**, 283 (1954).

(20) R. A. Robinson and R. H. Stokes, "Electrolyte Solutions," 2nd Ed., appendix 7.1, Academic Press, Inc., New York, N. Y., 1959.

TABLE I

ELECTROMOTIVE FORCE OF THE CELL Pt; H_2(G. 1 ATM.), $(CH_2OH)_3CNH_3Cl(m_1)$ $(CH_2OH)_3CNH_2(m_2)$, AgCl; Ag, FROM 0 TO 50° (IN V.)

m_1	m_2	0°	5°	10°	15°	20°	25°	30°	35°	40°	45°	50°
0.10153	0.10293	0.78294	0.78121	0.77932	0.77731	0.77526	0.77344	0.77102	0.76878	0.76647	0.76404	0.76145
.09122	.09266	.78509	.78338	.78159	.77967	.77765	.77561	.77343	.77119	.76885	.76642	.76392
.08077	.08188	.78737	.78566	.78382	.78197	.77984	.77816	.77581	.77365	.77139	.76896	.76642
.07479	.07521	.78860	.78697	.78525	.78334	.78149	.77944	.77725	.77508	.77276	.77035	.76793
.07012	.07123	.79015	.78851	.78674	.78496	.78306	.78112	.77888	.77650	.77441	.77170	.....
.06046	.06130	.79287	.79131	.78958	.78777	.78594	.78422	.78196	.77993	.77779	77530	77322
05506	05537	79460	79304	79141	78961	.78782	.78597	.78379	.78174	.77949	.77716	.77468
.04969	.05047	.79685	.79527	.79365	.79203	.79028	.78839	.78637	.78433	.78218	.77987	.76746
.04452	.04477	.79877	.79721	.79568	.79403	.79235	.79053	.78853	.78635	.78434	.78215	.77987
.03972	.04027	.80143	.79986	.79833	.79673	.79500	.79332	.79088	.78927	.78730	.78516	.78282
.02988	.03035	.80713	.80574	.80431	.80274	.80106	.79947	.79763	.79561	.79367	.79160	.78945
.02040	.02069	.81474	.81338	.81208	.81081	.80932	.80796	.80604	.80447	.80261	.80071	.79864
.015066	.015150	.82108	.81989	.81869	.81741	.81601	.81459	.81293	.81136	.80962	.80779	.80590
.010299	.010462	.82921	.82822	.82713	.82599	.82484	.82363	.82204	.82061	.81904	.81741	.81560
.007605	.007648	.83534	.83447	.83353	.83237	.83132	.83041	.82895	.82760	.82619	.82451	.82280

solutions was diluted by weight with distilled water to prepare five cell solutions. Hydrogen was bubbled through each solution to remove dissolved air. The cells were filled as usual, air being excluded. The preparation of the electrodes has been described elsewhere.[21]

The initial measurements were made at 25°. After the equilibrium values of the cells had been recorded, the temperature of the bath was lowered overnight to near 0°, and measurements from 0 to 25° were made on the second day. On the third day, the e.m.f. values from 25 to 50° were obtained, and a final reading at 25° was made when possible. The reproducibility and stability of the cells containing tris was excellent. The initial and final readings at 25° differed usually by no more than 0.1 mv., and duplicate combinations of electrodes in the same cell agreed, on the average, well within ±0.05 mv.

Results

The e.m.f. data are summarized in Table I. Each number is the average of two electrode combinations in the same cell. The e.m.f. was used to compute $-\log K_{bh}'$, the right side of equation 2, with various values of a^*, the ion-size parameter. A curvature was apparent when a^* values of +2 and −2 were used. The best straight-line plots of -log K_{bh}' with respect to m_1 were obtained with $a^* = 0$. The results at 0, 25 and 50° are shown in Fig. 1.

The value of $-\log K_{bh}'$ at $m_1 = 0$ (*i.e.*, the intercept $-\log K_{bh}$) and the slope of the extrapolation line ($-\beta$) were found by the method of least squares. The values of -log K_{bh} are summarized in Table II, together with σ_i, the standard deviation of the intercept. Values of the basic dissociation constant (K_b) are readily calculated from K_{bh} and the autoprotolysis constant for water[22] by the relation, $K_b = K_w/K_{bh}$.

The present value of 8.075 for $-\log K_{bh}$ at 25° is in excellent agreement with 8.076 found by Bates and Pinching.[8] At 20°, the present result is 8.214 and the earlier one 8.221. At 30°, the two values are, respectively, 7.934 and 7.937. From measurements with a glass electrode, Glasstone and Schram[7] found $-\log K_{bh} = 8.03$ at 25°. The values of $-\log K_{bh}$ in 0.6 *M* potassium chloride at 5 to 50° found by Bernhard[23] are about 0.3 unit higher than those given in Table II. The dissociation constants were calculated from electro-

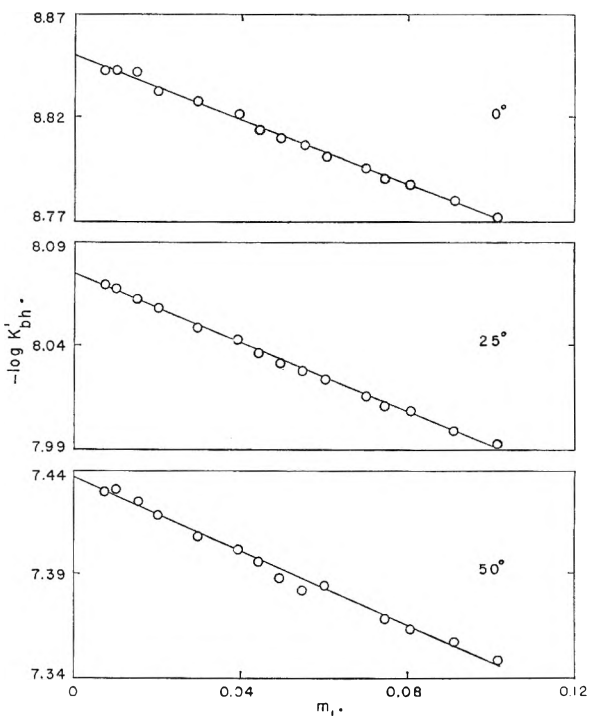

Fig. 1.—Plot of $-\log K_{bh}'$ as a function of m_1 at 0, 25 and 50°. Calculations made with $a^* = 0$.

TABLE II

ACIDIC DISSOCIATION CONSTANT (K_{bh}) FOR THE PROTONATED CATION OF TRIS-(HYDROXYMETHYL)-AMINOMETHANE FROM 0 TO 50°. ΔG^0, ΔH^0, ΔS^0 AND ΔC_p^0 AT 25°

t, °C.	−log K_{bh}	σ_i
0	8.8500	0.0008
5	8.6774	.0008
10	8.5164	.0008
15	8.3616	.0008
20	8.2138	.0009
25	8.0746	.0006
30	7.9344	.0010
35	7.8031	.0010
40	7.6772	.0011
45	7.5543	.0015
50	7.4365	.0013

t	ΔG^0, j. mole^{-1}	ΔH^0, j. mole^{-1}	ΔS^0, j. deg.$^{-1}$ mole^{-1}	ΔCp^0, j. deg.$^{-1}$ mole^{-1}
25	46,075	47,600	5.1	−64

(21) R. G. Bates, "Electrometric *p*H Determinations," John Wiley and Sons, Inc., New York, N. Y., 1954, pp. 166 and 205.

(22) H. S. Harned and B. B. Owen, "The Physical Chemistry of Electrolyte Solutions," 3rd Ed., Reinhold Publ. Corp., New York, N. Y., 1958.

(23) S. A. Bernhard, *J. Biol. Chem.*, **218**, 961 (1956).

metric titration data obtained with the glass electrode.

Thermodynamic Quantities.—In order to derive the thermodynamic constants for the dissociation process, the values of $-\log K_{bh}$ were fitted to an equation of the form suggested by Harned and Robinson.[24] The resulting equation, the constants of which were determined by the IBM 704 computer, is

$$-\log K_{bh} = \frac{2981.4}{T} - 3.5888 + 0.005571T \quad (3)$$

where T is the temperature in deg. Kelvin. The mean difference between the "observed" values of -log K_{bh} and the values calculated by equation 6 for the 11 temperatures is ± 0.0012 unit.

By application of the customary thermodynamic relations to this equation for the change of $-\log K_{bh}$ with T, the following expressions for the standard changes of free energy (ΔG^0), enthalpy (ΔH^0), entropy (ΔS^0), and heat capacity (ΔC_p) for the dissociation of the protonated cation of tris-(hydroxymethyl)-aminomethane, were derived

$$\Delta G^0 = 57{,}078 - 68.706T + 0.10666T^2 \text{ j. mole}^{-1} \quad (4)$$

$$\Delta H^0 = 57{,}080 - 0.1067T^2 \text{ j. mole}^{-1} \quad (5)$$

$$\Delta S^0 = 68.71 - 0.2133T \text{ j. deg.}^{-1} \text{ mole}^{-1} \quad (6)$$

$$\Delta C_p^0 = -0.213T \text{ j. deg.}^{-1} \text{ mole}^{-1} \quad (7)$$

These equations are valid from T = 273.16°K. to T = 323.16°K. The values of the quantities at 25° are given at the bottom of Table II. The estimated uncertainties are as follows: ΔG^0, ± 6 j. mole^{-1}; ΔH^0, ± 100 j. mole^{-1}; ΔS^0, ± 0.5 j. deg.$^{-1}$ mole^{-1}; and ΔC_p^0, ± 5 j. deg.$^{-1}$ mole^{-1}.

The equation for the variation of the basic dissociation constant (K_b) of tris with absolute temperature (T) is readily obtained by subtracting the expression for $-\log K_{bh}$ (equation 3) from the corresponding equation[25] for $-\log K_w$ as a function of T. The resulting equation is

$$-\log K_b = \frac{1489.9}{T} - 2.4958 + 0.011482T \quad (8)$$

from which the following values of the thermodynamic quantities for the basic dissociation at 25° are obtained

Process: $B + H_2O \rightleftharpoons BH^+ + OH^-$

ΔG^0 = 33,819 j. mole^{-1}

ΔH^0 = 8,980 j. mole^{-1}

ΔS^0 = −83.3 j. deg.$^{-1}$ mole^{-1}

ΔC_p^0 = −131 j. deg.$^{-1}$ mole^{-1}

Sturtevant[10] has reported a calorimetric determination at 25° of the enthalpy of ionization of the protonated (cationic) form of tris (BH^+) in dilute solutions (the ionic strength of the final solutions was 0.013). His measurements lead to a value of 45,700 ± 400 j. mole^{-1}, and this result may be regarded as ΔH^0 provided that the small enthalpy effect of dilution to zero concentration is ignored. The value found in this investigation is higher than Sturtevant's by nearly 2,000 j. Two determinations of the change in molar enthalpy for the ionization of BH^+ in a 0.1 M solution of the base which was 0.6 M with respect to potassium chloride have also been made. One of them,[11] a direct calorimetric measurement, gave 48,500 ± 400 j. mole^{-1} and the other,[23] utilizing electrometric titrations with the glass electrode to determine $-\log K_{bh}$ from 5 to 50°, gave 48,950 ± 800 j. mole^{-1}.

(24) H. S. Harned and R. A. Robinson, *Trans. Faraday Soc.*, **36**, 973 (1940).

(25) Reference 20, p. 363.

Discussion

Dissociation Constants.—Tris is a trihydroxy derivative of *t*-butylamine, with one hydrogen of each of the three methyl groups attached to the tertiary carbon atom replaced by a hydroxyl group. As would be expected from the electron-attracting nature of the hydroxyl group,[26] the substitution of OH groups results in a decrease of base strength. Inasmuch as -log K_{bh} for the *t*-butylammonium ion[27] is 10.45 at 25°, this reduction amounts to approximately 2.4 units in log K_b. Glasstone and Schram[7] found that the related compounds, 2-amino-2-methyl-1-propanol and 2-amino-2-methyl-1,3-propanediol, which have, on the tertiary carbon atom, one and two hydroxymethyl groups, respectively, are intermediate in strength, the latter being the weaker base.

Entropy.—The thermodynamic constants for the dissociation of the conjugate acid form of tris in the standard state are compared in Table III with the corresponding quantities for the cation acids of 18 other nitrogenous bases. With the exception of 2,2′-bipyridinium ion and triethanolammonium ion, the tris cation is the strongest acid listed in the table. It is unique among acids of its charge type in displaying an increase of entropy upon dissociation. (Positive changes in entropy have, however, been found for the first dissociation steps of ethylenediammonium ion and hexamethylenediammonium ion.) Furthermore, the change of heat capacity appears to have a larger negative value than that for any other univalent cation acid so far studied.

A fruitful, detailed interpretation of the changes of these thermodynamic quantities with changes in the structure of the cation acid is, unfortunately, not possible at the present time. It seems certain, however, that solvation, with its accompanying changes in entropy and heat capacity, plays a significant part. Evans and Hamann[29] explained the increasingly negative values of ΔS^0 with substitution on the nitrogen in terms of changes in the solvation shell surrounding the (approximately spherical) ion. Bulky groups attached to the nitrogen atoms tend to exclude solvent and to increase the entropy of hydration of the ion, thus making the value of ΔS^0 increasingly negative. Furthermore, the hydrophobic character of the alkyl groups added may well enhance this effect.[28]

It has likewise been observed[29] that the value of ΔS^0 becomes less negative as the alkyl chain lengthens. The increase in ΔS^0 is from 2 to 7 j. for each added CH_2 group, or always somewhat less than the rotational entropy of an additional carbon–carbon bond.[37] This observation has led to the

(26) A. E. Remick, "Electronic Interpretations of Organic Chemistry," 2nd Ed., John Wiley and Sons, Inc., New York, N. Y., 1949, p. 64; J. F. J. Dippy, *Chem. Revs.*, **25**, 151 (1939).

(27) N. F. Hall and M. R. Sprinkle, *J. Am. Chem. Soc.*, **54**, 3469 (1932).

TABLE III

COMPARISON OF $-\text{LOG } K_{bh}$, ΔH^0, ΔS^0 AND ΔC_p^0 FOR THE DISSOCIATION OF 19 CATION ACIDS (BH^+) AT 25°

Process: $BH^+ \rightleftharpoons B + H^+$

Acid	$-\log K_{bh}$	ΔH^0, j. mole^{-1}	ΔS^0, j. deg.$^{-1}$ mole^{-1}	ΔC_p^0, j. deg.$^{-1}$ mole^{-1}
Ammonium[13]	9.245	52,200	− 1.9	−14
Methylammonium[28]	10.624	54,760	−19.7	33
Dimethylammonium[28]	10.774	49,620	−39.7	97
Trimethylammonium[28]	9.800	36,880	−63.6	183
Ethylammonium[29]	10.631	56,820	−13.0	..
Diethylammonium[29]	10.933	53,430	−30.1	..
Triethylammonium[30]	10.715	44,200	−56.9	193
Ethanolammonium[31]	9.498	50,540	−12.3	− 5
Diethanolammonium[32]	8.883	42,410	−27.8	49
Triethanolammonium[33]	7.762	33,450	−36.4	52
n-Propylammonium[30]	10.568	57,180	−10.5	31
n-Butylammonium[30]	10.640	58,090	− 8.9	12
Ethylenediammonium (2nd step)[34]	9.928	49,450	−24.2	40
Hexamethylenediammonium (2nd step)[34]	10.930	58,200	−13.8	35
Piperidinium[14]	11.123	53,390	−33.9	88
4-Aminopyridinium[15]	9.114	47,090	−16.5	−15
2,2′-Bipyridinium[35]	4.352	14,120	−36.1	103
Ephedrinium[36]	9.544	45,150	−31.3	67
Tris-(hydroxymethyl)-aminomethane, protonated cation (this investigation)	8.075	47,600	5.1	−64

belief that free internal rotation is impeded to some extent by the solvation shell at the charge center ("chain-stiffening effect").

The positive change in entropy for the dissociation of the cation acid of tris can be interpreted qualitatively in terms of solvation. The free base is a primary amine structurally similar to *t*-butylamine. The value of ΔS^0 for *n*-butylammonium ion is −9 j. deg.$^{-1}$ mole^{-1}, but that for *t*-butylammonium ion has not been determined. By the reasoning of Evans and Hammann, the total restriction of internal rotation by the solvation shell should, however, be greater in *t*-butylammonium ion than in *n*-butylammonium ion, for there are three carbon–carbon bonds (instead of one) within range of the ionic charge.

It is evident from the data of Table III that the chain-lengthening effect does indeed fall off with the distance of the bond from the charged nitrogen atom. To obtain an estimate of ΔS^0 for *t*-butylammonium ion, therefore, one should add to ΔS^0 for ethylammonium ion about twice the increment observed on passing from methylammonium to ethylammonium, namely 2 (6.7) or 13 j. deg.$^{-1}$ mole^{-1}. We thus estimate $\Delta S^0 \approx 0$ for *t*-butylammonium ion. Furthermore, a comparison of ΔS^0 for triethylammonium with that for triethanolammonium shows that three hydroxyl groups may account for a further increase of 20 j. in ΔS^0. The positive value of ΔS^0 for the dissociation of the conjugate acid of tris is thus quite reasonable.

Heat Capacity.—The negative value of ΔC_p^0 for the dissociation of the tris cation is also reasonably consistent with the other values of ΔC_p^0 listed in Table III. No value for ethylammonium ion is available, but a comparison of the changes in heat capacity for the dissociation of methylammonium and *n*-propylammonium ions, by the same reasoning applied to the estimate of ΔS^0, makes it seem likely that ΔC_p^0 for *t*-butylammonium ion lies in the vicinity of 30 j. deg.$^{-1}$ mole^{-1}. It is evident, however, that the three hydroxyl groups may lower ΔC_p^0 by well over 100 j. (from 193 for triethylammonium ion to 52 for triethanolammonium ion). The value of ΔC_p^0 for the tris cation, −64 j. deg.$^{-1}$ mole^{-1}, is therefore not unreasonable.

Although the importance of ion–solvent interactions in accounting for the thermodynamic effects observed on the dissociation of an acid or base seems well established, it is impossible, on this basis alone, to show how an increase in ΔS^0 can be accompanied by a decrease in ΔC_p^0. A release of water molecules from combination would indeed be expected to increase both the entropy and the heat capacity. A clue to the contrary variation of these two quantities may possibly reside in the fact that restriction of the freedom of simple harmonic motion and hindered rotation can, under certain circumstances, lead to a fall of entropy with, however, an attendant increase of heat capacity.[38]

(28) D. H. Everett and W. F. K. Wynne-Jones, *Proc. Roy. Soc. (London)*, **177A**, 499 (1941).

(29) A. G. Evans and S. D. Hamann, *Trans. Faraday Soc.*, **47**, 34 (1951).

(30) D. H. Everett, unpublished results. Quoted by Robinson and Stokes (Reference 20, appendix 12.1).

(31) R. G. Bates and G. D. Pinching, *J. Research Natl. Bur. Standards*, **46**, 349 (1951).

(32) V. E. Bower, R. A. Robinson and R. G. Bates, to be published.

(33) R. G. Bates and G. F. Allen, *J. Research Natl. Bur. Standards*, **64A**, 343 (1960).

(34) D. H. Everett and B. R. W. Pinsent, *Proc. Roy. Soc. (London)*, **215A**, 416 (1952).

(35) R. Näsänen, *Suomen Kemistilehti*, **28B**, 161 (1955).

(36) D. H. Everett and J. B. Hyne, *J. Chem. Soc.*, 1636 (1958).

(37) M. L. Huggins, *J. Chem. Phys.*, **8**, 181 (1940).

(38) D. H. Everett, D. A. Landsman and B. R. W. Pinsent, *Proc. Roy. Soc. (London)*, **215A**, 403 (1952).

VOLTAMMETRIC MEMBRANE ELECTRODES. III. CONTROLLED CURRENT VOLTAMMETRY

By Richard C. Bowers, George Ward, Carol M. Wilson and D. D. DeFord

Department of Chemistry, Northwestern University, Evanston, Illinois

Received November 18, 1960

Voltammetric membrane electrodes are found to be ideally suited for controlled current voltammetry, the rigid structure of the membrane acting to minimize stirring and convection effects. Equations for transition times for constant current chronopotentiometry and linear current-scan chronopotentiometry under conditions of linear finite diffusion are derived, and it is shown that these reduce to those for infinite diffusion at short transition times. Good agreement between theory and experiment is obtained in cases where no interaction between the electroactive species and the cellophane membrane occurs.

Introduction

A theoretical treatment and an experimental study of diffusion currents obtained at voltammetric membrane electrodes have been reported in a previous publication.[1] The results obtained indicated that the membrance provides a fairly rigid diffusion layer so that the diffusion process is not disturbed by stirring or convection. This type of electrode should thus be ideally suited for controlled current voltammetry even in stirred solution.

The solution of the boundary value problem in the case of constant current voltammetry (chronopotentiometry), under conditions where infinite diffusion can be assumed, is well known. Delahay[2,3] has given excellent discussions of the theory and application of this method and Reilley, *et al.*,[4] have made an extensive experimental evaluation of the method as an analytical tool.

The theoretical equation governing the transition time for linear current-scan chronopotentiometry, assuming linear infinite diffusion, has been given by Reinmuth[5] and by Kambara and Tachi.[6] To the authors' knowledge, however, no experimental study of this technique has been reported in the literature.

This paper reports the results of a theoretical treatment and an experimental evaluation of constant current and linear current-scan chronopotentiometry at a membrane electrode where conditions of linear finite diffusion exist.

Theoretical

Constant Current Chronopotentiometry.—In this case, Fick's second law is solved with the initial condition; $C_{(x,0)} = C_l$ and the boundary conditions; $C_{(l,t)} = C_l$ and $(\partial C/\partial X)_{x=0} = i/nFAD$. Here l is the membrane thickness, n the number of electrons involved in the electrode process; F the faraday; A the cross sectional area through which diffusion occurs and D the diffusion coefficient in the membrane. The quantity C_l is the concentration of electroactive species in the membrane at the membrane–solution interface and may or may not be equal to the concentration of this species in the aqueous solution. It is assumed, however, that with rapid stirring of the solution, C_l remains constant throughout electrolysis.

Employing the Laplace transformation, the following is obtained as a solution to this boundary value problem

$$C_{(x,t)} = C_l - \frac{2i}{nFA}\sqrt{\frac{t}{\pi D}}\sum_{m=0,1,2,3....}^{m=\infty}(-1)^m \left\{\exp\left(-\frac{[2ml+x]^2}{4Dt}\right) - \exp\left(-\frac{[2ml+2l-x]^2}{4Dt}\right) - \frac{2ml+x}{2\sqrt{Dt}}\sqrt{\pi}\,\mathrm{erfc}\left(\frac{2ml+x}{2\sqrt{Dt}}\right) + \frac{2ml+2l-x}{2\sqrt{Dt}}\sqrt{\pi}\,\mathrm{erfc}\left(\frac{2ml+2l-x}{2\sqrt{Dt}}\right)\right\} \quad (1)$$

Upon setting $C_{(x=0)} = 0$, the following is obtained for the transition time, τ.

$$\tau^{1/2} = \frac{nFA\sqrt{\pi D}\,C_l}{2i(1-\sigma)} \quad (2)$$

where σ is defined by

$$\sigma = -2\sum_{m=1,2,3,....}^{m=\infty}(-1)^m\left\{\exp\left(-\frac{m^2l^2}{d\tau}\right) - \frac{ml}{\sqrt{D\tau}}\sqrt{\pi}\,\mathrm{erfc}\left(\frac{ml}{\sqrt{D\tau}}\right)\right. \quad (3)$$

Values of σ as a function of $l/\sqrt{D\tau}$ can be computed with the aid of tables of error functions.[7] It is found that when $l/\sqrt{D\tau} \geqslant 1.9$, $\sigma \leqslant 0.0055$ and equation 2 reduces essentially to that for infinite diffusion.

Current-scan Chronopotentiometry.—This problem differs from that treated above only in the boundary condition for the concentration gradient at the electrode surface. In the case of linear current-scan this gradient is given by $(\partial C/\partial X)_{x=0} = \beta t/(nFAD)$, where β is the rate at which the current changes with time. The solution of this boundary value problem can be written as

$$C_{(x,t)} = C_l + \frac{4\beta t^{3/2}}{3nFA\sqrt{\pi D}}\sum_{m=0,1,2,...}^{m=\infty}(-1)^m \left\{\left(1+\frac{[2ml+2l-x]^2}{4Dt}\right)\exp\left(-\frac{[2ml+2l-x]^2}{4Dt}\right) - \left(1+\frac{[2ml+x]^2}{4Dt}\right)\exp\left(-\frac{[2ml+x]^2}{4Dt}\right) - \left(\frac{3}{2}+\frac{[2ml+2l-x]^2}{4Dt}\right)\frac{[2ml+2l-x]}{2\sqrt{Dt}}\sqrt{\pi}\,\mathrm{erfc}\right.$$

(1) R. C. Bowers and A. M. Wilson, *J. Am. Chem. Soc.*, **80**, 2968 (1958).

(2) P. Delahay, "New Instrumental Methods in Electrochemistry," Interscience Publishing Co., New York, N. Y., 1954, chapter 8.

(3) P. Delahay and G. Mamantov, *Anal. Chem.*, **27**, 478 (1955).

(4) C. N. Reilley, G. W. Everett and R. H. Johns, *ibid.*, **27**, 483 (1955).

(5) W. H. Reinmuth, *ibid.*, **32**, 1509 (1960).

(6) T. Kambara and I. Tachi, *J. Phys. Chem.*, **61**, 1405 (1957).

(7) See, for example, J. Crank, "The Mathematics of Diffusion," Oxford University Press, London, 1956.

$$\left(\frac{2ml + 2l - x}{2\sqrt{Dt}}\right) + \left(\frac{3}{2} + \frac{[2ml + x]^2}{4Dt}\right) \frac{[2ml + x]}{2\sqrt{Dt}} \sqrt{\pi}\ \mathrm{erfc}\left(\frac{2ml + x}{2\sqrt{Dt}}\right)\Bigg\} \quad (4)$$

The transition time is given by

$$\tau^{1/2} = \frac{3nFA\sqrt{\pi D}\, C_t}{4\beta(1 - \sigma')} \quad (5)$$

where σ' is defined by

$$\sigma' = -2 \sum_{m=1,2,3....}^{m=\infty} (-1)^m \left\{\left(1 + \frac{m^2l^2}{D\tau}\right) \exp\left(-\frac{m^2l^2}{D\tau}\right) - \left(\frac{3}{2} + \frac{m^2l^2}{D\tau}\right) \frac{ml}{\sqrt{D\tau}} \sqrt{\pi}\ \mathrm{erfc}\left(\frac{ml}{\sqrt{D\tau}}\right)\right\} \quad (6)$$

When $l/\sqrt{D\tau} \geq 1.6$, $\sigma' \leq 0.0056$ and equation 5 reduces to that for infinite diffusion.[5,6]

Transition Time for the Reduction of a Second Species.—When two electroactive species, whose reduction potentials are different, are present, the transition time for the second step cannot be expressed by the relatively simple equations given above. The boundary value problem, under conditions of linear infinite diffusion and with constant current, has been solved by Berzins and Delahay[8] with the result

$$(\tau_1 + \tau_2)^{1/2} - \tau_1^{1/2} = \frac{n_2FA\sqrt{\pi D_2}\, C_2^0}{2i} \quad (7)$$

An analogous equation, valid for linear current-scan under conditions of infinite diffusion, is obtained by solving the following boundary value problem. Setting $t' = t - \tau_1$, the initial ($t' = 0$) conditions for species 1 and species 2 are given by

$$C_{1(x,0)} = C_1^0 - \frac{4\beta\tau_1^{3/2}}{3n_1FA\sqrt{\pi D_1}}\left[\left(1 + \frac{x^2}{4D_1\tau_1}\right) \exp\left(-\frac{x^2}{4D_1\tau_1}\right) - \left(\frac{3}{2} + \frac{x^2}{4D_1\tau_1}\right) \frac{x}{2\sqrt{D_1\tau_1}} \sqrt{\pi}\ \mathrm{erfc}\left(\frac{x}{2\sqrt{D_1\tau_1}}\right)\right] \quad (8)$$

and

$$C_{2(x,0)} = C_2^0 \quad (9)$$

In addition the following boundary conditions can be written

$$n_1D_1\left(\frac{\partial C_1}{\partial x}\right)_{x=0} + n_2D_2\left(\frac{\partial C_2}{\partial x}\right)_{x=0} = \frac{\beta t}{FA} \quad (10)$$

$$C_{1(0,t')} = 0 \quad (11)$$

$$C_{1(\infty,t')} = C_1^0 \quad (12)$$

and

$$C_{2(\infty,t')} = C_2^0 \quad (13)$$

Utilizing equations 8, 11 and 12 and proceeding in a manner analogous to that outlined by Berzins and Delahay,[10] the following is obtained as the Laplace transform of the flux of species 1 at $x = 0$ as a function of t'.

$$\left(\frac{\partial \bar{C}}{\partial x}\right)_{(0,p)} = \frac{C_1^0}{\sqrt{pD_1}} - \frac{A}{\sqrt{pD_1}} - \frac{6Aa^2\sqrt{D_1}}{p^{3/2}} + \frac{3Aa\sqrt{\pi}}{2p} + \frac{6Aa^3D_1\sqrt{\pi}}{p^2} - \frac{6Aa^3D_1\sqrt{\pi}}{p^2} \exp\left(\frac{p}{4a^2D_1}\right) \mathrm{erfc}\left(\frac{\sqrt{p}}{2a\sqrt{D_1}}\right) \quad (14)$$

where

$$A = \frac{4\beta\tau_1^{3/2}}{3n_1FA\sqrt{\pi D_1}} \text{ and } a = \frac{1}{2\sqrt{D_1\tau_1}}$$

By employing equation 14 in boundary condition 10 and utilizing equations 9, 10 and 13, Fick's second law for species 2 can be solved by the method of Laplace transforms with the result

$$C_{2(x=0)} = C_2^0 - \frac{4\beta}{3n_2FA\sqrt{\pi D_2}}[(t' + \tau_1)^{3/2} - \tau_1^{3/2}] \quad (15)$$

and

$$(\tau_2 + \tau_1)^{3/2} - \tau_1^{3/2} = \frac{3n_2FA\sqrt{\pi D_2}\, C_2^0}{4\beta} \quad (16)$$

Equation 16 predicts a decrease in the transition time of the second species with increasing transition times of the first species. This is opposite to the behavior with constant current chronopotentiometry.

It should be noted that equations 7 and 16 are valid only under conditions of linear infinite diffusion. Since at the voltammetric membrane electrode, conditions for attaining linear finite diffusion exist, the above equations are valid for this electrode only under specific limiting conditions. In order to predict accurately what these limitations are, it would be necessary to derive analogous equations but under conditions of finite diffusion. Such derivations would be exceedingly cumbersome. It is reasonable, however, to expect that $l/\sqrt{D_2\tau_2}$ must be equal to or greater than 1.9 or 1.6 for constant current or current-scan, respectively, in order that the diffusion of the second species corresponds essentially to infinite diffusion. Furthermore, since the fraction of the applied current expended for reduction of species 1 is explicit in the derivations of equations 7 and 16, and since infinite diffusion of this species is assumed, the further restriction that $l/\sqrt{D_1(\tau_1+\tau_2)}$ must be greater than 1.9 or 1.6, respectively, for constant current and current-scan chronopotentiometry is reasonable.

Charging Current Error.—The influence of the double layer in chronopotentiometry has been considered by Gierst[9] and by Delahay and Mamantov.[3] According to the treatment of the latter authors the time, t_c, required to charge the double layer in the absence of any electrochemical reaction is given by

$$t_c = \frac{\bar{C}\Delta E}{i} \quad (17)$$

where $\bar{C}$ is the average double layer capacity and ΔE is the change in potential of the electrode. The ratio of the charging current time to the transition time is then given by

$$\left(\frac{t_c}{\tau}\right)_{c.c.} = \frac{4\bar{C}\Delta Ei}{(nFAC)^2\pi D} \quad (18)$$

Equation 17 can be applied to linear current-scan chronopotentiometry, by setting $i = \beta\bar{t}$ where $\bar{t}$ is the average time, measured from the beginning of the current-scan, over which the charging process occurs.

Thus

(8) T. Berzins and P. Delahay, *J. Am. Chem. Soc.*, **75**, 4205 (1953).

(9) L. Gierst, Thesis, University of Brussels, 1952.

$$\left(\frac{t_c}{\tau}\right)_{c.s.} = \frac{(4/3)^{2/3}\bar{C}\Delta E}{\beta^{1/3}\bar{i}(nFAC)^{2/3}(\pi D)^{1/3}} \qquad (19)$$

Equation 19 predicts a much greater distortion of the current-time curve, due to charging of the double layer, at the beginning of the current-scan than in the vicinity of the transition time.

If the charging current error in the region of the transition time alone is considered ($\bar{i} \cong \tau$), it is possible to compare the approximate charging current errors associated with the two different techniques, constant-current and linear current-scan. This is most easily done assuming conditions such that the transition times for the two techniques would be the same. Under such circumstances, one finds that $(t_c)_{c.s.}/(t_c)_{c.c.} = {}^2/_3$. Thus, if charging of the double layer occurs predominately in the vicinity of the transition time, the charging current errors associated with the two different techniques will be approximately equal. However, if any appreciable charging of the electrode double layer occurs prior to reduction (or oxidation) of the electroactive species, the current-scan technique will give rise to a considerably larger charging current error.

Experimental

Reagents.—All supporting electrolyte solutions used were prepared from reagent grade chemicals. Stock solutions of thallous chloride were prepared from the recrystallized salt. Cadmium nitrate solutions were prepared from reagent grade chemicals and standardized according to the procedure of Wiley[10] or by titration with standard ethylenediaminetetraacetic acid solution. The mercury employed in the electrode was purified by treatment with 10% nitric acid followed by distillation at reduced pressure.

Electrode.—The electrode used was constructed in the manner previously described[1]; the cellophane employed was donated by E. I. du Pont de Nemours and Company.

Apparatus.—Three electrodes were used in all experiments. A platinum electrode having a fairly large area served as an auxiliary electrode and a Beckman #1170 saturated calomel electrode as the reference electrode. A jacketed electrolysis cell connected to a constant temperature water-bath was used to maintain a temperature of 25.0 ±0.1°. All solutions were deaerated with Linde H. P. nitrogen prior to each experiment. Potential–time curves were recorded with a variable speed Varian recorder having a response time of one second. The recorder was coupled to a general purpose electroanalytical instrument[11] which also served to maintain a constant current or to provide a current varying linearly with time. A constant current could be maintained to within ±0.1%; in the case of current-scan, the current was linear with time to within ±0.1% of the maximum current.

Results and Discussion

Experimental Verification of Equation 2 and 5.—It has been shown[1] that the diffusion coefficients of electroactive substances in cellophane can be calculated from the steady-state limiting current, i_∞, at voltammetric membrane electrodes by means of the equation

$$D = \frac{i_\infty l}{nFAC^0} \qquad (22)$$

Here l is the membrane thickness and A is the cross sectional area through which diffusion occurs. The latter has been shown to be essentially equal to the total area of the cellophane membrane.[1] This experimental evaluation of D allows a calculation of the theoretical proportionality constants relating transition times to concentration and current (or rate of current-scan) in chronopotentiometric experiments.

Case A. Infinite Diffusion Conditions.—In the theoretical discussion, the conditions under which infinite diffusion could be assumed were pointed out. Under such conditions, σ and σ' in equations 2 and 5 are negligibly small. The data in Tables I and II substantiate this conclusion.

Table I

Constant Current and Linear Current-scan Reduction of Thallous Ion

Supporting electrolyte: 0.5 M NH_4NO_3; 0.5 M NH_3. A = 0.273 cm.²; $l = 2.67 \times 10^{-2}$ cm.; D (calcd. from i_∞) $= 4.10 \times 10^{-6}$ cm.²/sec.

A. Constant-current

$$\left(\frac{\tau^{1/2}i}{C^0}\right)_{theor.} = 47.6$$

C^0_{Tl}(mM)	i(μamp.)	τ(sec.)	$\frac{\tau^{1/2}i}{C^0}$
1.00	10.0	21.8	46.6
2.00	20.0	21.7	46.5
4.00	40.0	21.8	46.6
8.00	80.0	20.5	45.2
12.0	120.0	22.8	47.7

Av. = 46.5 ± 0.5

For infinite diffusion $\tau \leqslant \frac{l^2}{1.9D} \leqslant 91$ sec.

B. Linear current-scan

$$\left(\frac{\tau^{3/2}\beta}{C^0}\right)_{Theor.} = 71.5$$

C^0_{Tl}(mM)	β(μamp./sec.)	τ(sec.)	$\frac{\tau^{3/2}\beta}{C^0}$
1.00	0.50	28.4	75.7
2.00	1.00	28.2	74.7
4.00	2.00	27.8	73.7
8.00	4.00	27.1	70.4
12.00	5.00	30.9	71.4

Av. = 73.2 ± 1.8

For infinite diffusion $\tau \leqslant \frac{l^2}{1.6D} \leqslant 108$ sec.

The data in Tables I and II indicate that the agreement between experiments at different concentrations is better with the constant current technique. Plots of $\tau^{3/2}\beta$ *vs.* C^0, however, yield good straight lines having slopes very nearly equal to the theoretical but not passing through the origin. The trend to larger values of $\tau^{3/2}\beta/C^0$ as the concentration is decreased is thought to be caused by the increasing relative error resulting from the charging of the double layer.

Case B. Influence of Finite Diffusion.—Constant current and linear current-scan experiments, in which $l/\sqrt{D\tau}$ was less than 1.9 and 1.6, respectively, were run in order to verify equations 2 and 5 more completely (Tables III and IV). Values of σ and σ' (equations 3 and 6) were obtained from plots of these quantities as a function of $l/\sqrt{D\tau}$.

Although the experimental values of $\tau^{1/2}i(1 - \sigma)/C^0$ and $\tau^{3/2}\beta\ (1 - \sigma')C^0$ deviate to some extent from the theoretical values, it is apparent that a satisfactory correction can be made for the finite

(10) R. C. Wiley, *Ind. Eng. Chem., Anal. Ed.*, **3**, 14 (1931).

(11) D. D. De Ford, "Symposium on Electroanalytical Techniques," 133rd American Chemical Society Meeting, San Francisco, California, April 1958.

TABLE II

CONSTANT CURRENT AND LINEAR CURRENT-SCAN REDUCTION OF Cd(II) ION

Supporting electrolyte: 0.50 M NH_4NO_3; 0.50 M NH_3. A = 0.273 cm.^{2}; $l = 2.41 \times 10^{-2}$ cm.; D (calcd. from i_∞) $= 1.05 \times 10^{-6}$ cm.^{2}/sec

A. Constant current

$$\left(\frac{\tau^{1/2}i}{C^0}\right)_{\text{Theor.}} = 47.9$$

C^0_{Cd}(mM)	i (μamp.)	τ (sec.)	$\frac{\tau^{1/2}i}{C^0}$
1.00	7.00	38.9	43.6
4.00	28.0	39.3	43.9
8.00	56.0	38.7	43.5
12.00	84.0	38.9	43.6

Av. = 43.6 ± 0.1

For infinite diffusion $\tau \leqslant \frac{l^2}{1.9D} \leqslant 291$ sec.

B. Linear current-scan

$$\left(\frac{\tau^{3/2}\beta}{C^0}\right)_{\text{Theor.}} = 71.8$$

C^0_{Cd}(mM)	β (μamp./sec.)	τ (sec.)	$\frac{\tau^{3/2}\beta}{C^0}$
1.00	0.50	28.0	73.9
4.00	2.00	27.5	72.3
8.00	4.00	27.4	71.8
12.0	4.00	35.5	70.5

Av. = 72.1 ± 1.0

For infinite diffusion $\tau \leqslant \frac{l^2}{1.6D} \leqslant 345$ sec.

TABLE III

CONSTANT CURRENT REDUCTION OF THALLOUS ION

Supporting electrolyte: 0.100 M KNO_3, A = 0.374 cm.^{2}; $l = 1.46 \times 10^{-2}$ cm.; D (calcd. from i_∞) $= 3.50 \times 10^{-6}$ cm.^{2}/sec.

$$\left(\frac{\tau^{1/2}i\,(1-\sigma)}{C^0}\right)_{\text{theor.}} = 59.8$$

C^0_{Tl} (mM)	i (μamp.)	τ (sec.)	$l/\sqrt{D\tau}$	σ	$\frac{\tau^{1/2}i}{C^0}$	$\frac{\tau^{1/2}i}{(1-\sigma)C^0}$
1.50	20.0	22.4	1.65	0.016	63.2	62.1
2.00	25.0	26.4	1.52	.028	64.2	62.3
0.909	10.0	36.7	1.29	.067	66.7	62.2
1.50	15.0	47.3	1.14	.111	68.9	61.2
2.00	20.0	50.0	1.10	.126	70.6	61.7

Av. = 61.9 ± 0.4

TABLE IV

LINEAR CURRENT-SCAN REDUCTION OF THALLOUS ION

Supporting electrolyte: 0.5 M NH_4NO_3; 0.5 M NH_3. Concn. of $TlNO_3$ = 2.00 mM; A = 0.272 cm.^{2}; $l = 2.49 \times 10^{-2}$ cm. D (calcd. from i_∞) $= 3.40 \times 10^{-6}$ cm.^{2}/sec.

$$\left(\frac{\tau^{3/2}\beta\,(1-\sigma')}{C^0}\right)_{\text{theor.}} = 64.3$$

β(μamp./sec.)	τ(sec.)	$l/\sqrt{D\tau}$	σ'	$\frac{\tau^{3/2}\beta}{C^0}$	$\frac{\tau^{3/2}\beta}{(1-\sigma')C^0}$
0.500	41.5	2.09	0.000	67.1	67.1
.400	48.2	1.95	.000	66.9	66.9
.200	76.7	1.54	.008	67.2	66.7
.100	124.5	1.21	.033	69.4	67.1
.050	207.0	0.94	.096	74.4	67.2

diffusion occurring when $l/\sqrt{D\tau}$ is not within the limits required for infinite diffusion.

Reduction of a Second Species.—Potential–time curves, using a linear current-scan technique, were recorded using solutions containing various amounts of thallous and cadmium ion (Table V). These experiments were performed under conditions where linear infinite diffusion could be assumed.

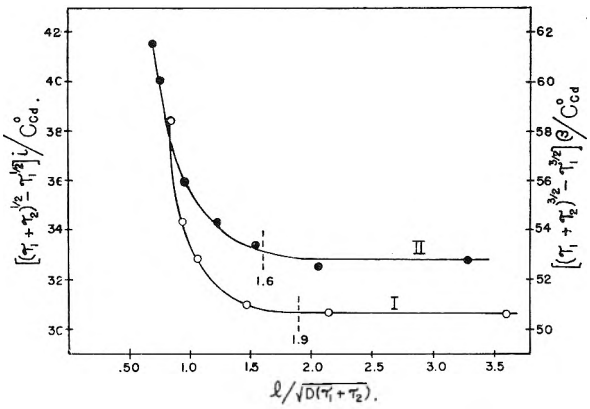

Fig. 1.—Dependence of the chronopotentiometric constant for the reduction of a second species on $l/\sqrt{D(\tau_1+\tau_2)}$. Concentration of Tl^+ = 1.00 mM; concentration of $Cd(NH_3)_4^{++}$ = 1.00 mM. I, constant current; II, linear current-scan.

TABLE V

STEPWISE REDUCTION, BY LINEAR CURRENT-SCAN TECHNIQUES, OF THALLOUS AND CADMIUM ION

Supporting electrolyte: 0.50 M NH_4NO_3; 0.50 M NH_3. A = 0.273 cm.^{2}; $l = 2.26 \times 10^{-2}$ cm.; 2.00 mM $TlNO_3$; D_{Tl^+} (calcd. from i_∞) $= 2.93 \times 10^{-6}$ cm.^{2}/sec.; $D_{Cd(NH_3)_4^{++}}$ (calcd. from i_∞) $= 0.774 \times 10^{-6}$ cm.^{2}/sec.

$$\left(\frac{\tau_1^{3/2}\beta}{C^0_{Tl}}\right)_{\text{Theor.}} = 59.9$$

$$\left(\frac{[(\tau_1+\tau_2)^{3/2}-\tau_1^{3/2}]\beta}{C^0_{Cd}}\right)_{\text{Theor}} = 61.7$$

C^0_{Cd}(mM)	β (μamp./sec.)	τ_1 (sec.)	$\tau_1+\tau_2$	$\frac{\tau_1^{3/2}\beta}{C^0_{Tl}}$	$\frac{[(\tau_1+\tau_2)^{3/2}-\tau_1^{3/2}]\beta}{C^0_{Cd}}$
0	1.00	24.2	24.2	59.5	..
0	0.50	38.6	38.6	60.0	..
0.865	2.00	14.2	18.4	53.5	58.7
0.865	1.00	22.1	28.8	52.0	58.5
2.02	2.00	15.1	24.2	58.7	59.7
2.02	1.00	24.2	38.9	59.5	61.2
2.66	2.00	14.8	26.5	57.0	59.7
2.66	1.00	23.0	41.7	55.5	59.7
2.66	0.50	37.1	66.5	56.5	59.3

For infinite diffusion

$$\tau_2 \leqslant \frac{l^2}{1.6D_2} \leqslant 413 \text{ sec.}$$

$$(\tau_1+\tau_2) \leqslant \frac{l^2}{1.6D_1} \leqslant 109 \text{ sec.}$$

The data in Table V substantiate equation 16, although the agreement between the experimental and "theoretical" values is not as good as when only one reducible species is present in solution.

The results of experiments run in order to determine the validity of the prediction that infinite diffusion occurs as long as $l/\sqrt{D_1(\tau_1+\tau_2)}$ is equal or greater than 1.9 or 1.6, for constant current or linear current-scan chronopotentiometry, respectively, are shown in Fig. 1. These plots indicate

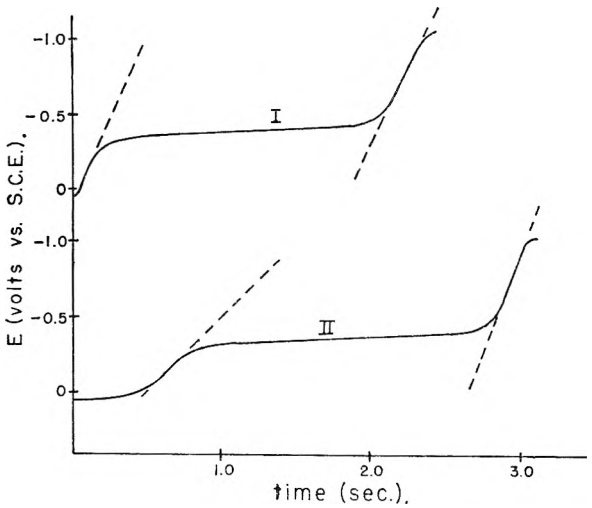

Fig. 2.—Constant current and linear current-scan chronopotentiograms of 1.00 mM $TlNO_3$. I, constant current, i = 100 μamp.; II, linear current-scan, β = 50 μamp./sec.

that below these limits an appreciable error is incurred, the error increasing with increasing $\tau_1 + \tau_2$ as expected. Since, in all cases, the quantity $l/\sqrt{D_2\tau_2}$ was within the limits for assuming infinite diffusion for cadmium, the error is due to the finite diffusion of thallous ion.

Charing Current Distortion of Potential–Time Curves.—Figure 2 allows comparison of the distortions of the potential–time curves using constant-current and linear-current-scan techniques. It is apparent that the distortion is nearly the same in the two techniques in the vicinity of the transition time. As expected, however, the distortion in the initial portion of the potential–time curve is much greater with the linear current-scan technique than with the constant-current technique.

Acknowledgments.—A portion of this work was supported through Grant #G7333 from the National Science Foundation. G.W. gratefully acknowledges a fellowship from Phillips Petroleum Company.

CHLOROGERMANIUM(IV) SPECIES IN ACID MEDIA

BY R. L. BENOIT AND P. CLERC

Département de Chimie, Université Laval, Québec, Canada

Received November 29, 1960

The solvent extraction method has been used to study the germanium(IV)–chloride system in acid media. $GeCl_4$ is the main germanium species extracted in CCl_4. The variation of the Ge distribution ratio with the solution composition is interpreted in terms of a series of $GeCl_i(OH)_j(H_2O)_k^{(i+j-4)-}$ species. At constant levels of total HCl–$HClO_4$ molality, the average value of i increases from 0 at low HCl concentration to close to 4 at the highest HCl concentration. In HCl–LiCl solutions of constant total molality, the average value of j decreases with increasing acidity from close to 4 to minimum values, these minimum values are in turn lower at higher molality levels. In HCl solutions, $GeO_2(H_2O)_k$ is the main Ge species up to 5.6 m HCl; at higher HCl concentrations, anionic complex species are present but complete formation of $GeCl_6^{2-}$ is not attained.

Introduction

The stability of the halide complexes of most metal ions decreases in the order $F^- >> Cl^- > Br^- > I^-$; the reverse sequence of stability holds for the complexes of a few transition and heavy metal ions and is attributed to dative π-bonding.[1-3] Ge(IV) and Sn(IV) halide complexes apparently fall into the first class whilst Pb(IV) is expected to belong to the second class.

As part of a study undertaken to establish the stability trends among the halide complexes of Ge(IV), Sn(IV) and Pb(IV), an investigation of the nature and stability of chlorogermanium(IV) species is reported. So far only qualitative predictions have been made as to the state of germanium(IV) species in hydrochloric solutions.[4,5]

The solvent extraction method was selected to investigate the Ge(IV)–Cl^- system. By establishing successively the influence of the metal, the ligand and the hydrogen ion concentrations on the metal distribution between solution and immiscible solvent, the formulas and stability constants of the $M_hL_i(OH)_j$ species in solution can be determined.[6,7] CCl_4 was chosen as solvent because it is nearly immiscible with water, a poor solvent for HCl and likely to extract $GeCl_4$ and give ideal solution.

Experimental Materials and Methods

Reagents.—An aqueous 4 × $10^{-2}M$ stock solution of germanium(IV) was prepared from 99.9% germanium dioxide kindly provided by the Tsumeb Corporation. Reagent grade hydrochloric acid, perchloric acid and lithium chloride were used. Reagent grade carbon tetrachloride was employed without purification once it was found that identical results were obtained with the purified solvent.[8]

Procedure.—Aqueous solutions of $HClO_4$, LiCl and HCl were mixed and cooled in a separatory funnel, after which the Ge solution was added. A known volume of CCl_4, in most cases equal to the volume of the aqueous phase, was added and the separatory funnel was shaken mechanically for 60 minutes. Tests showed that distribution equilibrium was reached in 12 seconds. The phase separation was achieved by decantation and when necessary by centrifugation. The experiments were carried out at 23 ± 2°.

Aliquots of the aqueous phase were taken for analysis.

(1) B. G. F. Carleson and H. Irving, *J. Chem. Soc.*, 4390 (1954).
(2) S. Ahrland, *Acta Chem. Scand.*, **10**, 723 (1956).
(3) S. Ahrland, J. Chatt and N. R. Davies, *Quart. Rev.*, **12**, 265 (1958).
(4) G. Brauer and H. Müller, *Z. anorg. Chem.*, **287**, 71 (1956).
(5) D. A. Everest and J. C. Harrison, *J. Chem. Soc.*, 1820 (1957).
(6) H. Irving, F. J. C. Rossotti and R. J. P. Williams, *ibid.*, 1906 (1955).
(7) R. M. Diamond, *J. Phys. Chem.*, **61**, 69 (1957).
(8) E. B. Sandell, "Colorimetric Determinations of Traces of Metals," Interscience Publ., New York, N. Y., 1959, p. 173.

The total acidity was obtained after addition of an excess of sodium carbonate and back titration with standardized HCl; GeO_2 being a very weak acid[9] does not interfere. Chloride was determined by the Volhard method and Ge(IV) by the phenylfluorone method,[10,11] according to the procedure developed by Sandell.[11] A Beckman model DU spectrophotometer was used.

The organic phase was analyzed, after extraction with water, as indicated above.

A germanium material balance provided a check of the technique. The germanium recovery amounted to a minimum of 90% when the germanium distribution ratio was less than 10^2, the recovery decreased to 80% for a distribution ratio $10^{3.5}$. Germanium losses appeared to take place during the making up of the germanium aqueous solution and were apparently caused by the high volatility of the germanium tetrachloride. To eliminate these errors, the germanium distribution ratios when high were calculated from the concentration in both phases.

Experimental Results

Nature of the Ge(IV) Species in CCl_4.—The analysis of ten CCl_4 extracts corresponding to various hydrochloric solutions of germanium are reported in Table I. When the extracts are equilibrated with water, hydrolysis of the germanium species proceeds according to

$$GeCl_i(OH)_{4-i} + (i-2)H_2O \longrightarrow GeO_2 + iCl^- + iH^+$$

The value of i can be deduced from the analytical ratios Cl^-/Ge or H^+/Ge. Corrections for the HCl coextracted in CCl_4 were calculated from a value $10^{-7.4}$ obtained for the HCl partition coefficient[12] and found to be negligible in the concentration range studied.

TABLE I

ANALYSIS OF CCl_4 EXTRACTS

Composition of initial aqueous phase, mole/l.			Analytical ratios		
Ge	HCl	$HClO_4$	Ge	Cl^-	H^+
10^{-2}	7.00	..	1.00[a]	4.03[a]	3.97[a]
10^{-2}	8.00	..	1.00	3.98	4.02
10^{-2}	8.96	..	1.00	4.16	4.08
5×10^{-3}	0.095	6.91	1.00[b]	3.94[b]	3.81[b]
10^{-2}	0.164	6.84	1.00	4.03	4.11
10^{-2}	0.620	6.74	1.00	3.93	3.90

[a] Average of 4 extractions. [b] Average of 2 extractions.

The analytical ratios Cl^-/Ge and H^+/Ge are in good agreement and come close to 4.

The amount of water present in CCl_4 extracts as determined by the Karl Fischer method using the Townson and Mercier apparatus appeared to be independent of the Ge concentration.

Distribution of Ge(IV) between HCl–$HClO_4$–LiCl Solutions and CCl_4.—The germanium(IV) distribution ratio D = (GeCl_4)org./Σ(Ge)aq. was studied as a function of four concentrations: those of germanium, chloride and hydrogen ions and hydrochloric acid.

(1) Influence of the Germanium Concentration.—The following values of D were obtained when the germanium concentration was varied in these solutions: 8.90 m HCl (1), 1.44 m HCl–6.58 m $HClO_4$ (2), 0.071 m HCl–9.85 m $HClO_4$ (3).

(9) C. E. Gulezian and J. H. Müller, *J. Am. Chem. Soc.*, **64**, 3142 (1932).

(10) H. J. Cluley, *Analyst*, **76**, 517 (1951).

(11) Ref. 8, p. 485.

(12) Unpublished results by C. Barbeau and P. Clerc.

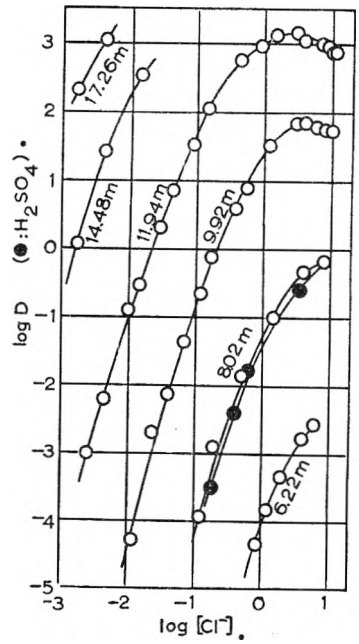

Fig. 1.—Germanium distribution ratio as a function of Cl^- concentration at various levels of total molality: open circles, HCl–$HClO_4$, filled circles, HCl–H_2SO_4.

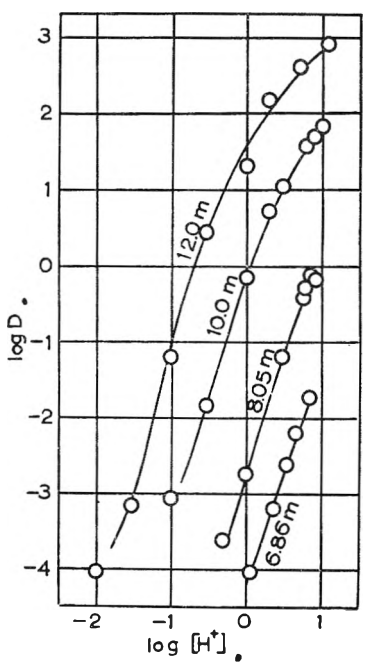

Fig. 2.—Germanium distribution ratio as a function of H^+ concentration at various levels of total molality.

(1) log Σ(Ge) aq.: -5.2 to -2.9, log $D = +0.80 \pm 0.03$
(2) log Σ(Ge) aq.: -3.4 to -1.7, log $D = -1.00 \pm 0.06$
(3) log Σ(Ge) aq.: -5.6 to -2.1, log $D = -1.34 \pm 0.04$

These results show no significant effect of the germanium concentration on the distribution ratio.

(2) Influence of the Chloride Ion Concentration at Constant Acidity and Total Molality.—Data are presented for solutions in which the HCl concentration was varied while acidity and total molality were maintained constant by means of $HClO_4$ at 6.22, 8.02, 9.92, 11.94, 14.88 and 17.26 m, and with H_2SO_4 at 8.02 m. The germanium con-

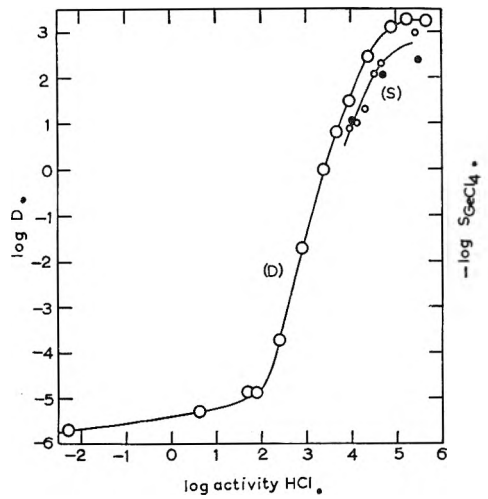

Fig. 3.—Dependence of the germanium distribution ratio and the solubility of $GeCl_4$ on HCl activity: ○, Brauer's solubility values; ●, Allison's solubility values.

centration was kept between 5×10^{-4} and 5×10^{-3}. Log D is plotted in Fig. 1 against the logarithm of the "free chloride" equilibrium concentration (Cl^-) in aqueous solution. This concentration was equal to the HCl concentration when the latter was not too low. A corrective term equal to the concentration of chloride bound to germanium, *i.e.*, $\bar{i}$ times the germanium concentration was subtracted from the HCl concentration at low HCl levels; $\bar{i}$ was obtained by using successive approximations, from the value of the slope of the curve. The distribution ratio increases with the chloride concentration. For total molality 9.92 and 11.94 *m*, D reaches a maximum value and then decreases. D increases markedly with increasing total molality at constant chloride concentration.

(3) **Influence of the Hydrogen Ion Concentration at Constant Chloride Concentration and Total Molality.**—The distribution ratios corresponding to solutions of variable HCl concentration and constant HCl + LiCl total molality of 6.86, 8.05, 10.0 and 12.0 *m* are plotted against log (H^+) in Fig. 2. D increases but less and less rapidly with increasing H^+ concentration. At constant acidity there is also a large increase of D with increasing total molality.

(4) **Influence of the HCl Concentration.**—Figure 3 presents the data for HCl solutions from 0.1 to 16 *m* HCl. The germanium initial concentration varied between 10^{-3} and 3.6×10^{-2}. The values of log D are plotted against the HCl activity logarithm calculated from Åkerlöf's data.[13] D varies at first slowly with the HCl concentration til 5 *m* HCl then D increases rapidly to reach a maximum value for 14 *m* HCl.

Interpretation of Results

The experimental results in Table I indicate that the germanium species extracted in CCl_4 is germanium tetrachloride. Recent determination of $GeCl_4$ vapor pressure[12] when compared with solvent extraction data support this conclusion and show further that the $GeCl_4$ solutions in CCl_4 are ideal. Irvine and co-workers[14] report values of Cl^-/Ge between 3.0 and 3.9 for extracted germanium species but no specific data are quoted so that it is difficult to discuss their results.

The lack of dependence of the distribution ratio on the metal concentration can be shown mathematically[6,7] to imply identical degrees of polymerization for the metal species in the aqueous and organic phases. $GeCl_4$ being present in CCl_4, the germanium species in the aqueous solutions studied are therefore mononuclear.

i and j, respectively, the number of Cl and OH bound per Ge atom in the $GeCl_i(OH)_j(H_2O)_k$ species in aqueous solutions, charges being omitted for convenience, are related to the slope of the curves plotted in Figs. 1 and 2. For sake of simplification it is assumed first that $GeCl_i(OH)_j(H_2O)_k$ is the only species present in a given concentration interval for Cl^- and OH^-. Calling K_{ij} the mass action constant for the equilibrium

$$GeCl_i(OH)_j(H_2O)_k + jH^+ + (4-i)Cl^- \rightleftharpoons GeCl_4 + (j+k)H_2O$$

and introducing the distribution ratio D_{ij} and P the $GeCl_4$ partition coefficient, the following expression is found

$$D_{ij} = K_{ij} \times P \frac{|H^+|^j |Cl^-|^{4-i}}{|H_2O|^{j+k}} \times f_{ijk} \qquad (1)$$

where | | means activity and f_{ijk} the activity coefficient of $GeCl_i(OH)_j(H_2O)_k$. Assuming now that various $GeCl_i(OH)_j(H_2O)_k$ species are present simultaneously the distribution ratio is such that

$$\frac{1}{D} = \Sigma \frac{1}{D_{ij}}$$

Taking the derivative with respect to $\log(Cl^-)$

$$\frac{d \log D}{d \log (Cl^-)} = D \Sigma \frac{1}{D_{ij}} \frac{d \log D_{ij}}{d \log (Cl^-)} \qquad (2)$$

Combining equations 1 and 2 and introducing $\bar{i}$ the average number of Cl bound per Ge atom

$$\bar{i} = \frac{\Sigma i (GeCl_i(OH)_j(H_2O)_k)}{\Sigma (GeCl_i(OH)_j(H_2O)_k)} = \Sigma \frac{iD}{D_{ij}}$$

and $\bar{j}$ and $\bar{k}$ are likewise defined. Then

$$\left[\frac{d \log D}{d \log (Cl^-)}\right]_{(H^+)} = (4-\bar{i}) + (4-\bar{i}) \frac{d \log f_{Cl^-}}{d \log (Cl^-)} + \bar{j} \frac{d \log f_{H^+}}{d \log (Cl^-)} + D\Sigma \frac{1}{D_{ij}} \frac{d \log f_{ijk}}{d \log (Cl^-)} - (\bar{j}+\bar{k}) \frac{d \log |H_2O|}{d \log (Cl^-)} \qquad (3)$$

If activity coefficients and water activity are kept constant, equation 3 becomes

$$\left[\frac{d \log D}{d \log (Cl^-)}\right]_{(H^+)} = 4 - \bar{i} \qquad (4)$$

Although the values of log D plotted against log (Cl^-) in Fig. 1 are for solutions of constant HCl–$HClO_4$ total molality, activity coefficients are likely to vary if the replacement of one constituent say $HClO_4$, by the other one HCl takes too large proportions.[15] The applicability of equation 4 to calculate $\bar{i}$ is therefore restricted to relatively low chloride concentrations. This point is illustrated

(13) G. Åkerlöf and J. W. Teare, *J. Am. Chem. Soc.*, **59**, 1855 (1937).

(14) G. O. Brink, P. Kafalas, R. A. Sharp, E. L. Weiss and J. W. Irvine, Jr., *ibid.*, **79**, 1303 (1957).

(15) P. G. Murdoch and R. C. Barton, *ibid.*, **65**, 4074 (1933).

by the results of the experiments made using H_2SO_4 in place of $HClO_4$ at the same total molality 8.02 *m*. The corresponding curves giving log *D* against log (Cl^-) are at first parallel and unexpectedly close but then slopes become different for 1.6 *m* (Cl^-). In this particular case, a 1.6 *m* Cl^- concentration, *i.e.*, a replacement of 20% of $HClO_4$ by HCl, is thus an upper limit for the applicability of equation 4.

Values of $\bar{\imath}$ were calculated for each total molality, from the slope of the curve giving log *D* against log (Cl^-) in Fig. 1, according to equation 4. For the lowest chloride concentrations, $\bar{\imath}$ was close to or equal to zero and then increased gradually with (Cl^-). The values of log (Cl^-) corresponding to $\bar{\imath} = i + {}^1/_2$ which are tabulated below for total molality 11.94 *m* give an indication of the stability of the chloro-complexes.

log (Cl^-)	−2.3	−1.2	−0.6	−0.1
$\bar{\imath}$	0.5	1.5	2.5	3.5

At 11.94 *m* total molality, *D* goes through a maximum leading to $\bar{\imath} = 4.0$, for 1.5 *m* (Cl^-), a chloride concentration for which equation 4 is still thought to be applicable. On the other hand, the value $\bar{\imath} = 4.0$ for 7.0 *m* (Cl^-) at 9.92 *m* total molality may not be significant.

An expression giving $[\mathrm{d} \log D/\mathrm{d} \log (H^+)]_{(Cl^-)}$ is obtained by following steps similar to those used for establishing relation 3. The application of the simpler form

$$\left[\frac{\mathrm{d} \log D}{\mathrm{d} \log (H^+)}\right]_{(Cl^-)} = \bar{\jmath} \qquad [5]$$

to the calculation of $\bar{\jmath}$ should be restricted to low H^+ concentrations to ensure the constancy of the activity coefficients. However, for solutions of constant total molality LiCl + HCl = 4 and 6 *m*, the HCl activity coefficient has been shown to be nearly independent of the HCl concentration.[16] If the constancy of the activity coefficient could be extended to higher total molality and to ionic activity coefficients, equation 5 could be used to calculate $\bar{\jmath}$ over the whole range of HCl concentration. The values of $\bar{\jmath}$ are plotted in Fig. 4, against log(H^+) for total molality 6.86 (1), 8.05 (2), 10.0 (3), and 12.0 *m* (4). $\bar{\jmath}$ is seen to decrease regularly with increasing H^+ concentration from close to 4.0 to minimum values which in turn decrease with increasing total molality.

Approximate values of $\bar{\imath}$ and $\bar{\jmath}$ for the $GeCl_i(OH)_j(H_2O)_k$ species present in HCl solutions are obtained from the limit slopes of the curves given in Figs. 1 and 2. For 12.0 *m* HCl, $\bar{\imath} = 4.2$ and $\bar{\jmath} = 0.7$ are found. This would indicate germanium species with an average charge −1 and suggest a coördination number 6 for germanium, water being coördinated. Migration experiments give also evidence that anionic Ge species are present.[4,17] Using the resin loading method, Everest[5] concludes that $GeCl_{5-j}(OH)_j^-$ species with $3 < j < 4$ are formed between 7.5 and 11 *m* HCl. However, this conclusion is not too dependable because the resin loading method is subject to criticism and most of the germanium solutions used were not in equilibrium with respect to hydrolysis.

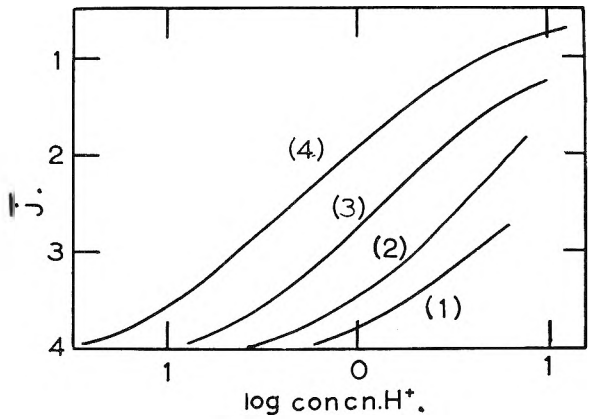

Fig. 4.—Variations of $\bar{\jmath}$, the average number of OH bound per Ge atom, with H^+ concentration at various levels of total molality: 1, 6.86 *m*; 2, 8.05 *m*; 3, 10.0 *m*; 4, 12.0 *m*.

The experimental values of *D* obtained for HCl solutions are in good agreement with those of Sandell[11] and Fischer[18] which are less complete but differ somewhat from those given by Irvine[14] particularly at low HCl concentrations.

Although the variations of log *D* against log (HCl) are related to $\bar{\imath}$, $\bar{\jmath}$ and $\bar{k}$ as

$$\mathrm{d} \log D/\mathrm{d} \log (\mathrm{HCl}) = [\mathrm{d} \log D/\mathrm{d} \log (H^+)]_{(Cl^-)} + [\mathrm{d} \log D/\mathrm{d} \log Cl^-)_{(H^+)}$$

the unknown values of the activity coefficient derivatives do not permit a complete quantitative interpretation of d log *D*/d log(HCl) in terms of solution equilibria. However, the maximum value 4.1 found for the slope of the curve giving log *D* *versus* log activity HCl (Fig. 3) near 5.6 *m* HCl is consistent with the presence of GeO_2, possibly hydrated, as the main germanium species in this solution; the value of d log *D*/d log |HCl| deduced from the equilibrium $GeO_2 + 4HCl \rightleftarrows GeCl_4 + 2H_2O$ would be somewhat above 4 because of two activity correction terms. Confirmation of the presence of GeO_2 up to 5 *m* HCl is found in the linear decrease of the GeO_2 solubility logarithm with the HCl concentration[4,5,19] which suggests a salting-out effect. The formation of a series of $GeCl_i(OH)_j(H_2O)_k$ species, where $\bar{\imath}$ increases towards 4 and $\bar{\jmath}$ decreases to low values, with increasing HCl concentration, accounts qualitatively for the observed decrease of d log *D*/d log |HCl| from 4.1 to 0. The constancy of *D* at the highest HCl concentrations indicates at least that complete formation of $GeCl_6^{2-}$ does not take place even though the existence of $GeCl_6^{2-}$ in a solid salt appears probable.[17] The formation of $GeCl_6^{2-}$ is also reported not to take place in liquid anhydrous HCl in contrast with that of $SnCl_6^{2-}$.[20]

The small variation of the distribution ratio up to 5 *m* HCl appears to be due to the presence of another CCl_4-soluble Ge species. That this species is likely to be GeO_2 is indicated: the GeO_2 solubility in CCl_4 was determined as 3.3×10^{-7} *m* giving

(16) J. E. Hawkins, *ibid.*, **54**, 4480 (1932).

(17) A. W. Laubengayer, O. B. Billings and A. E. Newkirk, *ibid.*, **62**, 546 (1940).

(18) W. Fischer, W. Harre, W. Freese and K. G. Hackstein, *Angew. Chem.*, **66**, 165 (1954).

(19) W. Pugh, *J. Chem. Soc.*, 1537 (1929).

(20) T. C. Waddington and F. Klanberg, *Naturwiss.*, **46**, 578 (1959).

-5.1 for log solubility GeO_2 in CCl_4/log solubility GeO_2 in H_2O, in fair agreement with -5.5, the value of log D extrapolated to zero HCl concentration. The slow rise of D with HCl concentration up to 5 m would result from a salting-out of GeO_2.

It is of interest to compare the variations of distribution ratio and $GeCl_4$ solubility between 9 and 16 m HCl as D and S_{GeCl_4} are related

$$\log D = A - \log S_{GeCl_4} \qquad (6)$$

The experimental values of $-\log S_{GeCl_4}$ as determined by Brauer[4] and Allison[21] are plotted in Fig. 3, against the HCl activity. Although the points are somewhat scattered, they fall approximately on a line parallel to the log D curve as indicated by expression 6. These results also confirm that $GeCl_4$ is the extracted species and that the $GeCl_4$ solution in CCl_4 is ideal.

An exact definition of the nature and stability of the chlorogermanium species has not proved possible. As OH^- is much more firmly bound to Ge than Cl^-, measurable substitution takes place only in concentrated H^+Cl^- solutions where the unknown values of the activity coefficients make the interpretation difficult. The existence of a series of species with similar stabilities further complicates the situation.

Acknowledgment.—One of the authors (P.C.) gratefully acknowledges the aid given him in the form of a fellowship sponsored by the Consolidated Mining and Smelting Co. The authors wish to thank the National Research Council of Canada for a grant.

(21) E. R. Allison and J. H. Müller, *J. Am. Chem. Soc.*, **54**, 2833 (1932).

VOLTAMMETRY IN LIQUID SULFUR DIOXIDE. I. TECHNIQUE AND THEORETICAL PROBLEMS[1]

BY PHILIP J. ELVING, JOSEPH M. MARKOWITZ AND ISADORE ROSENTHAL

Departments of Chemistry, The University of Michigan, Ann Arbor, Michigan, and The Pennsylvania State University, University Park, Pa.

Received December 15, 1960

The feasibility of voltammetry and polarography in solutions of a totally non-protonic solvent, sulfur dioxide, has been investigated. Apparatus, procedures and orientative work with various inorganic and organic solutes are described for two indicating electrodes, the dropping mercury electrode and the stationary cylindrical platinum electrode, and two reference electrodes, the mercury calomel pool and the silver–silver chloride electrode. The specific methodological findings are discussed critically, as are the theoretical aspects and practical effects for the general practice of voltammetry of the non-existence of a suitable background electrolyte, the possibility of reference electrode polarization, and the presence of a characteristic high solution resistance.

Although non-aqueous media[2] have been investigated as solvents for polarography and, more generally, voltammetry, use of a totally non-protonic solvent has not been reported. Consequently, the feasibility of voltammetry in liquid sulfur dioxide was studied. Sulfur dioxide was selected because of its exceptional effectiveness as a reaction medium[3-6] in stabilizing free radicals; this would permit investigation of the electrochemical behavior of free radicals and of the frequent postulation of free radical intermediates in the electroreduction of organic species.

This paper covers the development of experimental apparatus and procedures, orientative studies with various solutes, and exploration of certain theoretical problems involved in voltammetry in sulfur dioxide. A subsequent paper[7] describes the behavior of triphenylchloromethane.

Discussion

The fundamental experimental requirements for successful voltammetry of (a) a reliably responsive indicating electrode, (b) a totally non-polarizable reference electrode, and (c) the availability of soluble electrolytes with relatively high decomposition potentials to serve as background electrolytes and provide solutions with appreciable conductivity, are only partially satisfied in sulfur dioxide. The effects of this situation can be evaluated from the following considerations of electrode systems, observed electroactivity of various solutes, and factors which may produce error in the determination of characterizing potentials, *e.g.*, presence of a large migration current component in the limiting current, reference electrode polarization and solution iR drop.

Electrode Systems.—The dropping mercury electrode (DME) is relatively inferior to the cylindrical platinum electrode (CPE) under the experimental conditions used. Compared to its behavior in aqueous solution, the DME is unstable, showing non-reproducible drop-rate changes and other unfavorable electrokinetic characteristics; frequent clogging or streaming also occurs. Elec-

(1) Abstracted from the Ph.D. theses of I. Rosenthal, The Pennsylvania State University, 1951, and J. M. Markowitz, The University of Michigan, 1958.

(2) For example, the excellent studies in acetonitrile (I. M. Kolthoff and J. Coetzee, *J. Am. Chem. Soc.*, **79**, 870, 1852, 6110 (1957) and in ammonia (H. A. Laitinen and C. J. Nyman, *J. Am. Chem. Soc.*, **70**, 2241, 3002 (1948); H. A. Laitinen and C. E. Shoemaker, *ibid.*, **72**, 663, 4975 (1950); A. D. McElroy and H. A. Laitinen, *J. Phys. Chem.*, **57**, 564 (1953)).

(3) L. F. Audrieth and J. Kleinberg, "Non-Aqueous Solvents," John Wiley and Sons, New York, N. Y., 1953.

(4) G. Jander, "Die Chemie in Wasserahnlichen Losungsmitteln," Springer-Verlag, Berlin, 1949.

(5) J. M. Markowitz, Ph.D. Thesis, The University of Michigan, 1958.

(6) K. Cruse, *Z. Elektrochem.*, **46**, 571 (1940).

(7) P. J. Elving and J. M. Markowitz, *J. Phys. Chem.*, **65**, 686 (1961).

trocapillary curves are erratic with doubtful maxima and sharp, apparently random discontinuities; the principal difficulty was poor electrode stability over the long period of the experiment; differences between two electrodes or between the characteristics of one electrode before and after cleaning are so marked that failure of an electrode required termination of a run. The necessity for "renewal" of the CPE by a.c. is a practical disadvantage, as is the greater complexity of the theoretical relations involving current, potential, concentration and other polarographic variables, compared to the corresponding relations for the DME; the nature of the current–potential relation also makes difficult the resolution of consecutive waves.

Experimentally observed peak potentials and currents are reported for the CPE. For the DME, the "half-height potential," $E_{h/2}$, measured at one-half of the limiting current is reported; since no supporting electrolyte was present, $E_{h/2}$ cannot be assumed to equal the customary half-wave potential, $E_{1/2}$ (*cf.* subsequent Discussion).

Both calomel–pool and silver–silver chloride electrodes were used as reference electrodes; the former with the DME; the latter with the CPE. Cruse[6] recommends the latter as being better poised in sulfur dioxide; both may become slightly polarized in the solutions used (*cf.* subsequent discussion).

Effect of Absence of a Background Electrolyte.—Table I is a qualitative summary of the electroactivity observed for the compounds examined.

No suitable background electrolyte was found. From the literature,[8] it appears that the number of compounds having the correct properties to fulfil this function cannot be large; elimination of many on the basis of chemical similarity leaves an even smaller group to be tested. Investigation of several inorganic and organic compounds revealed that substances with high solubility and low solution resistance, *e.g.*, triphenylchloromethane and tetra-*n*-butylammonium iodide, exhibit large faradaic currents at low potentials; highly soluble substances, which are not easily decomposed, are invariably non-electrolytes, *e.g.*, thionyl chloride. The consequences of voltammetry in the absence of a background electrolyte will, consequently, be considered using DME relationships; the results are also applicable to the CPE.

In a polarographic electrolysis, the observed limiting current, i_l, is the algebraic sum of the diffusion current, i_d, and the migration current, i_m

$$i_l = i_d \pm i_m \qquad (1)$$

The minus sign is applicable if the species undergoing reduction is an anion; the plus sign, if it is a cation. Since i_m is approximated by the product of i_l and the transference number, $t_\pm$, of the reducible ion[9]

$$i_l = i_d/(1 \mp t_\pm) \qquad (2)$$

As a first approximation[10]

(8) P. J. Elving and J. M. Markowitz, *J. Chem. Ed.*, **37**, 75 (1960).

(9) I. M. Kolthoff and J. J. Lingane, "Polarography," 2nd ed., Interscience Publishers, New York, N. Y., 1952.

(10) S. Glasstone, "Introduction to Electrochemistry," D. Van Nostrand Co., Inc., New York, N. Y., 1942.

TABLE I

SUMMARY OF VOLTAMMETRIC BEHAVIOR OF VARIOUS SOLUTES IN LIQUID SULFUR DIOXIDE[a]

Solute	Results
Water	No current production; charging current increases with increasing water concn.
Potassium chloride	Two prominent maxima in cathodic branch and two waves in anodic branch, of which the more positive is more prominent
Potassium bromide	Two waves in anodic branch, similar to those for KCl
Potassium iodide	One prominent wave in anodic branch; none in cathodic branch
Ammonium thiocyanate	One wave in cathodic branch
2-Bromopropanoic acid	No current production except for traces in the presence of water
α,α'-Dibromosuccinic acid	No current production
Thionyl chloride	No current production; large increase in charging current in the presence of water
Triethylamine	No current production; charging current increases with increasing concn.
Tetra-*n*-butylammonium iodide	An enormous current production in the cathodic branch resembling hydrogen discharge in aqueous polarography; visible color change due to electrode reaction
Triphenylchloromethane[b]	One large cathodic branch wave and two waves in the anodic branch
p-Xenyldiphenylchloromethane[b]	One wave in the cathodic branch and a possible wave in the anodic branch

[a] Behavior at the DME *vs.* mercury–calomel pool at −25° except for compounds marked with a superscript *b*. Solution concentrations were *ca.* 1 m*M*, except that saturated solutions were used for very sparingly soluble compounds. [b] Behavior at the CPE *vs.* Ag–AgCl electrode at −22.7°.

$$t_\pm = t_\pm^0 + AC^{1/2} \qquad (3)$$

where $t_\pm^0$ is the transference number at infinite dilution, A is a constant, whose sign and magnitude depend on the nature of the ion, and C is its concentration. If the simple Ilkovic equation is introduced, $i_d = kC$, and at a cathode

$$i_l = kC/(1 \mp t_\pm^0 \mp AC^{1/2}) \qquad (4)$$

where the upper signs refer to a cation reduction; for processes at an anode, signs are reversed. Therefore, the precise value of i_l depends on the magnitude of $t_\pm$; its variation with concentration on the value of A.

The magnitude of $t_\pm$ and its variation with concentration for a specific electrolyte can be approximated from the Debye–Hückel–Onsager theory of ionic conductance; the calculation will be described for triphenylchloromethane, which apparently ionizes completely to the triphenylmethylcarbonium and chloride ions.[11] The transference numbers of cation and anion for a uni-univalent electrolyte are[10]

$$t_+ = \frac{\lambda_+^0 - (0.5A + B\lambda_+^0)C^{1/2}}{\Lambda_0 - (A + B\Lambda_0)C^{1/2}} \qquad (5)$$

$$t_- = \frac{\lambda_-^0 - (0.5A + B\lambda_-^0)C^{1/2}}{\Lambda_0 - (A + B\Lambda_0)C^{1/2}} \qquad (6)$$

where the constants A and B are defined by

(11) L. C. Anderson, *J. Am. Chem. Soc.*, **47**, 1674 (1935).

$$A = 82.4/\eta(DT)^{1/2} \quad (7)$$

$$B = 8.20 \times 10^{6}/(DT)^{3/2} \quad (8)$$

λ^0 is the ionic conductance at infinite dilution; Λ_0, equivalent conductance of the electrolyte at infinite dilution; D, dielectric constant; η, viscosity of the solvent; T, absolute temperature (all in conventional c.g.s. units). Introducing the relevant data[12] into equation 6 yields

$$t_- = \frac{0.920 - 3.29C^{1/2}}{1 - 4.34C^{1/2}} \quad (9)$$

The triphenylmethylcarbonium ion transference number is then

$$t_+ = 1 - t_- = \frac{0.080 - 1.05C^{1/2}}{1 - 4.34C^{1/2}} \quad (10)$$

The difference in transference number magnitude at infinite dilution (0.92 for Cl^-; 0.08 for ϕ_3C^+) seems reasonable, considering their relative sizes.

From the derivative of t with respect to $C^{1/2}$, it can be seen that for a 20-fold concentration increase in the 1 mM range, corresponding to the present experimental conditions, the anion transference number will increase about 1% and that of the cation will decrease about 12%.

From equation 2 (i_d replaced by kC) and its counterpart for processes at an anode (signs reversed), four separate electrode-ion combinations can be distinguished, which, on introducing the transference numbers for ϕ_3C^+ and Cl^-, have the forms

(a) Cathode, cation: $i_l = kC/0.92$ (11)

(b) Cathode, anion: $i_l = kC/1.92$ (12)

(c) Anode, cation: $i_l = kC/1.08$ (13)

(d) Anode, anion: $i_l = kC/0.08$ (14)

The magnitude of the denominators shows the difference between i_l and i_d to be appreciable only in cases b and d. Only in d does the concentration-sensitive cation transference number, 0.08, appear alone in the denominator; the other cases involve either the almost constant anion transference number or the added term, 1. Thus, a small change in transference number due to a concentration change will markedly affect the current only in case d; i_l should increase about 12% for a 20-fold concentration increase.

Because of the presence in equations 11 to 14 of the Ilkovic constant, k, i_l must be subject to the same instrumental laws as i_d (with minor qualification due to the approximate nature of the classical Ilkovic equation); in particular, the quotient, $i_l/h^{1/2}$ (h = head of mercury), will be constant and independent of h at a given concentration[4] for the DME and for a good many other electrode types and geometries.

The following general conclusions can then be drawn: In the absence of a background electrolyte, i_l is likely to differ considerably from i_d, unless the transference numbers of cation and anion differ greatly, in which case, the two processes, anion reduced at a cathode and cation oxidized at an anode (if they occur), will have limiting currents only a few per cent. different from i_d. The concentration dependence of i_l is almost linear unless the cation and anion transference numbers differ greatly; this will result in a non-linear concentration dependence of one of the processes, anion oxidized at anode or cation reduced at cathode.

Absence of a background electrolyte will affect the accuracy of $E_{1/2}$ measurement, even after correction for i_m on the basis of the approximate treatment given. Measured $E_{1/2}$ depends to some degree on the slope of the rising portion of the recorded i–E curve; simple correction for i_m corrects only the limiting portion. Therefore, only half-height potentials are reported; these differ from $E_{1/2}$ by probably a few millivolts.

TABLE II

POLAROGRAPHY OF POTASSIUM CHLORIDE IN LIQUID SULFUR DIOXIDE[g]

Hg head, cm.	Wave I $E_{h/2}$, v.	Wave I i, μa	Wave II $E_{h/2}$, v.	Wave II i, μa.	Notes
63	−0.03	13			a,e
63	− .03	12			a,e
99	− .02	44			a,e,b
96	− .08	25	−0.49	38	a,e,b
100	− .2	9	− .6	9	a,e
100	− .2	10	− .6	40	a,e
100	− .13	27	− .96	30	a,e,b
63	.06	3.5	1.56	7.2	f
63			1.62	7.1	f
63	.07	3.4			f
99	.07	5.7	1.55	9.6	f
66	.07	4.2	1.45	6.0	f
66	.06	3.6	1.46	6.0	f
96		4.9	1.43	7.9	f
77	.05	5.0	1.45	13.0	f
62	.02	4.3	1.47	9.1	f
100	.02	6.2	1.43		f
100	.06	6.0	1.51	17.5	f
100	.04	6.3	1.45	15.0	f,b
70	.05	5.0	1.48	10.7	f,b
100	.02	7.0	1.43	15.0	f,c
70	.03	5.8	1.44	11.1	f,c
100	.10	5.4	1.54	10.4	f,d
70	.02	5.0	1.46	7.4	f,d

[a] Maximum occurs. Tabulated i and E for first wave are peak values. [b] About 28 mM in H_2O. [c] About 40 mM in H_2O. [d] About 40 mM in H_2O and 5 mM in HCl (added as the concentrated acid). [e] Cathodic branch. [f] Anodic branch. [g] All solutions saturated with KCl (*ca.* 5 mM) and run at −25°, using the DME *vs.* the mercury–calomel pool.

Effect of High Solution Resistance.—Solution resistances in SO_2 exceeded 5K ohms and frequently were as high as 50K ohms, resulting in iR corrections of the order of several hundred millivolts and necessitating more precise resistance measurement than is ordinarily the case in polarography.

If maximum currents are used, the resistance must be measured at the corresponding point. Detecting final bridge balance just before the drop separates from the DME capillary requires an

(12) At the experimental temperature of −23°, A and B are calculated[18] to be 248 and 2.68, respectively. Extrapolation of the equivalent conductivity data for triphenylchloromethane at infinite dilution[18a] yields the value of 150 ohms^{-1}. No data could be found for ionic conductivities in liquid sulfur dioxide. However, results accurate to a few per cent. can be expected from calculating the transference number for chloride ion by Walden's rule,[10] which states that the function $\eta\lambda_0$ is approximately constant in all solvents and independent of temperature. Since λ_0 is 76.3 ohms^{-1} for chloride ion in water[10] at 25° (viscosity = 0.895 centipoise), its ionic conductance in sulfur dioxide is 138 ohms^{-1}.

TABLE III

POLAROGRAPHY OF KI, NH_4SCN AND KBr IN LIQUID SULFUR DIOXIDE[g]

Solute	Concn., m*M*	Temp., °C.	Hg head, Cm.	Wave I $E_{h/2}$, v.	Wave I i, μa.	Wave II $E_{h/2}$, v.	Wave II i, μa.	Notes
KBr	67	−25	80	0.09	1.8	1.7	2.4	*a, d*
KI	60	−30		.25	90			*a, d, f*
	29	−33		.30	72			*a*
				.28	78			*a*
				.16	80			*a*
				.18	86			*a*
					75			*a*
					75			*a*
NH_4SCN	3.3	−25	65	−0.58	49			*b, c*
				− .65	39			*b*
				− .47	23	13	−2.4	*b, e*
				− .47	22			*b*
				− .47	22			*b*

[a] Anodic branch. [b] Cathodic branch. [c] No waves observed in anodic branch. [d] No waves observed in cathodic branch. [e] Only case in which two waves were observed for this solute. [f] Mercury head was not recorded for this solute. [g] Run using the DME *vs.* the mercury–calomel pool.

unusual degree of personal judgment, which may cause an error in $E_{1/2}$ of several millivolts, if solution resistance is about 10K ohms and the current exceeds 10 μa. This difficulty is not encountered with the CPE; the effect of high solution resistance is here related to the theory of the method,[14] and is considered in the study of triphenylchloromethane.[7]

Electroactivity of the Alkali Halides.—Data (Tables II and III) on the electrolysis at the DME of several alkali halides and a pseudohalide, were gathered during apparatus development, and should only be considered as semiquantitative.

The most extensive study was of KCl in saturated solution (about 5 m*M* at 0°). The curves had the ragged appearance mentioned earlier with indifferent current reproducibility; $E_{h/2}$ shows little variation. In the cathodic curve, a large maximum occurs at *ca.* −0.1 v., and a very poorly defined wave at *ca.* −0.6 v.; heights of both are profoundly affected by the addition of water. Since both are also observed before adding water, it is possible that the KCl used contained a minute amount of water. Cathodic waves were not observed for any other alkali halide; polarography of water by itself leads to no electroactivity. These facts suggest interaction between KCl and water in SO_2. Two anodic waves occur at *ca.* 0.05 and 1.45 v.; the more positive is twice the height of the other. Current reproducibility was insufficient to permit precise determination of its proportionality to $h^{1/2}$, although lower currents do correspond to lower mercury heads. Water and HCl (added as the concentrated acid) had little effect on either current or $E_{h/2}$.

KI shows one anodic wave (*ca.* 0.25 v.) and KBr two (*ca.* 0.1 and 1.68 v.). The behavior of the three halides is thus consistent with their chemical activity; the first anodic wave occurs at 0.05, 0.1 and 0.25 v. for KCl, KBr and KI, respectively, and the second at 1.45 and 1.68 for KCl and KBr, respectively (a second KI wave would occur at a higher potential than was available). These waves may result from a process similar to that postulated in the case of triphenylchloromethane,[7] *i.e.*, perhalide formation, but the available evidence is inconclusive.

NH_4SCN behaves unlike the alkali halides; it gives two cathodic waves at *ca.* −0.5 and −2.4 v.; the latter was only observed once. The consistent decrease in current magnitude (all runs were made in the same solution over a period of several days) may indicate a reaction, *e.g.*, with the cell mercury, which slowly decreases the NH_4SCN concentration.

Electroactivity of Other Solutes.—2-Bromopropanoic acid (Table I) showed no activity; there was some indication of a current-producing process when a small amount of water was added. The need for water for electrochemical reaction is emphasized by the absence of reaction in dibromosuccinic acid. Unlike the 2-bromoalkanoic acids, which undergo a substitution reaction (H for Br) at an electrode in aqueous solution,[15] dibromosuccinic acid undergoes an elimination reaction, splitting out Br.[16]

With Bu_4NI, as soon as electrolysis commenced, an enormous cathodic current was produced and a deep wine-red color appeared, which soon obscured the DME tip. Iodine is wine-red in liquid sulfur dioxide, but it is difficult to account for its electrochemical formation; Bu_4NI itself is colorless. Formation of a solvate, $(Bu_4N)_2(SO_2)_x$, which is electrochemically reasonable, may account for the color.

The necessity for keeping solutions perfectly dry was perhaps unduly emphasized in the present work. In many cases, trace quantities of water had no adverse effect on the quality of the data. In precise conductivity measurements on sulfur dioxide solutions, a high standard of dryness must be maintained, but it appears that this is not always the case in voltammetry. Relaxation of the dryness requirement would allow modification of the apparatus to permit greater experimental convenience.

(13) (a) N. N. Lichtin and H. P. Leftin, *J. Phys. Chem.*, **60**, 160 (1956); (b) G. P. Luchinskii, *J. Phys. Chem.* (*USSR*), **12**, 280 (1938); (c) A. L. Vierk, *Z. anorg. Chem.*, **261**, 279 (1950).

(14) M. M. Nicholson, *J. Am. Chem. Soc.*, **76**, 2539 (1954).

(15) P. J. Elving, J. M. Markowitz and I. Rosenthal, *J. Electrochem. Soc.*, **101**, 195 (1954).

(16) P. J. Elving, I. Rosenthal and A. J. Martin, *J. Am. Chem. Soc.*, **77**, 5218 (1955).

Reference Electrode Polarization.—The contingency of concentration polarization[17] of the reference electrode is seldom considered in conventional polarography since stability of reference electrode potential is readily ensured by introducing a large excess of an electrolyte, to one of whose ions the electrode is reversible, and by passing only small currents through the cell. There are several reasons for considering reference electrode polarization: no discussion of the effect on polarograms of such polarization is apparently available in the literature; Cruse[6] has reported related effects on the potentials of certain electrodes, including the calomel, in liquid sulfur dioxide; the ideas developed will be helpful in interpreting some features of the potential data.

In absence of a background electrolyte, a solute ion will evidently participate in the reference electrode reaction, causing the latter's potential to be concentration-dependent. Consider the Ag–AgCl electrode as anode in the polarographic cell

$$\text{In}/\text{C}^+, \text{Cl}^-/\text{AgCl}/\text{Ag} \qquad (15)$$

where In is an indicating electrode at which the cation C^+ is being reduced.

The chemical reaction at the reference electrode is

$$\text{Ag} + \text{Cl}^- = \text{AgCl} + \text{e} \qquad (16)$$

Since the reversible potential for this half-cell is

$$E = E^0 + (RT/F) \ln a_{\text{Cl}^-} \qquad (17)$$

an increase in solute activity (or concentration) will cause the electrode potential to become more positive, and will widen the gap between reference and fixed (negative) cathode potentials ($E_{1/2}$ for the C^+ reduction is experimentally nearly always independent of concentration). A plot of measured $E_{1/2}$ *vs.* ln concentration should show a positive slope of RT/F; this would also be true for an analogous anodic process.

If concentration polarization can occur, a more subtle process will occur during the recording of each polarogram. Consider the same cell with the reference electrode as anode. At any point on the polarographic wave for a solution of Cl^- activity a without concentration polarization, the applied potential

$$E_{\text{app}} = E_{\text{In}} - [E^0 + (RT/F) \ln a] + iR \qquad (18)$$

where E_{In} is the assumed fixed cathode potential corresponding to the rate of discharge of reducible ions measured by the current i, and R is the solution resistance. Concentration polarization corresponding to i will decrease the surface concentration at the anode to a'; the actual applied potential is then

$$E_{\text{app}}' = E_{\text{In}} - [E^0 + (RT/F) \ln a'] + iR \qquad (19)$$

The difference indicates the concentration polarization

$$\Delta E_{\text{p}} = E_{\text{app}}' - E_{\text{app}} = (RT/F) \ln (a/a') \qquad (20)$$

Since $a' < a$, ΔE_{p} is positive. Thus, concentration polarization effectively augments the (negative) applied potential at every value of the current; $E_{1/2}$ measurements based on the applied potential will therefore be low by the magnitude of the polarization. If the reference electrode functions as a cathode, the mathematical description is similar, except that ΔE_{p} is negative since now $a' > a$; however, the applied potential is now positive, and concentration polarization leads again to a diminution of the measured potential with respect to the true potential throughout the wave.

Additional information about the magnitude of the concentration polarization may be obtained by assuming a linear concentration gradient at the reference electrode-solution interface, *i.e.*

$$i = K(a - a') \qquad (21)$$

where K is a constant depending on electrode area, Cl^- diffusion constant and diffusion layer thickness, and a' is the surface activity of Cl^-. Substitution into equation 20 gives

$$\Delta E_{\text{p}} = -(RT/F) \ln [1 - (i/aK)] \qquad (22)$$

By expanding the logarithm in Taylor's series and, since the polarization is assumed small, retaining only the first term, the polarization is approximately

$$\Delta E_{\text{p}} = iRT/aKF \qquad (23)$$

Thus, for small polarization effects, the polarization is directly proportional to the current; in a given polarogram, distortion of the wave from this effect becomes progressively greater up to i_l. A background electrolyte increases a without a corresponding increase in i, thus suppressing the polarization. Since i at $E_{1/2}$ is proportional to a, an increase in concentration of electroactive material will not affect the extent of polarization at $E_{1/2}$; consequently, concentration polarization at the reference electrode cannot be detected from the variation of $E_{1/2}$ with concentration.

Concentration polarization at the reference electrode may also be kinetically controlled, related, *e.g.*, to the slowness of the solute dissociation process. In this situation, the argument would be the same except that K would be interpreted as proportional to the rate constant for the forward reaction in

$$\text{CX} \rightleftarrows \text{C}^+ + \text{X}^- \qquad (24)$$

Means for distinguishing between these possibilities are not available from the present data; addition of an indifferent salt to the CX solution would reduce polarization whether it derives from kinetic or diffusion effects.

Experimental

Materials.—Anhydrous grade sulfur dioxide (Matheson; stated purity: 99.988%; stated impurites: 0.002% H_2O, 0.010% non-condensable gases) was treated to remove H_2O, SO_3 and non-condensable gases. SO_2 from tank O (Fig. 1) is bubbled through concentrated sulfuric acid *in vacuo* (M) (safety trap N protects tank from accidental acid surges), passed through two 2 × 45-cm. columns (L) containing P_2O_5 suspended on glass wool, and condensed in storage trap K, containing a few grams of P_2O_5 and cooled by a saturated Dry Ice–2-propanol bath; K has a flat, enlarged bottom which permits mixing of condensed SO_2 and P_2O_5 by the sealed-in-glass impeller of a magnetic stirrer. When sufficient SO_2 has been condensed, the bath is removed and the SO_2 is allowed to warm up under rapid stirring until its vapor pressure equals atmospheric pressure. The first

(17) Concentration polarization is generally defined as the change in electrode potential caused by local concentration changes near the electrode surface during the passage of current. If the current passed is sufficiently large and the rate of diffusion of electroactive species to or from the electrode surface sufficiently slow, the surface concentration will be sufficiently different from that in the bulk solution to cause an appreciable shift in potential.

portion of vapor to distil at this pressure is discarded *via* the blowoff system (J, P); the middle fraction is transferred by vacuum distillation to the appropriate spot in the apparatus for utilization in measurement; the last few ml. are discarded. Purity of SO_2 thus obtained was checked by its vapor pressure–temperature relation from −40 to −10°; agreement with literature data[18] was excellent.

Oil-pumped nitrogen (Linde; specified to contain less than 0.03% H_2O) was dried by passage over Drierite and P_2O_5. Mercury was chemically purified, dried and triple distilled. Reagent grade inorganic compounds were suitably dried. Apiezon M stopcock lubricant and Dow-Corning high vacuum stopcock grease were used to lubricate stopcocks and standard taper joints.

Triphenylchloromethane (I) and *p*-xenyldiphenylchloromethane (II) had been synthesized at the University of Michigan. I, recrystallized from 70:30 benzene–AcCl and then from petroleum ether (75° fraction), gave white crystals (m. 111–112°; lit. 111–113°). II, crystallized several times from benzene–AcCl and then washed with petroleum ether, gave white crystals, which decomposed to a red oil at 135–140°. Tetra-*n*-butylammonium iodide was provided through the courtesy of Dr. P. A. S. Smith. 2-Bromopropanoic acid and thionyl chloride were Eastman Kodak white label. *meso*-α,α'-Dibromosuccinic acid was synthesized.[17]

Gas-Handling System.—The glass vacuum line (schematically shown in Fig. 1) consists of a pumping section (A–C), a purification section (K–O), a main manifold with attachments, and a vent system.

Evacuation is accomplished with a two-stage mercury diffusion pump B (fore-pressure provided by mechanical pump A). After prolonged use, virtual leaks developed due to the slow release of strongly adsorbed SO_2 from the main manifold glass surface, resulting in a slow pressure rise on stopping the pumps; since this is due to the experimental material, the effect is not important. Cold traps C protect pump A and prevent distillation of mercury into the main manifold, which is a 2 × 120-cm. tube connected through a large stopcock to the pumping section; the opposite end has a 24/40 outer joint for the DME cell. Pressures are measured with McLeod gauge D (H. S. Martin Co.) and mercury manometer E.

A vent system allows for safety, and pressure regulation and manipulation. The blowoffs are mercury U-tube manometers; the mercury height can be adjusted by a leveling bulb connected to a T-seal at the U bottom. The U-tube arm sealed to the vacuum line is at least 76 cm. and contains a check valve or trap. The vent arms are connected *via* manifold P to a hood. Liquid SO_2 was disposed of by allowing it to distil off as a gas *via* the blowoff system, using a mercury level of about 1 cm. as a seal.

Dropping Mercury Electrode.—The most satisfactory cell (Fig. 2A) is a 2.5 × 20-cm. tube, whose lower portion is enlarged to 5-cm. diameter and is flattened except for a slight center bulge; the top is an outer 29/42 joint for attaching the cell head; a capped tube, joined just above the enlarged portion, is used for introducing solid solutes; a narrower tube, similarly joined, is closed near the top with a capillary-bore stopcock, whose end is capped with a serum-bottle rubber stopper, through which liquid solutes are added *via* a long hypodermic needle.

The head is a glass tee, whose 24/40 side joint fits the vacuum manifold (I, Fig. 1); the lower joint fits the cell top; the upper 19/38 outer joint holds the DME. A 6-mm. glass tube running downward from a point near the center of the cross is closed at the other end by sealing in a short length of platinum wire; the latter is less than a millimeter from the cell bottom; filling this tube with mercury provides contact to the pool electrode.

The DME, constructed of capillary tubing, drawn to a fine lumen and cut at a point beyond the narrowest section,[2] is sealed to a tube of the same outside diameter (8 mm.), which is ring-sealed through a 19/38 inner joint and connected to a mercury reservoir by Tygon tubing.

Cylindrical Platinum Electrode.—The CPE cell (Fig. 2B) is constructed from a 100-ml. Pyrex graduated cylinder by closing the lower end with a test-tube bottom and sealing a 24/40 outer joint to the upper end. A side tube terminates in a stopcock and a 14/35 outer joint for attachment to the

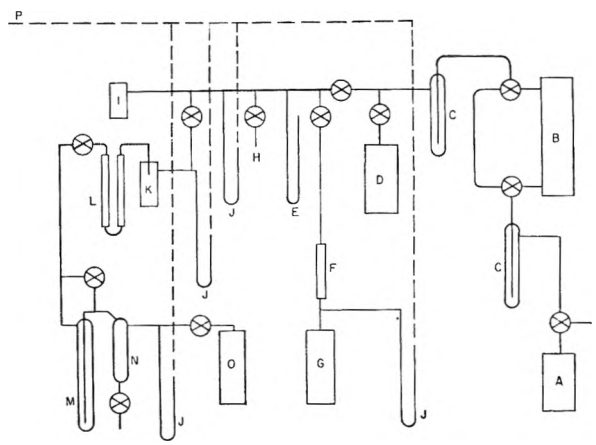

Fig. 1.—Schematic diagram of vacuum line apparatus for voltammetry in liquid sulfur dioxide: A, mechanical pump; B, diffusion pump; C, cold traps; D, McLeod gauge; E, absolute mercury manometer; F, nitrogen dryer; G, nitrogen cylinder; H, utility outlet; I, cell assembly for dropping mercury electrode; J, blow-off manometer; K, sulfur dioxide purification trap; L, phosphoric anhydride tubes; M, sulfuric acid bubbler; N, safety trap; O, sulfur dioxide cylinder; P, blow-off vent system.

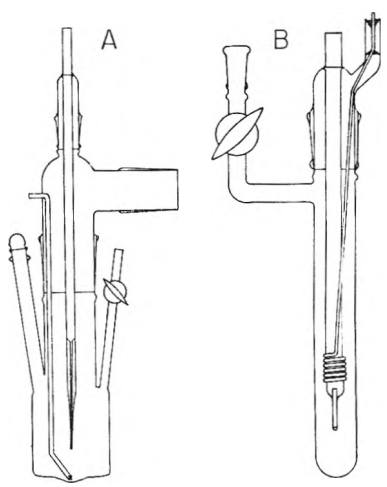

Fig. 2.—Cell assemblies for use with liquid sulfur dioxide: A, dropping mercury electrode; B, cylindrical platinum electrode,

manifold (H, Fig. 1). The engraved volume scale is calibrated.

The electrode assembly is built around a 24/40 inner joint. The indicating electrode is a 1.5-cm. × 1.10-mm. platinum tube, sealed into the end of an 8-mm. tube ring-sealed in the cell cap and coated at its lower end with a small Pyrex glass bead to eliminate end effects and to make the electrode geometry cylindrical.[16] The Ag–AgCl reference electrode is a 10-turn silver wire helix upon whose surface AgCl is deposited electrolytically.[19] A sufficiently long length of silver wire is left and is brought out through the capillary in the cell cap; the space is filled with Apiezon Wax W to make the cap vacuum-tight.

Temperature Control.—DME curves were run at −15, −25° or as specified, using 2-propanol–Dry Ice baths, which were manually controlled *via* frequent temperature checks and Dry Ice addition. CPE curves were run in the equilibrium liquid–solid CCl_4 bath of −22.6°, which was brought to temperature by adding liquid nitrogen. Both baths were kept in well stirred 5-l. Dewar flasks; temperature variation was ±0.3° for manual control (with more attention, better control was achieved) and less than ±0.1° for the CCl_4 bath.

Instrumentation.—Current-potential curves were re-

(18) R. T. Sanderson, "Vacuum Manipulation of Volatile Compounds," John Wiley and Sons, Inc., New York, N. Y., 1948.

(19) R. G. Bates, "Electrometric pH Determinations," John Wiley and Sons, Inc., New York, N. Y., 1954.

corded by a Sargent Model XXI polarograph; trial runs utilized the full 6 v. of available potential both positively and negatively compared to the reference electrode. Because of the high solution resistance, the potential actually applied at the indicating electrode in the presence of large current flow was possibly no more than a volt or so. The charging current was generally of the order of a microampere. Solution resistance was measured with a Jones-type conductivity bridge (estimated error: ±0.1%).

DME Procedure.—About 5 ml. of mercury was added to the thoroughly dried cell; 0.5 g. of prepared calomel was placed on it. The entire system was evacuated for an hour at the lowest available pressure; SO_2 was then condensed in K (volume of 30–70 ml.) and distilled into a graduated cylinder at H. The cold bath was removed from the latter and the SO_2 allowed to warm up to the temperature of the subsequent electrical measurements; after noting the liquid volume, the SO_2 was distilled into the cell.

The cell was warmed to operating temperature; the pressure in the system raised to a value slightly greater than atmospheric by admitting dry N_2, regulated by the main manifold blowoff; the cell cap removed to permit rapid introduction of a solute sample (1–100 mg., weighed directly in a short melting point tube) and the DME (care was taken to insure a vacuum-tight seal). The N_2 supply was shut off, and the system flushed several times with SO_2 vapor, using the mechanical pump to reduce the pressure (care needed to avoid flashing some condensed SO_2 into vapor).

An alternative procedure for removing N_2 was to freeze the solution with liquid nitrogen and evacuate the system to a very low pressure. For volumes of a few ml., the freezing procedure is much preferred; the freezing of large volumes, *e.g.*, 50 ml., is inconvenient. Because of possible flashing of the liquid due to the large temperature gradient during cooling and the danger of mechanical and thermal shock, particularly to the metal–glass seals, it was found that the flushing procedure is superior, especially if account is taken of the loss of solvent (*ca.* 1 ml.) by either returning the lost solvent to the cell by distillation from the pump trap or estimating the amount lost and correcting the concentration.

After N_2 removal, several polarographic electrolyses were made at each solute concentration and the electrical resistance measured.

CPE Procedure.—The cell was attached to H, the system thoroughly pumped out, SO_2 distilled directly into the cell, and N_2 introduced at slightly greater than atmospheric pressure. The cell was momentarily opened to introduce the solute, the N_2 shut off and removed by careful flushing, and the cell brought to operating temperature. Both stopcocks connecting cell to manifold were closed, and the entire cell assembly removed and placed in a constant temperature bath. On reaching temperature equilibrium, the solution volume was read and electrical measurements made. For dilution or addition of more solute, the cell was replaced on the vacuum line and the procedures described repeated.

Voltammetric curves were recorded with "renewal" of the solid electrode surface after each electrolysis by use of a moderate frequency alternating current[15]; the "renewal," utilizing the 1000-cycle signal generator of the resistance bridge, was incorporated into the cell resistance measurement which followed each electrolysis. Often, "renewal" treatment periods of 0.5 hr. or more were necessary to secure reproducible curves.

Acknowledgment.—The authors wish to thank the U. S. Atomic Energy Commission and the Office of Naval Research which helped support the work described.

VOLTAMMETRY IN LIQUID SULFUR DIOXIDE. II. BEHAVIOR OF TRIPHENYLCHLOROMETHANE. REDUCTION OF THE TRIPHENYLMETHYL FREE RADICAL

BY PHILIP J. ELVING AND JOSEPH M. MARKOWITZ

Department of Chemistry, The University of Michigan, Ann Arbor, Michigan

Received December 15, 1960

The voltammetric and polarographic behavior of triphenylchloromethane in liquid sulfur dioxide has been investigated, using the stationary cylindrical platinum electrode and the dropping mercury electrode; results with the latter are unsatisfactory due to reaction of mercury with the solute. Triphenylchloromethane gives one cathodic wave and two anodic waves, the more positive of the latter two being larger. The cathodic wave represents the reduction of triphenylmethyl cation to triphenylmethyl. The larger anodic wave is likely due to oxidation of the undissociated solute to the perchloride. No definite assignment can yet be made for the less prominent anodic wave. The fit of the data to Nicholson's equation for the cylindrical platinum electrode and the effect of high solution resistance on such data are discussed.

Since one of the objectives which led to the evaluation of liquid sulfur dioxide as a polarographic and voltammetric medium was the desire to study free radicals, which are often stable in that medium, the behavior of triphenylchloromethane was investigated at the stationary cylindrical platinum electrode, CPE, and the dropping mercury electrode, DME; the Ag/AgCl reference electrode was used with the former; the calomel pool electrode with the latter. The background for such study has been presented.[1]

Behavior at the Cylindrical Platinum Electrode.—The behavior of triphenylchloromethane at the CPE can be interpreted in terms of the theory developed for such an electrode[2]; the equation for the current–potential curve is

$$i = 1.475 \frac{n^{3/2}F^{3/2}}{R^{1/2}T^{1/2}} AD^{1/2}Cv^{1/2}\psi \qquad (1)$$

where n is the number of electrons per molecule electrolyzed; A the electrode area, cm.^{2}; C the solution concentration, moles/cm.^{3}; D the diffusion coefficient, cm.^{2}/sec.; v the polarization rate, *i.e.*, the rate of change of applied potential, v./sec.; and ψ a numerically derived function which measures the concentration gradient at the electrode surface and depends on the variables $(D/nv)^{1/2}/r_0$ and $nF(E - E_{1/2})/RT$, where r_0 is the electrode radius in cm. and E the applied potential.

Equation 1 and the relations[2] of ψ *vs.* E for various values of E predict a i–E curve for cylindric diffusion of form 1 in Fig. 1A.[3] The peak current, i_p, is directly proportional to concentration; $E_{1/2}$

(1) P. J. Elving, J. M. Markowitz and I. Rosenthal, *J. Phys. Chem.*, **65**, 680 (1961).

(2) M. M. Nicholson, *J. Am. Chem. Soc.*, **76**, 2539 (1954).

(3) The data used in deriving this theoretical curve were the following: A, 0.52 cm.^{2}; D, 1.6×10^{-5} cm.^{2}/sec.; v, 3.6 mv./sec.; T, 250°K.; r, 0.055 cm.; and $E_{1/2}$, −0.18 volts.

TABLE I

VOLTAMMETRY OF TRIPHENYLCHLOROMETHANE IN LIQUID SULFUR DIOXIDE[a]

Concn., mM	Wave I E_p, v.	Wave I i_p, μa.	Wave I i_p/C	Wave II E_p, v.	Wave II i_p, μa.	Wave II i_p/C	Resistance, ohms	Notes
				Cathodic branch				
0.104				−0.22	4.1	39	46,100	
.121				− .25	4.8	39	41,400	
.140				− .22	5.3	38	36,900	
.179				− .27	6.8	38	31,800	
.255				− .25	9.7	38	23,100	
1.57				− .40	56	36	7,450	
1.62				− .46	66	41	7,310	b
1.91	−0.074	23	52	− .55	74		6,480	b,c,d,e
1.91	− .086	26	59	− .48	56		5,660	b,c,d,e
				Anodic branch				
0.104	0.69	0.45	4.3	1.38	6.6	64	46,700	
.121	.70	.51	4.2	1.38	7.8	64	41,500	
.140	.67	.63	4.5	1.37	9.5	68	37,000	
.179	.71	.90	5.0	1.30	11	63	32,300	
.255	.65	1.2	4.5	1.28	17	66	23,600	
1.57				1.60	105	67	7,420	f
1.62				1.70	126	78	7,210	b
1.91				1.82	150	80	5,850	b,c

[a] Cylindrical platinum indicating electrode and Ag–AgCl reference electrode at −22.6°. Values are averages of from 2 to 5 runs. Peak potentials are corrected for iR drop. [b] Solution is 2.3 mM in LiCl. [c] Solution is 0.44 mM in p-xenyldiphenylchloromethane. [d] Results fell into two groups at this concentration. Since they differed markedly, averages of both are presented. [e] No attempt was made to resolve the current of the second wave for reasons explained in the text. Values of i_p for wave II in the runs at 1.91 mM represent the total current for both waves. [f] First wave disappears.

can be calculated from i_p, using the ψ function and the curves relating it to potential.

A typical cathodic polarogram for triphenylchloromethane at the CPE in sulfur dioxide, without and with iR drop correction, is generally similar in shape to the theoretical curve (Fig. 1A). The vertical agreement of peak positions is less conclusive than it appears. The peak height is dependent on the choice of D; in the absence of literature values, D was deliberately picked to bring the peaks into coincidence, in order to emphasize that the important difference is in curve shapes, which presumably results from the high solution resistance due to the absence of a background electrolyte. The value of $E_{1/2}$ used was determined by successive approximation; the other data are experimental and instrumental.

The disparity in the curve shapes is due to the theoretical results[2] being derived for constant v; in the present work, the rate of potential increase at the electrode is not uniform in spite of a uniformly increasing potential because of the substantial iR drop. Since the current changes nonuniformly during an electrolysis, the iR correction changes similarly, *e.g.*, consider the applied potential to be distributed between electrode and solution iR

$$E_{app} = E_{CPE} + iR \quad (2)$$

$$\frac{dE_{app}}{dt} = \frac{dE_{CPE}}{dt} + R\frac{di}{dt} \quad (3)$$

$$v = \frac{dE_{CPE}}{dt} = -R\frac{di}{dt} + \frac{dE_{app}}{dt} \quad (4)$$

Evidently, v equals the rate of change of applied potential only when R is negligible (corresponding to the theoretical curve) or when $di/dt = 0$, *i.e.*, at the peak.

Quantitative interpretation of the non-constancy of v poses a difficult mathematical problem. Since the use of Nicholson's relations for calculating $E_{1/2}$ is consequently a doubtful procedure and since it is difficult to estimate D for the solutions used, no general attempt was made to calculate $E_{1/2}$ from the CPE data. Instead, experimental peak potentials are reported. Aside from possible reference electrode polarization which would not be sufficient to influence the data significantly, E_p is only slightly concentration-dependent.

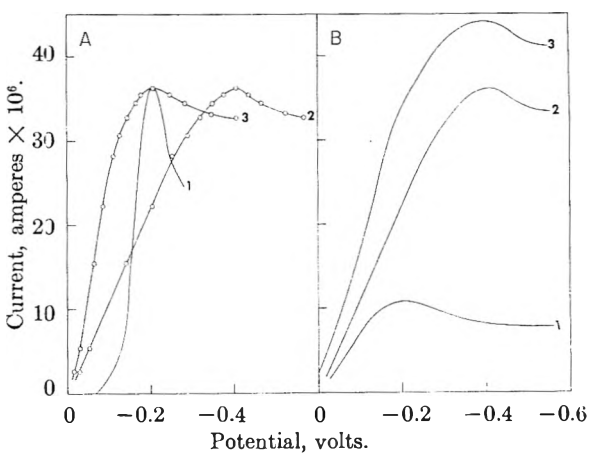

Fig. 1.—Current–potential curves at a stationary cylindrical electrode. (A) One electroactive solute present: (1) theoretical curve; (2) experimental curve; (3) experimental curve, corrected for cell iR drop. (B) Two electroactive solutes present: (1) hypothetical curve for p-xenyldiphenylchloromethane alone; (2) experimental curve for triphenylchloromethane alone; (3) hypothetical composite curve for triphenylchloromethane and p-xenyldiphenylchloromethane.

Effect of Addition of Other Substances.—Figure 1B shows the effect of adding a second solute, present in lower concentration and reducible at less negative potential (Table I runs with

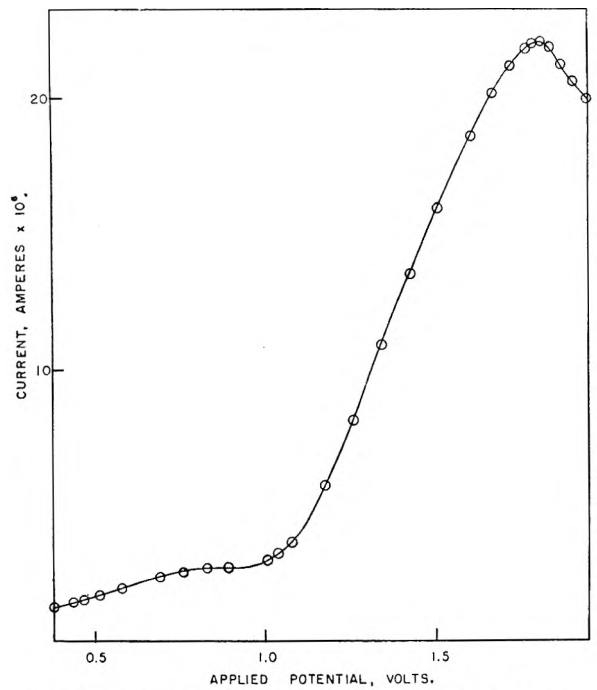

Fig. 2.—Anodic wave for triphenylchloromethane, showing two widely spaced peaks. Potential not corrected for iR drop.

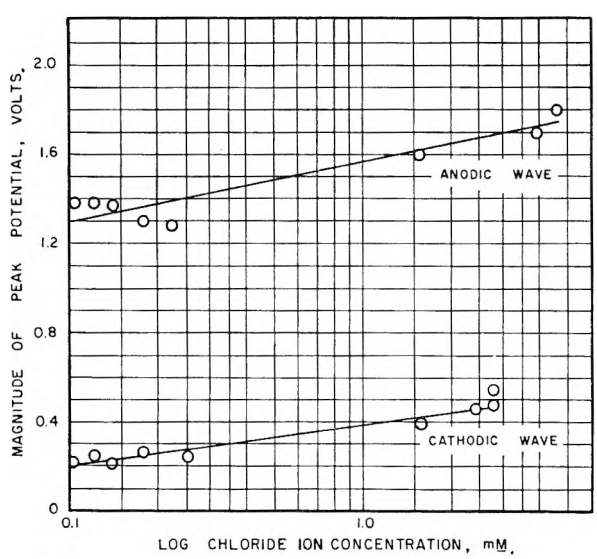

Fig. 3.—Peak potential *vs.* the logarithm of total chloride ion concentration for the cathodic wave and for the more prominent anodic wave of triphenylchloromethane. For the data pertaining to 1.62 and 1.91 mM triphenylchloromethane, the chloride concentration includes contributions from the dissolved LiCl and *p*-xenyldiphenylchloromethane.

p-xenyldiphenylchloromethane present). Curve 3 is the hypothetical sum of polarograms 1 and 2 for each individual solute. The total i_p is not the sum of peak currents for each solute; it is impossible from the composite curve alone to resolve the individual peaks. However, E_p of the composite curve corresponds to the more negative E_p of the individual curves; the slight bulge on the steep portion of the composite curve corresponds to the less negative individual peak.

Figure 2 shows the appearance of anodic polarograms with two widely spaced peaks.

The constancy of i/C over a fifteen-fold concentration range for both cathodic and anodic waves (Table I) is in accord with the theoretical linear dependence of i_p on concentration.[2]

E_p varies linearly with log of total Cl^- concentration (including contributions from LiCl and *p*-xenyldiphenylchloromethane), corresponding to the normal behavior of the reference electrode[1] (Fig. 3). The cathodic and anodic wave slopes are 0.016 and 0.027, respectively; the theoretical slope is 0.048 (the near ratio of the preceding numbers to 1:2:3 is fortuitous; n in RT/nF can only be 1 for the Ag–AgCl electrode).

Nature of Wave-producing Processes at CPE. Cathodic Processes.—In agreement with the results of some early electrolyses of triphenylbromomethane,[4] the cathodic wave can be assigned to reduction of the triphenylmethyl cation

$$(C_6H_5)_3C^+ + e^- = (C_6H_5)_3C \qquad (5)$$

No other reducible entity exists in the solution aside from the solvent itself, reduction of which would not lead to a limiting current. More importantly, production of a similar wave by *p*-xenyldiphenylchloromethane at a slightly less negative potential supports the assignment. The explanation[5] of the electrical conductivity of hexaphenylethane solutions in terms of an equilibrium between triphenylmethyl cation and triphenylmethyl has recently been refuted[6]; the latter work, however, does not preclude the coexistence, at least temporarily, of these two species.

Anodic Processes.—Assignment of the anodic waves is more problematical. Several arguments militate against the obvious possibility that the larger, more positive wave results from oxidation of chloride ion: (a) In a solution without background electrolyte, the limiting current function, i/C, for an anion being oxidized at the anode, when the transference number of the anion is much larger than that of the cation, should increase about 12% over the concentration range of Table I[1]; no such increase is observed (the last pair of concentration points, for which the current function is higher than the average, pertain to solutions containing substantial additions of other solutes). (b) The plot of E_p *vs.* log $[Cl^-]$ (Fig. 3) is linear within experimental error; consequently, the peak potentials accurately reflect $[Cl^-]$. If Cl^- were being oxidized, the limiting current function should reflect the same increase, *e.g.*, i/C for the solution 1.62 mM in triphenylchloromethane and 2.3 mM in LiCl, should be about 66 (the average value for the preceding concentration points) whereas it actually is about 38. (c) No evolution of chlorine gas was observed at the anode, even during very long (several hours) electrolyses.

If oxidation of chloride is rejected as the anodic phenomenon producing the more positive wave, several possibilities remain, none of which seem completely satisfactory. The oxidizable species present in addition to chloride are the undissociated

(4) W. Schlenk, T. Weickel and A. Herzenstein, *Ann.*, **372**, 1 (1910).
(5) L. C. Anderson, *J. Am. Chem. Soc.*, **57**, 1674 (1935).
(6) H. P. Leftin and N. N. Lichtin, *ibid.*, **78**, 2475 (1957).

triphenylchloromethane and the triphenylmethyl radical and anion, produced by the processes

$$2Ag + 2\phi_3CCl = \phi_3C\text{–}C\phi_3 + 3AgCl \quad (6)$$

$$\phi_3C\text{–}C\phi_3 = 2\phi_3C\cdot \quad (7)$$

$$\phi_3C\text{–}\phi C_3 = \phi_3C^+ + \phi_3C^- \quad (8)$$

Reaction 6, a normal heterogeneous reaction, is likely to be very slow (the source of Ag is the reference electrode); consequently, the amount of radical or anion in solution must be very small.[7] Consequently, while the smaller anodic wave may be due to reduction of radical or anion, another explanation is required for the larger wave.

The most likely cause is oxidation of undissociated triphenylchloromethane, followed by reaction of the oxidation product with Cl^- to form a perchloride. Both inorganic and organic perhalides are well known; the alkali perhalides occur as MX_3 and MX_5 (there is some doubt about the true molecular nature of higher perhalides) with the anion composed of either a single or a mixture of halogens. Assuming formation of a simple perhalide, the following reaction scheme may be postulated

$$\phi_3CCl = \phi_3CCl^{++} + 2e \quad (9)$$

$$\phi_3CCl^{++} + 2Cl^- = \phi_3CCl_3 \quad (10)$$

Identification of the reaction product in a voltammetric electrolysis is not normally possible because of the minute current densities used. Attempted identification of the postulated triphenylmethyl perbromide after electrolysis of triphenylbromomethane at high current densities was uncertain.[4] Thus, assignment of the oxidation wave to perhalide formation has yet to be positively established.

On the other hand, the assignment fits the voltammetric results very well. The resulting current function should be independent of the total $[Cl^-]$ to the extent that Cl^- enters the reaction at the electrode (equation 10) in an amount stoichiometrically equivalent to the triphenylmethyl cation. The small increase in the current function on LiCl addition is also explicable. If triphenylchloromethane is completely dissociated in sulfur dioxide,[5] the proposed mechanism requires that the rate of association be rapid compared with the electrode reaction rate, otherwise the former would be rate controlling. Therefore, undissociated triphenylchloromethane probably exists only in the immediate neighborhood of the electrode, and the diffusing species consist of the cation and anion. Consequently, migration effects from both cation and anion contribute to the limiting current, i_l, the cation subtracting from it and the anion adding to it in a complicated manner. The transference numbers previously calculated[1] probably do not apply directly to the present situation, since cation and anion are required by the reaction stoichiometry to react at the electrode in equivalent amounts. Chloride ion may be carrying more than its share of current, since the cation is being forced, as it were, to move upstream. The net effect would be to reduce the magnitude of i_l. Addition of LiCl would then be equivalent to adding a small amount of background electrolyte to the solution, thus increasing the current slightly.

One feature of the anodic data remains unexplained: If the small wave is assigned to oxidation of triphenylmethyl free radical, the reason for its disappearance at higher concentrations is not obvious.

The failure to detect an oxidation wave for *p*-xenyldiphenylchloromethane is likely due either to its being masked by the large triphenylchloromethane wave or to its appearing at a potential greater than that available.

Behavior at the Dropping Mercury Electrode.—Triphenylchloromethane polarographic waves were for the most part clear and relatively free from the irregular drop behavior generally exhibited[1] by the DME in SO_2 and conformed more closely to conventional polarographic wave forms. However, the data for series of runs at different concentrations and mercury heights were not entirely satisfactory, *e.g.*, currents did not vary linearly with concentration. Potentials ($E_{h/2}$ *vs.* calomel reference electrode) in both anodic and cathodic branches at −15° were fairly constant, though scattered. The only trend observable in the cathodic branch at −25° was a moderate general decrease as concentration increased, which is opposite to that theoretically expected from the effect of concentration on the calomel electrode potential; the latter, like the Ag–AgCl electrode,[1] becomes more positive with increasing $[Cl^-]$, so that the polarographic potentials should increase.

Increasing the temperature, as expected, substantially increases the currents observed at any given concentration. The cathodic potentials increase with increased temperature; the anodic do not.

The cause for these current inconsistencies, which exceed in magnitude any reasonable estimate of systematic or accidental experimental error, was found to be an unsuspected reaction of triphenylchloromethane with mercury.

On warming a mixture of mercury, triphenylchloromethane and SO_2, sealed in a bomb tube under vacuum, to room temperature, a copious blue-gray precipitate soon appeared and the solution color changed from its normal lemon yellow to a brownish green. The precipitate contained bound mercury, and probably resulted from the abstraction of chlorine by mercury to form Hg_2Cl_2 and hexaphenylethane. No peroxide formation was observed when the tube was opened and exposed to air; this is consistent with Anderson's observation.[5] Although the reaction is rapid at room temperature, it certainly occurs more slowly at experimental temperatures (−25 and −15°). The current inconsistencies can therefore be ascribed to the slow decrease in solution concentration caused by reaction of the solute with mercury from the pool electrode and, possibly, DME.

Behavior of Calomel Reference Electrode.—The moderate decrease in the cathodic $E_{h/2}$ as concentration increases at −25° cannot be ascribed to

(7) The possibility that reaction 6 went to completion in the experiments described, resulting in the complete consumption of triphenylchloromethane, is contradicted both by the potential data, which shows the presence of chloride ion in constant amount at each concentration, and by the solution resistances, which are constant at each concentration and decrease with each solute addition.

solution depletion by the solute–mercury reaction, since the current, in contrast with the current function, $i/Ch^{1/2}$, actually increases at each nominally greater concentration (nominal concentration equals the "as-prepared" concentration), *i.e.*, while the true solute concentration is less than the nominal one due to depletion, the former, as indicated by the current, is in all cases greater than the last preceding nominal concentration. Although the solute–mercury reaction may so interfere with the normal chemical processes at the reference electrode surface as to produce the potential anomaly, the potential changes observed are more likely part of a more general pattern of behavior for the calomel electrode in sulfur dioxide, first noted by Cruse,[8] who studied the cell

$$Ag/AgCl/SO_2,\ Et_2NH_2Cl/Hg_2Cl_2/Hg \qquad (11)$$

in which the calomel electrode acts as a cathode. For the first few hours, the potential remained fairly constant at 50 mv., which is close to the value calculated from thermal data; subsequently, it increased over a period of 12 hr. to a new and fairly constant value of 280 mv. This aging effect was observed in other cells, using either the calomel or $Hg–Hg_2Br_2$ electrode, but not in cells in which the Ag–AgCl electrode was used with, *e.g.*, a hydrogen electrode. Cruse concluded that the aging is characteristic of mercury–mercurous halide electrodes in sulfur dioxide, and that such electrodes are not suitable for measurements of more than a few hours duration.

The potential change found in the present study, in which the calomel electrode functions as an anode, is logically in the opposite sense to Cruse's observation.

(8) K. Cruse, *Z. Elektrochem.*, **46**, 571 (1940).

Experimental

The material, apparatus and procedures used have been described.[1]

Acknowledgment.—The authors wish to thank the U. S. Atomic Energy Commission which helped support the work described.

NOTES

DISSOCIATION OF MOLYBDENUM(V) CHLORIDE IN CARBON TETRACHLORIDE SOLUTION[1]

By Irving M. Pearson[2] and Clifford S. Garner

Department of Chemistry, University of California, Los Angeles 24, California

Received April 11, 1960

Molybdenum(V) chloride is a blue-black dimeric[3a] solid having normal melting and boiling points[3b] of 194 and 268°, respectively. The dark red-brown vapor apparently consists of $MoCl_5$ trigonal bipyramids,[4] easily decomposed to lower chlorides and Cl_2 under appropriate conditions. Many studies of $MoCl_5$ require specialized handling techniques because of the extreme sensitivity to moisture and oxygen, which form oxychlorides and, respectively, HCl and Cl_2.

We give here observations on the hitherto unreported solubility and dissociation of $MoCl_5$ in CCl_4 solution, as well as on the behavior of $MoCl_5$ in vacuum distillation and the removal of oxychloride contaminants from $MoCl_5$.

Experimental

Argon, Hydrogen, Nitrogen.—Tank Ar (Linde), oil-pumped tank N_2 (Liquid Carbonic Co.) and electrolytic grade tank H_2 (Liquid Carbonic Co.) were each passed through Drierite and Ascarite, then through finely-divided U metal at *ca.* 800° (Ar, N_2) or *ca.* 600° (H_2).

Chlorine, Hydrogen Chloride.—Matheson tank Cl_2 was purified by the method of Downs and Johnson.[5] Matheson tank HCl was dried by passage through $Mg(ClO_4)_2$.

Carbon Tetrachloride.—J. T. Baker "Analyzed" CCl_4 was purified (76.8° normal b.p.) essentially by the method of Wallace and Willard.[6]

Molybdenum(III) Chloride.—$MoCl_3$ (Climax Molybdenum Co.) was boiled with 12 *f* HCl, then washed with absolute ethanol and dried in a vacuum desiccator.

Molybdenum(V) Chloride.—For most of these studies $MoCl_5$ was synthesized[7,8] from purified Cl_2 and Mo metal (obtained by reduction of J. T. Baker "Analyzed" MoO_3 with purified H_2 at 1000°, followed by heating in anhydrous HCl to remove possible oxide impurities). Climax Molybdenum Co. $MoCl_5$ (special lots selected for large lump size) was used in spectrophotometric studies of the dissociation. $MoCl_5$ prepared from MoO_3 and CCl_4 at 400°[9] was supplied by Professor S. Y. Tyree, Jr., and used in oxychloride-removal studies with the same general results as our own $MoCl_5$.

Removal of Oxychloride Contaminants from Molybdenum(V) Chloride.—$MoCl_5$ from the above sources generally had brown and green oxychloride coatings. When coatings were removed mechanically in the best dry boxes available to us new coatings formed rapidly. Distillation in a Cl_2 atmosphere appeared to distil oxychloride with the $MoCl_5$; attempts to fractionate were unsuccessful. Heating *in vacuo* or in N_2 gave essentially no distillation except on approaching the melting point whereupon extensive release of Cl_2 resulted, in accord with findings of Hönigschmid and Wittmann[8] and thermodynamic estimates of Brewer and co-workers,[10] but in apparent conflict with a claim[11] that

(1) Supported by U. S. Atomic Energy Commission under Contract AT(11-1)-34, Project 12.

(2) Electronics Division. The National Cash Register Company, Hawthorne, California.

(3) (a) D. E. Sands and A. Zalkin, *Acta Cryst.*, **12**, 723 (1959); (b) H. Debray, *Compt. rend.*, **66**, 732 (1868).

(4) R. V. G. Ewens and M. W. Lister, *Trans. Faraday Soc.*, **34**, 1358 (1938).

(5) J. J. Downs and R. E. Johnson, *J. Am. Chem. Soc.*, **77**, 2098 (1955); J. J. Downs, Ph.D. Thesis, Florida State University, August, 1954.

(6) C. H. Wallace and J. E. Willard, *J. Am. Chem. Soc.*, **72**, 5275 (1950).

(7) A. Voigt and W. Biltz, *Z. anorg. Chem.*, **133**, 277 (1924).

(8) O. Hönigschmid and G. Wittmann, *ibid.*, **229**, 65 (1936).

(9) K. Knox, S. Y. Tyree, Jr., R. D. Srivastara, V. Norman, J. Y. Bassett, Jr., and J. H. Holloway, *J. Am. Chem. Soc.*, **79**, 3358 (1957).

(10) L. Brewer, L. A. Bromley, P. W. Gilles and N. L. Lofgren, in L. L. Quill (ed.), "The Chemistry and Metallurgy of Miscellaneous

$MoCl_5$ can be vacuum sublimed away from $MoCl_4$ at 120° and the claim that $MoCl_5$ can be vacuum distilled at 150°[12a] or even at 60–70°.[12b] The latter paper also stated that solid $MoCl_5$ and gaseous $MoCl_5$ in equilibrium with it decompose to Cl_2 and solid $MoCl_4$ at 98–162°. Apparently $MoCl_5$ cannot be purified by vacuum distillation at these temperatures unless the distillation is substantially faster than the dissociation.

Repeated extraction of solid $MoCl_5$ with CCl_4 *in vacuo* in a Pyrex apparatus allowing filtration of the solid from the extract and evaporation and re-use of the CCl_4 gave purified $MoCl_5$ with a Cl/Mo atom ratio of 5.00. The red-brown final CCl_4 extracts (including Cl_2 in gas phase) had Cl/Mo atom ratios close to 5, whereas the first CCl_4 extracts were bright red with Cl/Mo atom ratios of 3.4–4.2.

Measurement of Chlorine Produced by Dissociation of Molybdenum(V) Chloride in Carbon Tetrachloride Solution.—In the course of working with $MoCl_5$ in CCl_4 *in vacuo* Cl_2 was found present in amounts grossly in excess of that which could be formed from any O_2 possibly present. Two methods were used (and a third attempted) to measure the Cl_2 formed. Concentrations of Cl_2 in the $MoCl_5$–CCl_4 solutions and in the vapor phase above each solution were deduced from either the Cl_2 in the vapor phase or the total Cl_2 with the aid of the perfect-gas and Henry's laws.[13]

1. **Distillation Method.**—Aliquots (10- or 20-ml.) of $MoCl_5$ (purified by extraction method) in CCl_4 were delivered from an evacuated buret equipped with a bellows-type brass vacuum valve with Cu–Pyrex seals into an evacuated Pyrex evaporator[5] and the CCl_4, Cl_2 and any HCl distilled in 2 min. ("fast") or in 18 min. ("slow") into traps immersed in liquid N_2. The trap contents were distilled into O_2-free aqueous KI, and the I_3^- formed titrated with standard $Na_2S_2O_3$, after which any HCl was determined iodometrically.

2. **Aqueous KI Method.**—Aliquots of the same $MoCl_5$–CCl_4 solutions were delivered into the evaporator, then O_2-free aqueous KI was rapidly added with vigorous stirring and the I_3^- formed titrated with standard $Na_2S_2O_3$. Cl_2 so determined is a measure of the "equilibrium" concentration if the assumptions be made that the $MoCl_5$ is instantaneously hydrolyzed before further dissociation occurs and that oxidation–reduction is negligible here except between Cl_2 and I_3^-.

3. **Spectrophotometric Method.**—Spectrophotometric measurement of Cl_2 in $MoCl_5$–CCl_4 solutions was not considered feasible because of complications. At the suggestion of Professor J. D. McCullough, we attempted to measure the intensity of the Cl_2 absorption band at 328 mμ in known aliquots of the gas phase in apparent equilibrium with $MoCl_5$–CCl_4 solutions. Because of considerable attack of $MoCl_5$ by moisture during the extensive handling the results were useful only in showing independently of the other two methods that Cl_2 is released when $MoCl_5$ dissolves in CCl_4.

Molybdenum and Chlorine Analyses.—$MoCl_5$ and its CCl_4 solutions and residues were hydrolyzed in sealed apparatus with excess 1 *f* NaOH, the Mo oxidized to Mo(VI) with 30% H_2O_2, then excess H_2O_2 and any CCl_4 present removed by boiling. Aliquots of the colorless solutions were used for determining Mo by the α-benzoinoxime gravimetric method[14] and Cl by Clarke's method[15] (satisfactory at *p*H 3.0–3.5 in the presence of Mo(VI)).

Dry Box.—Among several dry boxes used, the best was a Lucite box equipped with an air lock, a Na-arc purification system (No. 106, Caemco Inc., Florida), and two Neoprene gloves treated with Fluorolube M to reduce diffusion of O_2 and moisture into the box. A second pair of Neoprene gloves was worn by the operator. A purified Ar flow was used inside the box. Although the box contained fresh P_2O_5 and gave negative tests[16] for O_2 with liquid Na–K eutectic alloy and with a mineral-oil suspension of sodium benzophenone ketyl for 15–30 min. periods, $MoCl_5$ exposed to the dry-box atmosphere formed coatings within a minute or less.

Results and Discussion

Our experiments show clearly that Cl_2 is released when $MoCl_5$ dissolves in CCl_4 at 2–26°, unlike PCl_5 and in contradiction with the impression gained from the literature that $MoCl_5$ dissolves in CCl_4 without reaction. Because of the fantastic sensitivity of $MoCl_5$ to moisture and the low solubility of $MoCl_5$ in CCl_4, our experiments do not establish the nature of the Mo species formed in the dissociation. $MoCl_3$ appears improbable since CCl_4 equilibrated for days with $MoCl_3$ powder had a solubility of $\leqslant 10^{-6}$ *f* at 25° and our $MoCl_5$–CCl_4 solutions gave no solid phase on centrifugation. Residues from the total distillation of Cl_2 and CCl_4 from $MoCl_5$–CCl_4 solutions were brown-black solids with green discolorations and Cl/Mo atom ratios of 3.35–3.37, suggesting the presence of oxychlorides and possibly $MoCl_4$ (attack of $MoCl_5$ by moisture in at least one distillation was shown by finding 0.106 mmole of HCl in addition to 0.066 mmole of Cl_2). Thermodynamic estimates of Brewer, *et al.*,[10] and our own data are compatible with dissociation by the path

$$2MoCl_5(soln.) \overset{K}{\rightleftharpoons} 2MoCl_4(soln.) + Cl_2(soln.)$$

$$Cl_2(soln.) \rightleftharpoons Cl_2(g)$$

for which $K \sim 0.2$ *M* at 2–26° from our aqueous KI data.

The degree of dissociation α of $MoCl_5$ in CCl_4 in the presence of a vapor phase is affected by the ratio of vapor volume V_g to liquid volume V_l. Since we are uncertain of the dissociation stoichiometry, the results are given in Table I in terms of β, the ratio of total mmoles of Cl_2 found to the initial apparent mmoles of $MoCl_5$. If $MoCl_5$ dissociates to Cl_2 and either $MoCl_3$ or an equimolar mixture of $MoCl_2$ and $MoCl_4$, β will be equal to α; in all other cases β will be less than α.

TABLE I

DISSOCIATION OF $MoCl_5$ IN CCl_4 SOLUTION

Method[a]	Temp., °C.	V_g/V_l	$(MoCl_5)_0$, m*f*	β
Fast dist.	~23	..	11.2	0.57
Slow dist.	~23	..	5.6	.59
Aqueous KI	2	21.8	6.6	.45
Aqueous KI	26	16.3	5.1	.46

[a] See Experimental.

The values of β obtained by the two methods are in rough agreement. As expected, β is larger in the distillation experiments than in the aqueous KI experiments, which presumably more nearly indicate the equilibrium conditions. A Soviet group[12a] has interpreted their data on the partial pressure of Cl_2 over solid $MoCl_5$ at 98–162° in terms of dissociation of $MoCl_5(g)$, in equilibrium with $MoCl_5(s)$, into $MoCl_4(g)$ and $Cl_2(g)$; from their dissociation constants we have estimated α to be 0.76 at 162°, 0.53 at 98°, and, by extrapolation, 0.09 at 25°. Although comparison of our β-

Materials: Thermodynamics," McGraw-Hill Book Co., Inc., N. Y., 1st ed., 1950, Paper 8, pp. 276–311.

(11) D. E. Couch and A. Brenner, NES Report No. 5326, June 14, 1957, p. 11.

(12) (a) S. A. Schukarev, I. V. Vasil'kova and B. N. Sharupin, *Zhur. Obshchei Khim.*, **26**, 2093 (1956); (b) Vestnik Leningrad Univ., **14**, No. 10, *Ser. Fiz. i Khim.*, No. 2, 72 (1959).

(13) Henry's law constants were calculated from the data of W. J. Jones, *J. Chem. Soc.*, **99**, 392 (1911), and N. W. Taylor and J. H. Hildebrand, *J. Am. Chem. Soc.*, **45**, 682 (1923).

(14) H. B. Knowles, *Bur. Standards J. Research*, **9**, 1 (1932).

(15) F. E. Clarke, *Anal. Chem.*, **22**, 553 (1950).

(16) T. R. P. Gibb, Jr., *ibid.*, **29**, 584 (1957).

values with these α-values would be more meaningful if we could extrapolate our values to zero V_g/V, and if the α-values had been obtained in the absence of solid $MoCl_5$, the comparison suggests that the degree of dissociation is substantially greater in CCl_4 solution than in the vapor–solid system at the same temperature, providing the dissociation stoichiometry is the same.

The distillation data suggest that the dissociation of $MoCl_5$ in CCl_4 solution is fairly rapid.

The literature implies that $MoCl_5$ is fairly soluble in CCl_4 at room temperature. We find the solubility to be only *ca.* 0.011 *f* (at a vapor-to-liquid volume, which affects the solubility slightly, of 5).

Acknowledgments.—Our thanks are due Professor S. Y. Tyree, Jr., University of North Carolina, for sending us a sample of his $MoCl_5$ and Climax Molybdenum Company, New York, for donation of $MoCl_5$ and $MoCl_3$ samples. Assistance with some of the apparatus by Mr. Glenn Crabbs is gratefully acknowledged.

A METHOD OF PHASE STUDY IN SOME TERNARY LIQUID–SOLID SYSTEMS[1]

BY E. L. HERIC

Department of Chemistry, University of Georgia, Athens, Georgia

Received September 6, 1960

Often the major barrier to a study of phase equilibrium is the lack of a desirable analytical procedure.[2] For ternary liquid–solid systems in particular, the commonly used method of Schreinemakers[3] requires that the weight per cent. of at least two of the three components in each phase be determined. Some of the analytical difficulty may be eliminated by use of the method of algebraic extrapolation.[4] The latter still requires that the weight per cent. of two of the components in the solution phase be determined, however, and thus may be of limited use where analysis presents difficulty.

Analysis for one of the components in the solution phase is frequently comparatively simple. If, for example, the system consists of water and two salts whose anhydrous forms are thermally stable, the weight per cent. water in the solution phase may be determined by evaporation of a weighed fraction.

A method of phase study of ternary liquid–solid systems requiring the determination of the weight per cent. of but a single component in only the solution phase would be useful in some instances. Such a method is presented here, being based upon arguments stated earlier.[5] Application of the method to the systems potassium chloride–sodium chloride–water (I) and sodium bromide–sodium nitrate–water (II) at 25° is described.

The Method

Consider the triangular phase diagram (temperature and pressure constant) of a ternary system composed of water and two salts, the components identified, respectively, as 1, 2, and 3. Assume a tie line joining a solid phase D with the solution A in equilibrium with the solid. This tie line is the locus of points of mixtures from which the phases A and D will form at equilibrium. Consider two such mixtures on this tie line, B and C. If the points B and C are fixed, the direction of the tie line is known, although this would not fix the location of either A or D. If, however, any one of the coördinates A_1, A_2 or A_3 of A were also known,[6] that point would be fixed. This follows from the linearity of tie lines, which requires that

$$\frac{A_1 - B_1}{B_1 - C_1} = \frac{A_2 - B_2}{B_2 - C_2} = \frac{A_3 - B_3}{B_3 - C_3} \qquad (1)$$

In like manner knowing any one of the coördinates D_1, D_2 or D_3 suffices to fix point D, because

$$\frac{D_1 - B_1}{B_1 - C_1} = \frac{D_2 - B_2}{B_2 - C_2} = \frac{D_3 - B_3}{B_3 - C_3} \qquad (2)^7$$

Thus in order to apply the method described here, the following must be known: (1) the location of point B, (2) the location of point C, (3) one coordinate of point A, (4) one coördinate of point D.

The first of these is available upon synthesis of mixture B. While in principle C could also be established by synthesis, this would be highly impractical. Instead that point is found indirectly, as described below, after determination of the third quantity. By the methods used here the third quantity is A_1. It is determined by evaporation to dryness of a weighed fraction of the solution phase of mixture B. The fourth quantity is determined as in the method of algebraic extrapolation, after the location of point C is fixed. A knowledge of A_1 found for the solution phase of mixture B would fix point C if A_1 were known as some systematic function of the compositions of mixtures. Such a relationship can be established by the determination of A_1 for a series of mixtures having an arbitrary but fixed weight per cent. water and variable ratios of the two salts, *i.e.*, variable $C_2/C_2 + C_3$ at constant C_1. Because the location of point C on the tie line is, in principle, arbitrary, C may be considered a member of the series of mixtures at constant C_1. Thus data are available for a reference plot of A_1 *vs.* $C_2/C_2 + C_3$ at known C_1. For a value of A_1 determined for the solution phase of mixture B it is thus possible to fix the composition of the corresponding point C from this plot; points B and C must have the same A_1 value if they lie on the same tie line. A determination of A_1 for a number of such mixtures as B thus fixes corresponding points C on the same tie lines, and defines both the solubility curve and the solid phase.

As there are no tie lines in an invariant region, an invariant point cannot be established by the above method. This point must be fixed instead by extrapolation of the solubility curves to their

(1) Presented at the Southeastern Sectional Meeting of the American Chemical Society, Richmond, Virginia, November 5, 1959.

(2) See, for example: A. N. Campbell and E. M. Kartzmark, *Can. J. Chem.*, **37**, 1409 (1959).

(3) F. A. H. Schreinemakers, *Z. physik. Chem.*, **11**, 80 (1893).

(4) A. E. Hill and J. E. Ricci, *J. Am. Chem. Soc.*, **53**, 4305 (1931).

(5) E. L. Heric, *J. Chem. Educ.*, **35**, 510 (1958).

(6) The coördinates (in weight per cent.) of a point such as A are given by A_1, A_2 and A_3, where the subscripts refer to the components.

(7) Equation 2 will be recognized as the basis of solid phase identification by the method of algebraic extrapolation,[4] except that the composition of the solution phase has been replaced by that of a second mixture lying on the same tie line.

point of intersection with one another. Determination of points on the solubility curves in the vicinity of the invariant point reduces the uncertainty in fixing the latter. The extrapolation is also rendered less uncertain in that the two curves should intersect at the A_1 found experimentally by evaporation of fractions of the solution phase of mixtures in the invariant region.

The applicability of the method will depend upon the nature of the system. As applied here, it obviously would not be applicable to a system where a solubility curve had an essentially unvarying value of A_1. It would also be invalid for systems in which the salts are either volatile or decomposed by heat. In addition for some systems with such characteristics as metastability or a relatively large number of solid phases, it is possible that the method would not be practical.

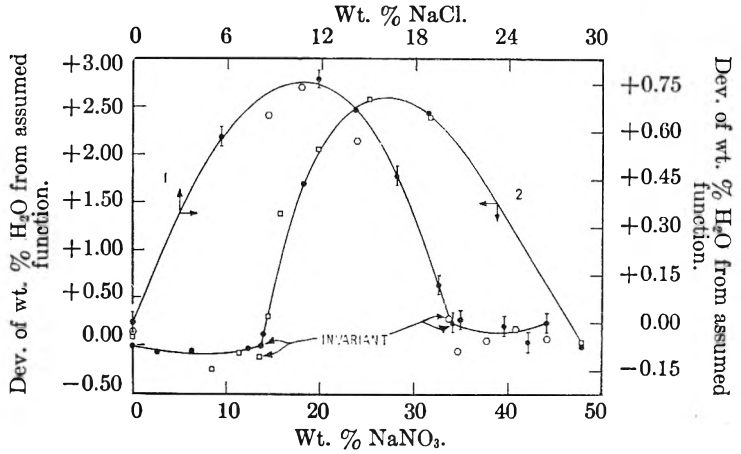

Fig. 1.—Solubility curves expressed as difference plots—(1) the system KCl–NaCl–H_2O at 25°: ⬭, lit. values[8]; ⬮, present work. (2) The system NaBr–$NaNO_3$–H_2O at 25°: □, lit. values[12]; ●, present work.

Experimental

Salts, ACS or reagent grade, were recrystallized before use and dried until a sample showed no weight loss when heated overnight in a 100° vacuum oven. Salts were stored at 150°. Water was singly distilled and protected from CO_2 during storage. Mixtures attained equilibrium at 25 ± 0.05° while constantly agitated with a magnetic stirring device.

Two types of mixtures are required, corresponding to either B or C as identified above. To distinguish between the two, the former will be referred to as scanning mixtures and the latter as reference mixtures. While data for the systems were available from the literature, this fact was essentially ignored to simulate conditions which might be encountered in unknown systems. Before preparing the mixtures a crude preliminary study of the solubility curves was made by adding water to known mixtures of the two salts, with stirring, until the solid phase had been reduced to a few small crystals. This is a convenient method of establishing optimum compositions of the scanning mixtures to be prepared, as well as indicating the general form of the solubility curve. Scanning mixtures were selected so that their compositions would lie near the solubility curves in order to minimize extrapolation errors inherent in the use of equation 1.

The desired values of C_1 to be maintained constant in the reference mixtures were estimated visually during the preliminary crude study. For best results C_1 should approach D_1, but not so closely that insufficient solution phase is available for removal. For the liquid–solid two-phase regions of both systems, a C_1 of 30 to 40 weight % was suitable. Mixtures were prepared by weighing *in situ* each component after it had been added to the solubility bottle. Total weights of scanning mixtures were a minimum of 15 g., while those of reference mixtures were 25 g.; weighings were made to the nearest whole mg. The latter mixtures were in larger amount to minimize the difficulty in obtaining a precisely preselected C_1 value.

Compositions of mixtures used in the determination of the weight per cent. water of an invariant point were not precisely known. As the approximate location of the point was known from the preliminary study, the only restriction in these invariant mixtures was that the composition should fall within the limits estimated for the invariant region. Like values of A_1 for the solution phases of several supposedly invariant mixtures were accepted as evidence that this value had been established.

For both systems 12 hours were sufficient to attain equilibrium. Duplicate determinations from under- and oversaturation indicated no supersaturation tendencies. Fractions removed from solution phases weighed a minimum of 1 g., and were withdrawn through filters. Solution fractions were weighed and dried in 100-ml. glass-stoppered volumetric flasks. These were used because the extended necks prevented loss of solids by spattering during evaporation to dryness. Evaporation was continued at 150° until no further weight loss occurred over a 12 hour period. The minimum weight of residue obtained was 0.6 g. Weighings concerned with solution fractions were made to the nearest 0.2 mg. Duplicate determinations of the weight per cent. water of solution phases agreed typically within ±0.05 weight % water.

Results

System I.—Results are compared with accepted values, using the data of Reinders,[8] in Fig. 1. The comparison is made with a difference plot as departure from the straight lines formed by joining the invariant point to those of the individual salts in water. The plot is based upon the best curves, by eye, drawn through the data obtained in the present work. The solubilities of KCl and NaCl in water reported here are, respectively, 26.43 and 26.44 weight %. Accepted values are 26.30–26.73 for the former[9] and 26.40–26.52 for the latter.[10] For the invariant point the values 11.13, 20.46 and 68.41 KCl, NaCl and H_2O, respectively, compare with accepted values of 11.14–11.26, 20.28–20.44 and 68.42–68.46.[8,11] The directly determined value of the weight per cent. water at the invariant point is 68.35.

By tie line extrapolation the solid phases were identified as the anhydrous salts. Departure of indicated solid composition from the correct values exceeds the theoretical uncertainty for only one tie line. The theoretical uncertainties were calculated assuming that each tie line was anchored at points B with an uncertainty in its direction due to variation of ±0.03 weight % in either C_2 or C_3.

System II.—Results are compared with accepted values[12] in Fig. 1, again using a difference plot.

The solubilities of NaBr and $NaNO_3$ in water reported here, respectively, 48.50 and 47.90 weight %

(8) W. Reinders, *Z. anorg. Chem.*, **93**, 202 (1915).

(9) (a) A. Seidell, "Solubilities of Inorganic and Metal Organic Compounds," third edition, Vol. I, D. Van Nostrand Co., Inc., New York, N. Y., 1941, pp. 750–775; (b) A. Seidell and W. F. Linke, "Solubilities of Inorganic and Organic Compounds," Supplement to the third edition, D. Van Nostrand Co., Inc., New York, N. Y., 1952, pp. 280, 285.

(10) Reference 9a, pp. 1217–1245; reference 9b, pp. 451–452.

(11) (a) W. C. Blasdale, *Ind. Eng. Chem.*, **10**, 344 (1918); (b) K. Uyeda, *Mem. Coll. Sci. Eng. (Kyoto)*, **2**, 245 (1909–1910).

(12) J. E. Ricci, J. Budish and N. Borodulia, *J. Am. Chem. Soc.*, **59**, 868 (1937).

compare with accepted values of 48.22–48.81 for the former[13] and 47.78–47.87 for the latter.[14] For the invariant point the values of 40.87, 13.73 and 45.40 NaBr, $NaNO_3$ and H_2O, respectively, compare with accepted values of 41.05, 13.62 and 45.33.[12] The directly determined value of the weight per cent. water at the invariant point is 45.39. Tie line extrapolation indicated the solid phases to be anhydrous $NaNO_3$ and $NaBr \cdot 2H_2O$. Agreement between errors in indicated solid composition and the theoretical uncertainty again is as noted above.

Discussion

Solubilities of the individual salts agree within experimental error with the accepted values, indicating that purification, drying and equilibrium attainment were adequate. Presumably these procedures were equally satisfactory for the ternary mixtures. One reason for the use of the above systems in testing the proposed method is that their solubility curves show relatively small variations in weight per cent., thereby providing a sensitive test of the method. Consequently, and in view of the internal consistency of the results obtained, it appears that the method is capable of yielding precise data. Only one point reported here for both systems fails to fall on the smoothed solubility curves of Fig. 1.

Comparison with the data of Reinders shows that the present values exhibit in general a lower salt content along both solubility curves. While Reinders' experimental methods were not reported, it is significant that his values for the solubilities of the individual salts also lie toward the higher of the accepted values, indicating the probability of such a systematic disagreement between the two sets of data. The present values show no such systematic disagreement with those accepted for System II.

It is of interest to compare the results of the present method with those obtainable for system I using chemical analysis, the determination of chloride as AgCl. If the analysis were performed on solution fractions of the weights used in this work, say 2.4 g., for a solution of given weight per cent. water a change in weight of AgCl of 0.2 mg. would correspond to a change of 0.03 weight % of either salt.

It should be noted that in the solubility data determined with equation 1 there is an added uncertainty to that in the direct determination of A_1 for the scanning mixtures. This results from the use in equation 1 of interpolated C_2 or C_3 values in determining A_2 or A_3. The former reflect the uncertainty in the A_1 values of the mixtures used in constructing the reference plots. It can be shown, however, that this additional error is small, amounting to as much as 0.01 weight % for only three of the fourteen points so determined. These errors are small because of the proximity of the scanning mixtures to the solubility curves.

Although the solid phases of the systems studied here are of definite composition, extension of the method to systems with solid solution formation should be straightforward.[15]

(13) (a) Reference 9a, pp. 1155–1159; (b) reference 9b, pp. 421–424.
(14) (a) Reference 9a, pp. 1158, 1281, 1403; (b) reference 9b, p. 476.
(15) J. E. Ricci, *J. Am. Chem. Soc.*, **57**, 805 (1935).

HEAT OF COMBUSTION OF ETHYLENE CARBONATE

By Gayton Silvestro and Charles Lenchitz

Propellants Research Section, Picatinny Arsenal, Dover, New Jersey

Received September 1, 1960

The heat of combustion of ethylene carbonate

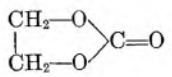

is not reported in the literature. As this compound is used as an ingredient in propellant formulations, an accurate heat of combustion is necessary in order to calculate the thermochemical constants of the propellant.

Experimental

Material.—The ethylene carbonate sample used was obtained from the Jefferson Chemical Company and recrystallized from isopropyl alcohol. This sample has a freezing point of 35.8° and an index of refraction of 1.4151 at 50°.* An examination of columns 2 and 3 of Table II shows that the purity of this sample is 99.97%, based on the carbon content of the ethylene carbonate. Literature values for the melting point of pure ethylene carbonate is inconclusive.

Vorlander in 1894[1] reported a freezing point for ethylene carbonate of 39°. In his analysis for carbon and hydrogen however, an excess of 0.4% carbon and 8% hydrogen is reported. Tilitschejew in 1923[2] obtained a 28% yield of ethylene carbonate in the thermal decomposition of glycolide. His analysis of the sample show melting points ranging between 38.5 and 40° and only 99.08% of the theoretical amount of carbon. In 1933 Hill and Carothers[3] identified ethylene carbonate in the depolymerization of a polyester. A melting point of 39° and an index of refraction of 1.4158 at 50° is reported, but no mention is made of any chemical analysis. It is therefore concluded that none of the reported freezing points can be used with confidence.

In the more recent literature two values are reported, one in the "Handbook of Chemistry and Physics,"[4] the other in the "Condensed Chemical Dictionary."[5] A freezing point of 35.7°. is listed in ref. 4 under the section "Physical Constants of Industrial Chemicals." This value is reported by another manufacturer of ethylene carbonate, but there is no indication of sample purity. The freezing point and index of refraction listed in ref. 5 are 36.4° and 1.4158 at 50° respectively, but here too there is no indication of sample

Table I

Calorimeter Calibration with Benzoic Acid 6318

cal./g.

1 cal. = 4.184 j.

Wt. sample, g.	Δe_1, j./ohm	ΔRc, ohms	q_i, j	q_n, j	E_s, j./ohm
1.12397	13.3	0.165341	69.0	7.6	180,125
1.08490	12.9	.159619	69.0	8.7	180,121
1.09996	13.1	.161747	69.0	8.1	180,208
1.10787	13.1	.162922	69.0	9.3	180,198
1.13797	13.5	.167373	69.0	10.5	180,166
1.00790	12.0	.148366	69.0	3.5	180,032
				Mean	180,142
				Stand. dev. of mean	±26

* Analysis made by the Propellant Analysis Unit of the Arsenal.

(1) A. Vorlander, *Ann. Chem.* (*Liebig*), **280**, 187 (1894).

(2) M. Tilitschejew, *Ber. Deutschen Chem. Gesellschaft*, **56**, 2218 (1923).

(3) J. W. Hill and W. H. Carothers, *J. Am. Chem. Soc.*, **55**, 5031 (1933).

(4) "Handbook of Chemistry and Physics," 41st Edition, 1959–1960.

(5) "Condensed Chemical Dictionary," 5th Edition, Reinhold Publ. Corp., New York, N. Y., 1956.

TABLE II

HEAT OF COMBUSTION OF ETHYLENE CARBONATE

Mol. wt. = 88.062

Sample wt. vac., g. (1)	Theoretical CO_2, g. (2)	CO_2 recovered, g. (3)	Δe_2, j./ohm (4)	ΔR_c, ohms (5)	q, 28°, j. (6)	q_i, j. (7)	q_n, j. (8)	$-\Delta E_b$ 28° j./g. CO_2 (9)
1.60425	2.40522	2.40316	30.6	0.119406	21,513.7	69.0	5.8	8921.1
1.78164	2.67091	2.67106	34.0	.132315	23,840.0	69.0	5.8	8897.3
1.51918	2.27768	2.27775	29.0	.112862	20,334.5	69.0	6.4	8894.3
1.56722	2.34970	2.34799	29.9	.116512	20,992.2	69.0	6.9	8908.2
1.47437	2.21049	2.21037	28.2	.109697	19,764.2	69.0	5.8	8907.7
							Mean	8905.7
							Standard dev. of mean	±4.7

purity. The freezing points listed in the more recent literature, references (4) and (5), although not substantiated, checks more closely the values obtained in this report.

Apparatus and Procedure.—The heat of combustion was determined in a National Bureau of Standards calorimeter, manufactured by the Precision Scientific Company. Resistance measurements were made with Leeds and Northrop type, G-2 Mueller Bridge and a platinum resistance thermometer calibrated by the National Bureau of Standards. All combustions were made in a 340 cc. "Parr" Combustion bomb using purified oxygen. The bath temperature of the calorimeter was maintained at 29.99 ±02° and calibrated with "Parr" Benzoic acid (calorific value 6318 cal./g.). The sample was dried in a vacuum desiccator at room temperature to constant weight. A moisture analysis by the "Karl Fischer" method showed an insignificant quantity of water.

Results

The results of the calibration are listed in Table I. In Table II is listed the results on the heat of combustion of ethylene carbonate. After correcting to 25°, constant pressure, and including a modified "Washburn" correction, calculated according to Prosen,[6] a value of 3179.0 ± 1.7 cal./g. is obtained.

Acknowledgments.—The authors wish to acknowledge the assistance of Mr. R. Trask of Picatinny Arsenal, Dover, N. J.

(6) F. D. Rossini, "Experimental Thermochemistry," Editor, Ch. 6, Interscience Publishers, Inc., New York, N. Y., 1956.

FERROCENE AS A RADICAL "SCAVENGER" IN THE RADIOLYSIS OF CARBON TETRACHLORIDE

BY E. COLLINSON, F. S. DAINTON AND HUGH GILLIS

Department of Physical Chemistry, The University, Leeds, 2, England

Received September 19, 1960

Values of the radical yield, G_R, for the radiolysis of deaerated, liquid carbon tetrachloride, using radiations of comparable linear energy transfer, differ widely. Using diphenylpicrylhydrazyl (DPPH) as a scavenger, Chapiro[1] obtained 19 ± 1; using the polymerization method, Seitzer and Tobolsky[2] found a value of 10.2; with methyl methacrylate to scavenge the primary radicals and ferric chloride to oxidize the polymethyl methacrylate radicals so formed, the highest value obtained was 8.7[3]; and the radiation-induced exchange of Cl^{36}-labelled chlorine with carbon tetrachloride suggests that $G_{CCl_3} = 3.5 \pm 0.35$ and that G_R is perhaps ~ 7.[4] The solubility of ferrocene (Fn) in this solvent, its small positive oxidation potential and ability to react with free radicals,[5] together with the recent evidence of Brand and Snedden[6] that it can be oxidized by iodine atoms generated photochemically, all point to the probability that ferrocene would efficiently scavenge chlorine atoms produced by irradiation of CCl_4 according to the reaction 1

$$Fn + Cl \longrightarrow Fn^+Cl^- \qquad (1)$$

where Fn^+Cl^- denotes ferricinium chloride. We here report our observations on this system.

Experimental

May and Baker carbon tetrachloride was saturated with chlorine and then illuminated for 90 min. with an unscreened medium pressure mercury lamp in a quartz envelope, after which it was washed successively with 5 *M* aqueous NaOH and water, dried over calcium chloride and carefully distilled. Ferrocene was recrystallized once from methanol, dried *in vacuo* and sublimed *in vacuo* at 100° into the empty irradiation cell, the solvent being added subsequently. Co-60 γ-rays were used to provide a dose-rate of 3×10^{19} e.v. $l.^{-1}$ sec. in the solution.

Solutions of 5-ml. volume were degassed thoroughly before irradiation. The concentration of ferrocene during an experiment was followed by decanting the sample into a quartz spectrophotometer cell attached to the irradiation cell. Two sintered glass filters of porosities 2 and 3 between the irradiation cell and the spectrophotometric cell prevented the precipitate (Fn^+Cl^-; see Discussion) which was formed from interfering with the spectrophotometric measurements. The molar decadic extinction coefficients, determined from samples of freshly sublimed ferrocene weighed in air, were: $\epsilon_{max} = \epsilon_{307} = 785$; $\epsilon_{350} = 310$; $\epsilon_{360} = 185$; $\epsilon_{min} = \epsilon_{390} = 67$; $\epsilon_{max} = \epsilon_{450} = 105$. These values agree as nearly as can be determined with those given in curve (e) of Fig. 1 of reference 6.

Results and Discussion

The variation of [Fn] with dose was measured for solutions containing five different initial concentrations within the range 1.2 to 8.3 m*M*. In four of these the change in optical density was measured at three different wave lengths and in the fifth solution at two. The graphs of optical density with dose were linear down to a concentration of ~0.5 m*M* and correspond to $G(-Fn) = 2.34 \pm 0.07$.

(1) A. Chapiro, *J. Phys. Chem.*, **63**, 801 (1959), and earlier papers cited therein.

(2) W. H. Seitzer and A. V. Tobolsky, *J. Am. Chem. Soc.*, **77**, 2687 (1955).

(3) N. Colebourne, E. Collinson and F. S. Dainton, unpublished work.

(4) J. W. Schulte, *J. Am. Chem. Soc.*, **79**, 4643 (1957).

(5) P. L. Pauson, *Quart. Revs.*, **9**, 391 (1955).

(6) J. C. D. Brand and W. Snedden, *Trans. Faraday Soc.*, **53**, 894 (1957).

There was evidence for a small back reaction in that the initial slope at 307 mμ of a solution of initial concentration 1.2 mM was 0.052 whereas the slope for a solution in which the concentration had been reduced by irradiation from an initial value of 8.3 to 1.2 mM was 0.037. The possibility that the irradiation products of pure carbon tetrachloride in some way affect the ferrocene or other products was excluded by direct experiment.

To test the stoichiometry of the reaction, dry methanol was added under vacuum to the residue after the solvent had been pumped off an irradiated solution. The resulting solution was blue, having an absorption peak at 620 mμ. If this peak were due entirely to the ferricinium ion for which $\epsilon_{620} = 362$ in methanol,[6] then the concentration of Fn^+Cl^- present was within 5% of that of the ferrocene destroyed.

When a sufficiently large dose had been given completely to destroy the ferrocene, a small new absorption band (λ_{max} 320 mμ) was observed. This was not due to chlorine which in carbon tetrachloride solution has a spectrum with λ_{max} 332 mμ. Possibly a substituted ferrocene is responsible for this band. If so the yield is small.

If reaction 1 were the only origin of Fn^+Cl^- then we could conclude $G_{Cl} = 2.34$. However it is possible that ferrocene may be oxidized by CCl_3^+ (an abundant ion in the mass spectrum of CCl_4) and CCl_3 (almost certainly the precursor of the C_2Cl_6 found when pure CCl_4 is irradiated). It is also possible that a fraction of such reactive radicals as chlorine atoms may abstract a hydrogen atom, the resultant ferrocene radical being the immediate precursor of the substituted ferrocene thought to be responsible for the spectrum with λ_{max} at 332 mμ. An attempt to measure G(HCl) for a ferrocene solution was unsuccessful due to obscuration of the end-point by Fn and Fn^+Cl^-.

We conclude that although solutions of ferrocene in carbon tetrachloride respond to irradiation in a typical "indirect action" manner the value of $G(-Fn) = G(Fn^+Cl^-) = 2.34$ is merely a minimum value for G_R.

Acknowledgment.—We wish to thank the Rockefeller Foundation and the General Electric Research Laboratory for financial aid.

THE REACTION OF TOLUENE-2,4-DIISOCYANATE WITH *n*-BUTYL ALCOHOL

BY ARMAND DI GIACOMO

E. I. du Pont de Nemours & Company, Eastern Laboratory, Gibbstown N. J.

Received September 12, 1960

Although numerous studies of isocyanate concentration *vs.* time for the reaction of toluene-2,4-diisocyanate (TDI) with a primary alcohol have appeared in the literature,[1-5] no analysis of the data has ever been reported giving the concentrations of TDI, intermediates, and final product throughout the course of the reaction. Such data, applied to recently derived equations,[6] would permit more detailed characterization than has heretofore been possible of an important class of condensation polymers, polyurethans derived from TDI. Consequently, the following experiment and analysis were undertaken.

TDI was treated with *n*-butyl alcohol–xylene solution at 80°. The concentration of —NCO as a function of time was determined by transferring periodically withdrawn reaction samples to excess *n*-butylamine solution and back titrating with HCl. A representative curve is shown in Fig. 1. Values of —NCO, as read from the smoothed out curve of Fig. 1 are compiled in Table I, col. 2.

TABLE I

COMPARISON OF EXPERIMENTAL CONCENTRATIONS OF ISOCYANATE WITH CALCULATED VALUES

Time, hr.	Exptl.	Calcd. 1	Calcd. 2
0	0.250	0.25000	0.25000
0.100	.224	.22235	.22244
.200	.205	.20208	.20217
.300	.187	.18657	.18664
.400	.173	.17433	.17438
.500	.162	.16443	.16444
.750	.146	.14635	.14630
1.000	.134	.13409	.13400
1.250	.126	.12520	.12511
1.500	.118	.11843	.11834
1.750	.113	.11307	.11300
2.000	.109	.10869	.10865
2.500	.102	.10189	.10190
3.000	.097	.09673	.09680
4.000	.090	.08914	.08925
5.000	.084	.08352	.08358
6.000	.078	.07900	.07894

Constants (l./eq.-hr.)	k_1	k_2	k_3	k_4	Std. deviation meq./ml.
Calcd. 1	8.54	4.00	1.92	0.53	0.00118
Calcd. 2	9.21	6.00	1.20	0.63	0.00115

Assuming that reaction of each –NCO group in eq. 1 with a primary alcohol obeys second-order kinetics,[7] one obtains the following set of independ-

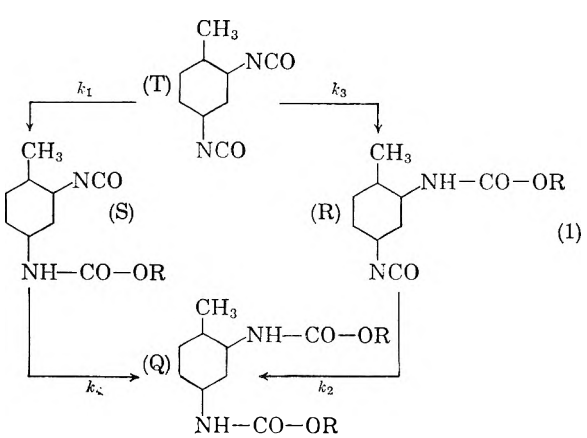

(1) I. C. Kogon, *J. Org. Chem.*, **24**, 438 (1959).
(2) M. E. Bailey, *et al.*, *Ind. Eng. Chem.*, **48**, 794 (1956).
(3) M. Morton and M. A. Deisz, Abstracts of Papers, Div. of Paints and Plastics, A.C.S. Meeting, September, 1956.
(4) J. J. Tazuma and H. K. Latourette, ref. 3.
(5) J. Burkus and C. F. Eckert, *J. Am. Chem. Soc.*, **80**, 5948 (1958).
(6) A. Di Giacomo, *J. Poly. Sci.*, in press.
(7) R. G. Arnold, *et al.*, *Chem. Revs.*, **57**, 47 (1957).

TABLE II

CALCULATED MOLES OF (T), (Q), (R) AND (S) *vs.* %-NCO CONSUMED

%-NCO Consumed	(T) Calcd. 1	(T) Calcd. 2	(Q) Calcd. 1	(Q) Calcd. 2	(R) Calcd. 1	(R) Calcd. 2	(S) Calcd. 1	(S) Calcd. 2
0	1.0000	1.0000	0.0000	0.0000	0.0000	0.0000	0.0000	0.0000
11.0	0.7819	0.7827	.0030	.0032	.0381	.0233	.1770	.1908
19.2	.6266	.6279	.0101	.0106	.0622	.0372	.3011	.3243
25.4	.5117	.5131	.0190	.0200	.0796	.0456	.3914	.4214
30.3	.4238	.4254	.0291	.0303	.0880	.0504	.4591	.4938
34.2	.3551	.3567	.0397	.0412	.0944	.0531	.5109	.5491
41.5	.2370	.2386	.0663	.0682	.1008	.0541	.5960	.6392
46.4	.1645	.1658	.0918	.0938	.1000	.0514	.6438	.6889
49.9	.1174	.1185	.1152	.1176	.0959	.1473	.6711	.7166
52.6	.0854	.0864	.1378	.1397	.0904	.0427	.6863	.7313
54.8	.0631	.0639	.1585	.1599	.0844	.0382	.6940	.7378
56.5	.0472	.0479	.1777	.1787	.0783	.0341	.6968	.7392
59.2	.0273	.0278	.2118	.2126	.0667	.0269	.6938	.7328
61.3	.0162	.0166	.2424	.2422	.0565	.0211	.6848	.7202
64.3	.0062	.0064	.2931	.2924	.0405	.0129	.6601	.6883
66.6	.0026	.0026	.3345	.3340	.0292	.0080	.6338	.6554
68.4	.0011	.0011	.3691	.3697	.0214	.0051	.6084	.6242

Constants (l./eq.-hr.)	k_1	k_2	k_3	k_4	Std. deviation, meq./ml.
Calcd. 1	8.54	4.00	1.92	0.53	0.00118
Calcd. 2	9.21	6.00	1.20	0.63	0.00115

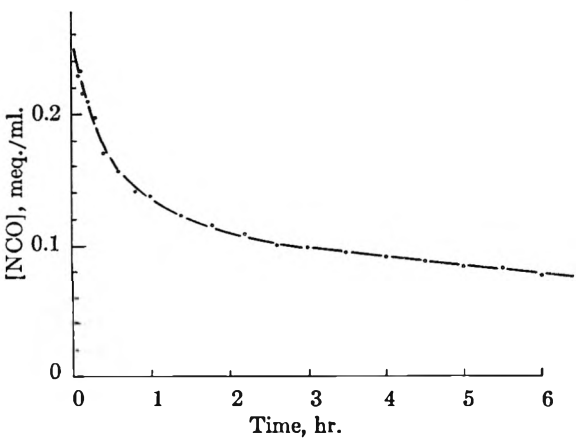

Fig. 1.—[NCO] *vs.* time. Reaction of TDI with *n*-butyl alcohol in xylene solution at 80°.

ent equations (where each rate "constant" depends slightly on hydroxyl[8] and urethan[9] concentration).

$$-d(T)/dt = (k_1 + k_3)(T)(OH)$$
$$-d(R)/dt = k_2(R)(OH) - k_3(T)(OH) \quad (2)$$
$$-d(S)/dt = k_4(S)(OH) - k_1(T)(OH)$$
$$2(T) + (R) + (S) = \text{total -NCO}$$

Equations 2 were fitted to the -NCO *vs.* time curve with the aid of a Bendix G-15 computer. This automatic curve fitting procedure was found to be insensitive to the value of k_2 as may be seen from Table I, columns 3 and 4. Nonetheless, the approximate values of $k_1 = 8.9$, $k_2 = 5$, $k_3 = 1.6$, $k_4 = 0.6$ all in liters/eq.-hr., are an improvement over reported values derived from similar data by analyses based on only two rate constants. Assignment of the largest value to the *para-* rather than the *ortho*-isocyanate group was based on studies[10] which demonstrated unequivocally its greater reactivity.

(8) J. W. Baker, *et al.*, *J. Chem. Soc.*, 9, 19, 24, 27 (1949).
(9) J. W. Baker and J. B. Holdsworth, *J. Chem. Soc.*, 713 (1947).

Notwithstanding the uncertainty in the values of the rate constants, the values, which were of primary concern, of (T) and of (Q) as a function of the % -NCO consumed were computed with satisfactory accuracy by this procedure. The nearly equal values obtained with each of two sets of rate constants are shown in Table II. Values of the intermediates, (R) and (S), which are subject to a greater uncertainty, are also tabulated.

The assistance of Dr. A. L. Squyres in running the computer is gratefully acknowledged.

(10) D. M. Simons and R. G. Arnold, *J. Am. Chem. Soc.*, **78**, 1658 (1956).

SPECTROPHOTOMETRIC EVIDENCE FOR INTERACTION BETWEEN CHLOROFORM AND MONOETHYLAMINE

BY LEON SEGAL

Southern Regional Research Laboratory,[1] New Orleans, Louisiana

Received October 6, 1960

In an earlier paper by Segal and Jonassen[2] evidence for interaction between chloroform and ethylamine was reported, based on heat of mixing, distillation, and water-washing of chloroform–amine and hexane–amine mixtures. A change in refractive index was also reported which seemed to indicate that a 1:1 complex was formed in the chloroform–amine system. From the data at hand the authors concluded that a hydrogen-bonded complex was formed, where the bonding was through the C–H←N bond. More recent evidence for the hydrogen bonding power of chloroform is discussed by Pimentel and McClellan.[3] An infrared spec-

(1) One of the laboratories of the Southern Utilization Research and Development Division, Agricultural Research Service, U. S. Department of Agriculture.
(2) L. Segal and H. B. Jonassen, *J. Am. Chem. Soc.*, **74**, 3697 (1952).

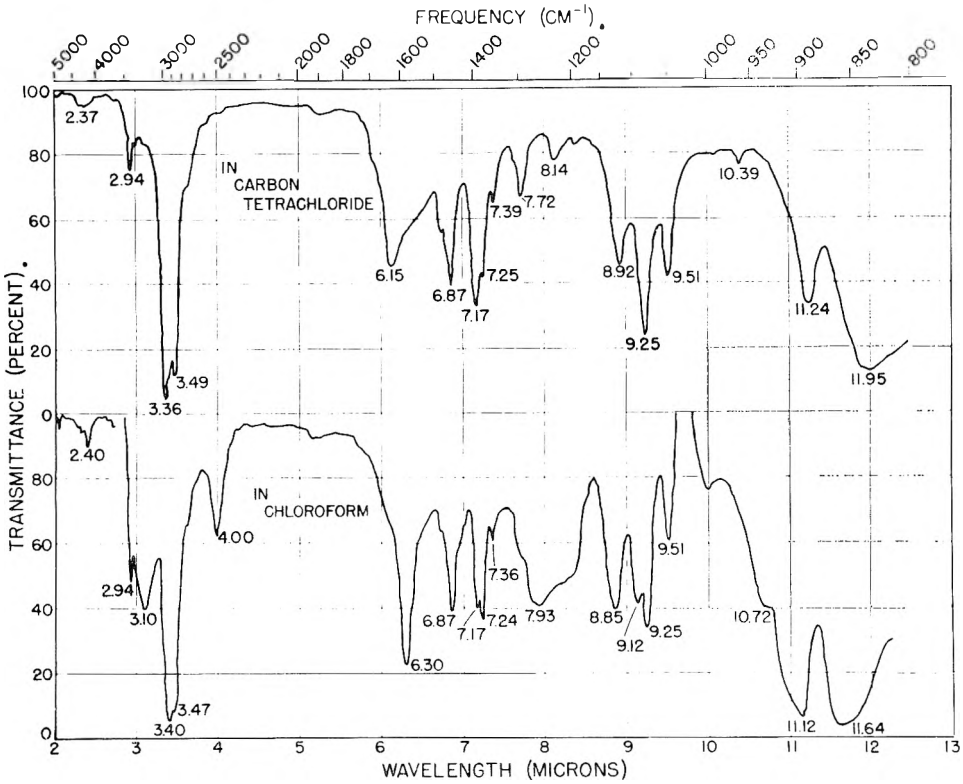

Fig. 1.—Infrared spectra of ethylamine in carbon tetrachloride and in chloroform.

trum of ethylamine in chloroform has been published in connection with studies on gossypol,[4] but the bands are poorly resolved and no cognizance was taken of any possible solvent–solute interaction and its effect on the infrared spectrum.

This paper reports infrared spectrophotometric evidence for an interaction between chloroform and ethylamine which further confirms hydrogen bonding of the type C-H←N.

Experimental

Anhydrous ethylamine was drawn as a vapor from a cylinder, condensed in an all-glass apparatus, and stored in a refrigerator over sodium hydroxide pellets. Samples titrated with standard hydrochloric acid indicated a purity of 100%. Carbon tetrachloride and chloroform were of spectrophotometric grade. Infrared absorption spectra were obtained at a rate of 0.5 μ per minute with a Perkin–Elmer Model 21[5]-double-beam infrared spectrophotometer with sodium chloride prism, operated with the following settings: resolution, 927; gain, 6; response, 1; and suppression, 3. Cell thickness was 0.48 mm., and solution concentrations were 20.8 g./l. (0.46 *M*).

Results and Discussion

In the infrared spectrum of ethylamine in carbon tetrachloride where association of the amine does not occur, only the absorptions of the NH_2 group are of interest here. These have been identified after extensive consultation of several works[6] as being the unbonded N–H and NH_2 stretching of a primary amine at 2.94 μ, the NH_2 scissoring mode at 6.15 μ, the NH_2 wagging mode at 8.92 μ, the C–N stretchings of a primary amine at 9.24 and 9.51 μ, an N–H bending at 10.39 μ, and NH_2 deformations at 11.24 and 11.95 μ (Fig. 1). The spectrum of ethylamine in chloroform shows shifts in the locations of several of these absorption bands and the presence of new bands. These shifts, and particularly the presence of the new bands, indicate the presence of hydrogen bonding in this system.

The strong absorption now appearing at 3.10 μ indicates a strongly bonded NH_2 group. The new mode at 4.00 μ definitely fixes the bonding as that of C–H←N. An amine band in this region does arise from an amine hydrochloride where the group is $-NH_3^+$, $=NH_2^+$, and $>NH^+$, but no hydrochloride is present here. Gordy,[7] after observing the appearance of an absorption band at 4 μ in systems involving chloroform, bromoform, pyridine, α-picoline, and piperidine, concluded that it was an NH vibrational band resulting from a hydrogen bond formed by sharing of the proton of the C–H haloform group and a N of the amine. He also concluded that this band is the most definite evidence yet for the existence of the hydrogen bond. Thompson and Pimentel[8] have more recently reported the appearance of a strong band in this region for the solid obtained by freezing a gaseous mixture of chloroform and triethylamine at 77°K.

(3) G. C. Pimentel and A. L. McClellan, "The Hydrogen Bond," Reinhold Publ. Co., New York, N. Y., 1960, pp. 196–199.

(4) R. T. O'Connor, P. Von der Haar, E. F. DuPre, L. E. Brown and C. H. Pominski, *J. Am. Chem. Soc.*, **76**, 2368 (1954).

(5) Use of a company and/or product named by the Department does not imply approval or recommendation of the product to the exclusion of others which may also be suitable.

(6) R. N. Jones and C. Sandorfy in "Chemical Application of Spectroscopy," ed. by W. West, Interscience Publ., New York, N. Y., 1956, pp. 247–580; H. M. Randall, R. G. Fowler, N. Fuson and J. R. Dangl, "Infrared Determination of Organic Structures," D. Van Nostrand Co., New York, N. Y., 1949; L. J. Bellamy, "The Infra-red Spectra of Complex Molecules," John Wiley and Sons, New York, N. Y., 1954; N. B. Colthup, *J. Opt. Soc. Am.*, **40**, 397 (1950).

(7) W. Gordy, *Nature*, **142**, 831 (1938); *J. Chem. Phys.*, **7**, 163 (1939).

(8) W. E. Thompson and G. C. Pimentel, *Z. Elektrochem.*, **64**, 748 (1960).

However, they attribute this band, which shifted to 5.32 μ when $CDCl_3$ was substituted for $CHCl_3$, to the C–H bending mode of hydrogen-bonded chloroform.

Other changes in the ethylamine spectrum arise from this association between chloroform and ethylamine. The NH_2 scissoring mode has shifted from 6.15 to 6.30 μ. In the 8-μ region now appears a strong, broad band whose origin is quite puzzling. The NH_2 wagging mode has shifted down to 8.85 μ, the N–H deformation at 10.39 has shifted down to 10.00 μ, and the NH_2 deformations at 11.24 and 11.95 μ have shifted down to 11.12 and 11.64 μ. Two new absorptions now appear in the C–N stretching region, located at 9.12 and 10.72 μ. The 9.12-μ band can be reasonably assigned to a new NH_2 deformation as it seems to be a harmonic of the bands at 3.10 and 6.30 μ, but assignment of the 10.72-μ band cannot be made yet.

Acknowledgment.—The author is indebted to Miss E. R. McCall for the infrared spectra.

THE SHARPNESS OF THE TRANSITION IN REVERSIBLE PROTEIN DENATURATION[1]

By H. A. Scheraga, R. A. Scott,[2] G. I. Loeb, A. Nakajima and J. Hermans, Jr.

Department of Chemistry, Cornell University, Ithaca, N. Y.

Received October 7, 1960

This is an addendum to a recent paper[3] on reversible protein denaturation, and makes use of the model presented therein. The purpose of this note is to show how permanent cross-links and side-chain hydrogen bonds affect the sharpness of the transition in reversible denaturation.

The observed standard free energy of denaturation is given by eq. 19, 33 and 34 for the model used previously.[3]

$$\Delta F^0_{obsd} = (n - 4)\Delta H^0_{res} - T\Delta S^0_0 + \Delta F^0_H \quad (33)$$

$$\Delta S^0_0 = (n - 1)\Delta S^0_{res} + \Delta S^0_x/\nu \quad (34)$$

$$\Delta F^0_H = -RT\sum \ln (1 - x_{ij}) \quad (19)$$

The fraction of the molecules denatured is given[3,4] by eq. 36.

$$\alpha = [1 + e^{\Delta F^0_{obsd}/RT}]^{-1} \quad (36)$$

Defining the sharpness[4] of the transition as $d\alpha/dT$ at the transition temperature, T_{tr}, where $\Delta F^0_{obsd} = 0$, we obtain

$$\left(\frac{d\alpha}{dT}\right)_{T_{tr}} = \frac{(n - 4)\Delta H^0_{res} + \Delta H^0_H}{4RT^2_{tr}}$$

where ΔH^0_H is given by eq. 20.[3] The terms ΔF^0_H and ΔH^0_H arise from the side-chain hydrogen bonds.

The pH-dependence of $(d\alpha/dT)_{T_{tr}}$ arises from the pH-dependence of ΔH^0_H and of T_{tr}. This is illustrated in Fig. 1 for the model previously described,[3] in which the crystalline unit is stabilized in the intermediate pH-region by one tyrosyl-carboxylate ion side-chain hydrogen bond. Thus, it can be seen that side-chain hydrogen bonding increases the sharpness of the transition. As shown previously,[3] it also increases the transition temperature.

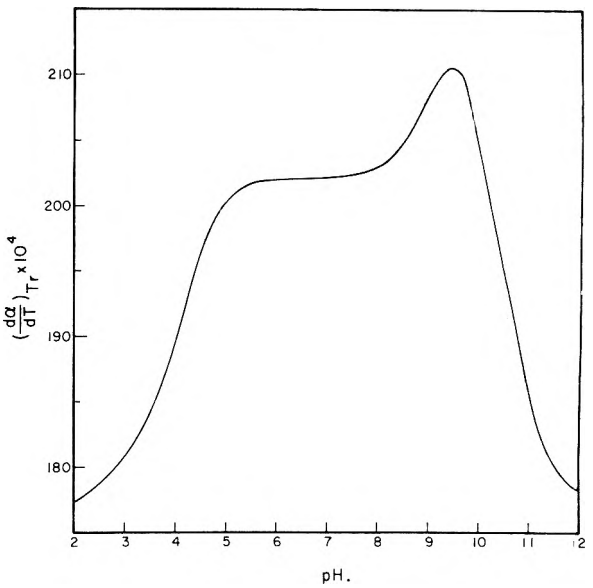

Fig. 1.—Effect of a tyrosyl-carboxylate ion hydrogen bond on the sharpness of the transition of Fig. 12 of the previous paper.[3]

It is easiest to see the effect of cross-linking at a pH where ΔH^0_H and ΔF^0_H are zero, *i.e.*, where no side-chain hydrogen bonds exist. Under these conditions, the transition temperature (from eq. 33) is

$$T_{tr} = \frac{(n - 4)\ \Delta H^0_{res}}{\Delta S^0_0}$$

and

$$\left(\frac{d\alpha}{dT}\right)_{T_{tr}} = \frac{(\Delta S^0_0)^2}{4R(n - 4)\ \Delta H^0_{res}}$$

Thus, since ΔS^0_x is negative,[5] T_{tr} is raised by cross-linking, as pointed out by Schellman[4] and Flory.[5] (See also Table I of previous paper.[3]) Further, $(d\alpha/dT)_{T_{tr}}$ decreases with increasing cross-linking, *i.e.*, the transition becomes broader. For example, in the model used previously,[3] the value of $(d\alpha/dT)_{T_{tr}}$ is decreased from 0.0250 to 0.0178 by the cross-linking.

The effect of increasing n was pointed out by Schellman.[4] In the absence of cross-links and side-chain hydrogen bonds large n leads to

$$T_{tr} = \Delta H^0_{res}/\Delta S^0_{res}$$

and to increased values of $(d\alpha/dT)_{T_{tr}}$.

Proteins may, therefore, differ from synthetic polypeptides, as far as the sharpness of the transition in reversible denaturation is concerned, if cross-links and side-chain hydrogen bonds are present in the protein but absent from the polypeptide. Obviously, any other phenomena which affect the enthalpy or entropy of the transition (such as breaks in the helix, hydrophobic bonds, etc.) may also affect the sharpness.

(1) This work was supported by research grant No. E-1473 from the National Institute of Allergy and Infectious Diseases of the National Institutes of Health, Public Health Service, and by grant G-6461 from the National Science Foundation.

(2) U. S. Public Health Service Pre-doctoral fellow, National Heart Institute, 1959–1960.

(3) H. A. Scheraga, *J. Phys. Chem.*, **64**, 1917 (1960).

(4) J. A. Schellman, *Compt. rend. trav. lab. Carlsberg, Ser. chim.*, **29**, 230 (1955).

(5) P. J. Flory, *J. Am. Chem. Soc.*, **78**, 5222 (1956).

PROTONATION IN N-METHYLACETAMIDE[1]

By Gideon Fraenkel[2]

Gates and Crellin Laboratories of Chemistry, California Institute of Technology, Pasadena, California

Aharon Loewenstein and

NMR Laboratory, Weizmann Institute, Rehovoth, Israel

Saul Meiboom

Bell Telephone Labs., Murray Hill, N. J.

Received September 21, 1960

In a recent note by Spinner[3] a discussion of the site of protonation in amides is given. In that note it is suggested that the n.m.r. evidence for O-protonation in N-methylacetamide and other amides is inconclusive. As we have shown previously,[4,5] the N-methyl proton resonance of this molecule in very acidic solution consists of a symmetrical doublet presumably due to spin–spin interaction with a single N-hydrogen. Spinner, however, interprets this doublet as being due to non-equivalence of the methyl groups in different isomeric forms resulting from hindered rotation. We wish to point out that the symmetry of the doublet makes such an interpretation highly improbable as the equal intensity of the components would lead to the conclusion that the two isomeric forms have very nearly the same energy.

Two experiments were performed to show unambiguously that the splitting of the N-methyl resonance in protonated N-methylacetamide is due to spin–spin interaction rather than a chemical shift.

1. The N-methyl resonance of a solution of N-methylacetamide in 100% H_2SO_4 consists of two equal lines while in 100% D_2SO_4 the same resonance consists only of a single line.

2. The separation of the M-methyl doublet in protonated N-methylacetamide is independent of the magnetic field (3.7 ± 0.3 c.p.s. both at 30 and 60 Mc.).

It is therefore clear that N-methylacetamide protonates predominantly on oxygen.

(1) Contribution No. 2580.

(2) Department of Chemistry, The Ohio State University, Evans Chemical Laboratory, 88 W. 18th Avenue, Columbus 10, Ohio.

(3) E. S. Spinner, *J. Phys. Chem.*, **64**, 275 (1960).

(4) G. Fraenkel and C. Niemann, *Proc. Natl. Acad. Sci. (U. S.)*, **44**, 688 (1958).

(5) A. Berger, A. Loewenstein and S. Meiboom, *J. Am. Chem. Soc.*, **81**, 62 (1959).

ANALYSIS OF THE INTRINSIC VISCOSITY OF A POLYMER UNDERGOING SIMULTANEOUS CROSSLINKING AND DEGRADATION

By Malcolm Dole

Department of Chemistry, Northwestern University, Evanston, Illinois

Received October 13, 1960

The effect of simultaneous crosslinking and degradation on the intrinsic viscosity of a polymer has recently been considered theoretically in this country by Kilb,[1,2] using the theory of Zimm and Kilb,[3] and in Japan by Saito,[4] Inokuti[5] and Inokuti and Katsuura.[6,10] Saito,[4] Kilb[1] and Charlesby and Pinner[7] all demonstrated that in the case of an initially random molecular weight distribution gelation is possible on irradiation only if the number of chain scissions is less than four times the number of crosslinks. Saito[4] and Inokuti[5,6] have concluded that in certain favorable cases the intrinsic viscosity of a polymer undergoing irradiation may actually decrease before rising rapidly at the gel point, even if the effect of the formation of branch points due to the crosslinking is neglected. Kilb,[1] however, demonstrated that the changes in intrinsic viscosity on irradiation are a function of the formation of branch points as well as of the scission to crosslink ratio. Black and Lyons[8] calculated the G-value for scissions from the initial decrease of intrinsic viscosity of polypropylene on irradiation neglecting both the effect of crosslinking and branch point formation on the molecular weight and shape of the molecules. In this connection it should be noted that Shultz, Roth and Rathmann[9] in their mathematical analysis of the intrinsic viscosity of polymers undergoing simultaneous degradation and crosslinking warned against "basing molecular weights of irradiated polymers, or polymers otherwise branched or degraded, on viscosity measurements without corroborative evidence from other methods." With this conclusion we are in complete agreement. Shultz, Roth and Rathmann assumed a random molecular weight distribution. Very recently Katsuura[10] has extended the treatment of Saito[4] and Inokuti[5,6] to allow for the effect of branching on the intrinsic viscosity.

It is the purpose of this note to demonstrate that if the initial molecular weight distribution is random and if the influence of branch points on the intrinsic viscosity is neglected, then contrary to the conclusions of Saito[4] and Inokuti[5,6] the intrinsic viscosity probably cannot decrease provided that gelation ultimately occurs. Suggestions will be made concerning experiments which could be performed to measure the effect of irradiation on the exponent of the intrinsic viscosity–molecular weight equation.

Nomenclature.—The symbols of Charlesby and Pinner[7] will be adopted for the most part. Let

r, r_g = total dose, and dose to the gel point, resp. in e.v./g.
p, q = total no. of scissions and crosslinked units per chain unit resp., after the dose r
p_0, q_0 = no. of scissions and crosslinked units per e.v.
$p = p_0 M_0(r/N_A)$, $q = q_0 M_0(r/N_A)$ where
M_0 is the molecular weight of one chain unit and
N_A is Avogadro's number
$G(X)$, $G(S)$ = G-values for crosslinks and scissions produced per 100 e.v.
$G(X) = 100q_0/2$; $G(S) = 100p_0$

(1) R. W. Kilb, *J. Phys. Chem.*, **63**, 1838 (1959).

(2) R. W. Kilb, *J. Polymer Sci.*, **38**, 403 (1959).

(3) B. H. Zimm and R. W. Kilb, *ibid.*, **37**, 19 (1959).

(4) O. Saito, *J. Phys. Soc. Japan*, **13**, 198, 1451, 1465 (1958).

(5) M. Inokuti, *ibid.*, **14**, 79 (1959).

(6) M. Inokuti and K. Katsuura, *ibid.*, **14**, 1379 (1959).

(7) A. Charlesby and S. H. Pinner, *Proc. Roy. Soc.* (*London*), **A249**, 367 (1959).

(8) R. M. Black and B. J. Lyons, *ibid.*, **A253**, 322 (1959).

(9) A. R. Shultz, P. I. Roth and G. B. Rathmann, *J. Polymer Sci.*, **22**, 495 (1956).

(10) K. Katsuura, *J. Phys. Soc.* (*Japan*). Kindly loaned in advance of publication by M. Inokuti.

M_n, M_w = no. av. and wt. av. molecular weight
$[\eta]$, $[\eta]_0$ = intrinsic viscosity after and before irradiation
δ = no. of crosslinked units per initial wt. av. molecule
A, B = empirical constants of the intrinsic viscosity equation

$$\frac{[\eta]}{[\eta]_0} = 1 + Ar + Br^2 \qquad (1)$$

K, a = empirical constants of the intrinsic viscosity equation

$$[\eta] = KM_w^a \qquad (2)$$

b = empirical coefficient of the equation

$$M_w = bM_n \qquad (3)$$

The constants a, b and K will be assumed to be functions of the dose.

Mathematical Analysis.—In the case of many polymers, the change of intrinsic viscosity with dose over the initial period of irradiation follows the empirical eq. 1. Differentiating (1) with respect to dose, at zero dose, we have

$$\left[\frac{d[\eta]/[\eta_0]}{dr}\right]_{r=0} = A \qquad (4)$$

Similarly from (2) inasmuch as M_w, K and a are functions of r

$$\left[\frac{d[\eta]/[\eta]_0}{dr}\right]_{r=0} = \frac{a_0}{M_{w,0}}\left[\frac{dM_w}{dr}\right]_{r=0} + \ln M_{w,0}\cdot\left[\frac{da}{dr}\right]_{r=0} + \frac{1}{K_0}\left[\frac{dK}{dr}\right]_{r=0} \qquad (5)$$

Now, assuming that the production of scissions and crosslinking are independent processes

$$\frac{dM_w}{dr} = \left[\frac{dM_w}{dr}\right]_X + \left[\frac{dM_w}{dr}\right]_S \qquad (6)$$

where X and S represent the crosslinking and degradation processes, respectively. From (3)

$$\left[\frac{dM_w}{dr}\right]_{0,s} = b_0\left[\frac{dM_n}{dr}\right]_{0,s} + M_{n,0}\left[\frac{db}{dr}\right]_{0,s} \qquad (7)$$

In terms of p_0

$$\left[\frac{dM_n}{dr}\right]_{0,s} = -\frac{M^2_{n,0}P_0}{N_A} \qquad (8)$$

From gelation theories of Stockmayer[11] and Charlesby[12] provided that no degradation occurs

$$M_w = \frac{M_{w,0}}{1-\delta} \qquad (9)$$

From eq. 9 we have, therefore

$$\left[\frac{d\delta}{dr}\right]_{0,X} = \frac{1}{M_{w,0}}\left[\frac{dM_w}{dr}\right]_{0,X} \qquad (10)$$

and in terms of q_0

$$\left[\frac{d\delta}{dr}\right]_{0,X} = \frac{q_0 M_{w,0}}{N_A} \qquad (11)$$

Combining (10) and (11); (7), (8) and (6); and introducing the results into (5), we obtain finally

$$A = \frac{a_0}{b_0}\left(\frac{db}{dr}\right)_{0,S} + \ln M_{w,0}\cdot\left(\frac{da}{dr}\right)_0 + \frac{1}{K_0}\left(\frac{dK}{dr}\right)_0 + \frac{a_0 M_{w,0}}{N_A}\left\{q_0 - \frac{p_0}{b_0}\right\} \qquad (12)$$

In eq. 12 the first term on the right represents the change of the weight to number average molecular weight ratio as a consequence of the production of scissions, the second and third terms represent the change in the a exponent and K constant due to change of shape of the molecules with crosslinking and the fourth term the direct effect on the intrinsic viscosity of the production of scissions and crosslinking.

In the case of an initially random molecular weight distribution, b equal to 2 and constant,[1,4,7]

$$r_g = \frac{N_A}{M_{w,0}\left(q_0 - \frac{p_0}{2}\right)}; \qquad (13)$$

hence, in this case

$$A = \ln M_{w,0}\left(\frac{da}{dr}\right)_0 + \frac{1}{K_0}\left(\frac{dK}{dr}\right)_0 + \frac{a_0}{r_g} \qquad (14)$$

Discussion

Let us consider the case of a polymer whose initial molecular weight distribution is random, b equal to 2. On irradiation, if gel ultimately forms, the weight average molecule weight must always increase irrespective of the ratio of q_0 to p_0 (gel will not form if $2p_0/q_0$ is equal to or greater than four). However, the intrinsic viscosity may initially decrease due to the effect of the crosslinks in changing the shape of the resulting molecules inasmuch as branched molecules have a lower intrinsic viscosity than linear molecules at the same molecular weight. In addition to this effect, Saito[4] and Inokuti[5,6] have concluded that the intrinsic viscosity can also decrease due to a change in the molecular weight distribution. Neglecting the change of the viscosity exponent a with irradiation, they have calculated from viscosity theory that the term dK/dr of eq. 14 is negative, and in some cases outweighs the positive quantity a_0/r_g. Thus neglecting da/dr, eq. 14 becomes

$$A = \frac{1}{K_0}\left(\frac{dK}{dr}\right)_0 + \frac{a_0}{r_g} \qquad (15)$$

However, Price, Martin and Bianchi[13] found K to increase from 0.0805 to 0.326 and the viscosity exponent a to fall from 0.50 to 0.21 as the CH_3/Si ratio in polysiloxanes was changed chemically from 2.0 to 1.5, or, in other words, as the branching increased. Chemical treatment of polymers can produce three kinds of branches, intermolecular crosslinks, intramolecular crosslinks (ring links) and branches which terminate without further reaction. Only intermolecular crosslinks lead to gel formation whereas all three types of branches effect the intrinsic viscosity. Thus, Schaefgen and Flory[14] studied star-shaped polymers, up to the octachain type, in which the branches were all linear. From their data it can be shown that the constant K of eq. 2 decreased as the branching increased, but that the a exponent increased slightly or remained constant. Gel formation, of course, could not occur in this case. Limiting ourselves to polymers in which gelation did ultimately occur, as in the work of Price, Martin and Bianchi,[13] we can conclude that the constant A of eq. 15 cannot be negative provided that b is initially two, that da/dr is negligible and that

(11) W. H. Stockmayer, *J. Chem. Phys.*, **12**, 125 (1944).
(12) A. Charlesby, *Proc. Roy. Soc.* (*London*), **A222**, 542 (1954).
(13) F. P. Price, S. G. Martin and J. P. Bianchi, *J. Polymer Sci.*, **22**, 41 (1956).
(14) J. R. Schaefgen and P. J. Flory, *J. Am. Chem. Soc.*, **70**, 2709 (1948).

dK/dr is positive. As the transition is made from a linear polymer to a compact spherical molecule, a drops to zero and the K constant rises to $2.5/\rho$ where ρ is the density of the compact molecule and the intrinsic viscosity is expressed in units of g./cc. These values of a and K for compact spherical molecules follow from the hydrodynamic theory of solution viscosity of Einstein.[15] Thus, on the basis of Price, Martin and Bianchi's experimental results and of the Einstein theory, it would appear that dK/dr is positive and that the A of eq. 15 will always be positive in contradiction to the conclusions of Saito[4] and Inokuti.[5,6] It should be pointed out, however, that this conclusion is academic and without practical importance inasmuch as da/dr is negative; *i.e.*, it appears to be impossible to have K change without a also changing. Furthermore, in many vinyl type polymers, b is significantly greater than 2 initially so that the term $a_0/b_0\ (db/dr)_{0,S}$, of eq. 12 must be negative and far from negligible.

For illustrative calculations let us consider data of Shultz, Roth and Rathmann[9] and of Kilb[1] on polymers assumed initially to have a random molecular weight distribution. Kilb measured the intrinsic viscosity of polydimethylsiloxane; from his data a rough estimate of A equal to 29×10^{-22} g./e.v. can be made. From r_g equal to 10.3×10^{19} e.v./g. and a_0 equal to 0.79, a_0/r_g is 77×10^{-22} g./e.v.

By difference

$$\ln M_{w,0}\frac{da}{dr} + \frac{1}{K_0}\frac{dK}{dr} = -58 \times 10^{-22}\ \text{g./e.v.}$$

From the data of Price, Martin and Bianchi[13] quoted above, $(1/K_0)(dK/dr)$ appears to be about one tenth the magnitude of $\ln M_{w,0}(da/dr)$; neglecting it, we can estimate Δa to be about -0.04 to the gel point. A similar calculation from the data of Shultz, Roth and Rathmann[9] on polystyrene yielded an estimated Δa of -0.03, the same order of magnitude as the result of Kilb. In both cases these are estimates of the total change in a up to the gel point. Thus, the change in intrinsic viscosity beyond that due to the increase in molecular weight on irradiation up to the gel point can be explained on the basis of a decrease in a of about 0.03 to 0.04 unit.

We conclude that this method of analyzing the intrinsic viscosity data in the case of polymers ultimately undergoing gelation on irradiation and possessing initially a random molecular weight distribution can yield a first approximation of the extent to which the viscosity exponent a should change with the irradiation. Exact estimates would require a knowledge of dK/dr and, in general, db/dr.

(15) A. Einstein, *Ann. Physik*, [4] **19**, 289 (1906); **34**, 591 (1911).

Acknowledgments.—The work of this note stems from a project sponsored by the Air Research and Development Command, U.S.A.F. Grateful acknowledgment is expressed to R. W. Kilb and M. Inokuti for helpful comments.

ERRATUM TO THE PAPER ON THE KINETICS OF EVAPORATION[1]

BY S. S. PENNER

Div. of Engineering, Calif. Inst. of Tech., Pasadena, Calif.

Received January 19, 1961

Professor M. Boudart of Princeton University has kindly called my attention to an error in the derivation of the rate equation for the kinetics of evaporation from absolute reaction rate theory. He has pointed out that, if consistent estimates are made for the free volume in the equation for the partition function per molecule in the liquid, as well as in the vapor pressure equation, then the Hertz–Knudsen equation is obtained with or without the assumption that the communal entropy has its full value R. Thus the free volume v_f in the expression for the partition function

$$Q = \frac{(2\pi m\, kT)^{3/2}}{h^3} v_f$$

should not be v_f but[2] rather ev_f when the communal entropy is R and the usual expression is used for the vapor pressure, *viz.*,

$$p = \frac{kT}{v_f}\exp(-\Delta H_e/RT)$$

Introduction of the specified changes makes it unnecessary to assume that the fundamental equilibrium assumption of absolute reaction rate theory must be abandoned in order to obtain a theoretical relation that is in accord with the experimentally verified Hertz–Knudsen equation.

The result obtained from a straightforward application of absolute reaction rate theory, using a model in which the activated complex moves freely at the surface, is identical with the non-equilibrium theory of Mortensen and Eyring.[3] Professor Boudart states in a private communication that it is gratifying to note that all difficulties have been removed from a theory possessing "the beautiful simplicity of absolute rate theory with a transmission coefficient equal to unity and the usual equilibrium assumption."

(1) S. S. Penner, *J. Phys. Chem.*, **56**, 475–479 (1952).

(2) See, for example, K. F. Herzfeld and T. A. Litovitz, "Absorption and Dispersion of Ultrasonic Waves," Academic Press, Inc., New York, N. Y., 1959, p. 379.

(3) E. M. Mortensen and H. Eyring, *J. Phys. Chem.*, **64**, 846 (1960).

COMMUNICATIONS TO THE EDITOR

THE RADIOLYSIS OF BENZENE BY DENSELY IONIZING RADIATIONS[1]

Sir:

Previous comparisons of the chemical effects on aliphatic hydrocarbons of fast electrons with those of more densely ionizing particles have indicated little difference between the two types of radiations.[2] In aromatic systems, however, since the yields of most products are low, it might be expected that a change of linear energy transfer (LET) would result in an observable change in the over-all radiation chemistry of the system. In particular one might expect a pronounced effect on the yield of hydrogen from benzene since this product accounts for only a small fraction of the total decomposition in the case of γ-rays. Indications of variation of product yield with LET have been obtained in early work by Sworski and Burton[3] and more recently by Burns and co-workers[4] and by Boyd.[5] This problem is of considerable technological importance because of the use of aromatic systems as moderators and coolants in reactors. This communication reports preliminary experiments on the radiation decomposition of benzene by cyclotron helium ions and deuterons which further indicate that the yield of hydrogen produced by heavy particle radiations is considerably in excess of that produced by fast electrons. Little effect on the yields of polymeric products is observed.

Phillips research grade benzene was thoroughly degassed and dried over Molecular Sieves, distilled to the irradiation vessel and sealed. Irradiation techniques were similar to those employed in previous studies.[2] Hydrogen gas was measured in a McLeod gauge after pumping from the sample at $-196°$. Acetylene was pumped from the sample at $-120°$. Higher molecular weight products were measured gas chromatographically using DC710 silicone oil as the separating fluid. More than five components were found in the C_{12} region. The main products were biphenyl, phenylcyclohexadiene-2,5 and phenylcyclohexadiene-2,4. Details of the γ-ray and fast electron radiolysis will be published elsewhere.[6]

The yields of gaseous products are given in Table I. The present value for the hydrogen yield obtained in the γ-ray experiments compares very well with other published values. It is apparent from these data that the heavy particles produce a considerably higher yield of hydrogen than do fast electrons. This is in agreement with the work of Burns and of Boyd. Peculiarly the ratio of yields of acetylene to hydrogen for the densely ionizing radiations is essentially the same as for fast electrons. This indicates, as has been noted before,[7] that these compounds are produced from common precursors.

TABLE I
YIELDS OF GASEOUS PRODUCTS

Radiation	Dose[a] ev. $\times 10^{-21}$	H_2 produced moles $\times 10^6$	$G(H_2)$	C_2/H_2[b]
Co-60 γ-rays	2.52	1.57	0.0378	(0.49)[c]
	3.58	2.23	.0377	.53
18 Mev. deuterons	12.8	9.94	.047	.53
	25.0	19.0	.046	.54
31 Mev. helium ions	1.10	1.34	.074	.54
	3.70	4.8	.078	...
	8.55	11.6	.082	...
	12.5	15.5	.075	.55
	17.0	23.0	.082	.54
	32.0	39.7	.075	.55
	61.5	79.3	.078	.54

[a] In 10-ml. sample. [b] Mass spectrometric analysis shows this fraction to be 95–98% acetylene with small amounts of C_3 and C_4 as additional products. [c] *Cf.* ref. 6.

In the radiolysis of benzene the yields of C_{12} products other than biphenyl are dependent on total dose. For this reason a comparison of the effects of different types of radiation on the heavy products has only limited significance. Table II shows that the yield of biphenyl is little affected in going from electrons (LET $\sim$ 0.02 ev./Å.) to 32 mev. helium ions (LET $\sim$ 2 ev./Å.) although a slight change in product distribution was observed. This is in contrast to the large effect on hydrogen production but in agreement with the relatively small change found by Burns in polymer formation produced by fast neutrons.

TABLE II
YIELDS OF C_{12} PRODUCTS[a]

Radiation	G(biphenyl)	$\frac{\Sigma G(C_{12})}{G(\text{biphenyl})}$
Co-60 γ-rays	0.065	1.45
32 mev. helium ions	0.063	1.74
1.5 mev. helium ions[b]	...	2.03

[a] At total dose of 6×10^{19} ev./g. [b] Recoil radiations from B(n, α)Li reaction. Benzene containing 4.2 mg. of decaborane per ml. irradiated with thermal neutrons.

The above effects are certainly not understood in any detail at the present time. It does not seem likely that the increased hydrogen yield can arise from track recombination of hydrogen atoms because of the high reactivity of the solvent in this case nor would such an explanation predict a

(1) Work supported in part by the U. S. Atomic Energy Commission and the Swiss Kommission fur Atomwissenschaft. T. G. is indebted to the Centenarfonds of the Swiss Federal School of Technology for a Grant-in-Aid.

(2) R. H. Schuler and A. O. Allen, *J. Am. Chem. Soc.*, **77**, 507 (1955); H. A. Dewhurst and R. H. Schuler, *ibid.*, **81**, 3210 (1959); R. H. Schuler, *J. Phys. Chem.*, **63**, 925 (1959).

(3) T. J. Sworski and M. Burton, *J. Am. Chem. Soc.*, **73**, 3790 (1951).

(4) (United Nations) Proc. 2nd Intl. Conf. Peaceful Uses of Atomic Energy, **29**, 266 (1958).

(5) Abstracts 138th American Chemical Society Meeting, New York, N. Y., 1960.

(6) T. Gäumann, *Helv. Chim. Acta*, to be published.

(7) R. H. Schuler, *J. Phys. Chem.*, **60**, 381 (1956).

parallel increase in acetylene formation. Alternate explanations might involve the bimolecular reaction of long-lived excited species, multiple ionization of a single molecule or of near neighbors, or other specific effects which could occur at the end of the path of the ionizing particle. Further detailed studies are in progress.

EIDGENOSSISCHE TECHNISCHE HOCHSCHULE
ZURICH, SWITZERLAND — TINO GÄUMANN
MELLON INSTITUTE — ROBERT H. SCHULER
PITTSBURGH, PENNSYLVANIA, AND
BROOKHAVEN NATIONAL LABORATORIES
UPTON, NEW YORK

RECEIVED MARCH 20, 1961

THE ONSAGER COEFFICIENT L_{12} IN TRANSPORT OF BINARY ELECTROLYTES

Sir:

Miller[1] has pointed out the importance of the coefficient L_{12} in the Onsager phenomenological equations for diffusion, conductance, and transference of a binary electrolyte. He suggests that L_{12}/I (where I is ionic strength) approaches a common slope for electrolytes of different valences. As a matter of fact, the slope for a given electrolyte computed from the Debye–Onsager theory depends somewhat on specific properties, but turns out to be almost constant for various electrolytes.

The theoretical expression for L_{12} can be written compactly in terms of the equivalent concentration, c_e, Hittorf transference numbers, t_1 and t_2, and the so-called kinematic diffusion coefficient, D, which is equal to the Fick diffusion coefficient divided by $(1 + \mathrm{d} \ln y/\mathrm{d} \ln c)$

$$1000 \frac{L_{12}}{c_e} = \frac{\nu_1 t_1 t_2 \Lambda}{z_2 \mathfrak{F}^2} + \frac{\nu_1 \nu_2 D}{\nu RT}$$

where $z_2 < 0$ is the valence of the anion, and the other symbols have their usual significance[2] (ν is used in place of Miller's r). Differentiation by $\sqrt{c_e}$ gives the limiting slope of the L_{12}/c_e curve in terms of the limiting slopes $(S_\Lambda)_1$ and $(S_\Lambda)_2$ for equivalent ionic conductances and S_D for diffusion:

$$\frac{\mathrm{d}}{\mathrm{d}\sqrt{c_e}} \left(1000 \frac{L_{12}}{c_e}\right) \equiv S_{12} = \frac{\nu}{z_2 \mathfrak{F}^2} [t_1^2 (S_\Lambda)_2 + t_2^2 (S_\Lambda)_1] + \frac{\nu_1 \nu_2}{\nu RT}$$

Expressions for the S_Λ's and S_D can be taken from standard works[2] and evaluated for salts for which values of t_1, t_2, and Λ are available at infinite dilution. The theoretical values are given in Table I

(1) D. G. Miller, *J. Phys. Chem.*, **64**, 1598 (1960).
(2) *E. g.*, H. S. Harned and B. B. Owen, "The Physical Chemistry of Electrolytic Solutions," 3rd Edition, Reinhold Publishing Corp., New York, N. Y., 1958.

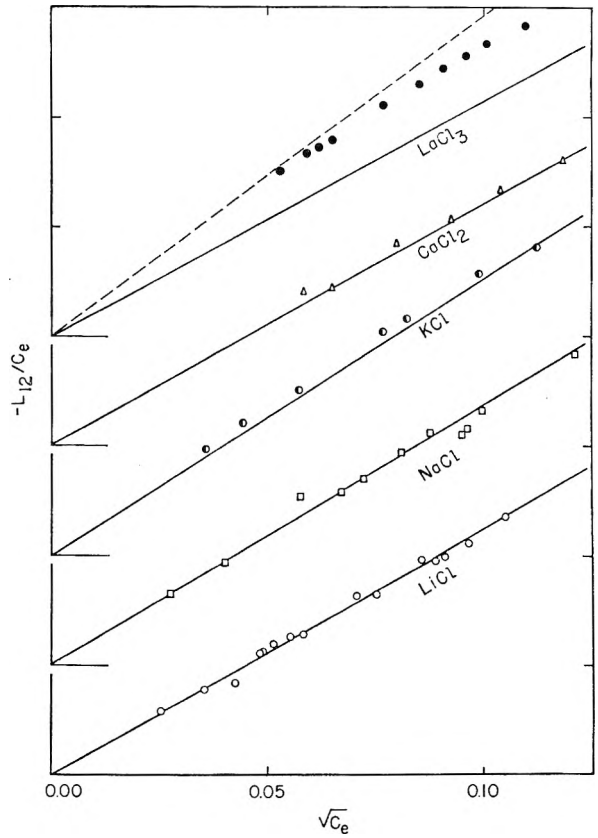

Figure 1.—Experimental and theoretical values of $-L_{12}/c_e$. The intercepts are separated by 0.1×10^{-16}.

TABLE I

THEORETICAL VALUES OF $S_{12} \times 10^{16}$

LiCl	NaCl	KCl	$CaCl_2$	$LaCl_3$
2.248	2.361	2.536	2.206	2.145

for several chlorides in water. Comparison with experimental values is shown in Fig. 1. The four lower-valent salts exhibit an exceptional conformance with the linear limiting laws (solid lines), up to $c_e > 0.1$, a property that is not shared by other quantities associated with electrolytes, including the Onsager coefficients L_{11} and L_{22}. It is a curious fact for these electrolytes that diffusion coefficients can be obtained more accurately from the theoretical value of L_{12} and the experimental value of Λ, than directly as the theoretical value on which calculation of L_{12} is based.

The data on $LaCl_3$ appear to be approaching a slope (dashed line) about 35% higher than the theoretical.

PETROLEUM RESEARCH CENTER
BUREAU OF MINES — PHILIP B. LORENZ
U. S. DEPARTMENT OF THE INTERIOR
BARTLESVILLE, OKLA.

RECEIVED JANUARY 16, 1961

CEC makes the only medium-priced
MASS SPECTROMETER
FOR ANALYTICAL LABORATORIES
that features human engineered packaging. This is it...

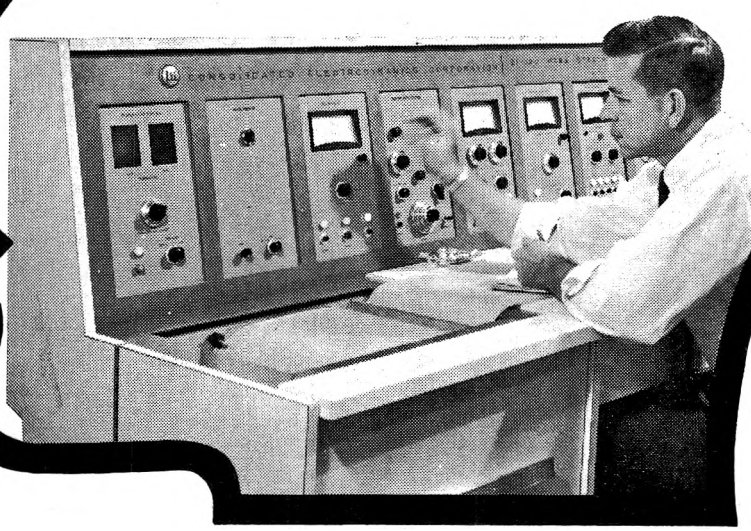

CEC's all-new 21-130 Mass Spectrometer offers the same accuracy, precision, sensitivity and scan speed you'll find only in the largest instruments of its kind.

All this plus a totally new "human" engineered packaging concept that means: Greater accessibility (modular electronics on pull-down chassis)... Convenience in the grouping of operating controls by function, with each operable and adjustable from the front... Lighter weight because it's built on a welded extruded aluminum frame with formica-over-honeycomb cabinet panels.

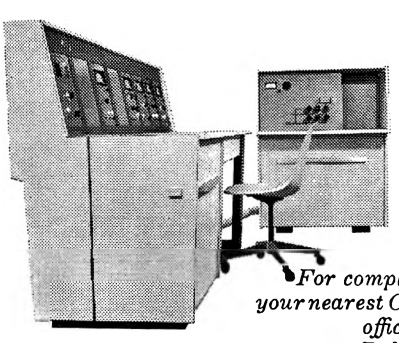

Look at its features: A built-in direct writing oscillograph recording system using five galvanometers... a stainless steel inlet system... a built-in micromanometer. And performance? Mass range from m/e 2 to 230 continuous with unit resolution up to m/e 200.

For complete information call your nearest CEC sales and service office or write today for Bulletin CEC 21130-X3.

Analytical & Control Division CEC

CONSOLIDATED ELECTRODYNAMICS / pasadena, california

A SUBSIDIARY OF **Bell & Howell** · *FINER PRODUCTS THROUGH IMAGINATION*